OCS Study
MMS 96-0067

Coastal Marine Institute

Numerical Simulation of Gulf of Mexico Circulation under Present and Glacial Climatic Conditions

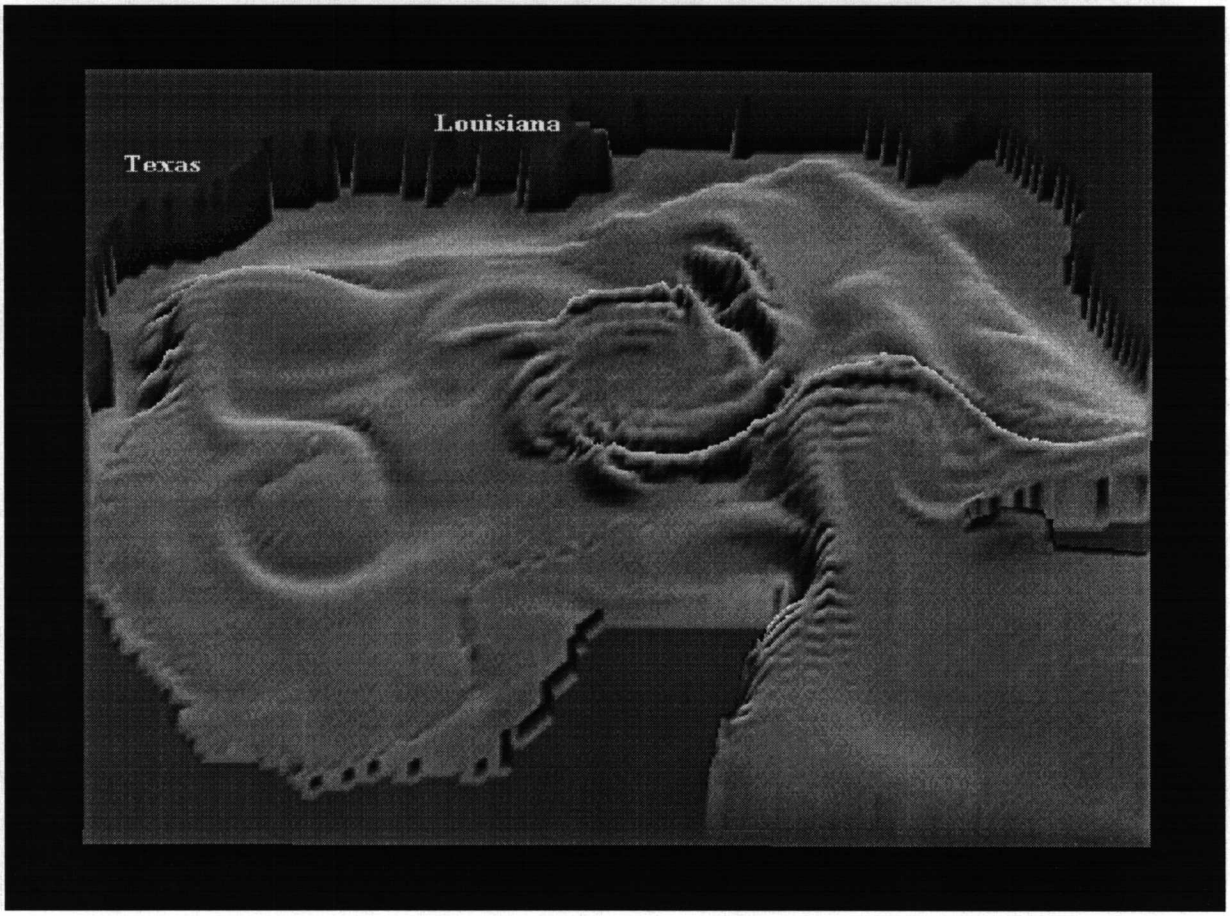

MMS U.S. Department of the Interior
Minerals Management Service
Gulf of Mexico OCS Region

OCS Study
MMS 96-0067

Coastal Marine Institute

Numerical Simulation of Gulf of Mexico Circulation under Present and Glacial Climatic Conditions

Authors

Masamichi Inoue
Susan E. Welsh

Prepared under MMS Contract
14-35-0001-30660-19908
by
Coastal Marine Institute
Louisiana State University
Baton Rouge, Louisiana 70803

Published by

U.S. Department of the Interior
Minerals Management Service
Gulf of Mexico OCS Region

New Orleans
March 1997

DISCLAIMER

REPORT AVAILABILITY

Extra copies of the report may be obtained from the Public Information Office (MS 5034) at the following address:

U.S. Department of the Interior
Minerals Management Service
Gulf of Mexico OCS Region
Public Information Office (MS 5034)
1201 Elmwood Park Boulevard
New Orleans, Louisiana 70123-2394

Telephone Number: (504) 736-2519
1-800-200-GULF

CITATION

Suggested citation:

Inoue, M. and S.E. Welsh. 1996. Numerical simulation of Gulf of Mexico circulation under present and glacial climatic conditions. OCS Study MMS 96-0067. U.S. Dept. of the Interior, Minerals Management Service, Gulf of Mexico OCS Region, New Orleans, La. 146 pp.

PREFACE

Recent increasing level of activity associated with offshore oil and gas exploration and production in the outer continental shelf and slope regions of the Gulf of Mexico (GOM) calls for a better understanding of the ocean environment and the need to assess various potential environmental effects of those activities. The MMS's interests in those regions resulted in the recently-funded oceanographic research programs specifically focused on those areas. This study represents one of those programs.

The usefulness of numerical models to simulate ocean circulation has been recognized by paleoceanographers, and paleoceanographic modeling has become an important tool in understanding the past oceanographic conditions. Numerical models offer means to test and verify various hypotheses concerning the past oceanographic conditions. This is necessary in order to arrive at the most plausible scenario. Paleoceanography based on planktonic foraminiferal assemblages, oxygen isotopes and sedimentary geology has helped in determining some of the characteristics of the past oceanographic conditions. However, paleoceanographic modeling of the GOM has not been attempted to take advantage of the usefulness of the numerical models to test and verify various hypotheses. Circulation in the Gulf during the last glacial period is of great interest not only to paleoceanographers but also to the oil and gas industry. As exploration moves to the shelf edge and beyond, instability hazards posed by late Wisconsin deltas, as well as older deposits, must be understood. This has a strong relevance to the late Quaternary shelf-margin deltas which are primary indicators of the position of ancient shelf margins, and are important for predicting sand occurrence in that environment as well as farther downslope.

In this project, we study circulation in the GOM under present and glacial climatic conditions by modeling not only the entire GOM but also a portion of the North Atlantic and the northwestern corner of the Caribbean. The first objective of this study is to examine the present circulation of the GOM. Then this model will be used to study the ocean circulation in the GOM during the last glacial period, for which a significant amount of supporting data is available. The objectives will be to study the effects of the atmospheric conditions and sea-level changes during the last lowstand of sea level on the general circulation in the Gulf with an emphasis on the Loop Current dynamics and the shelf-slope interaction.

This study consitutes the Ph. D. dissertation research of Susan E. Welsh, who was awarded a Ph. D. degree in the Department of Geology & Geophysics at the Louisiana State University in August 1996.

ABSTRACT

The Gulf of Mexico is an ideal location for paleoceanographic study using a three-dimensional ocean circulation model because of the availability of data to verify the model for the present. A description of the Gulf of Mexico circulation during the last glacial maximum is beneficial in interpreting the distribution of glacial fauna and adds to the understanding of global climate change because the Gulf of Mexico is an important link in the circulation of the Atlantic Ocean. The Florida Current originates in the Gulf of Mexico and contributes warm, salty water to the Gulf Stream. The Gulf Stream influences the climate of the North Atlantic and is a factor in the production of North Atlantic Deep Water, thus contributing to the global thermohaline circulation.

The Modular Ocean Model is used with fine horizontal grid resolution to be truly eddy-resolving and with a high number of vertical levels to resolve the bottom topography. A unique method of forcing the inflow through the Yucatan Channel is developed that results in a realistic annual cycle in the volume transport and baroclinic shear of the Loop Current. Seasonally varying wind forcing and surface relaxation toward observed temperature and salinity fields are implemented. The present-day seasonal simulations were able to realistically reproduce many of the observed features of the general circulation as well as the formation, migration, and decay of Loop Current rings. The model deep circulation is dominated by large cyclones that are associated with the upper layer Loop Current rings.

The model grid was then configured to represent the lowstand in sea level at 18,000 years before present and the model was forced with glacial estimates of wind stress and surface temperature. The response of the model to different inflow conditions through the Yucatan Channel was tested. Volume transport of the Florida Current during the last glacial maximum that is lower than present is supported by glacial estimates of the volume transport of the North Atlantic gyre and by the results of a global ocean circulation model for the last glacial maximum.

TABLE OF CONTENTS

PAGE

PAGE

CHAPTER

LIST OF FIGURES

FIGURE PAGE

FIGURE PAGE

FIGURE PAGE

FIGURE PAGE

LIST OF TABLES

LIST OF ACRONYMS AND ABBREVIATIONS

The following acronyms may be used throughout this report:

AVHRR	Advanced Very High Resolution Radiometer
B.P.	before present
ka	kiloannum or thousands of years before present
CLIMAP	Climate Long-Range Prediction and Mapping Project
GOM	Gulf of Mexico
LC	Loop Current
LGM	last glacial maximum
NADW	North Atlantic deep water
R	surface relaxation parameter
SC	shelfbreak current
SST	sea-surface temperature
Sv	sverdrup
WBC	western boundary current

ACKNOWLEDGMENTS

We would like to thank the Coastal Marine Institute at LSU that is funded by the Minerals Management Service for providing the necessary support of this project. We would also like to thank the Louisiana State University Board of Regents for providing the Graduate Fellowship for S. Welsh during the first four years of her Ph. D. program and the System Network Computing Center for the free usage of the IBM 3090. Our gratitude goes to Dr. Kutzbach at the University of Wisconsin for providing wind data for the last glacial maximum.

We would like to acknowledge all members of S. Welsh's graduate committee for their expertise on each of the different facets of the research: Dr. Sen Gupta in paleoceanography; Dr. William Wiseman in physical oceanography; Dr. Lui Chan in chemical oceanography; Dr. S.A. Hsu in meteorology and Dr. Greg Stone in geography, and for their helpful comments on the dissertation. In this study we made an extensive use of a computer animation software produced by Mr. Lingsong Bi. Our acknowledgments are extended to Dr. Tony Sturges, the staff of the Dept. of Geology and Geophysics and of the Coastal Studies Institute, in particular Mr. David Wilensky.

CHAPTER 1

INTRODUCTION

Presently there is much interest in the thermohaline circulation of the Atlantic Ocean during the last glacial maximum (LGM), approximately 18,000 years before present (B.P.). The main focus of these studies has been to determine the volume flux of glacial North Atlantic Deep Water (NADW), which may reflect changes in the intensity of the oceanic circulation (LeGrand and Wunsch 1995). This is part of an effort to piece together the past global circulation and understand the ocean-atmosphere response mechanisms to global climate change. Numerical models are useful in describing past environments by combining what we know about present-day environmental processes with data from the geologic record, which is incomplete and not a direct measurement of the ocean circulation. Although numerical models have been used to study the North Atlantic circulation during the LGM, the grid resolution has been too coarse to resolve the circulation in the Gulf of Mexico (GOM) (Lautenschlager et al. 1992) or did not extend into the GOM (LeGrand and Wunsch 1995). The GOM is an important link in the circulation of the North Atlantic gyre because the Gulf Stream derives the bulk of its warm, salty water from the Florida Current, which flows from the GOM into the North Atlantic through the Florida Straits. Consequently the volume transport and source waters of the Florida Current can influence the climate and general circulation of the North Atlantic.

The research presented here uses present-day boundary conditions to first develop and verify a primitive-equation numerical ocean model of the GOM. Some improvements of this study over other GOM modeling efforts are the eddy-resolving capability of the model, small grid size in the vertical and horizontal, low values for viscosity and diffusivity, and seasonal forcing. This present-day model can realistically simulate the upper-layer seasonal circulation in the GOM, the ring separation process of the Loop Current (LC), and LC ring characteristics. Detailed analysis of the lower layer temperature and velocity fields has also provided new insight into the deep circulation of the GOM.

The model is then used to simulate the paleocirculation of the GOM during the LGM by adjusting the grid to represent the lowstand in sea level and applying boundary conditions for 18,000 years B.P. The goals of the LGM simulations are to test hypotheses regarding the volume transport into the GOM during the LGM and help interpret the distribution of glacial fauna in the western GOM. An application of the LGM model results is to estimate coastal currents during the lowstand in sea level when rivers deposited sediment directly on the outer shelf and slope (Morton and Price 1987), which is a factor in finding mineral resources. Another reason to describe the paleoceanographic conditions in the GOM is to provide information regarding the climate over the North American continent during the LGM because the warm surface waters of the GOM are an active region for cyclogenesis to occur (Hsu 1988).

The use of numerical models to study the present ocean circulation has increased in recent years and has contributed significantly to our understanding of various ocean processes. Numerical models also help in the design and interpretation of observational studies which are limited in either spatial resolution or geographic extent as well as temporal resolution or length of record. Once the model has been tested and validated, the output can be sampled and analyzed with a high degree of resolution to help interpret observations or develop further sampling strategies. In addition, the verified model can be used to study the response of the study area to different environmental conditions.

Several numerical modeling studies have been made of the GOM using present-day environmental conditions. The two-layer model of H. Hurlburt and J.D. Thompson (1980) at the Naval Oceanographic Research and Development Activity (NORDA) has been useful in understanding LC ring separation dynamics. A major disadvantage of these models is their inability to adequately resolve bottom topography. The new generation of three-dimensional, primitive-equation, ocean circulation models allows for enhanced vertical and horizontal resolution, but also requires more powerful, high-speed computers (Cox 1984; Blumberg and Mellor 1987; Haidvogel et al. 1991). The Princeton model (Blumberg and Mellor 1987) has been useful in the study of GOM circulation (e.g. Oey 1995).

The GOM is an ideal basin for study using an eddy-resolving model due to the limited size of the domain and the dominance of the LC and rings shed by the LC. Sturges et al. (1993) used the Bryan-Cox model (Cox 1984) to study the GOM on a ¼-degree grid with 12 vertical levels that also included the entire Caribbean and adjacent portions of the North Atlantic Ocean to force the flow through the Caribbean with a volume transport equal to the wind-driven transport of the North Atlantic Gyre. Although the model was able to reproduce some of the observed features of the LC and associated anticyclonic rings, the maximum transport through the Florida Straits was only 18 Sv (1 Sverdrup = 10^6 $m^3 \cdot s^{-1}$) compared to the 30 Sv that is observed. The difference can be accounted for by the Schmitz et al. (1992) estimate that the wind-driven component of the Florida Current represents only 55% of the total volume transport.

The eddy-resolving numerical model of the GOM by Dietrich and Lin (1995) also extends outside of the GOM into the western Caribbean where the inflow is prescribed as a western boundary current with a fixed volume transport of 25 Sv. The horizontal grid resolution is 20 km and there are 16 levels in the vertical. The model does not include surface forcing or salinity effects. Many of the ring characteristics were close to the observed averages, such as swirl speed, westward migration speed, and period of ring separation. Although a goal of the Dietrich and Lin (1995) model was to describe the vertical structure of rings during the ring separation cycle, the vertical temperature distributions of the model rings and the ambient fluid are distinctly different from observations.

This modeling project features essentially the same model as Sturges et al. (1993), but with a reduced horizontal domain that permits doubling the horizontal grid resolution to ⅛° (13 km). Resolution of the eddy dynamics is essential in the GOM, where anticyclonic rings shed from the LC carry heat and momentum to the western GOM,

thereby coupling the eastern and western basins and influencing the heat and salt budgets of the GOM (Elliot 1982). Rings also impact the local surface current patterns, climate and biological productivity. The length scale of the rings is determined by the Rossby radius of deformation, which is approximately 30-40 km for the first baroclinic mode (Emery et al. 1984). A minimum of two grid boxes is necessary per radius of deformation in order to simulate realistic rings, which will be satisfied on an ⅛-degree grid. In this study, the term 'rings' will always be used when referring to the anticyclonic, warm-core rings shed by the LC, and 'eddies' applies to any other cyclonic or anticyclonic circulation features.

The verification of numerical models in the GOM has been possible because of the tremendous amount of observational data that is available and a small number of other modeling studies. Surface drifters (Lewis and Kirwan 1987), Advanced Very High Resolution Radiometer (AVHRR) data (Vukovich 1995) and NOAA satellite infrared images (Vukovich and Crissman 1986) have been used to study the dynamics and periodicity of the ring separation cycle. The structure and westward migration of the rings (Elliot 1982; Vukovich and Crissman 1986) and the interaction of the rings with the western wall of the GOM (Vidal et al. 1992; Indest 1992; Brooks 1984) have been described from hydrographic surveys, satellite images and drifters. Current meters and hydrographic surveys have been used to determine the general circulation (Molinari et al. 1978) and the deep flow in the GOM (Hamilton 1990).

Not all paleoceanographic modeling studies have included the model calibration phase using present-day conditions, which is difficult when there are large changes in the basin shape and size, as well as climate. Some modeling studies which were mainly used for hypothesis testing are the model simulation of the Cretaceous by Barron (1989) and the ocean circulation model for Pangaean time by Kutzbach et al. (1990). A more recent modeling study of the mid-Cretaceous ocean circulation by Barron and Peterson (1990) used an adaptation by Semtner (1974) of the model code by Bryan (1969), which is the same model used in this study. The model had been tested using present-day conditions, and then a present-day control simulation was made with the model code adapted for the Cretaceous experiments (Barron and Peterson 1990). The paleoceanographic model was then used for sensitivity studies to determine the importance of bathymetry of the ocean basins, air temperature, and the affect of changing wind stress by varying continental elevation (Barron and Peterson 1990).

Paleoceanographic models that focus on the LGM are not subject to changes in continental locations, and are more conducive to verification using paleontological and sedimentological data. A numerical model used in the study of the Indian Ocean during glacial and interglacial conditions (Luther et al. 1990; Prell et al. 1990) was not only extensively tested for the present (Luther and O'Brien 1985), but model results for the interglacial conditions were verified by comparison with the distribution of planktonic foraminifera and estimated sea-surface temperature (SST) (Prell et al. 1990).

Lautenschlager et al. (1992) constructed a global ocean general circulation model for the LGM to test the ocean's response to forcing by glacial estimates of wind stress and fresh water flux computed using the atmospheric general circulation model of Kutzbach

and Guetter (1986). Testing and verification of the ocean model was reported in a previous paper (Maier-Reimer et al. 1991) and a 750-year model simulation was performed as a present-day control experiment for comparison with the LGM simulations (Lautenschlager et al. 1992). Model simulated SST was compared to LGM estimates and model distributions of Cd/Ca and $\delta^{13}C$ were compared with data from deep-sea sediment cores. Although the model predicts intensification of Atlantic equatorial currents in response to stronger trade winds in the Atlantic (Prell et al. 1976), the westward flow in the Caribbean is reduced and the intensity of the Brazil Current is increased (Lautenschlager et al. 1992). The model resolution is too coarse to resolve the circulation in the GOM, but the results for the LGM circulation study indicate a decrease in the inflow to the GOM from the Caribbean (Lautenschlager et al. 1992). This particular result had a large impact on the way in which the inflow into the GOM was prescribed in this modeling study.

In this study the glacial-period simulations are made in exactly the same way as the present day, except with lowered sea level and with surface boundary conditions that reflect the climate of the LGM. The SST field is restored to Climate: Long-Range Investigation, Mapping, and Prediction (CLIMAP) data (CLIMAP Project Members 1981) and the wind stress estimates are from the glacial atmospheric general circulation model of Kutzbach and Guetter (1986). Paleontological and sedimentological data for the GOM are used to estimate the validity of the LGM model simulations. The circulation of the upper layers is compared to the circulation inferred from the estimates of glacial temperature and salinity patterns made by Brunner and Cooley (1976). Vertical profiles of model velocity through the Florida Straits for the present and LGM simulations are compared to determine the likelihood of stronger bottom currents in the Florida Straits during the LGM as suggested by Brunner (1986).

The research presented in this report is divided into two phases which have rather different purposes. The present-day simulations of the GOM will be of value to the GOM modeling community due to the realistic ring separation from the LC, the westward migration and decay of the rings, the seasonal cycle in the general circulation and new findings regarding the deep circulation in the GOM. Also the present-day model verification is necessary as a control run for modeling the LGM environment. The objectives of the paleoceanographic model simulations are to help interpret paleontological and sedimentological data from the geologic record, describe the circulation of the GOM during the LGM and test hypotheses regarding the volume transport of the Florida Current. The latter goal is important in describing the glacial climate and changes in the thermohaline circulation of the Atlantic Ocean.

The numerical model history and configuration, the model development under annual mean forcing conditions, and results of the annual mean forcing case are described in Chapter 2. The model configuration, initial conditions, and model forcing for the present-day, seasonally-forced simulations are discussed in Chapter 3. The results of the seasonal-forcing case and the model-data comparisons for the seasonal-forcing case are also presented in Chapter 3. A discussion of the sea level lowstand during the LGM, and comparisons of the SST and wind stress fields over the GOM for the present-day and

LGM are presented in Chapter 4. The LGM model configuration, initial conditions, model forcing, model results and model-data comparisons are presented in Chapter 4. For reference, a summary of all model simulations covered in Chapters 2 through 4 is provided in Table 1. The project summary and conclusions are presented in Chapter 5. Details of the numerical model formulation are presented in Appendix A and an explanation of how the forcing for the LGM simulations was determined is presented in Appendix B.

Table 1. Summary of all model simulations made in this study.

Type of Simulation	Length of Simulation weeks (years)	Rings
Present-day annual mean forcing		
High friction [1]		
Spin-up	156 (3.0)	
Production run	156 (3.0)	10
Parameter test with R=12 [2]	96 (1.8)	3
Production run	60 (1.2)	2
Low friction [3]		
Production run	120 (2.3)	4
Total	(11.3)	
Present-day seasonal forcing		
Spin-up	154 (3.0)	
Production run (upper layer study)	257 (5.0)	S0-S9
Production run (deep layer study)	206 (3.0)	S9-S13
Total	(11.0)	
LGM high transport case		
Spin-up	206 (4.0)	
Production run	206 (4.0)	H0-H5
Total	(8.0)	
LGM low transport case		
Spin-up	206 (4.0)	
Production run	206 (4.0)	L0-L5
Total	(8.0)	

[1] coefficients of viscosity and diffusivity are 200 $m^2 s^{-1}$ and 100 $m^2 s^{-1}$, respectively.

[2] R denotes relaxation time scale in weeks for surface boundary conditions. All model simulations used R=6 except the single case with R=12.

[3] coefficients of viscosity and diffusivity are 75 $m^2 s^{-1}$ and 75 $m^2 s^{-1}$, respectively.

CHAPTER 2

MODEL DEVELOPMENT AND VERIFICATION

2.1 Model Description

The bathymetry of the GOM features several broad, gently sloping shelves, steep escarpments and relatively shallow sill depths in the Yucatan Channel and Florida Straits (Figure 1). The circulation in the GOM is dominated by the presence of the LC and the anti-cyclonic rings that are shed from the LC. The Modular Ocean Model (Pacanowski et al. 1991) is a three-dimensional primitive equation model that is able to simulate the effects of bottom topography as well as resolve eddy dynamics on a small enough grid, both of which are important in the GOM. The Modular Ocean Model directly evolved from the Bryan-Cox numerical ocean model (Bryan 1969; Cox 1984; Semtner 1986a,b). Modular Ocean Model version 1.1, released in 1993, was used in this study. Details of the model physics and numerical formulation are presented in Appendix A.

The structure and transport of the flow into the GOM through the Yucatan Channel are very important for realistic simulation of the LC. In order to keep the size of the model domain limited and achieve a realistic inflow condition, this model domain extends outside the GOM into a synthetic return flow region that links the Straits of Florida with the western Caribbean (Figure 2). The bathymetry in the return flow region was altered and smoothed to allow flow exiting the GOM to recirculate around Cuba and enter the GOM through the western Caribbean. Flow through the western Caribbean was forced to acquire the observed shear and geostrophic transport of the Caribbean Current along a north-south transect at 82.375°W. West of the geostrophic forcing region the flow could adjust naturally to the bathymetry and local wind forcing, which resulted in a realistic inflow condition through the Yucatan Channel. This method of forcing the inflow eliminated the need to include the entire North Atlantic, which can be very costly in terms of computer resources, especially for a small grid-size and high vertical resolution. Another benefit of allowing the flow to recirculate was to avoid the difficulties in implementing open boundaries, while allowing the model to pick the natural inflow conditions through the Yucatan Channel.

The model grid was derived from the ETOP05, 1/12°-resolution, world topography data set available from the National Ocean Data Center. The bathymetric values were interpolated to ⅛° and then smoothed using three passes of a double Hanning filter to prevent topographically-induced instabilities in the numerical solution. The model domain extends from 97.75°W to 72.875°W and from 16.0°N to 30.875°N and has lateral dimensions of 200 by 120. There are 15 levels in the vertical with a maximum depth of 3600 m, which is approximately the deepest isobath in the GOM. It is preferable to use evenly-spaced levels in the vertical to reduce error in the finite difference formulation of the vertical velocity. Also it is desirable to have greater resolution near the surface for more accurate representation of the shelf bathymetry and to resolve the thermocline. Therefore, bimodal spacing of the vertical levels was chosen such that the

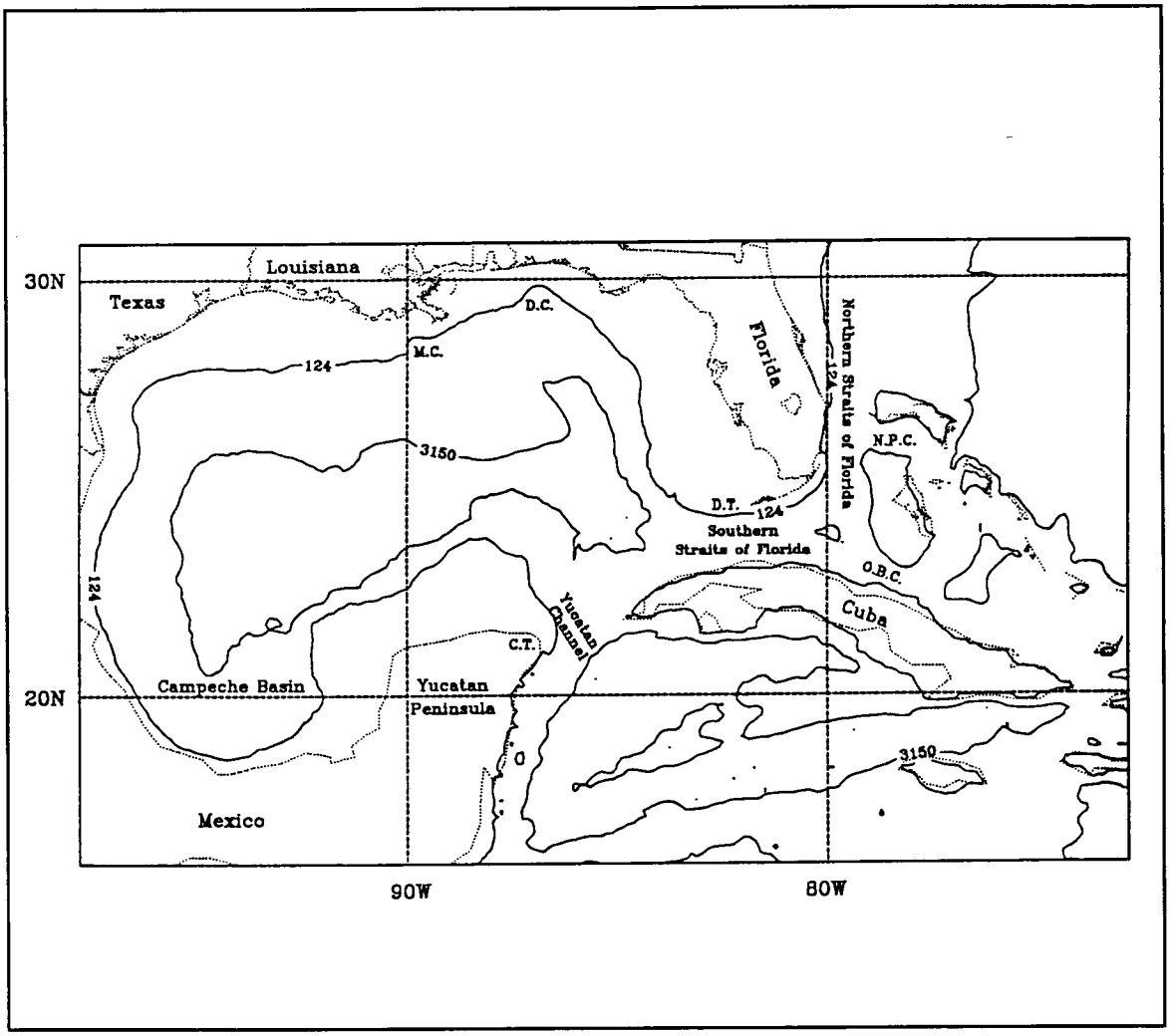

Figure 1. The Gulf of Mexico model domain. Depth contours in meters. stippled line represents observed coastline and geographic boundaries.

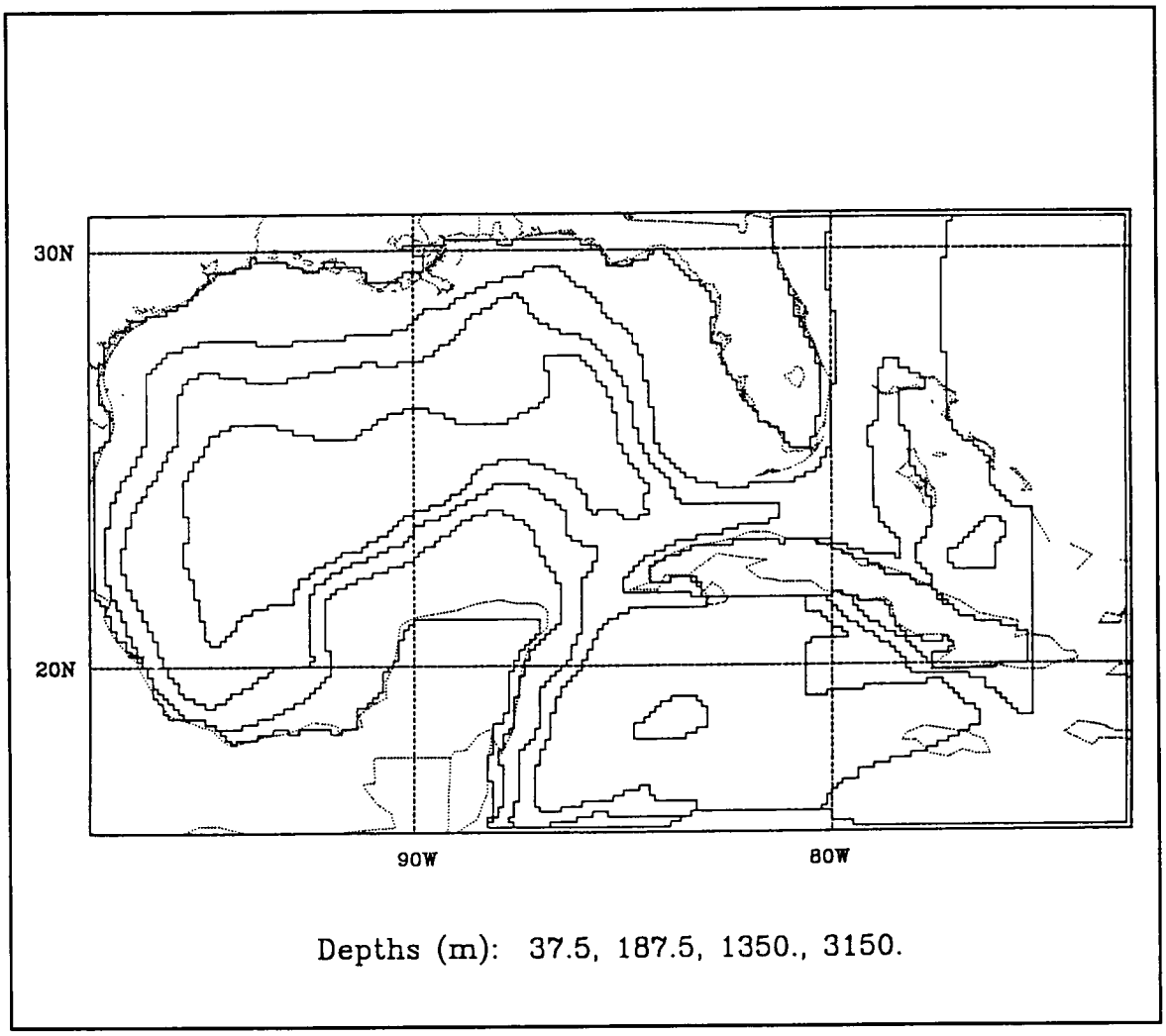

Figure 2. The present-day simulation model grid. Solid lines represent model grid levels. Stippled line represents observed coastline and geographic boundaries

thickness of each of the upper four levels is 75 m and the lower 11 levels are each 300-m thick.

The three-dimensional annual mean temperature and salinity fields used to initialize the annual-mean forcing case were derived from the Levitus Climatological Atlas of the World Ocean (Levitus 1982). The original data is available on a 1° horizontal grid with 33 levels in the vertical. The vertical interpolation of the hydrographic data to model depths was performed using a cubic spline algorithm from IMSL (1989) and then an IMSL two-dimensional quadratic spline algorithm was used to interpolate laterally to ⅛°.

Level 1 (vertically centered at a depth of 37.5 m) temperature and salinity were restored to climatological means to prevent a drift. This surface boundary condition allows for surface heat and moisture fluxes, which should be close to real surface fluxes. A parameter study was performed to determine the optimum value for the surface relaxation time scale, R, for Newtonian restoration of the temperature and salinity fields. An initial value of R=6 weeks was used, which is common in this type of model (Sturges et al. 1993) and produced level 1 temperature and salinity fields that were in good agreement with the Levitus climatology. It is noted that R=6 weeks is close to the range of 25-40 days computed from observed climatology (Han 1984; Hirst and Godfrey 1993). The simulation was repeated with R=3 weeks, but it was immediately obvious that this value prevented the surface fields from evolving freely. Parallel 96-week simulations were made with values of R=6 weeks and R=12 weeks for comparison. Although the circulation at level 1 was essentially identical after 96 weeks for the two cases, the northern section of the GOM was gaining heat and the southern portions of the model were losing heat in the R=12 weeks case. Therefore the choice of R=6 weeks was used for all simulations.

The surface wind stress field was derived from the Hellerman and Rosenstein (1983) normal monthly wind stress climatology. The global monthly mean wind stress values on 2° grid were calculated from over 35 million surface wind speed observations from 1870 to 1976 (Hellerman and Rosenstein 1983). The conversion from wind speed to wind stress is made using a quadratic bulk aerodynamic formulation,

$$|\tau| = \rho C_D (u^2 + v^2),$$

where $|\tau|$ is the modulus of the wind stress vector, ρ is the air density, u and v are the eastward and northward components of the wind and C_D is the non-dimensional drag coefficient based on wind speed and air temperature minus sea temperature (Hellerman and Rosenstein 1983). The original wind stress field was interpolated to ⅛° using the IMSL (1989) two-dimensional tensor product spline interpolant algorithm. For the annual mean forcing case, an annual average of the wind stress was applied over the entire GOM and in the Caribbean to the west of the geostrophic forcing region only.

The volume flux through the Yucatan Channel was controlled by adding an equal value of u-component of velocity to each grid point in the north-south and vertical directions within a longitudinal band centered at 82.375°W in the Caribbean. The desired

vertical shear was achieved by relaxing the temperature and salinity along this same vertical cross section to the observed values. A parameter study was performed to find the best value for the relaxation time scale for Newtonian restoration of the temperature and salinity fields to observations. The model was run with several values for the relaxation time scale ranging from 30 min to 12 weeks. The optimum value for the relaxation time scale for restoration of the vertical profiles of temperature and salinity fields to produce realistic geostrophic flow through the western Caribbean was six weeks. The temperature and salinity fields used for this purpose were also derived from the Levitus climatology.

Quadratic friction was implemented and the coefficients of horizontal viscosity and diffusivity were A_M=200 $m^2 \cdot s^{-1}$ and A_H=100 $m^2 \cdot s^{-1}$, respectively, for the initial runs with annual mean forcing. A value of 1×10^{-4} $m^2 \cdot s^{-1}$ was used for both vertical viscosity and diffusivity for all simulations. These values for friction were within the range of values used in previous modeling studies that focus on the dynamics of the LC and rings (Hurlburt and Thompson 1980; Sturges et al. 1993; Oey 1995). Bottom stress is applied with a drag coefficient of C_D =.001. A parameter study was made to determine the largest possible time step that would result in a stable numerical solution. A 30-min timestep is used for all simulations.

There were several indicators used to determine the stability of the model. The total kinetic energy averaged over the basin was monitored to determine if the model fields have come to equilibrium or were 'spun-up'. Also it was necessary to determine if the model was losing heat or salt, which could be assessed by monitoring the basin average of the absolute change in temperature and salinity. The volume averages of these three variables were plotted against time to detect any trend in the mean. The model equilibrium was assessed by evaluating the time series of each of these variables.

2.2 Model Simulations with Annual Mean Forcing

The first set of model simulations featured annual mean forcing and was necessary to determine model stability and to make adjustments to many of the model parameters and the method of forcing the inflow. Approximately three years of model integration were necessary for the annual-mean forcing model to become sufficiently spun-up. Then more than eight years of model integration were made for analysis, totalling more than 11 years of model integration with annual-mean forcing (refer to Table 1). All model integrations were performed on an IBM 3090 with vector capabilities. The average cpu time per time step was 4.3 s resulting in 21 hr of cpu time per model year of simulation.

This modeling study used a target value of 28 Sv to represent the annual mean volume transport through the southern Straits of Florida. This volume transport was based on time series of current meter measurements and cable-based transport measurements across each of the various channels that feed the Florida Current. SAIC (1992) estimated the annual mean transport through the Florida Straits at 27°N to be 31.1 Sv and the combined annual mean transport through the Old Bahama Channel and the

Northwest Providence Channel to be 2.8 Sv. Subtracting the combined transports through the Old Bahama Channel and the Northwest Providence Channel from the transport at 27°N results in an annual mean transport through the southern Straits of Florida equal 28.3 Sv. The widely accepted value for the transport of the Florida Current at 24°N is 30 Sv (Schmitz et al. 1992), which includes the 1.9 Sv flowing through the Old Bahama Channel measured by SAIC (1992).

Rings in the model separated from the LC with a constant ring-separation period of 30 weeks. This was somewhat shorter than the primary mode of 8-9 months observed by Sturges (1994) and also less than the primary mode of 9 months observed by Vukovich (1995), but well within the observed range of 6-17 months (Vukovich 1995). Both Vukovich (1995) and Sturges (1994) reported a secondary mode of 13-14 months, which was not reproduced in the model. This secondary mode is presumably forced by factors that are not included in the model.

The process of ring separation in the initial simulations using high values of viscosity and diffusivity was similar to that described by Sturges et al. (1993): "...a long gradual, process involving recirculation between the ring and the main flow for many weeks". The temperature and velocity fields of the LC and a ring during the separation are presented in Figure 3. The average diameter of the rings using annual mean forcing and high friction ($A_M = 200$ m^2·s^{-1} and $A_H = 100$ m^2·s^{-1}) was approximately 416 km in diameter with swirl speeds up to 40 cm·s^{-1} in the eastern GOM, decreasing to 20 cm·s^{-1} after 180 days. All rings followed the same migration path from east to west and merged with the western boundary flow along the Mexico Slope. The rings took approximately 270 days to reach the western slope. The rings were then advected into the northwestern corner where they would slowly decay until the next ring moved into the same location. The signature of the older rings disappeared when the new ring took its place, and the average life span of an individual ring was on the order of 500 days.

To improve the model, several test cases were performed to find the lowest reasonable values of viscosity and diffusivity that would generate more realistic eddy fields and continue to produce a numerically stable solution. A value of 75 m^2·s^{-1} was chosen for both viscosity and diffusivity for additional simulations with annual-mean forcing. This change in the friction had a great effect on the ring separation process and the westward migration of the rings. The LC became very unstable during the separation of a ring. Both the LC and the shed ring exhibited frontal waves and filaments along the outer boundaries from a time just before ring separation until after the ring was completely shed (Figure 4). Once the ring and the LC were moving away from each other, the frontal instabilities began to disappear. The rings no longer followed a predetermined path in the low friction simulations, although they did tend to move along two general paths. One path was just to the north of 24°N in the central GOM and the other was just to the south of 24°N. The maximum swirl speeds of the LC increased to over 100 cm·s^{-1} and maximum swirl speeds of the rings in the eastern GOM increased to over 70 cm·s^{-1} in the low friction simulations. Lowering the friction resulted in LC and ring behavior that compared more favorably with observations.

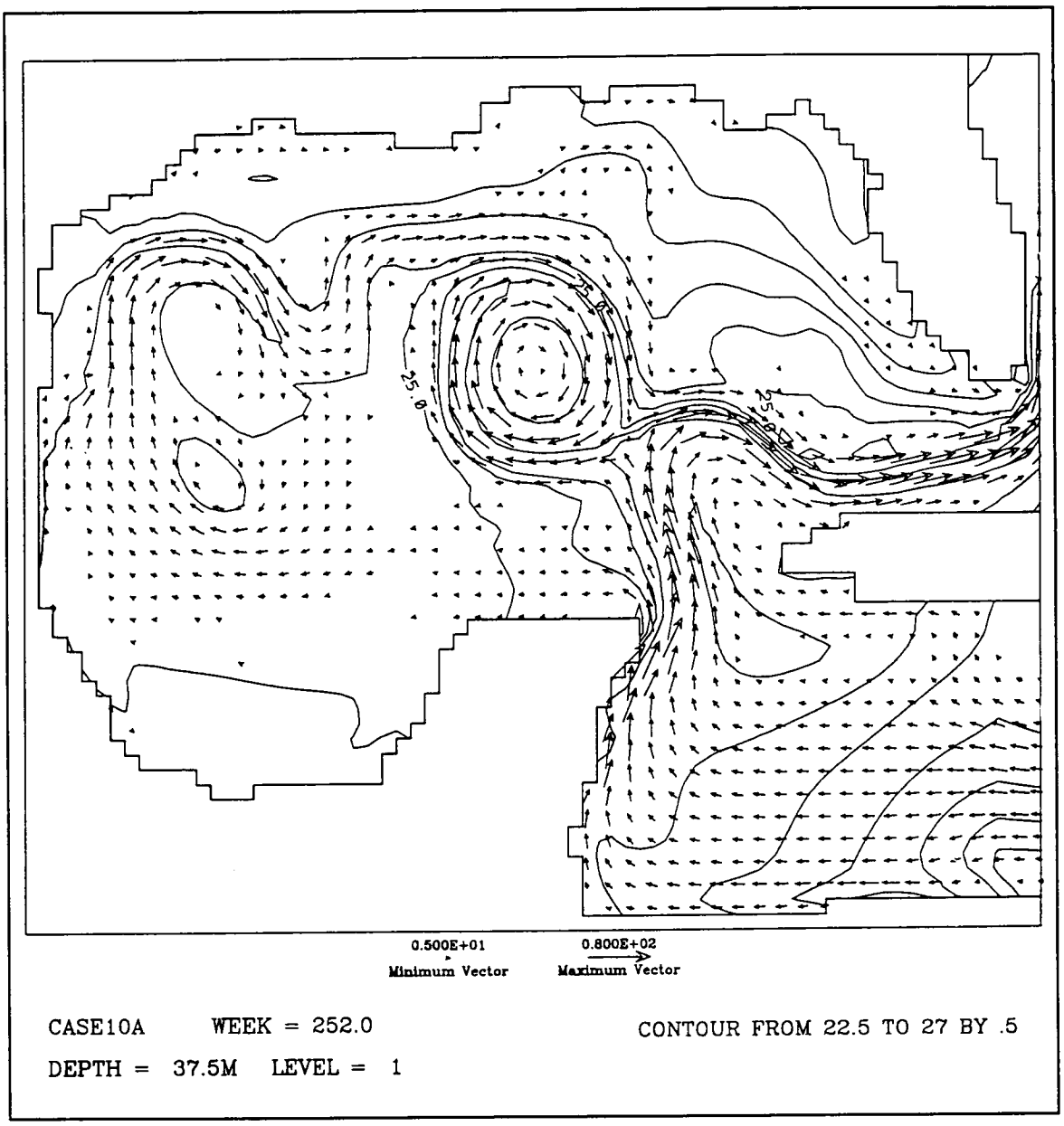

Figure 3. Level 1 (37.5 m) temperature (°C) and velocity ($cm \cdot s^{-1}$) fields for the annual-mean forcing case with high viscosity (200 $m^2 \cdot s^{-1}$) and diffusivity (100 $m^2 \cdot s^{-1}$) at model week 252.

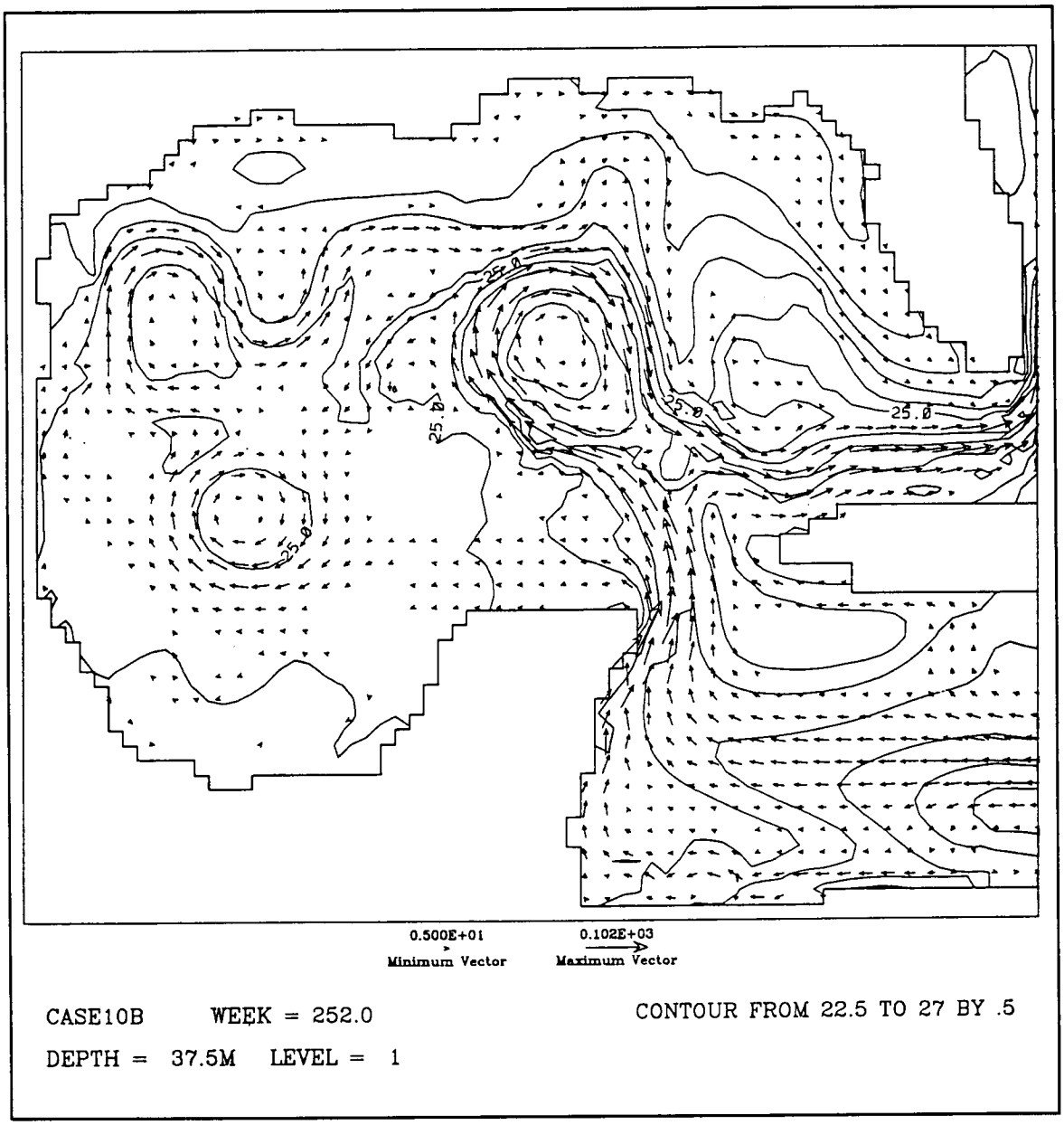

Figure 4. Level 1 (37.5 m) temperature (°C) and velocity ($cm \cdot s^{-1}$) fields for the annual-mean forcing case with low viscosity (75 $m^2 \cdot s^{-1}$) and diffusivity (75 $m^2 \cdot s^{-1}$) at model week 252.

CHAPTER 3

PRESENT-DAY SIMULATIONS

3.1 Introduction

The initial model simulations using annual mean forcing were necessary to develop a method for forcing the GOM and confirm the stability of the model and its ability to reproduce observed circulation features. The next phase in the model development was to implement the annual cycle in the forcing by applying monthly wind forcing and a seasonally-varying surface boundary condition. Further verification of the model's ability to simulate GOM circulation was possible using seasonal forcing. The model output from the seasonal forcing simulations is also a source of data to learn about processes in the present-day GOM that we do not have sufficient observations to understand completely. The last, but very significant, reason for the seasonal forcing simulations was to serve as a basis for comparison for the final stage in the dissertation, which was to model the GOM under LGM environmental conditions.

3.2 Model Description

The model configuration for the seasonal forcing simulations was exactly the same as for the initial annual-mean forcing simulations. The temperature, salinity, velocity, transport stream function and vorticity fields output from the low-friction, annual-mean forcing simulations were used to initialize the seasonal forcing simulations. The wind stress fields were derived from the Hellerman and Rosenstein (1983) monthly wind stress climatology. The seasonal-mean SST and salinity fields were interpolated from the Levitus seasonal climatology (1982). The Levitus climatology defined the seasons according to the following grouping of the months: winter - February, March, April; spring - May, June, July; summer - August, September, October; and fall - November, December, January. In order for the climatological surface forcing to vary smoothly in time, both the monthly mean wind stress field and the seasonal mean temperature and salinity fields at level 1 were linearly interpolated.

It was possible in the model to force a seasonal variation in the baroclinic shear of the inflow in the western Caribbean, therefore the temperature and salinity along the vertical transect centered at 82.375°W in the Caribbean were restored to the seasonal Levitus values. However, it was impractical to force seasonal changes in the volume transport, because the model was very sensitive to changes in the amount of u-component of velocity that is added along the north-south transect in the Caribbean. A minimum of one year of model spin-up time was needed for the model to adjust to small changes in the value of u added along 82.375°W. During spin-up, the added u-component of velocity is increased by very small increments until the target volume transport through the Yucatan Channel averaged over a year is achieved. Then the added value of u-component of velocity is kept constant over time for the production runs.

3.3 General Circulation

Under seasonal forcing the model transport through the southern Straits of Florida varies between 25 Sv and 31 Sv, with an average of 27.71 Sv (Figure 5). It is assumed that the mean inflow through the Yucatan Channel must equal the mean outflow through the Florida Straits. Schott et al. (1988) reported that the transport in the northern Straits of Florida at 27°N varies from approximately 26 Sv to 33 Sv with the maximum occurring in July, which includes approximately 5 Sv entering through the Old Bahama Channel and the Northwest Providence Channel. SAIC (1992) observed maxima in the flow during December and May for the observation period December 1990 to November 1991in the northern Straits of Florida. From Figure 5, it can be seen that the transport through the Yucatan Straits varies annually in the seasonal forcing simulations with the maximum transport occurring in late spring or early summer. Molinari et al. (1978) reported that the maximum transport through the Yucatan Channel in the upper 500 m is in June and the mean transport and phases of the maximum transports through the Yucatan Channel and Florida Straits are the same.

Upwelling is generated in the model along the northern coast of Yucatan in the vicinity of Cape Catoche, which is strongest in spring and weakest in summer (Figure 6). This upwelling has been observed by Ruiz Rentería (1979) to always occur in spring, but only occur sometimes in the summer and to be very weak or non-existent during the remainder of the year (Figure 7). The cool water is brought onto the Yucatan Shelf by Ekman transport due to local wind and possibly from bottom friction induced by the bottom current (Ruiz Rentería 1979). This process occurs when the core of the Yucatan Current flows along the eastern edge of the bank. A vertical cross-section of temperature from the eastern Yucatan Coast illustrates that the model upwelling is also fed by the cool waters along the eastern slope of the Yucatan Peninsula (Figure 8).

The observed circulation in the Campeche Bay features a semi-permanent cyclonic gyre that has an annual average geostrophic transport of approximately 3 Sv (Molinari et al. 1978; Vazquez de la Cerda 1993) (Figure 9). This seasonal gyre has its maximum geostrophic transport in fall and minimum transport in spring in response to seasonal changes in the local wind stress curl (Vazquez de la Cerda 1993). Molinari et al. (1978) reported that in the spring some flow separates from the Loop Current and moves west along the Campeche Bank into the Bay of Campeche. The model output features a well-developed cyclone in the Bay of Campeche in the fall and also flow enters the Bay of Campeche from the east over the Campeche Bank each spring (Figure 10).

A seasonal cycle is also apparent in the western boundary current (WBC) generated by the model. The maximum velocities in the model-generated WBC occur in the late summer and weaken in winter (Figure 11). The model-simulated WBC remains weak from November through January and then begins to strengthen. Molinari et al. (1978) computed geostrophic transports for the upper 500 m from observed temperature and salinity fields on a 1° grid over the entire GOM. The transport in a persistent anticyclone in the western GOM had maxima in summer and winter (Molinari et al. 1978), which agrees with the estimates made by Sturges and Blaha (1976) based on the

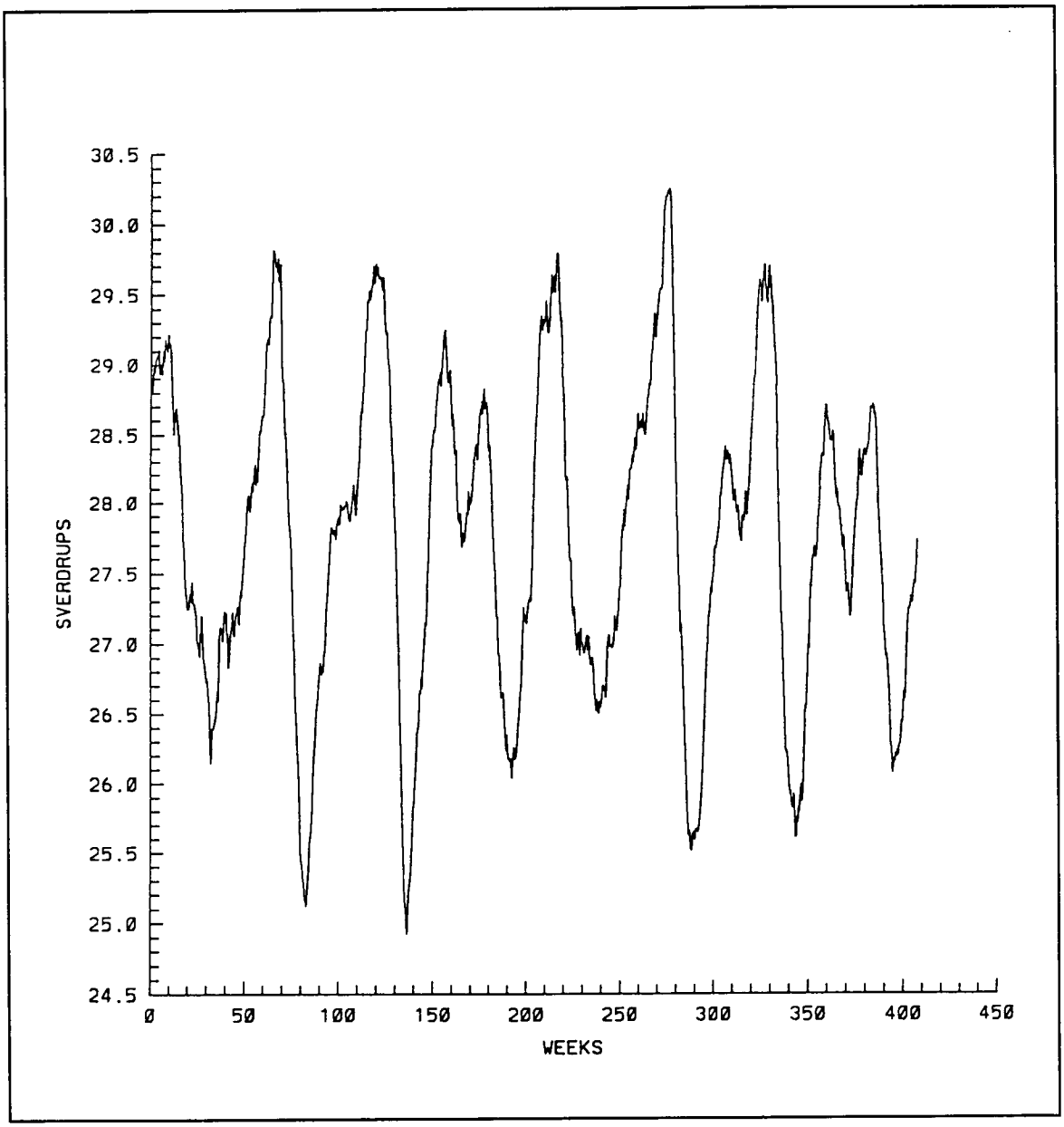

Figure 5. Time series of volume transport stream function (Sv) in the Florida Straits for the present-day seasonal forcing case. Model years 4-11. This data was processed with a 30-day running mean. The time axis begins with March 1.

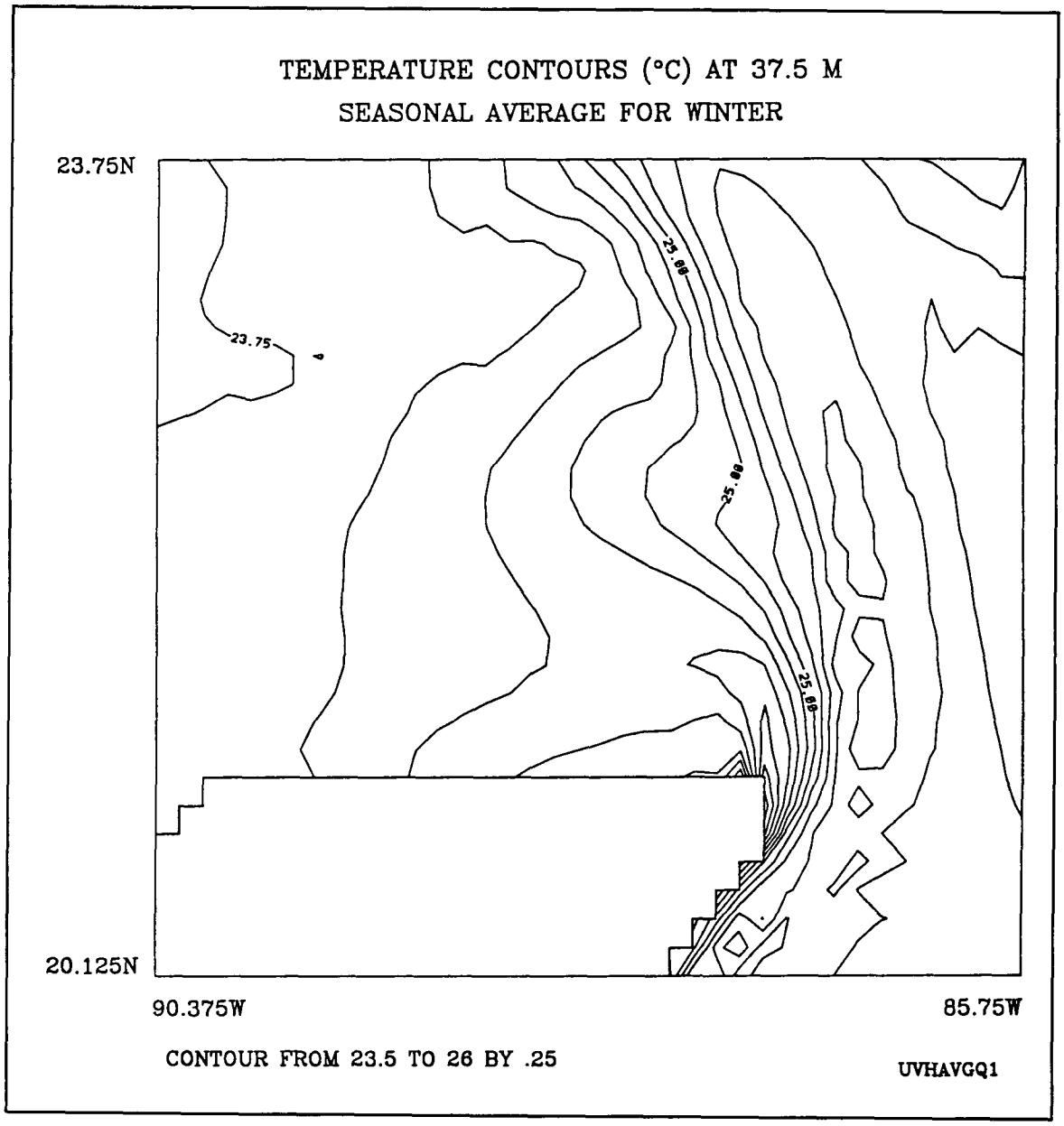

Figure 6a. Four-year averages of the level 1 (37.5 m) temperature field in the eastern Gulf of Mexico for the present-day seasonal forcing case for Winter.

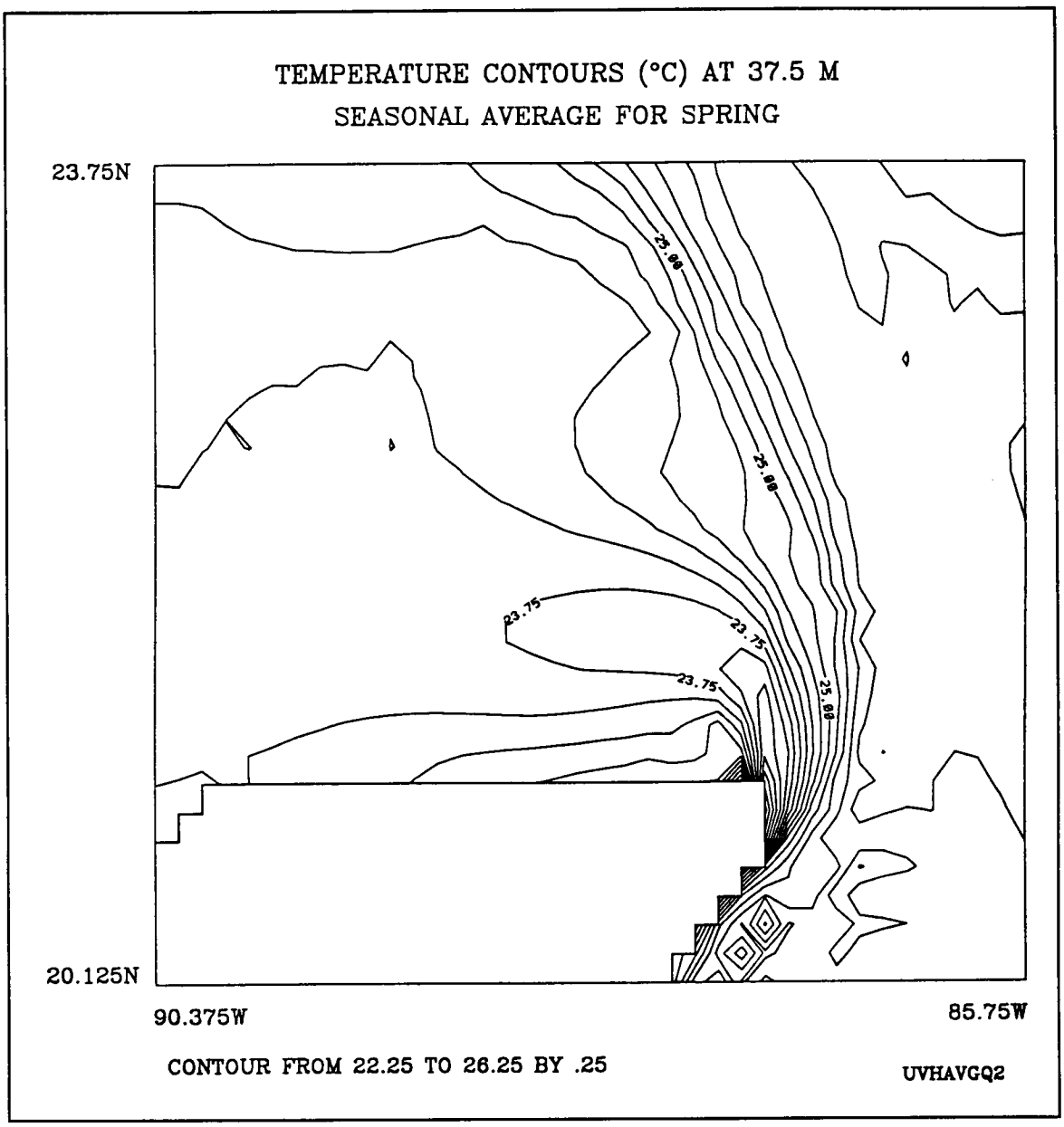

Figure 6b. Four-year averages of the level 1 (37.5 m) temperature field in the eastern Gulf of Mexico for the present-day seasonal forcing case for Spring.

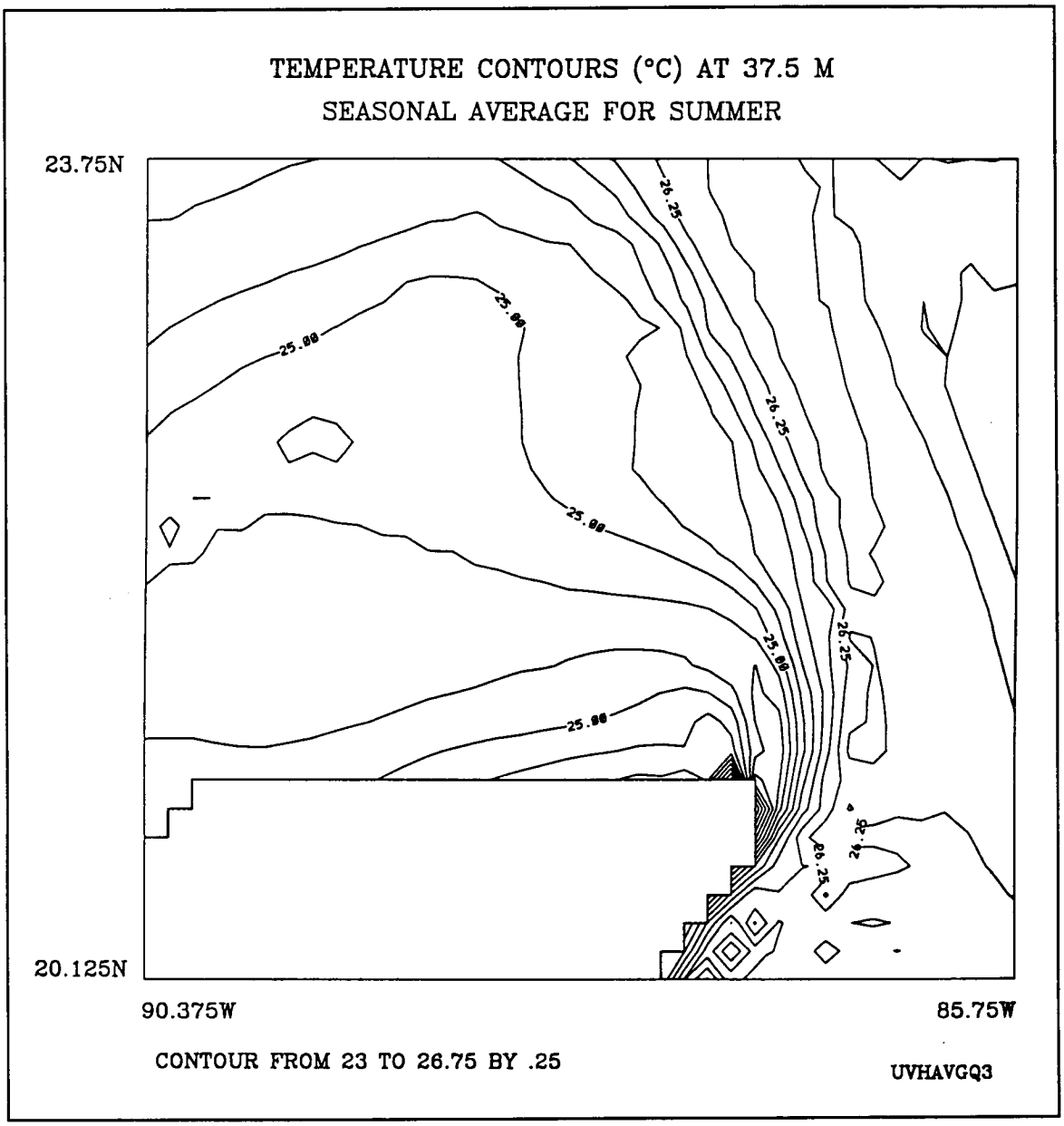

Figure 6c. Four-year averages of the level 1 (37.5 m) temperature field in the eastern Gulf of Mexico for the present-day seasonal forcing case for Summer.

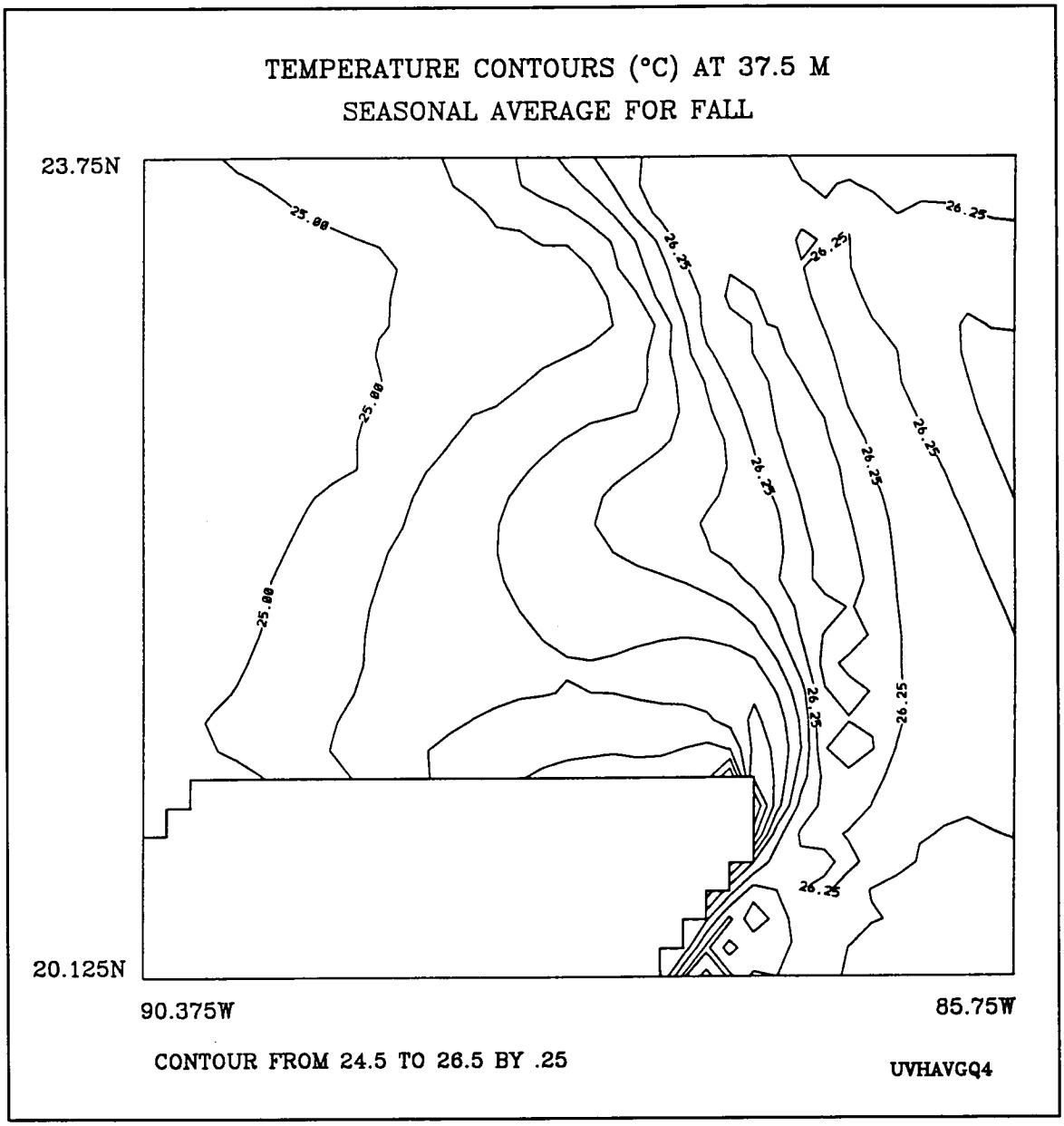

Figure 6d. Four-year averages of the level 1 (37.5 m) temperature field in the eastern Gulf of Mexico for the present-day seasonal forcing case for Fall.

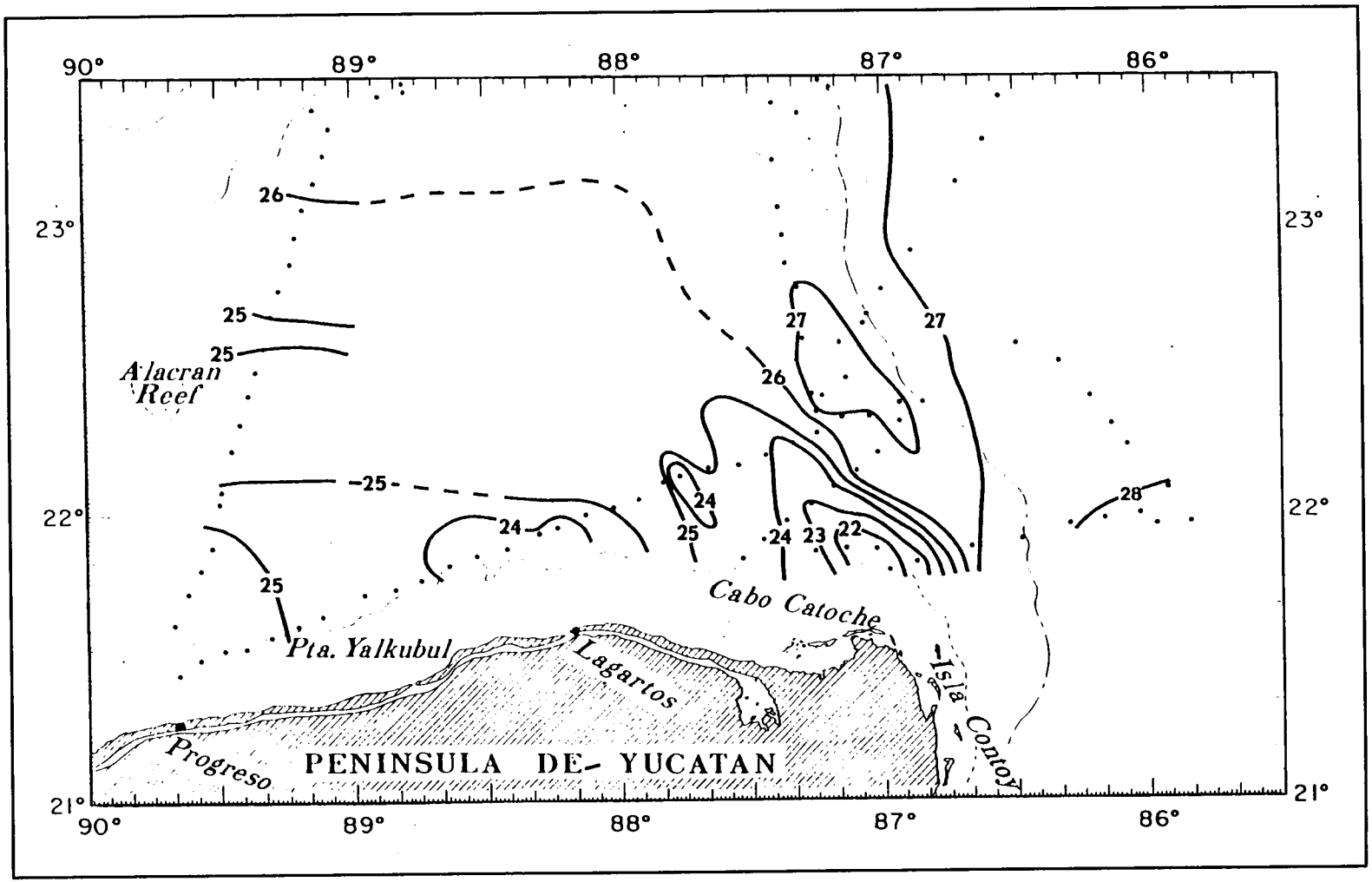

Figure 7a. Observed sea-surface temperature (°C) north of the Yucatan Peninsula during May 14-20, 1969.

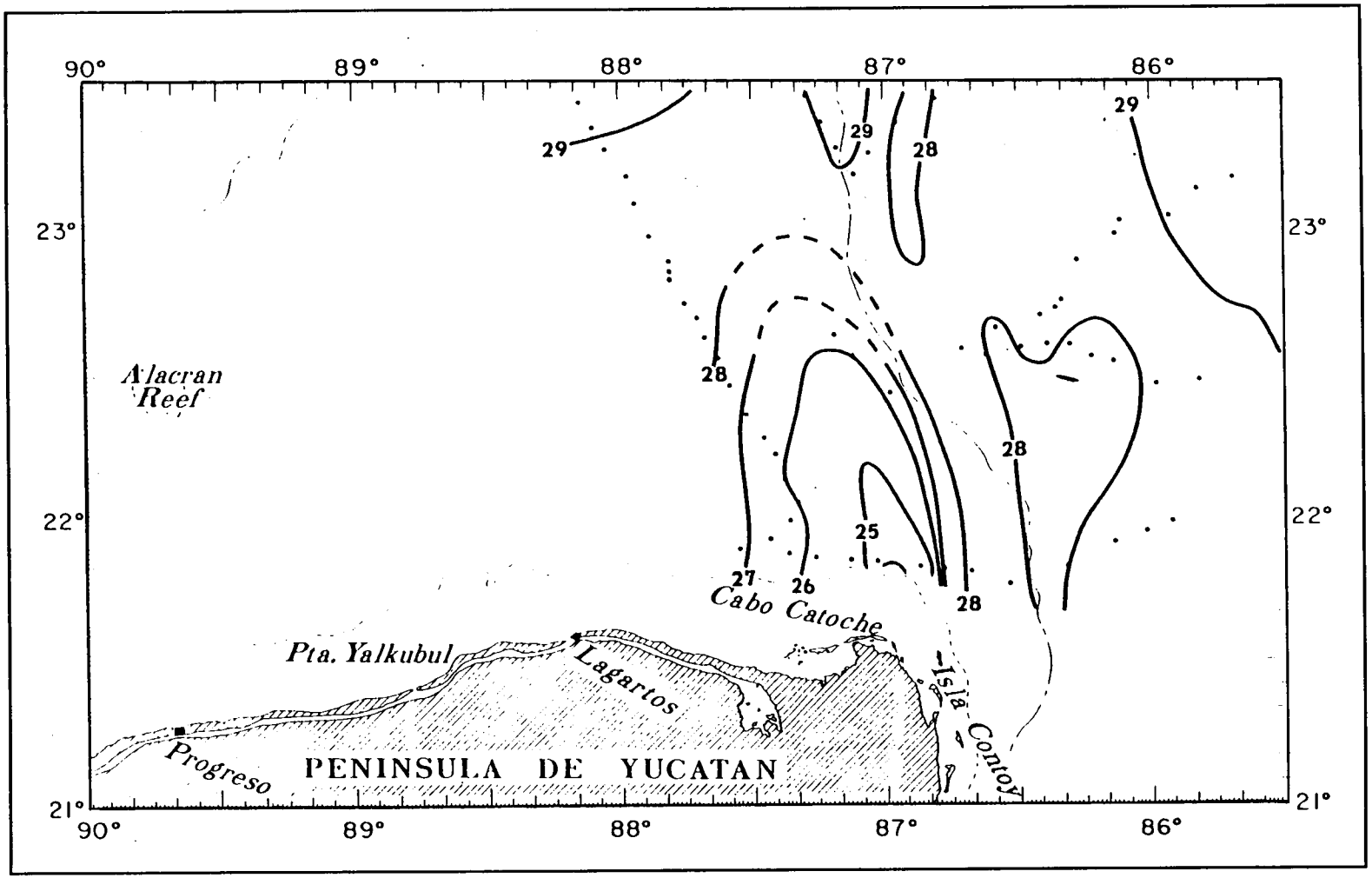

Figure 7b. Observed sea-surface temperature (°C) north of the Yucatan Peninsula during September 8-21, 1969 (from Ruiz Rentería 1979).

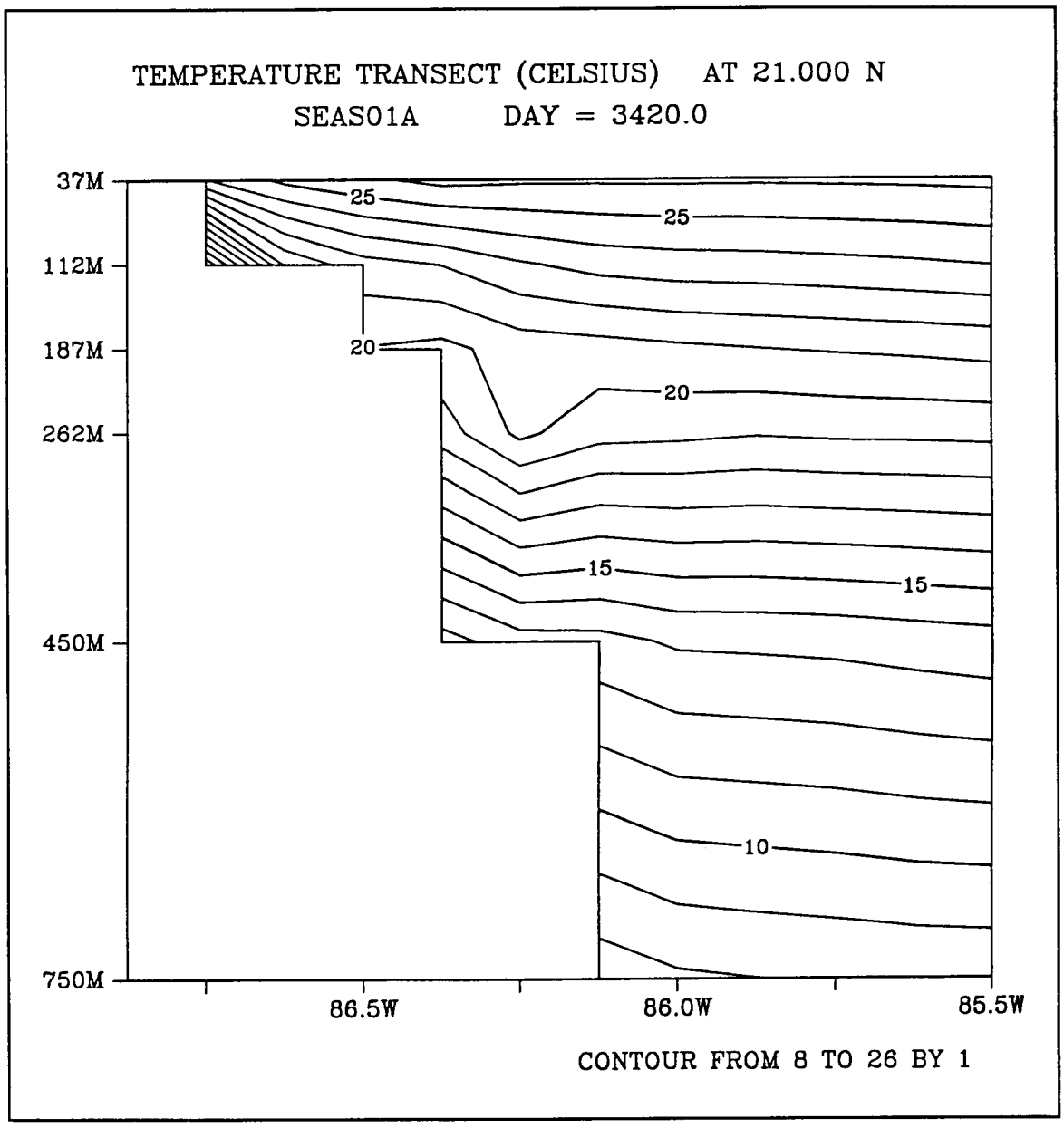

Figure 8a. West-east vertical profile of temperature for the present-day seasonal forcing case on model day 3240 (May).

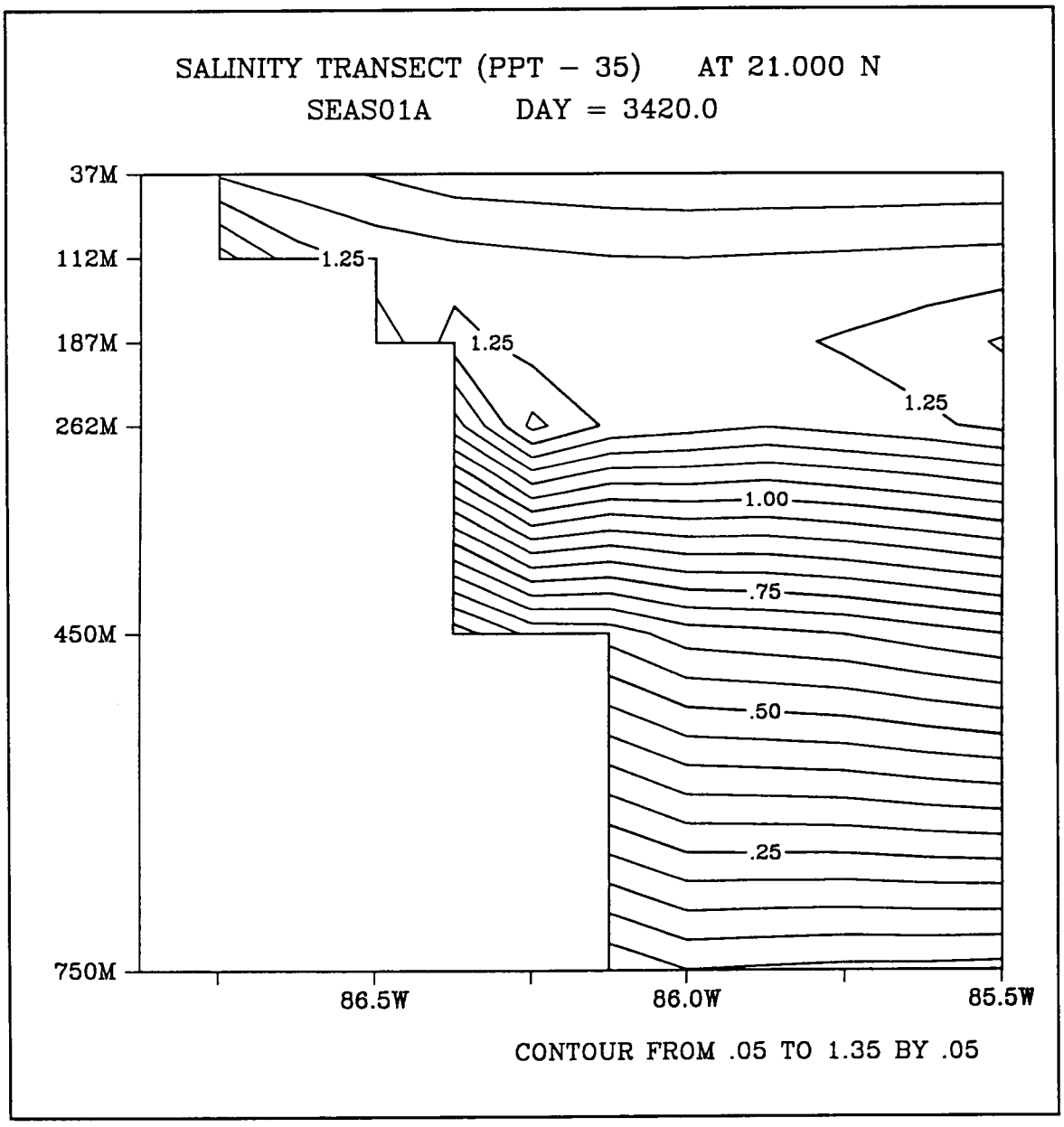

Figure 8b. West-east vertical profile of salinity for the present-day seasonal forcing case on model day 3240 (May).

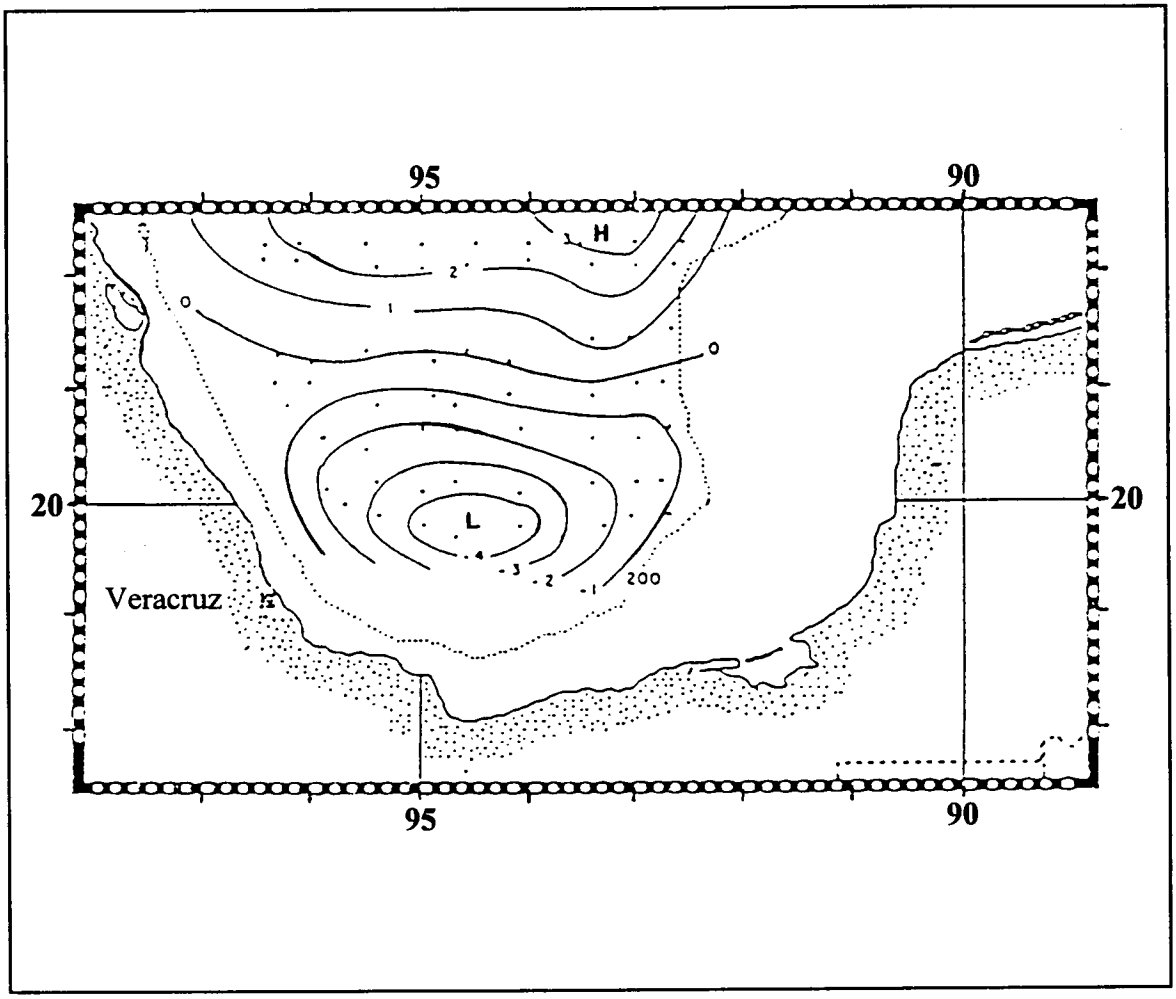

Figure 9. Contours of the average field of EOF mode 1 dynamic height (dyn·cm) of the sea surface relative to 425 db (from Vazquez de la Cerda 1993).

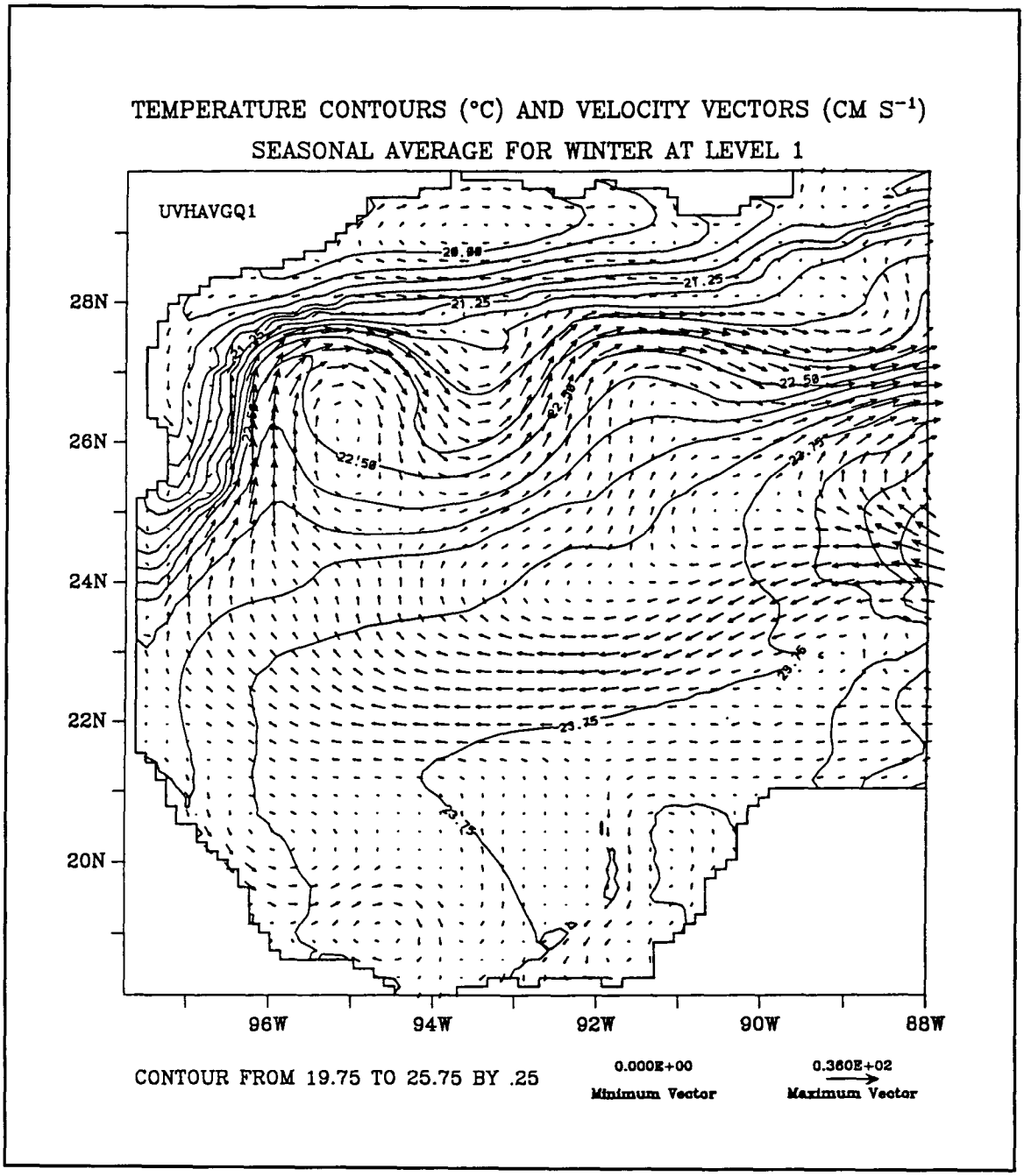

Figure 10a. Four-year averages of level 1 (37.5 m) temperature and velocity fields in the western Gulf of Mexico for the present-day seasonal forcing case in Winter.

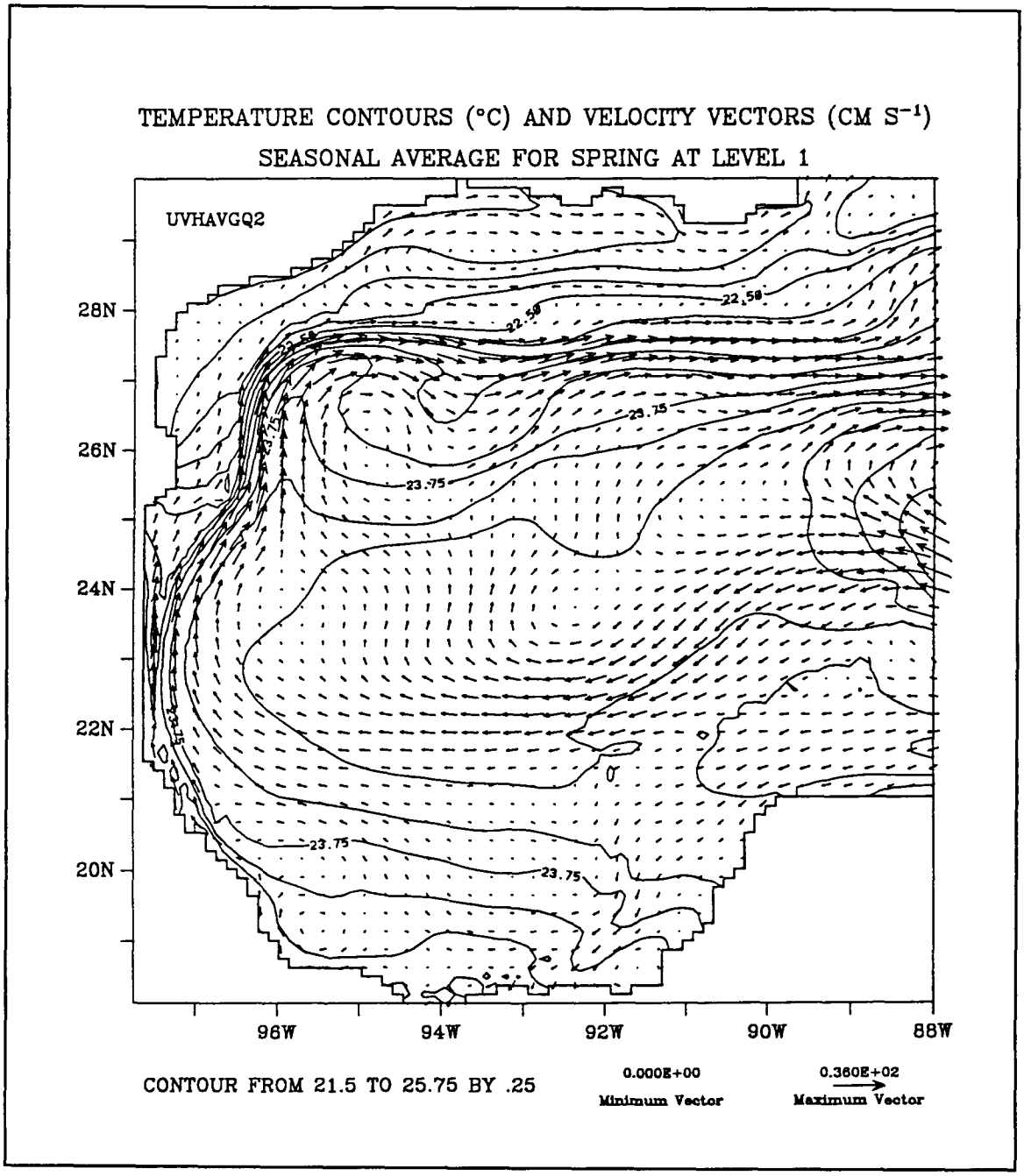

Figure 10b. Four-year averages of level 1 (37.5 m) temperature and velocity fields in the western Gulf of Mexico for the present-day seasonal forcing case in Spring.

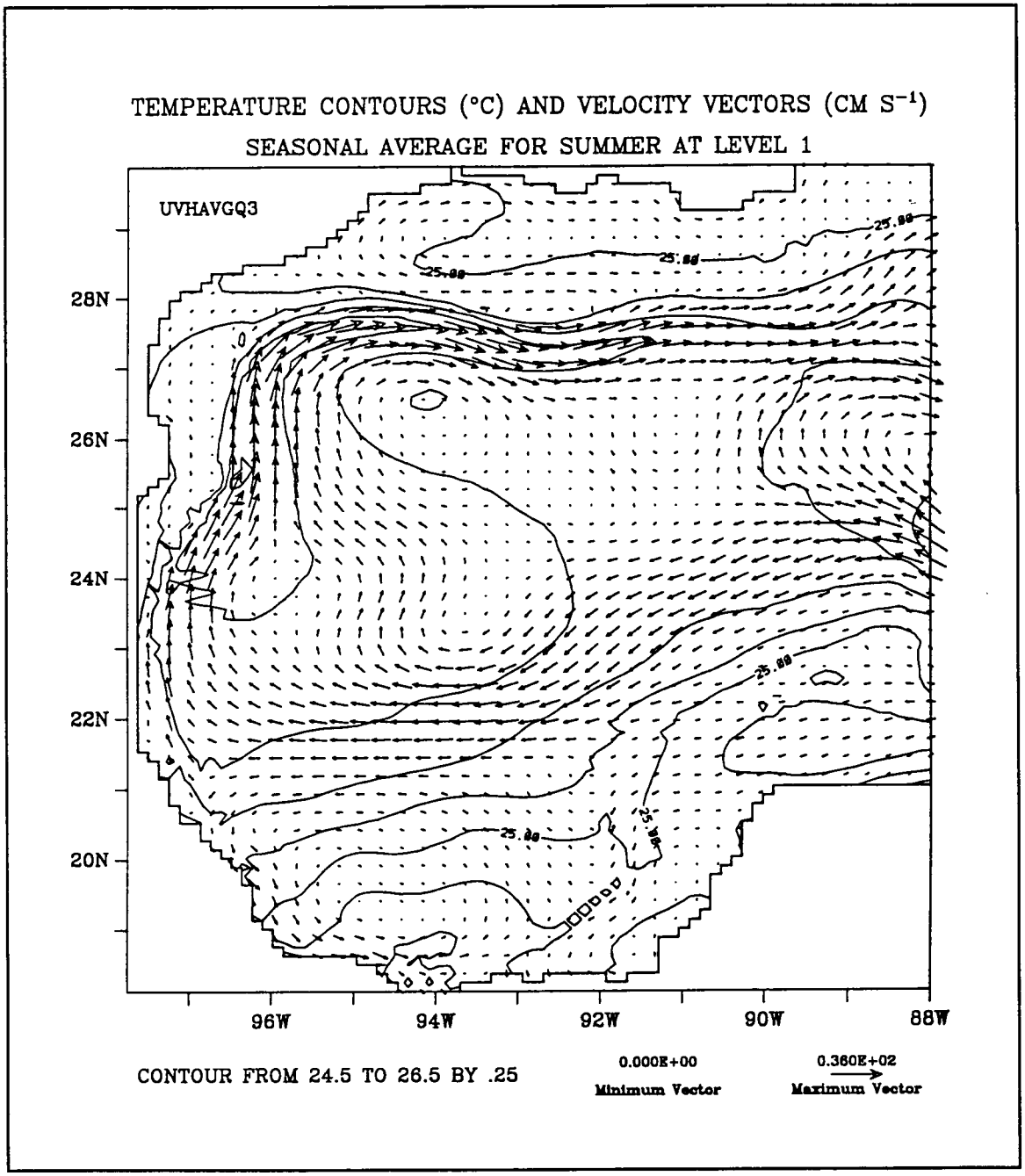

Figure 10c. Four-year averages of level 1 (37.5 m) temperature and velocity fields in the western Gulf of Mexico for the present-day seasonal forcing case in Summer.

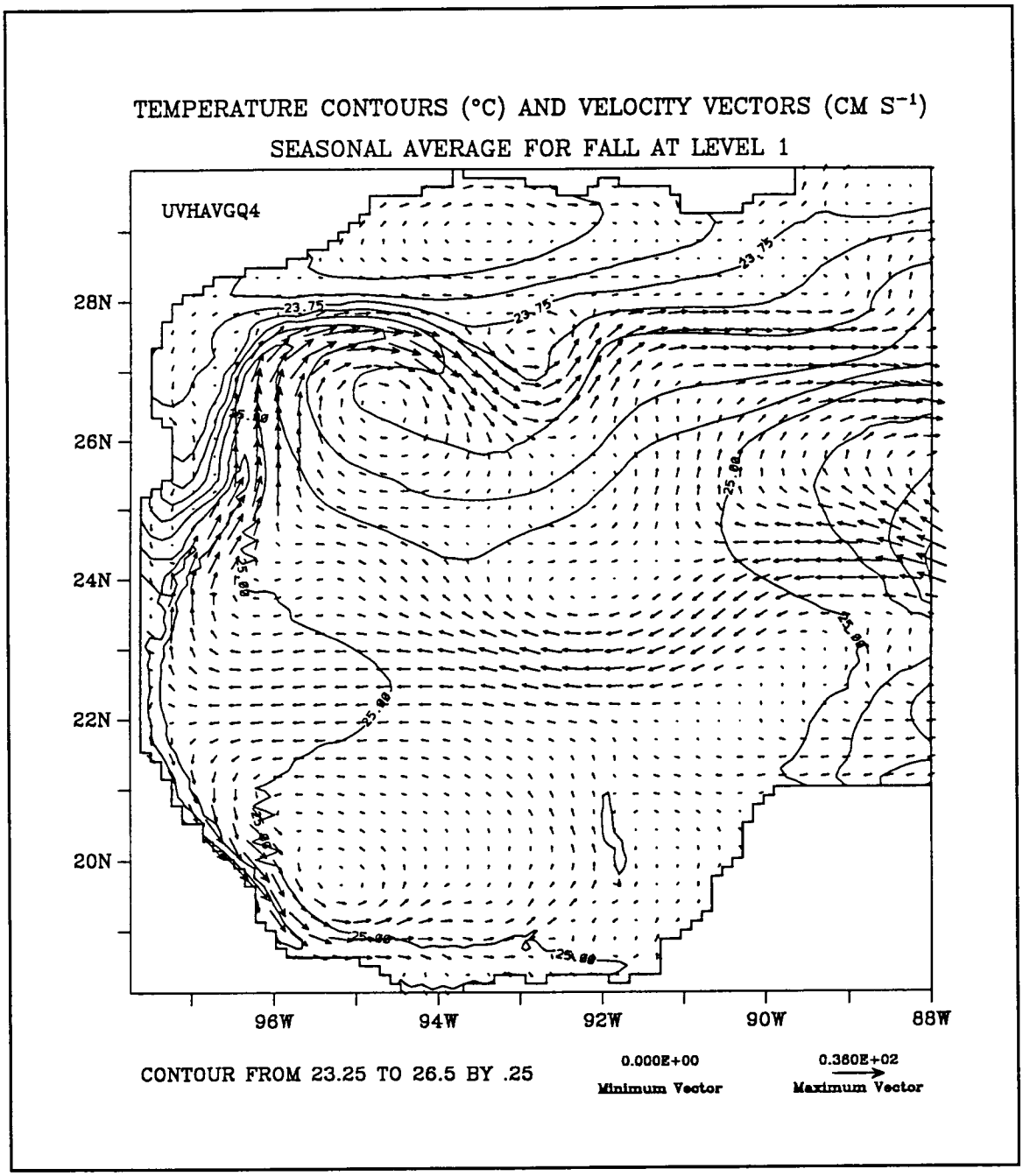

Figure 10d. Four-year averages of level 1 (37.5 m) temperature and velocity fields in the western Gulf of Mexico for the present-day seasonal forcing case in Fall.

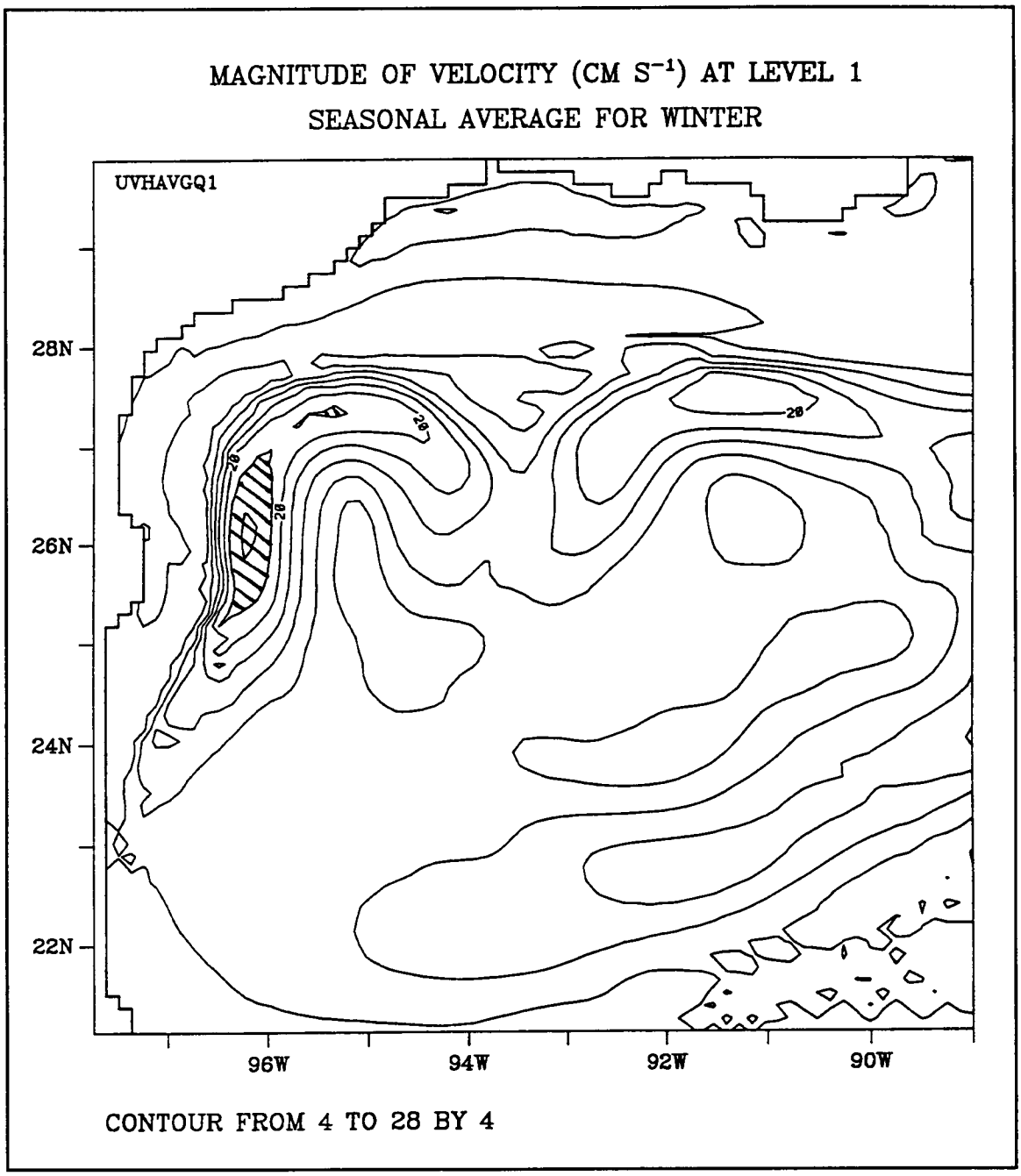

Figure 11a. Four-year averages of level 1 (37.5 m) velocity magnitudes in the northwest Gulf of Mexico for the present-day seasonal forcing case for Winter. Hatched areas denote magnitudes greater than 24 cm·s^{-1}.

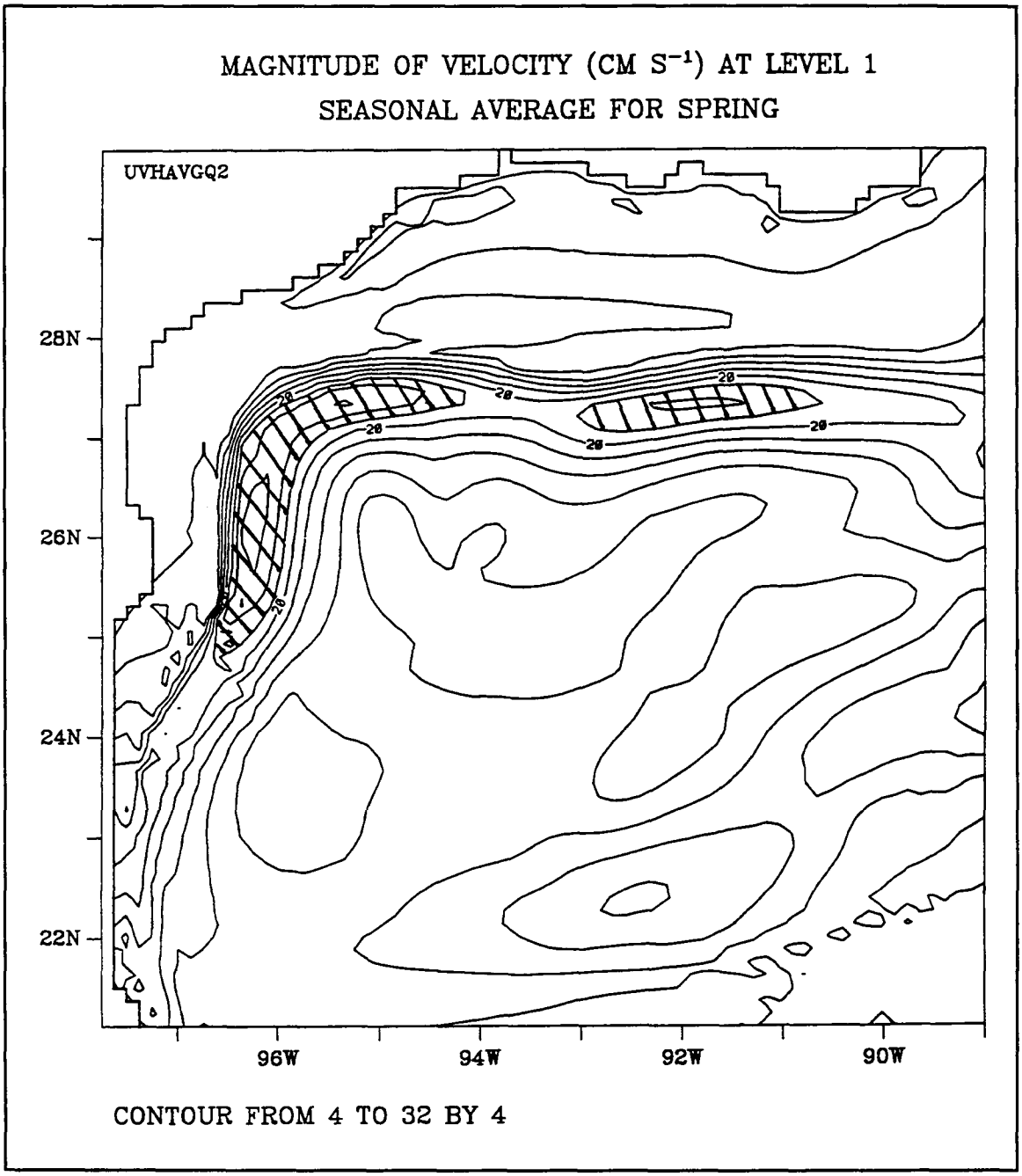

Figure 11b. Four-year averages of level 1 (37.5 m) velocity magnitudes in the northwest Gulf of Mexico for the present-day seasonal forcing case for Spring. Hatched areas denote magnitudes greater than 24 cm·s^{-1}.

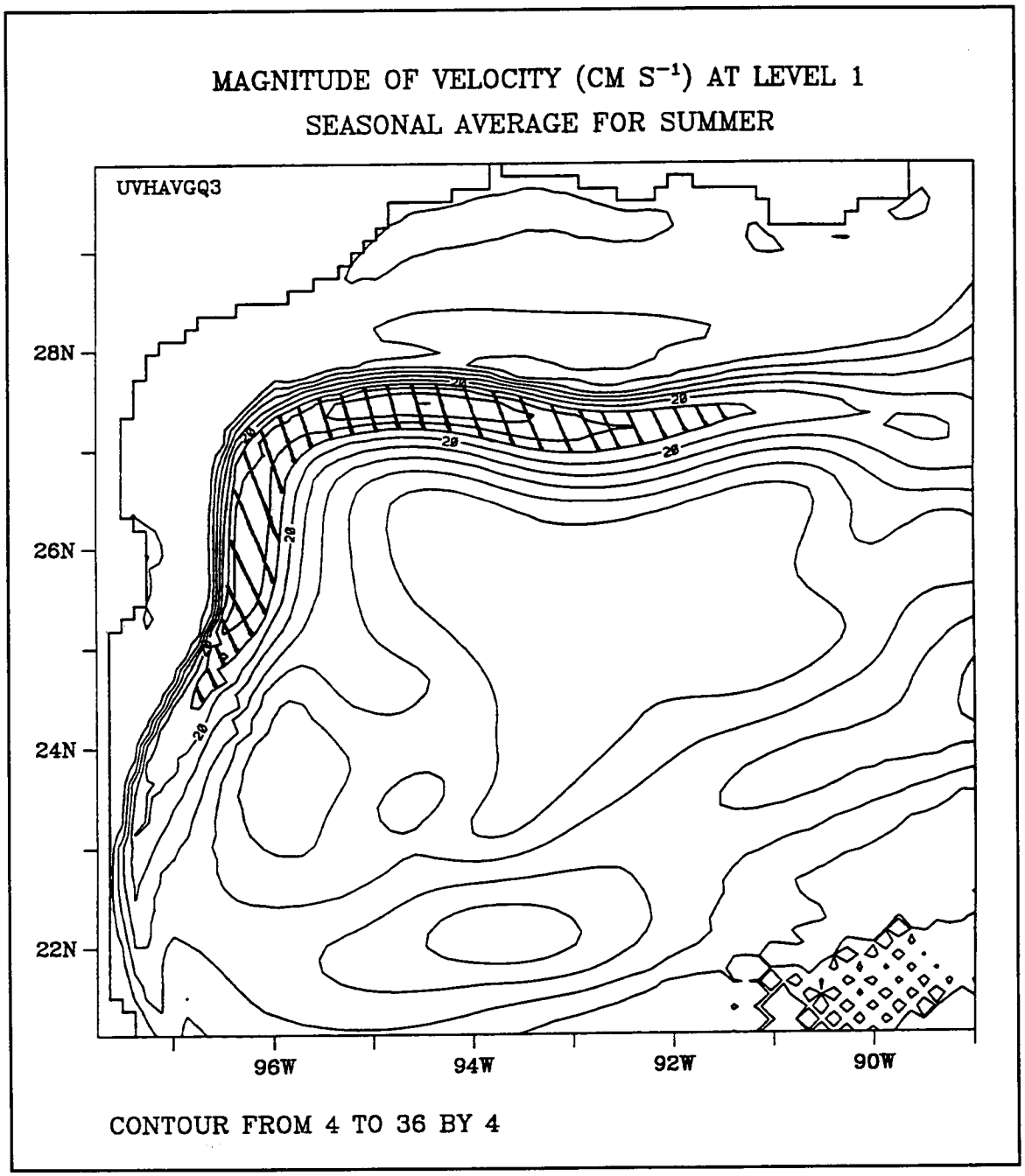

Figure 11c. Four-year averages of level 1 (37.5 m) velocity magnitudes in the northwest Gulf of Mexico for the present-day seasonal forcing case for Summer. Hatched areas denote magnitudes greater than 24 cm·s^{-1}.

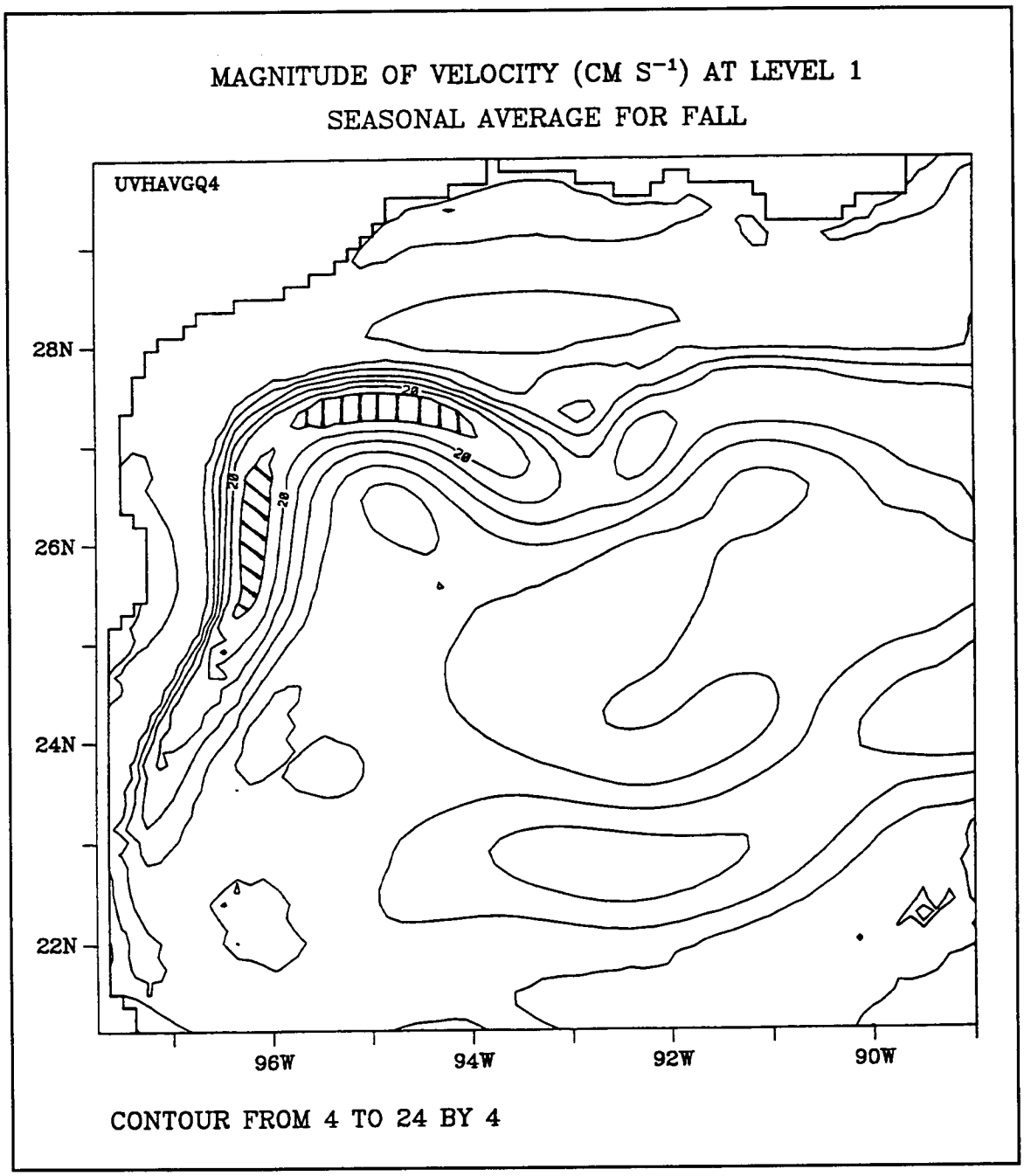

Figure 11d. Four-year averages of level 1 (37.5 m) velocity magnitudes in the northwest Gulf of Mexico for the present-day seasonal forcing case for Fall. Hatched areas denote magnitudes greater than 24 cm·s^{-1}.

observed curl of the wind stress. Sturges (1994) concluded that the WBC, which is observed to have a maximum in July and a minimum in October is driven by the curl of the wind stress and Ekman pumping over the western GOM.

A numerical modeling study was made by Oey (1995) to determine the relative importance of wind, rings, and bouyancy forcing from riverine flow on the cyclonic circulation on the Louisiana-Texas shelf region. The Princeton Model, which is a three-dimensional, primitive-equation, ocean model, was used with a horizontal grid resolution of 20 km and 20 cells in the vertical. The model domain of Oey (1995) extended outside the GOM into the northwestern Caribbean to the south and eastward to the Bahama Islands for the purpose of prescribing natural inflow and outflow conditions for the GOM. This model also featured seasonal wind forcing and produced a WBC that was strongest in July and August following the maximum in negative wind stress curl from May to July (Oey 1995).

A semi-permanent feature of these model results is the current that runs from the northwest corner of the GOM eastward along the shelf break toward the Mississippi Delta (see Figure 11). Oey (1995) also observed this current in his model results and referred to it as the shelf break current (SC). Oey (1995) noted that there is an increase in the transport of the SC from May through October. Since the transport of the SC continued to increase after the timing of the maximum transport of the WBC in the model, Oey (1995) concluded that the SC is partly forced by the WBC, partly by a change in the curl of the wind stress that occurs from September through October, and by the decay of rings in the northwest corner of the GOM. Molinari et al. (1978) also observed the SC and suggested that it may carry Texas Shelf water through the north central GOM and rejoin the LC. The process of entrainment of western GOM water by the LC via the SC is apparent in the model output. Transport of GOM waters on shore near the Mississippi Canyon by the SC is observed in this model output as well as in the model of Oey (1995) (see also Figure 11).

From current meter measurements, Cochrane and Kelly (1986) reported that currents off Freeport, Texas are northward in July, absent in June and August, and southward for the rest of the year. Currents on the south Texas shelf generated in the model by Oey (1995) were to the north in July and southward in October. This model produces southward flow over the south Texas shelf for most of the year with northward flow sometimes occurring briefly in spring or summer.

The circulation on the Louisiana-Texas shelf is characterized by an elongated cyclone with currents flowing westward near shore and eastward on the outer shelf and shelf break that is present during all months except July and August (Cochrane and Kelly 1986). The currents along most of the Texas-Louisiana Shelf are primarily wind-driven (Cochrane and Kelly 1986), although the numerical model of Oey (1995) demonstrated that rings and bouyancy forcing also contribute to the total shelf transport. The model circulation on the Louisiana-Texas shelf was exactly opposite in direction to what was observed. Although a realistic SC flows eastward in the model, the flow along the outer shelf was westward and the flow near the coast was eastward. The inability of the model to simulate the Texas-Louisiana shelf circulation is mainly due to the coarse spatial

resolution of the Hellerman and Rosenstein (1983) wind data, which is $2° \times 2°$, while the Texas-Louisiana shelf is less than two-degrees wide for most of its length. Another reason for the reverse circulation of the model on the Louisiana-Texas shelf is most likely due to the lack of buoyancy forcing that would be provided by the fresh water flux of the Mississippi River. Although the Levitus (1982) data is used for surface relaxation of temperature and salinity, the data set does include the inner shelf region west of the Mississippi Delta and the fresh water signal is not adequately represented.

The model produces flow along the West Florida shelf that is southerly throughout the year, but in the vicinity of the Dry Tortugas, a semi-permanent gyre develops in response to the ring-separation cycle (Figure 12). When the LC is penetrating well into the GOM, a cold-core cyclonic gyre, Tortugas Gyre, forms to the east of the Dry Tortugas off the southern portion of the west Florida Shelf. After a ring has shed from the LC and the LC is reforming, this cyclonic gyre is forced eastward into the entrance to the southern Straits of Florida and disappears. This process was observed by Lee et al. (1995) and SAIC (1992) using a combination of moored current meters, shipboard hydrography, and satellite images of surface temperature fields. Lee et al. (1995) explained that the Tortugas gyre forms when the LC is well-formed in the eastern GOM and flow from the LC overshoots the southern Straits of Florida. The cold-core features are approximately 200 km in size and exist for time scales of about 100 days (Lee et al. 1995). SAIC (1992) noted that during the eastward advection of the Tortugas Gyre water is exchanged between the outer shelf and upper slope due to the the cyclonic rotation of the gyre . Also the Tortugas Gyre is responsible for deflecting the Florida Current to the south, which forces the Florida Current offshore when the gyre moves to the east (SAIC 1992). Thus the Tortugas Gyre can affect the position of the Florida Current within the Florida Straits as well as the hydrography of the Florida Current. The Tortugas gyre generated in the model is also approximately 200 km in diameter when fully developed and persists over similar time scales as observed.

3.4 Loop Current Rings

The process of shedding rings in the GOM is of major importance in the GOM. The variability in the LC itself as well as some of the variability in the circulation on the Yucatan and west Florida shelves is due to the separation of rings. The ring-separation process also has a large influence on the heat and salt budgets of the GOM and is responsible for coupling the circulation in the eastern and western portions of the GOM. It is necessary then that a numerical model of the GOM realistically simulate the ring-separation process and the westward migration of the LC rings.

The formation of LC rings in the model appears similar to the following process described by Lewis and Kirwan (1987):

> The classical concept of Loop Current processes is one in which part of the Gulf Stream at first flows directly from the Yucatan Straits to the Florida Straits. Within this flow field, insta-

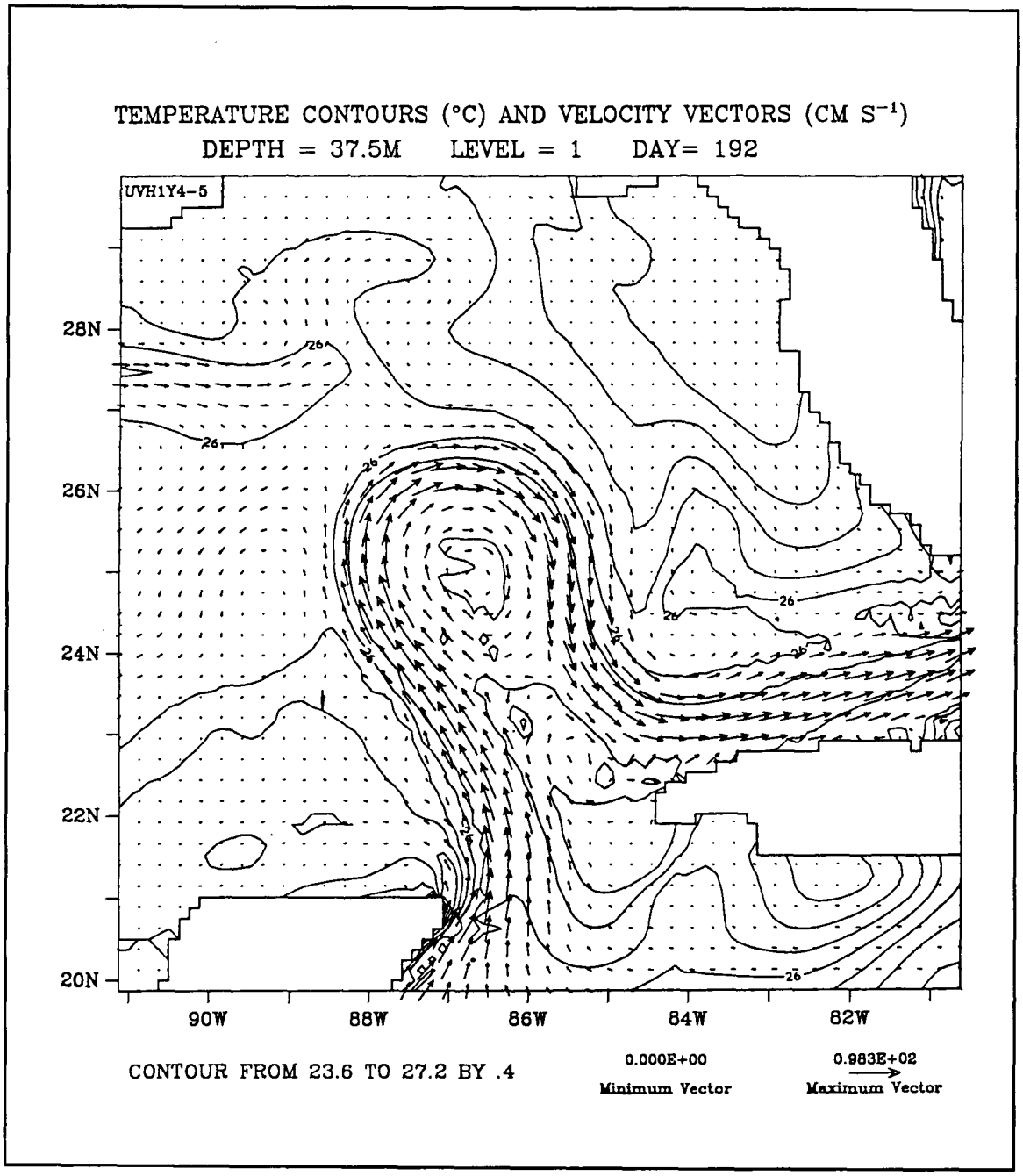

Figure 12a. Sequence of level 1 (37.5 m) temperature and velocity fields in the eastern Gulf of Mexico on model day 192.

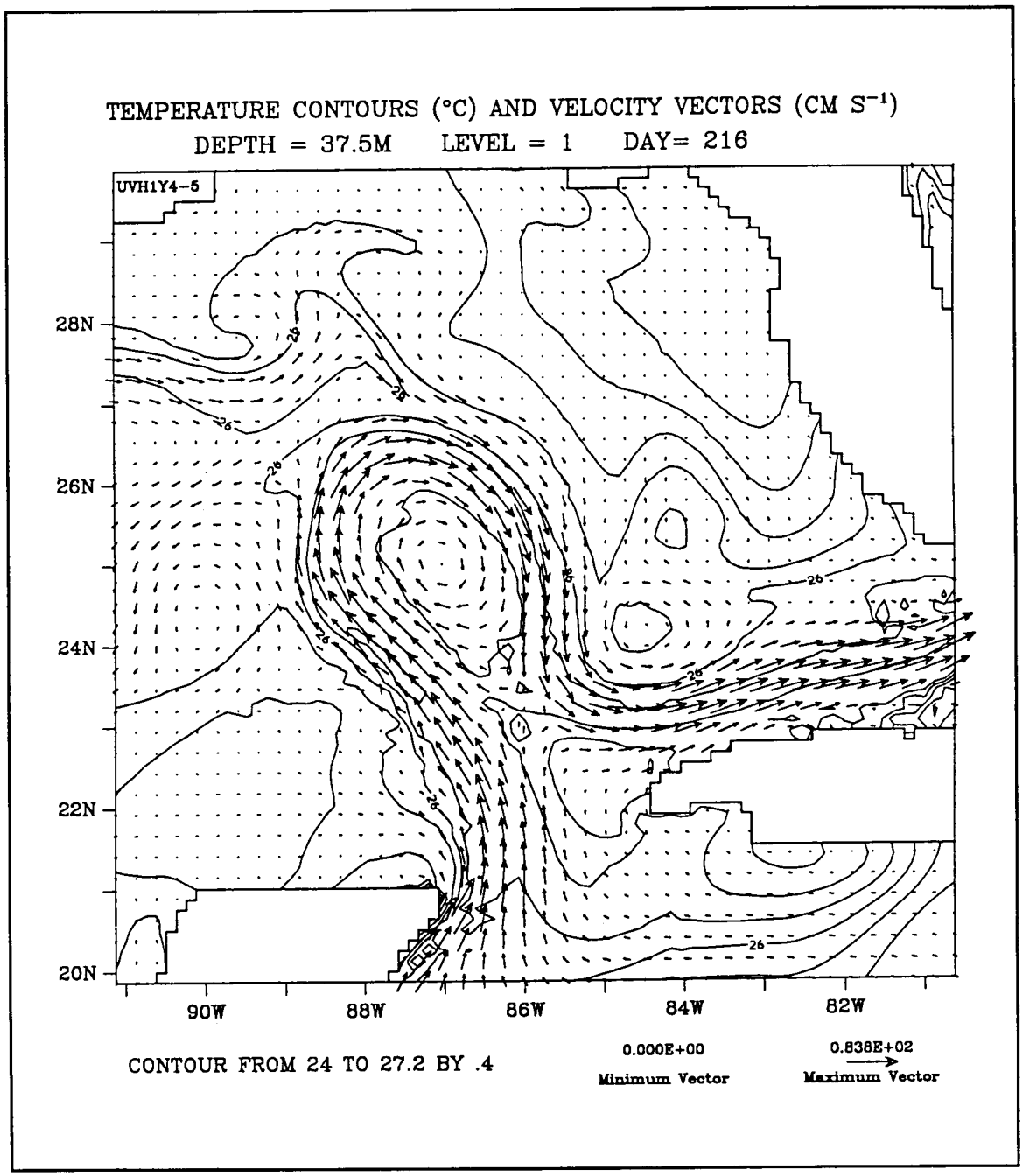

Figure 12b. Sequence of level 1 (37.5 m) temperature and velocity fields in the eastern Gulf of Mexico on model day 216.

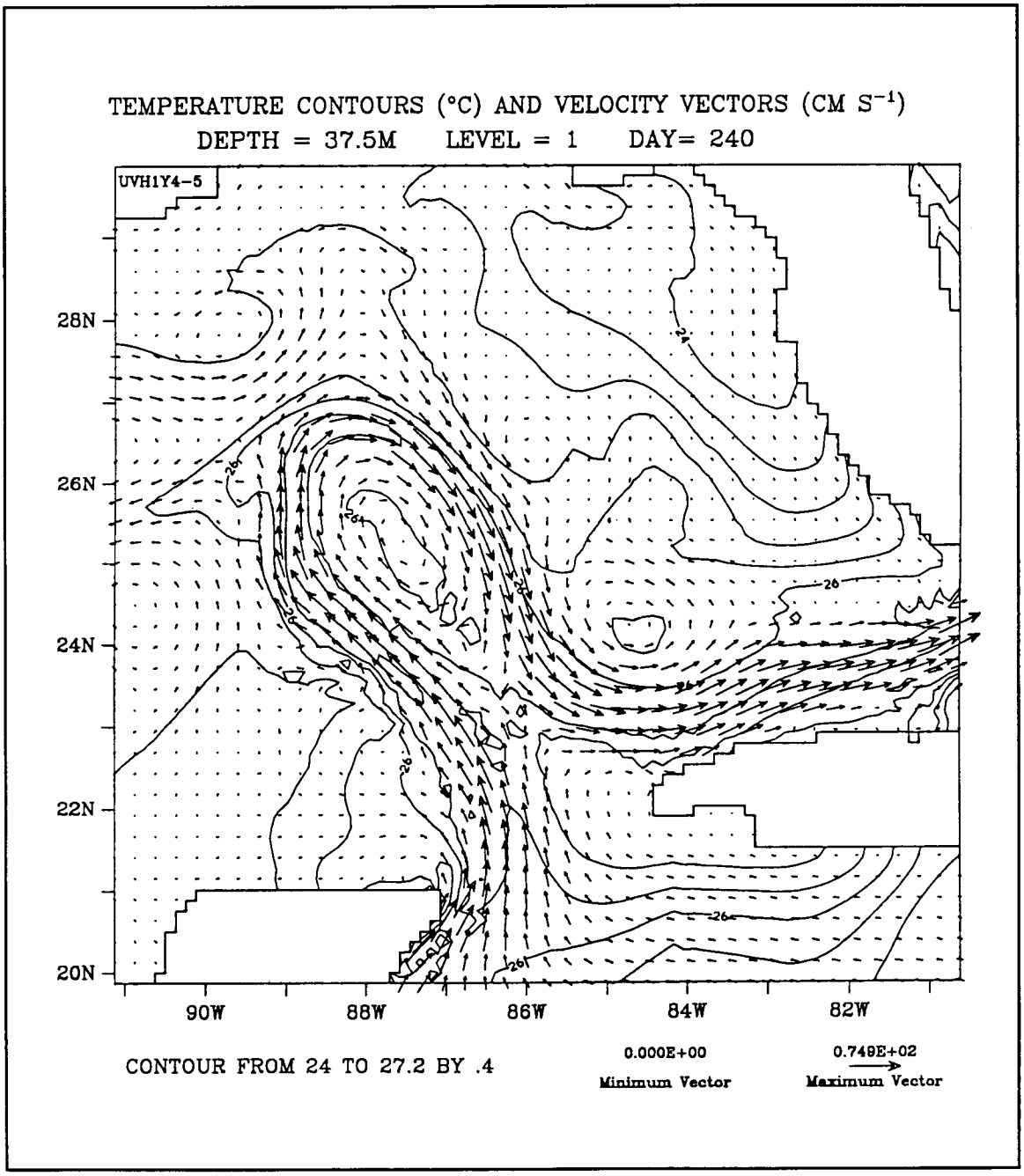

Figure 12c. Sequence of level 1 (37.5 m) temperature and velocity fields in the eastern Gulf of Mexico on model day 240.

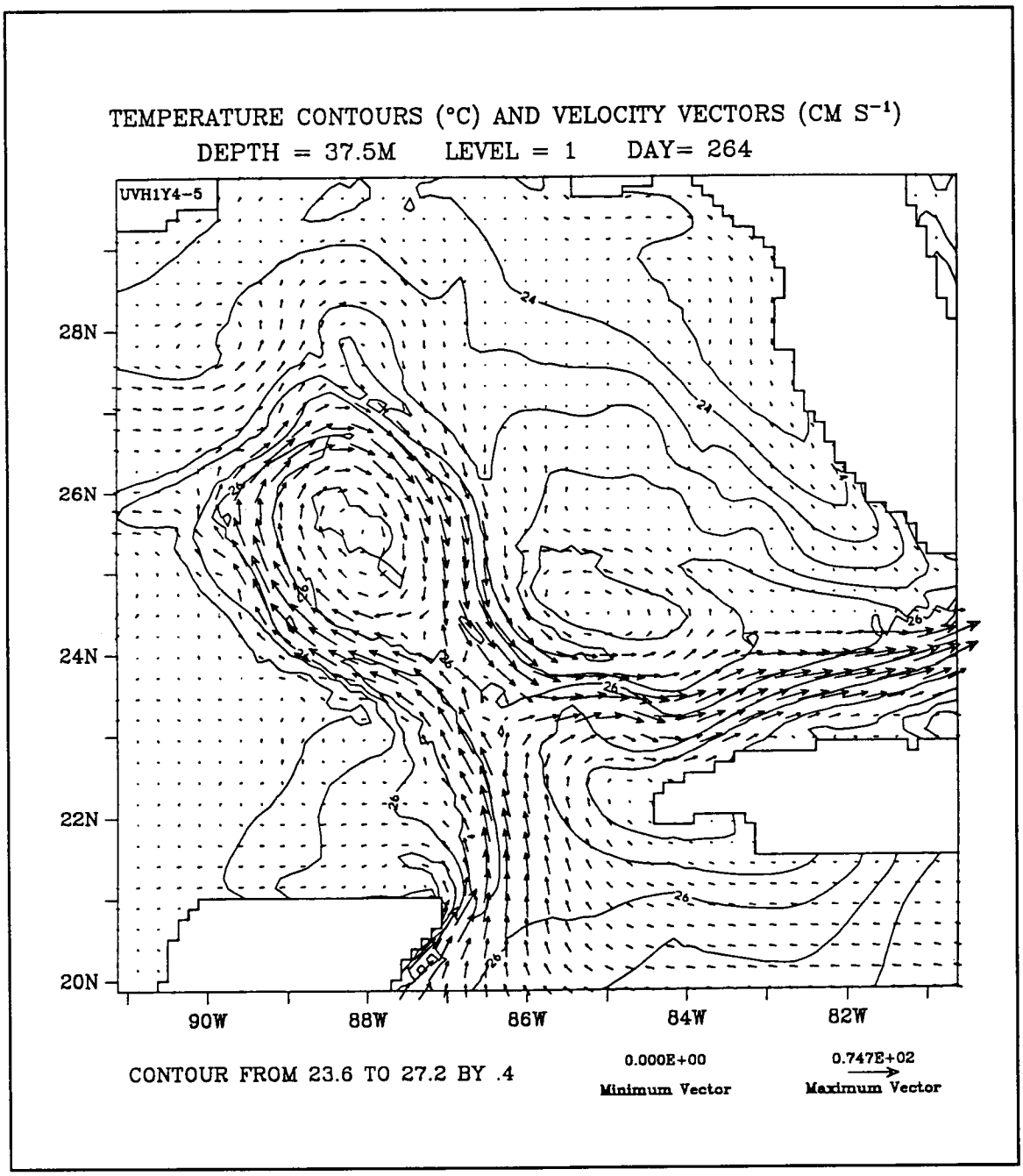

Figure 12d. Sequence of level 1 (37.5 m) temperature and velocity fields in the eastern Gulf of Mexico on model day 264.

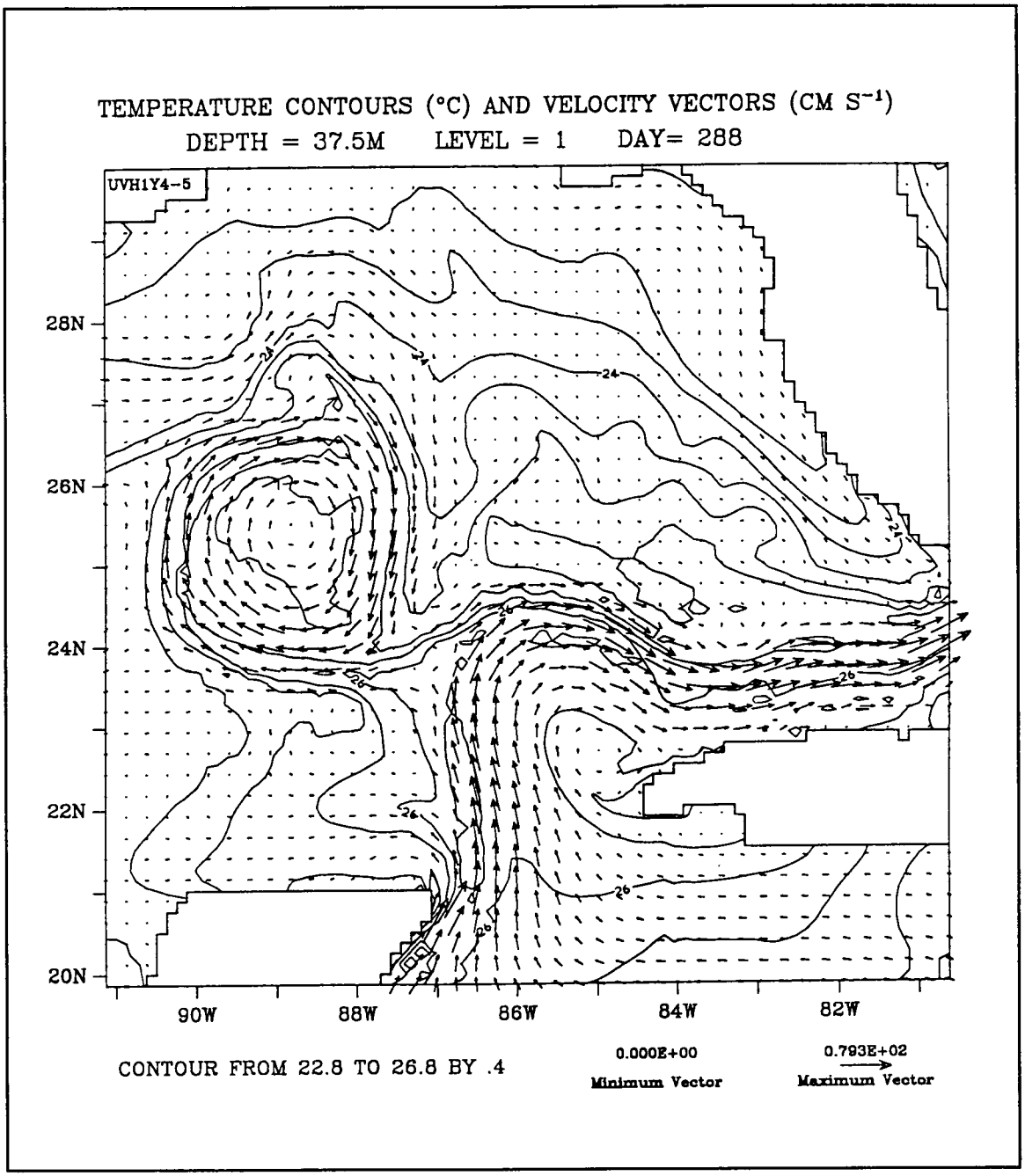

Figure 12e. Sequence of level 1 (37.5 m) temperature and velocity fields in the eastern Gulf of Mexico on model day 288.

> bilities exist which result in meandering of the Loop Current (Hurlburt and Thompson 1980). As the sizes of the meanders increase and reach northward, it is generally believed that the flow field wraps back onto itself and 'shorts' across the stream of flow: Part of the flow would still go northward around the Loop Current extension, while the remainder of the flow would take the more direct, southerly route to the Florida Straits.

The process of ring separation in the model is very gradual using high friction (A_M = 200 $m^2 \cdot s^{-1}$ and A_H = 100 $m^2 \cdot s^{-1}$) and resembles the model results of Sturges et al. (1993), who state: "it is difficult to point to any specific time at which one can say that the ring has just 'separated'". After friction was reduced ($A_M = A_H$ = 75 $m^2 \cdot s^{-1}$) in the annual-mean forcing simulations, the ring separation could be described as a much more catastrophic event. Both the LC and semi-attached ring exhibit rapid boundary fluctuations just as the ring is about to separate. Immediately following separation, the rapid boundary fluctuations cease and the flow fields of the LC and the ring become smooth again. As the ring is separating, frontal waves propagate along the northern boundary of the LC from west to east from the northern extension of the LC out through the Florida Straits. The anticyclonic flow within the model LC strengthens just following ring separation.

There are a great number of observations of individual rings from hydrographic surveys, current meter measurements, drifters, and satellite imagery. In comparison to observations, the model rings have reasonable lateral dimensions, vertical structure, swirl velocities (velocity about the ring center), translation speeds, migration paths, fine-scale boundary features, and life spans. Table 2 summarizes various model ring characteristics and compares them to observations. Some authors report swirl speeds in both the LC and rings that reach 200-300 $cm \cdot s^{-1}$, although speeds under 200 $cm \cdot s^{-1}$ are more representative. Swirl speeds for the model LC are generally under 130 $cm \cdot s^{-1}$ and under 100 $cm \cdot s^{-1}$ for the rings. This is partly due to the fact that peak velocities reported in the literature are observed at the surface and the level 1 (uppermost level) model velocities represent the mean for the upper 75 m of the water column. Also the model is forced with climatological forcing, i.e. surface wind stress and vertical hydrographic fields that are spatially averaged and vary smoothly in time.

The model's ability to simulate the vertical structure of the rings correctly has an important bearing on its ability to simulate the heat and salt balances of the GOM. Although LC rings are of the warm-core type, observed rings and the model rings sometimes have cooler surface water at the center compared to the outer portions. Drifter analysis by Lewis and Kirwan (1987) indicates that the kernel of the ring water is entrained from the waters off the northwest coast of Cuba. Figure 13 compares the model temperature structure with hydrographic data collected by ships of opportunity for the Minerals Management Service (after SAIC 1986). Note the divergence of the isotherms with depth in the LC and the rings below 450 m and the shape of the isotherms as they slope up from the ring to the LC.

Table 2. Characteristics of model Loop Current rings for the present-day seasonal forcing case.

Ring	Size [1] (km)	Migration Speed (km d^{-1})	(cm s^{-1})	Time to Wall [2] (days)	Lifespan (days)	Ring Interaction
S1	350	6.33	7.33	168	432	merge
S2	350	3.45	3.99	288	456	split
S3	364	3.89	4.50	288	408	split
S4	350	3.39	3.93	264	360	none
S5	434	3.71	4.30	288	312	none
S6	364	3.92	4.54	264	360	none
S7	392	3.69	4.27	264	300	merge
S8	364	4.69	5.43	184	300	merge
Mean	371	4.13	4.78	251	366	
Std. dev.	29.0	0.97	0.50	47.8	60.8	

Observed Values:

366 [3]	4 [4]		1 year [3]
300-400 [5]	5 [5]		

[1] Approximate diameter in the eastern GOM. Measured by taking an average of the north-south and east-west dimensions of each ring.

[2] Time to western wall is a visual estimate of the number of days that each ring took from just after separation to reach the outer shelf of the Mexico or Texas coast. The arrival of the ring at the western wall is characterized by some deformation of the ring, typically marked by a north-south elongation of the ring.

[3] Elliot (1982)

[4] Oey (1995)

[5] Vukovich and Crissman (1986)

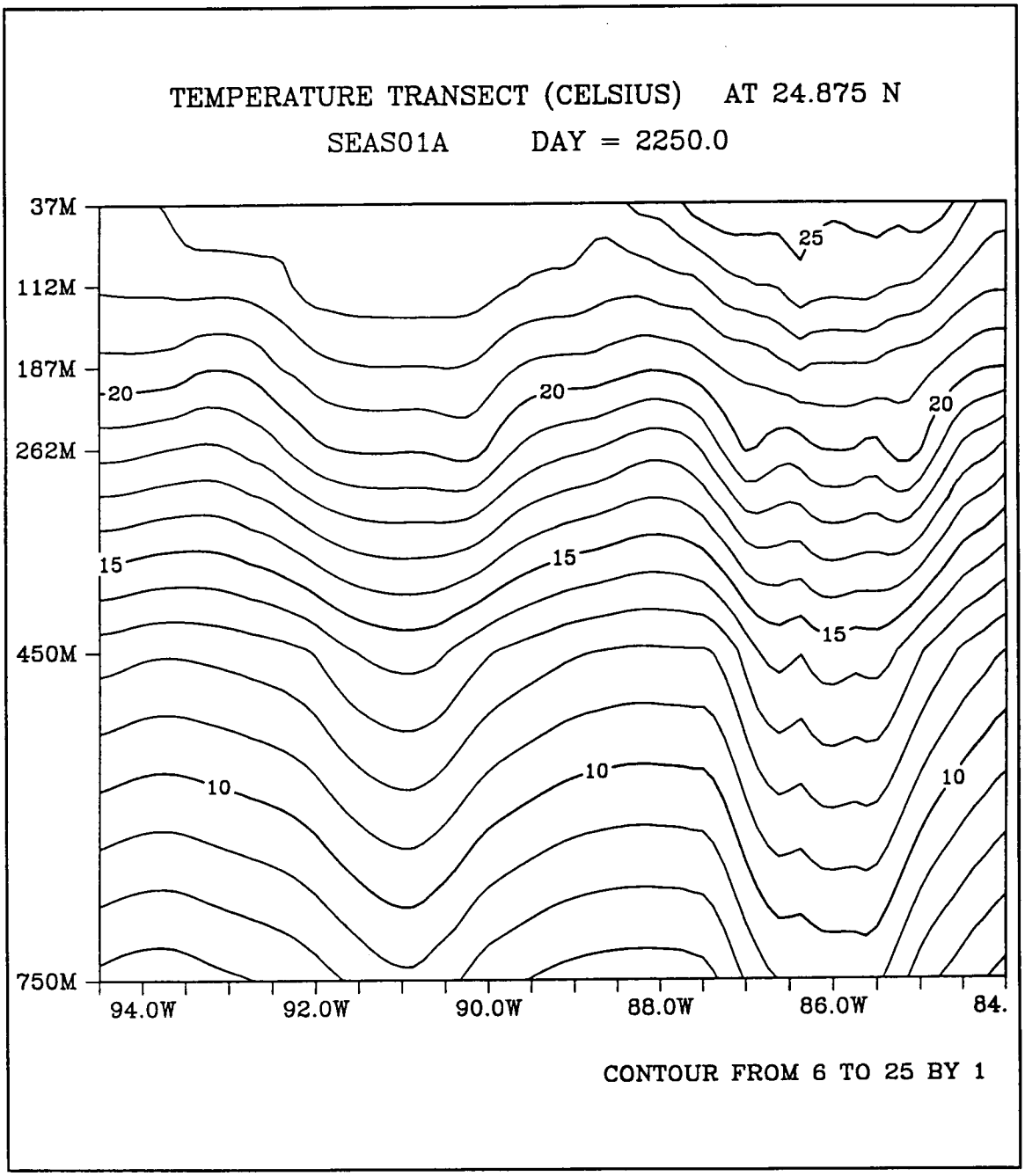

Figure 13a. Vertical cross-section of temperature through a ring and the Loop Current from the present-day seasonally forced model.

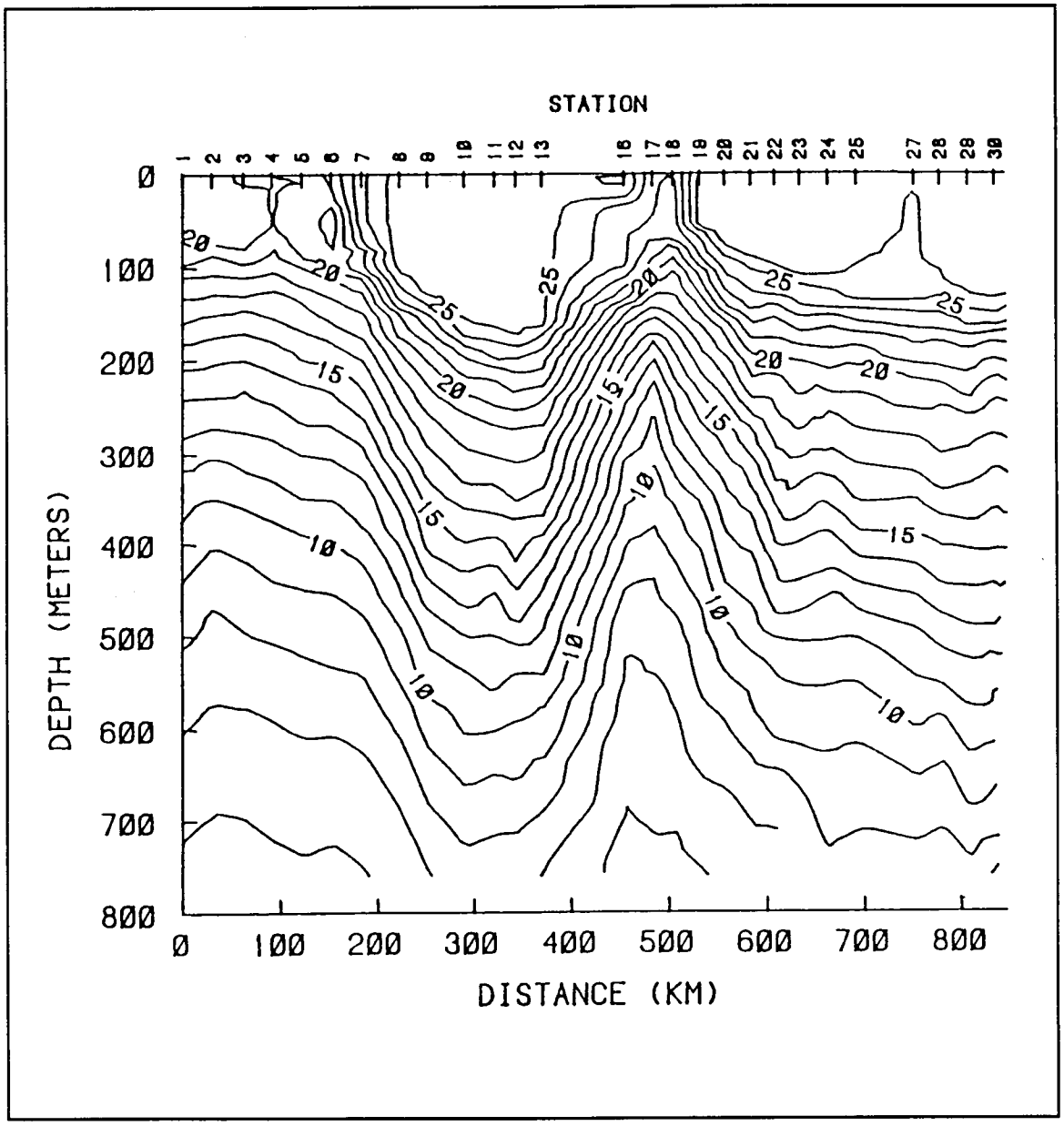

Figure 13b. Vertical temperature (°C) section through a ring and the the Loop Current in the Gulf of Mexico collected by the Nordic Wasa on January 7-8, 1984 (from SAIC 1986).

Observed rings in the eastern GOM are characterized by the high salinity maximum of 36.6 ppt with a potential temperature of 22.5°C at 200 m (Elliot 1982). This high salinity core represents Caribbean Subtropical Underwater (SUW) and is typically 70-m thick. As the ring migrates westward, convective mixing causes the SUW to eventually be transformed into Gulf Common Water with a salinity of 36.5 ppt and potential temperature of 22.5°C at 100 m (Elliot 1982). The degradation and shoaling of the high salinity core is illustrated in an east-west vertical cross-section through a ring in the central GOM and the LC in Figure 14. The salinity maxima in the model are somewhat less than observed because the vertical resolution of the model may be too coarse to resolve the salinity maximum. Also seasonally-averaged and spatially-averaged hydrographic data in the Caribbean are used to force the vertical shear of the Caribbean/Yucatan currents.

During the 8 years of model simulation for the seasonal forcing case, there were 13 complete ring migration paths. The model rings undergo shape transformation from initially elongated east-west to more circular or directed north-south as observed by Lewis and Kirwan (1987) using drifters to study the kinematics of ring separation. The model rings move westward with the observed average translation speed of approximately 4 km day^{-1} while decreasing in lateral dimensions with time. Although each ring follows a unique migration path, the rings tend to follow one of three characteristic paths which are illustrated in Figure 15. The model migration paths are tracked by monitoring the position of the 21.2°C isotherm at 187.5 m and are therefore continuous and not affected by seasonal surface heating and cooling.

The characteristic path that is followed by the majority of the model rings is to the southwest, south of 24°N in the region 91°W to 93°W, and then westward. These rings may elongate, but do not split. They remain intact and eventually move northward along the western wall into the northwest corner.

Rings that are at a latitude of 24°N between 91°W and 93°W typically split in a north-south direction. A portion of the ring moves directly into the northwest corner and the other portion continues to the southwest until it reaches the western wall and then moves northward into the northwest corner (Figure 16).

When a model ring moves directly into the northwestern GOM, it is generally larger than average and partially merges with an older ring in the northwest corner. These partial mergings are very similar to those described for Kuroshio warm core rings by Yasuda (1995). The partial mergings in the model and a model simulation of a larger ring merging with a smaller ring by Yasuda (1995) exhibit the following sequence: 1) a larger ring moving to the west and a smaller ring located to the northwest of it; 2) exchange of fluid via streamers wrapping around each other; 3) movement of the smaller ring to the east along the northern perimeter of the larger ring; 4) splitting off of some or most of the younger ring to the south or east; 4) the larger ring moving into the location formerly occupied by the smaller ring. A sequence of level 1 temperature and velocity fields illustrating a new ring merging with an old ring is presented (Figure 17).

Vukovich and Crissman (1986) observed that rings follow three characteristic paths during westward migration (Figure 18) which are similar to the model ring

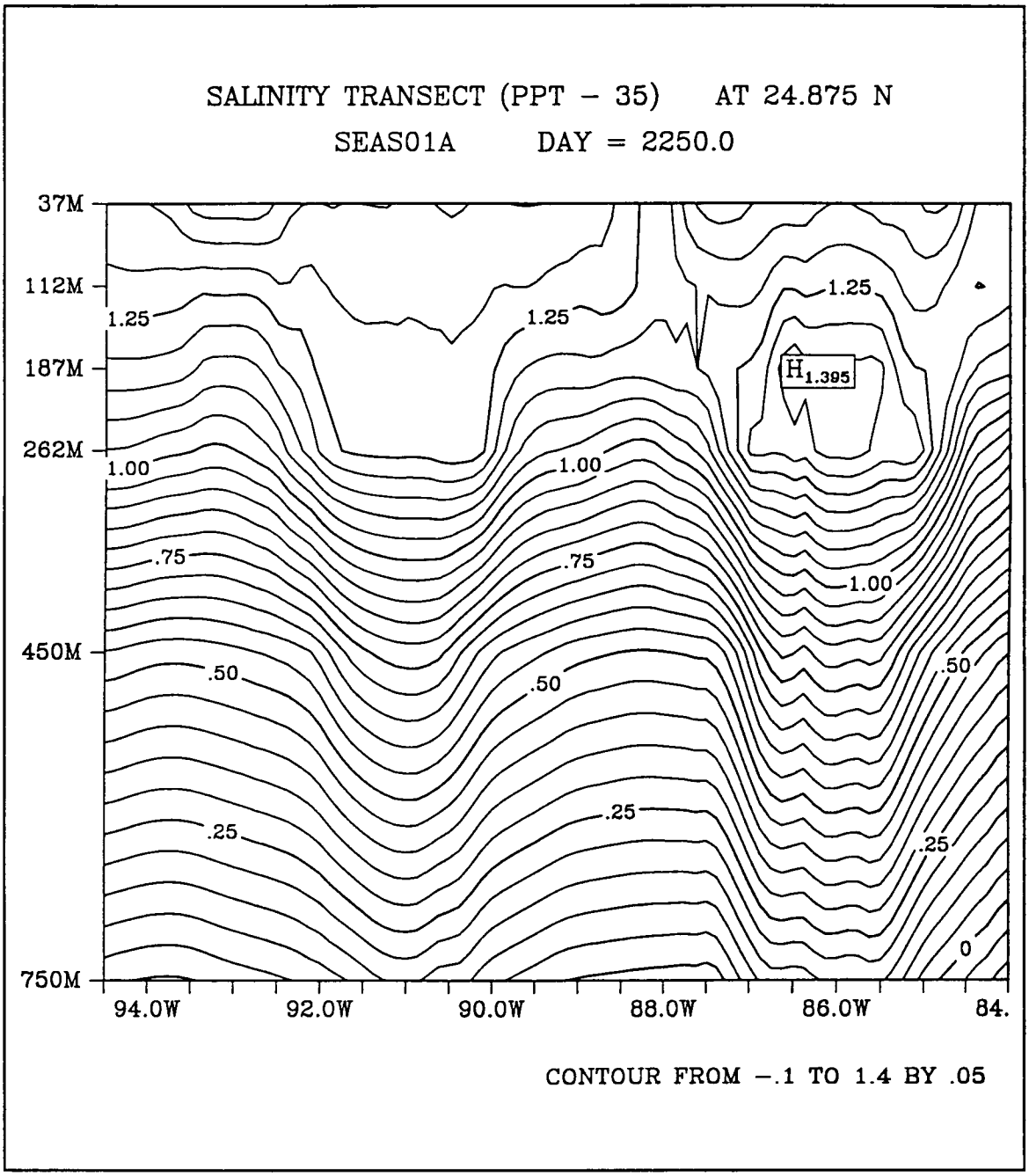

Figure 14. Vertical cross-section of salinity through a ring and the Loop Current from the present-day seasonal forcing model at model day 2250 (February).

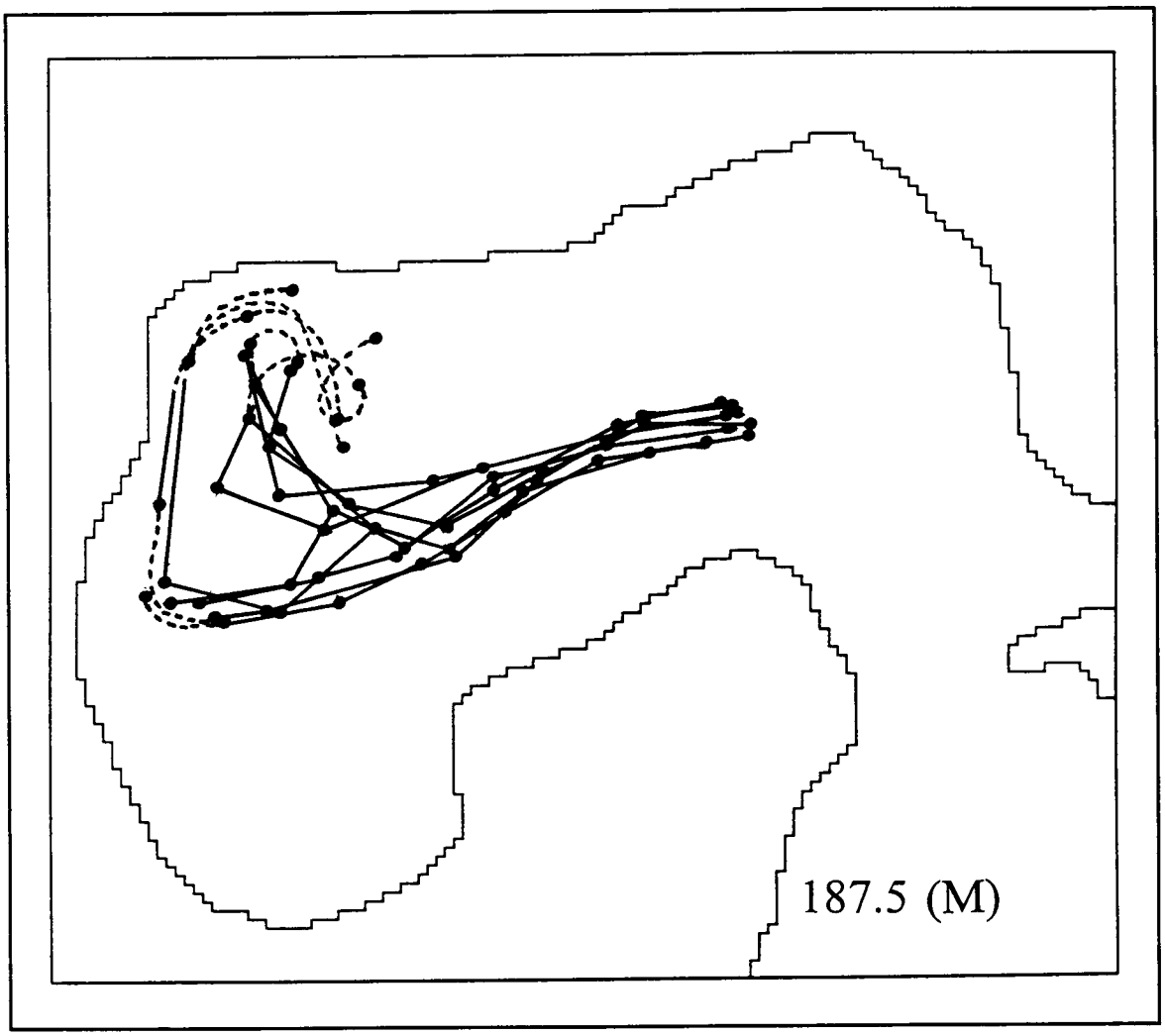

Figure 15. Migration paths of 8 Loop Current rings generated in a 5-year simulation using the present-day seasonally forced model.

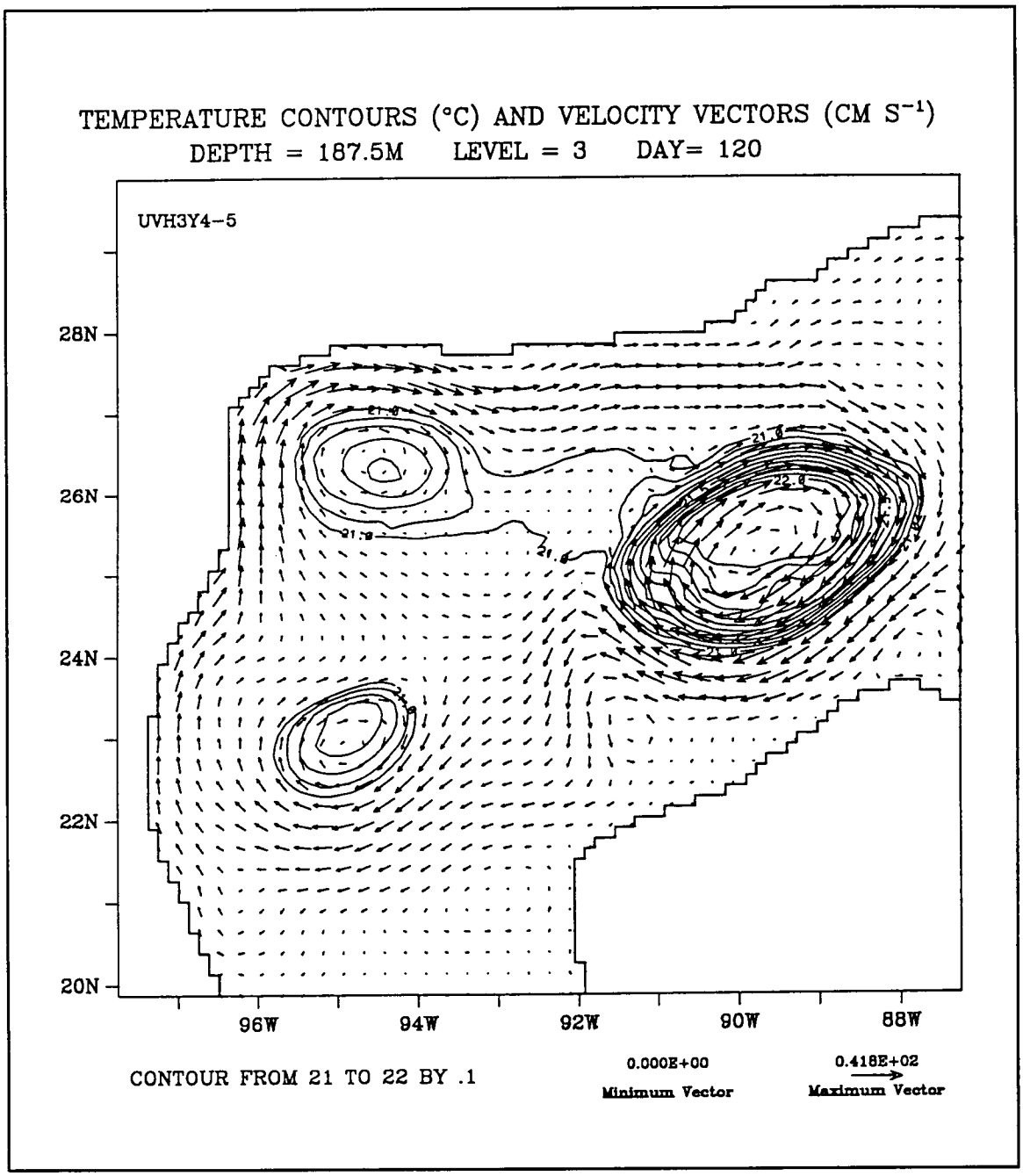

Figure 16a. Level 3 (187.5 m) temperature and velocity fields for the present-day seasonally forced model on day 120.

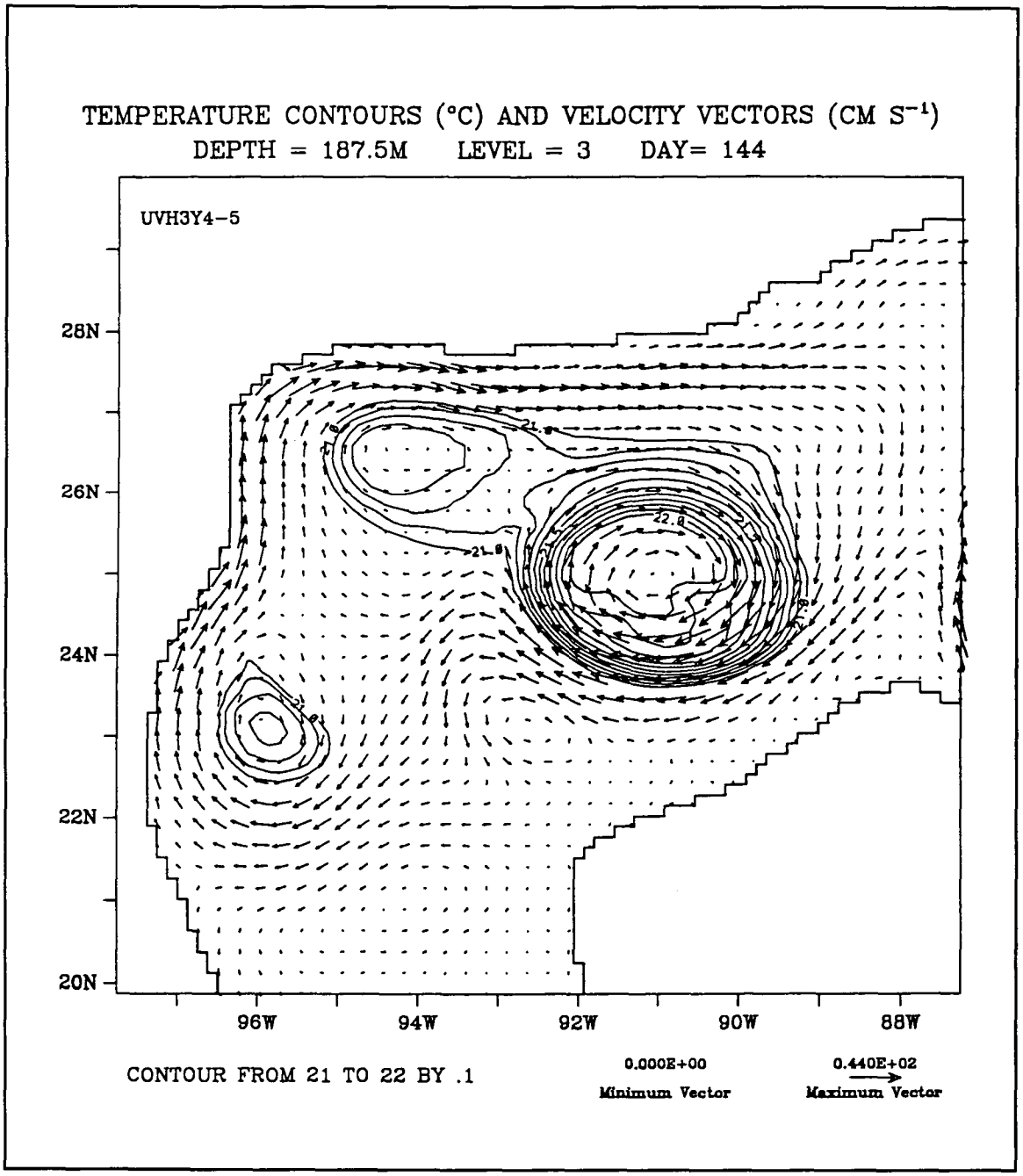

Figure 16b. Level 3 (187.5 m) temperature and velocity fields for the present-day seasonally forced model on day 144.

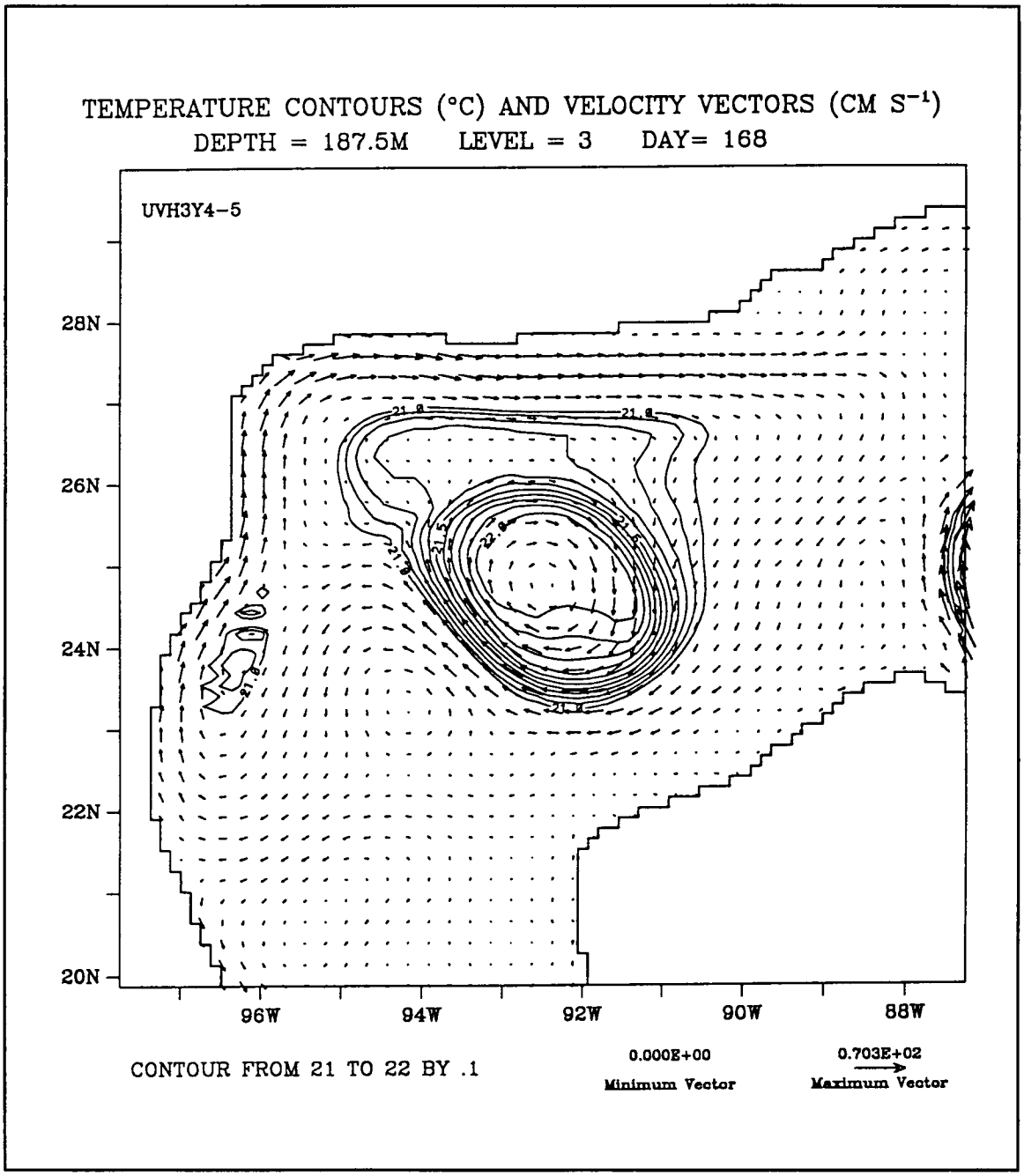

Figure 16c. Level 3 (187.5 m) temperature and velocity fields for the present-day seasonally forced model on day 168.

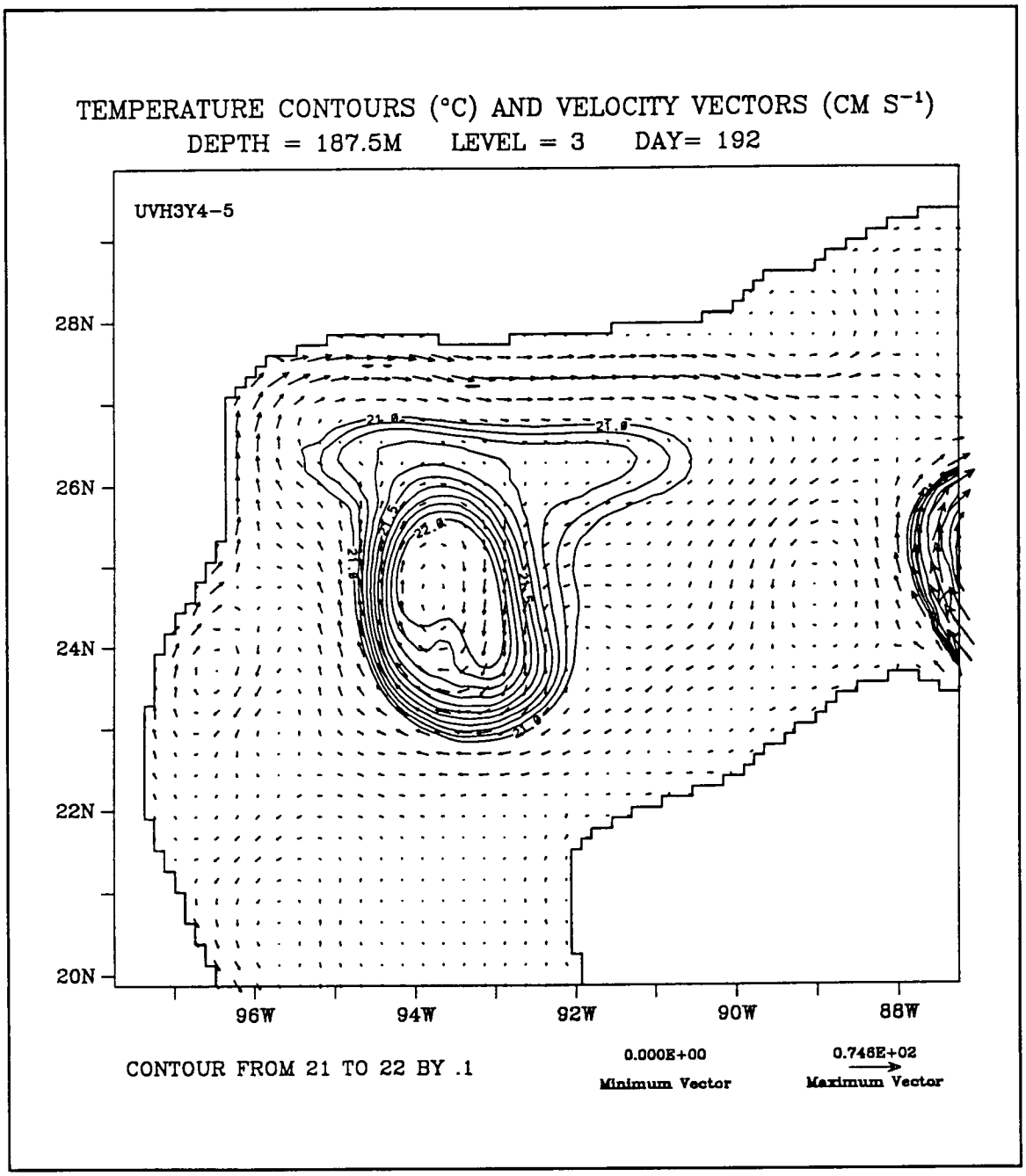

Figure 16d. Level 3 (187.5 m) temperature and velocity fields for the present-day seasonally forced model on day 192.

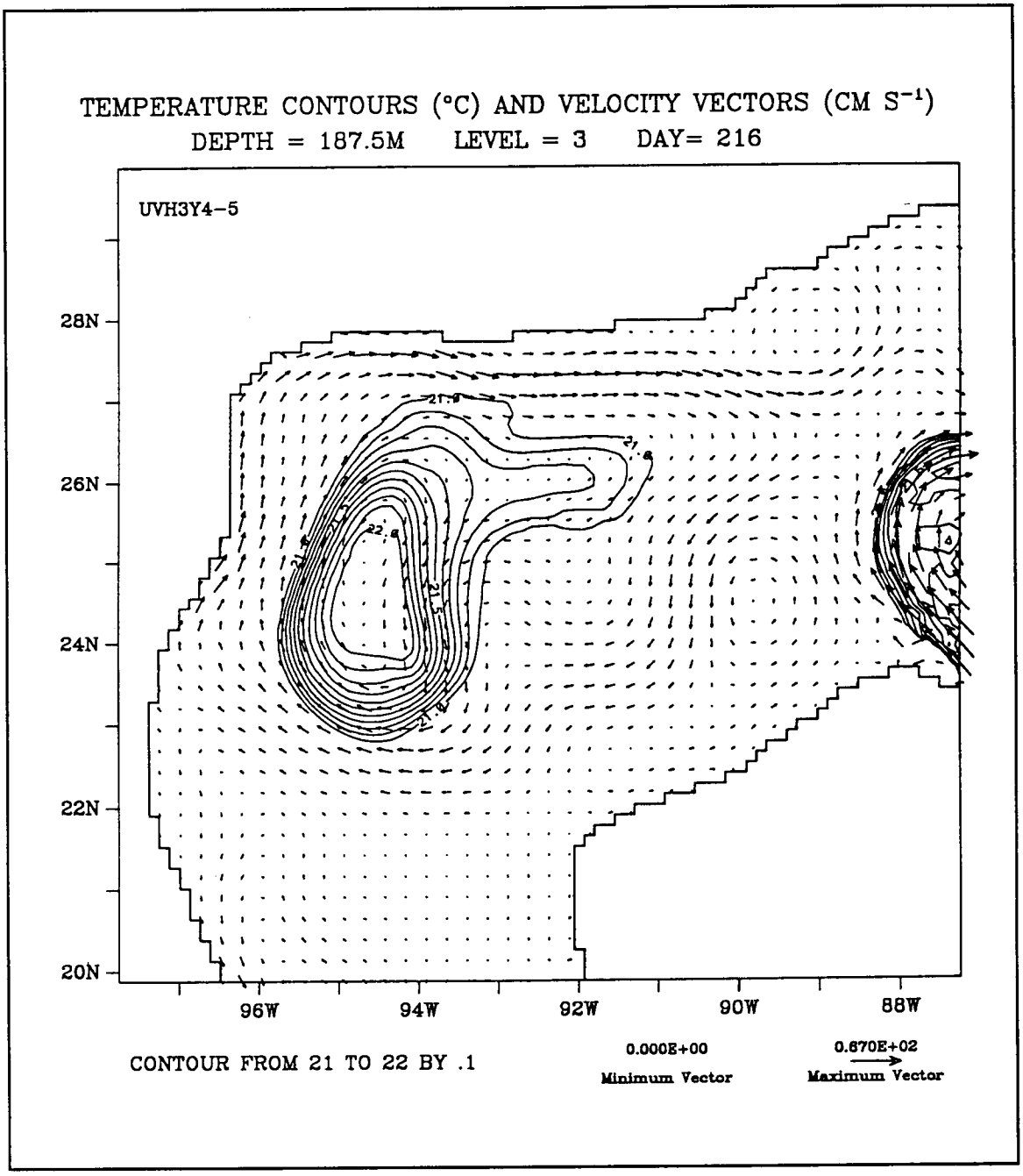

Figure 16e. Level 3 (187.5 m) temperature and velocity fields for the present-day seasonally forced model on day 216.

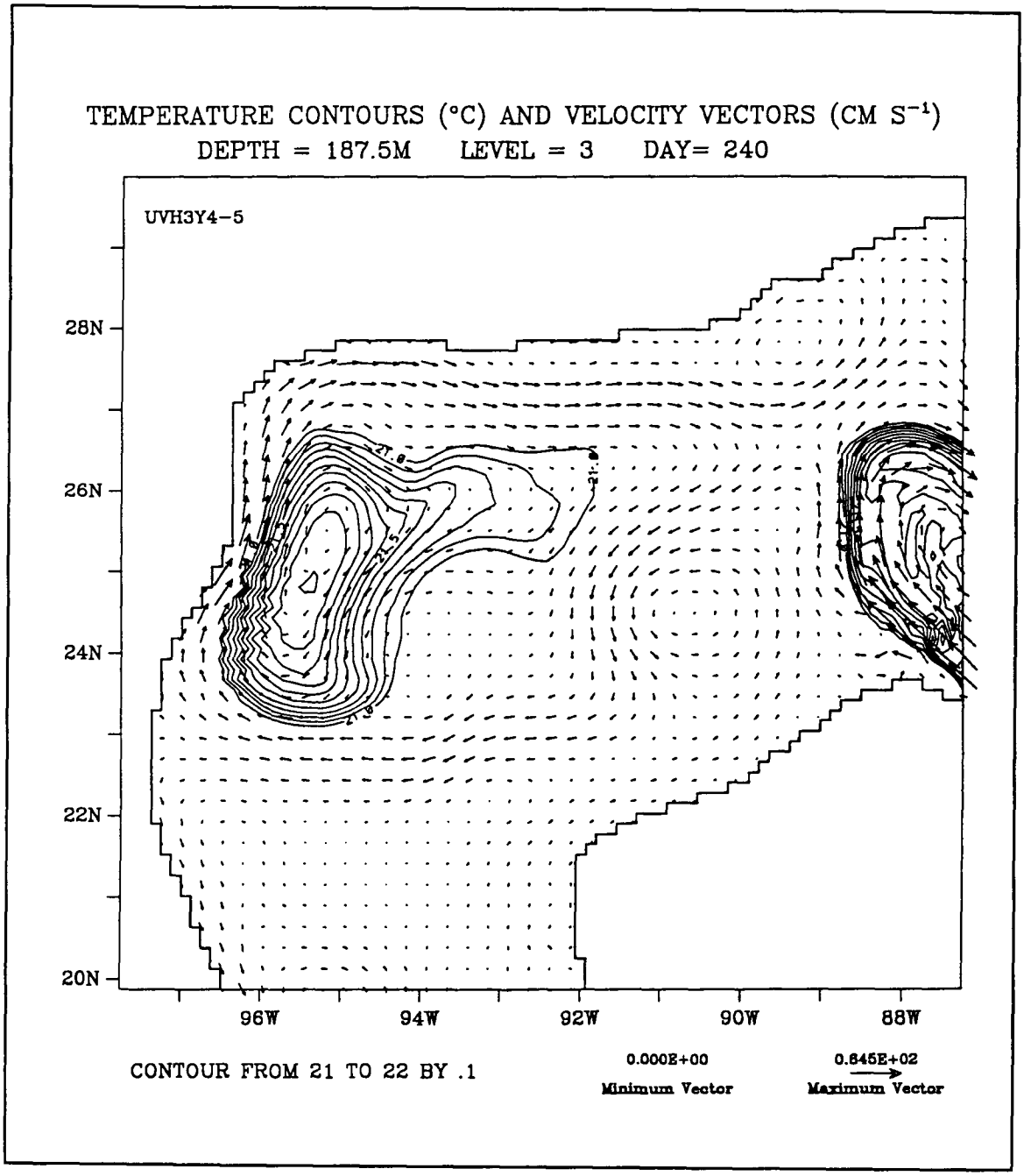

Figure 16f. Level 3 (187.5 m) temperature and velocity fields for the present-day seasonally forced model on day 240

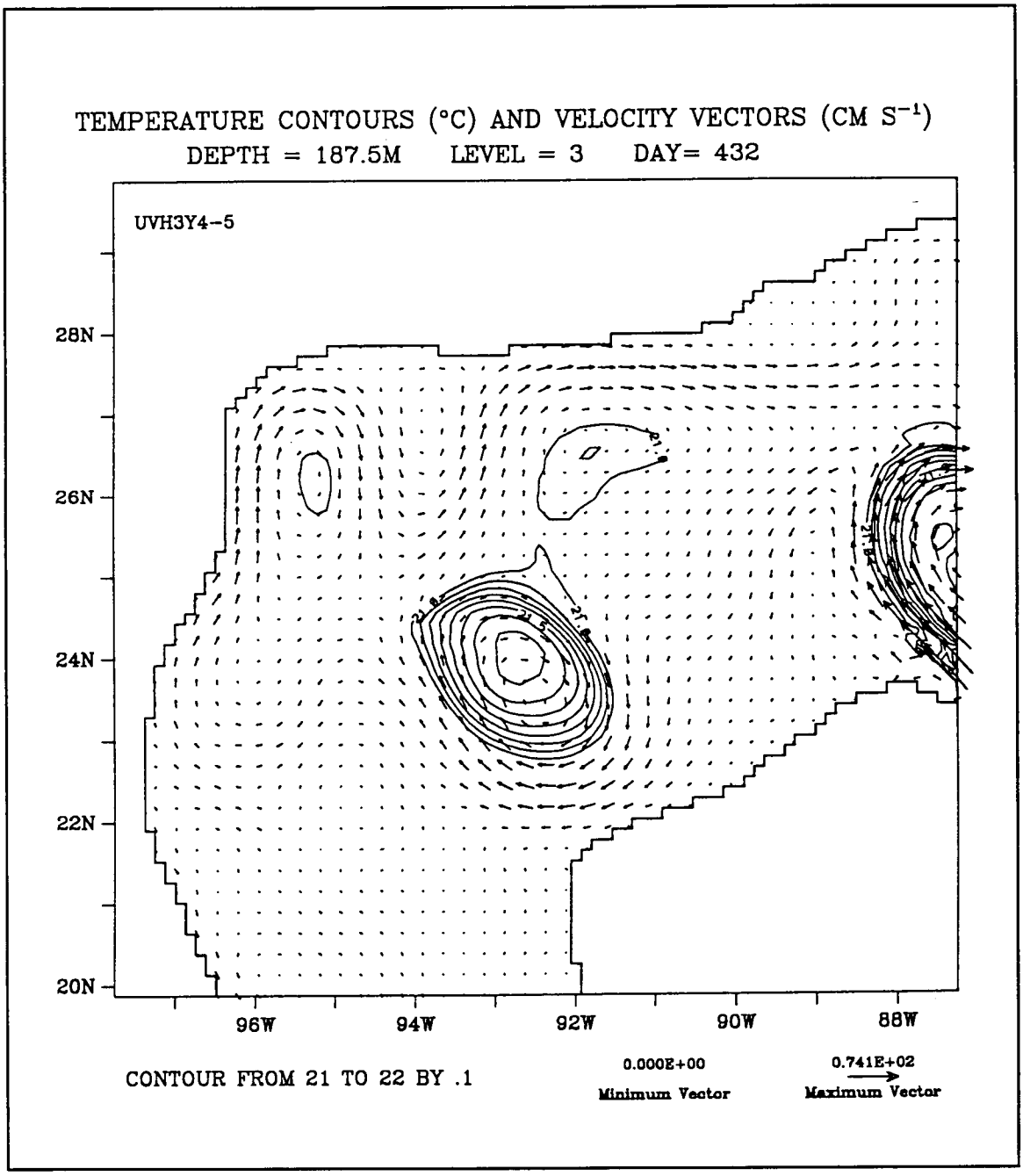

Figure 17a. Level 3 (187.5 m) temperature and velocity fields for the present-day seasonally forced model on day 432.

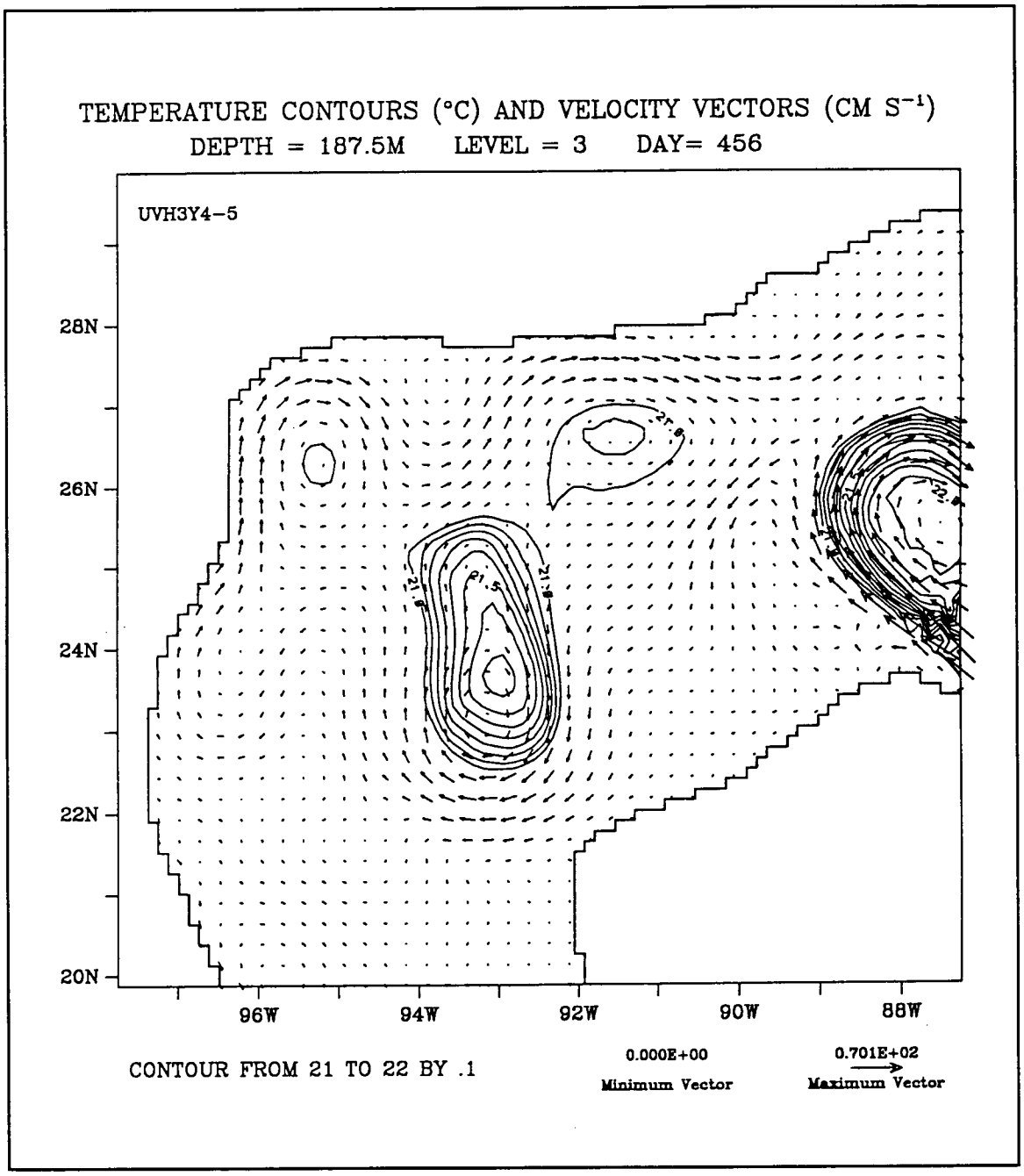

Figure 17b. Level 3 (187.5 m) temperature and velocity fields for the present-day seasonally forced model on day 456.

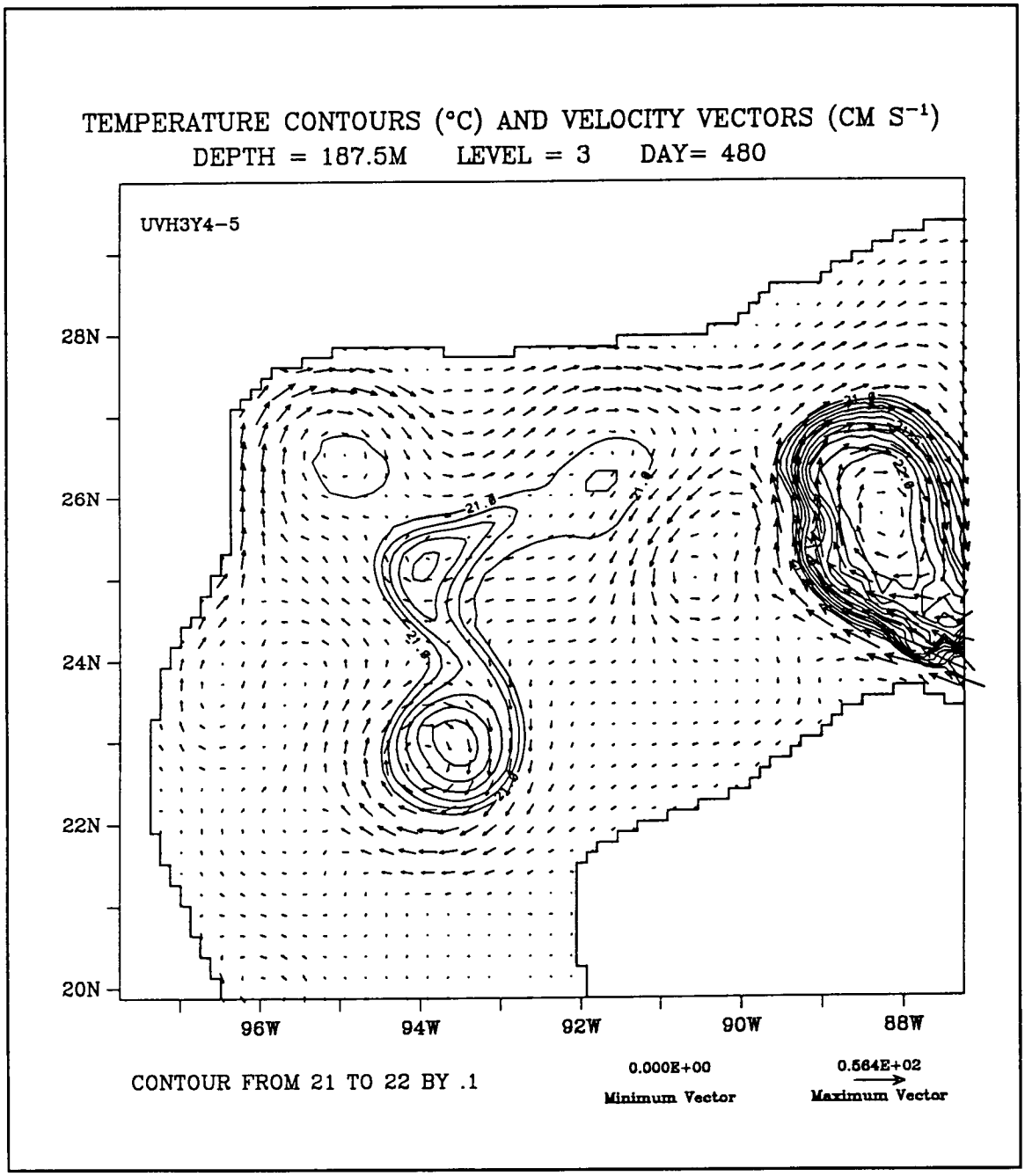

Figure 17c. Level 3 (187.5 m) temperature and velocity fields for the present-day seasonally forced model on day 480.

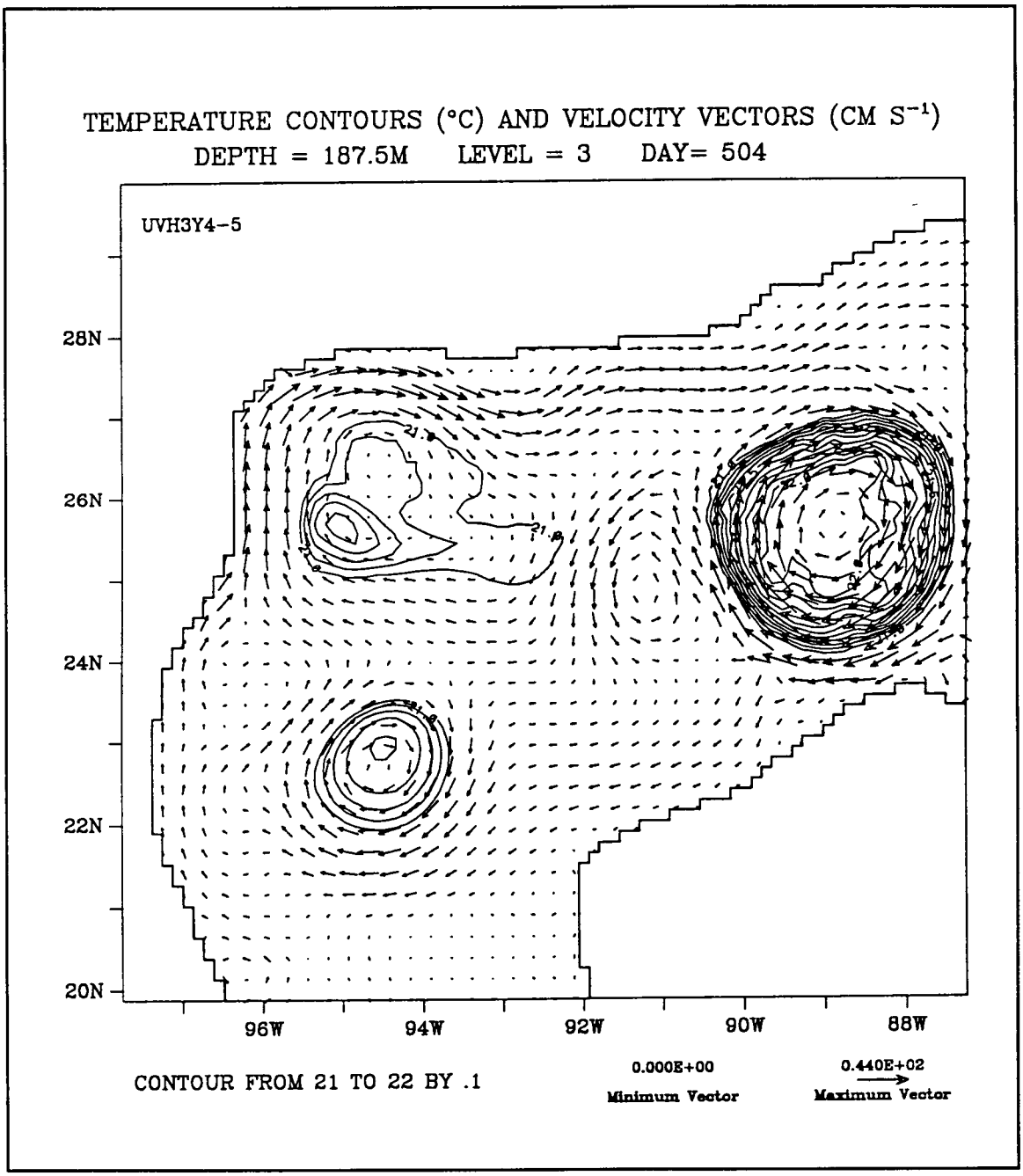

Figure 17d. Level 3 (187.5 m) temperature and velocity fields for the present-day seasonally forced model on day 504.

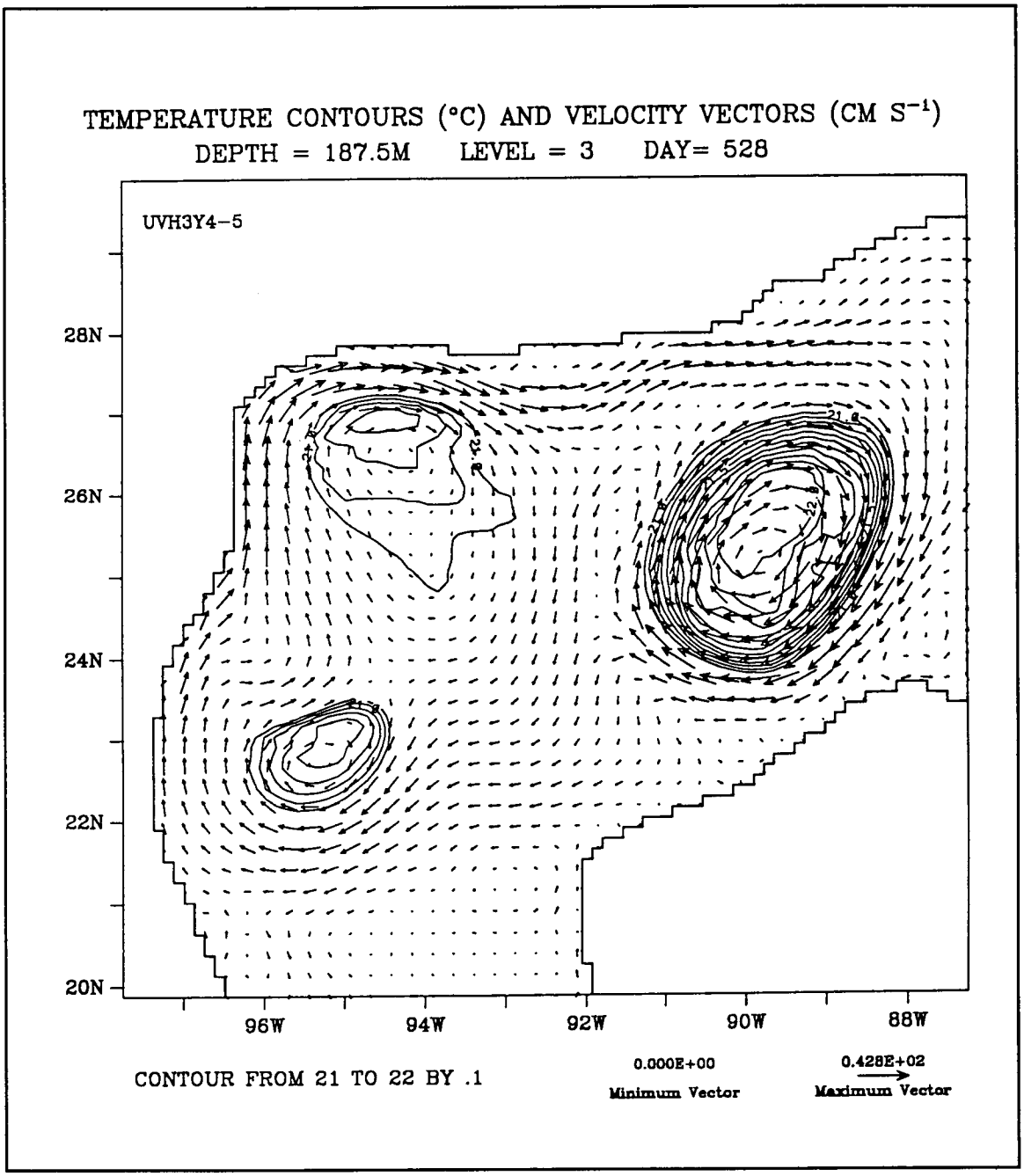

Figure 17e. Level 3 (187.5 m) temperature and velocity fields for the present-day seasonally forced model on day 528.

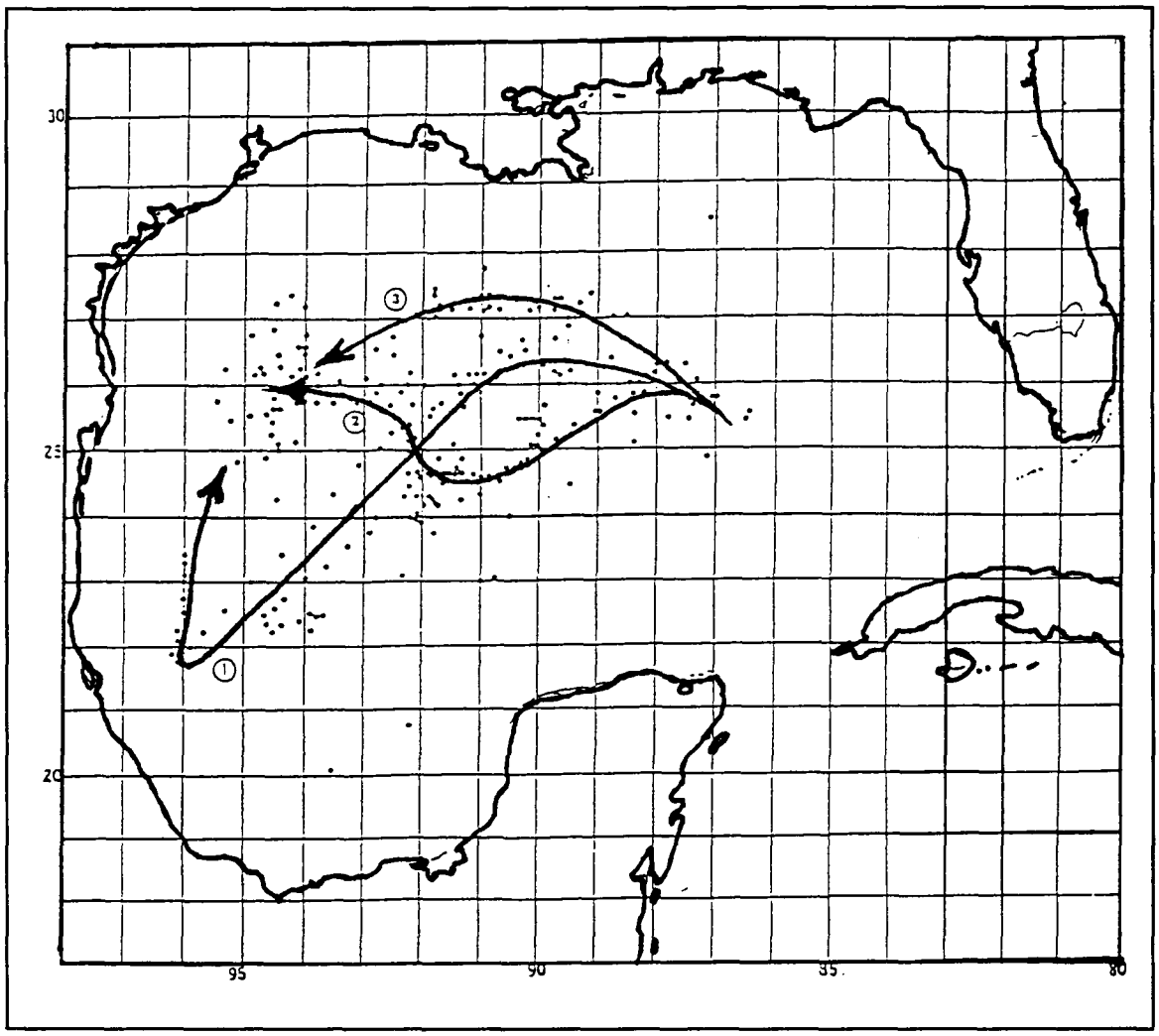

Figure 18. Characteristic paths of warm rings in the western Gulf of Mexico and the position of warm ring centers obtained using GOES and NOAA satellite data for the periods of 1973-1984 (from Vukovich and Crissman 1986).

migration paths. Of the nine long-term paths observed, six rings followed path 1, which was the predominant path. Many of the drifter tracks presented in Indest (1992) also follow a southwesterly course before turning northward along the Texas-Mexico coast. The majority of the model rings followed a path similar to path 1. Both of the characteristic migration paths 2 and 3 were based on only one long-term path and a number of isolated points (Vukovich and Crissman 1986). Only those model rings that split in the region of 24.5°N and 91.5°W follow a path similar to path 2, although Vukovich and Crissman (1986) do not report that any of the observed rings split. The model rings that migrate westward and merge with an older ring already resident in the northwest corner follow a path that is between paths 2 and 3. Some differences in the model migration paths and the observed paths are due to the monitoring of the model rings at 187.5 m, because the of the tilt of the isotherms with depth.

3.5 The Deep Circulation

Although many studies have been made of the upper layer circulation in the GOM, only a limited number of studies have been made of the deep circulation. The most recent observational study was made by Hamilton (1990) using moored current meters to make direct measurements of the currents below 1000 m. The current meter measurements were recorded at depths from 1000 m to 3174 m in the eastern, central and western portions of the GOM between 24.5°N and 27°N. Most of the current meter measure-ments reported in Hamilton (1990) are on the continental slope in the northwestern portion of the GOM and do not provide direct information about the deep circulation away from the continental slope and rise.

Hamilton (1990) reported that low frequency fluctuations with periods greater than 10 days were propagating from east to west with a group speed of 9 km·day^{-1} and that they had the characteristics of topographic Rossby waves. Hamilton (1990) also reported that the deep motions were travelling faster than the average westward migration speed of rings and he concluded that the deep motions were becoming progressively decoupled from the surface anticyclones. These deep motions are highly coherent in the vertical and exhibit bottom intensification (Hamilton 1990). Hoffman and Worley (1991) inferred from hydrographic data that, along with small circulation cells, there is a large cyclone in the deep western basin that opposes the upper layer circulation.

The velocity fields generated by this model are remarkably similar to the observations. To begin with, the deep motions in the model are highly coherent with depth from between 1000 and 1500 m all the way to the bottom (Figure 19) and the maximum velocities in the model also become stronger as the bottom is approached. The model results indicate that there are large cyclones dominating the deep circulation and that the location of the upper layer anticyclones (rings) are related to the position of the deep cyclones. The maximum swirl speeds of the deep cyclones in the model range from 10 cm s^{-1} to 20.6 cm s^{-1} at 2550 m which is in agreement with velocities measured at mooring GG in the central basin at 1650 m and 2500 m (Figure 20 after Hamilton 1990).

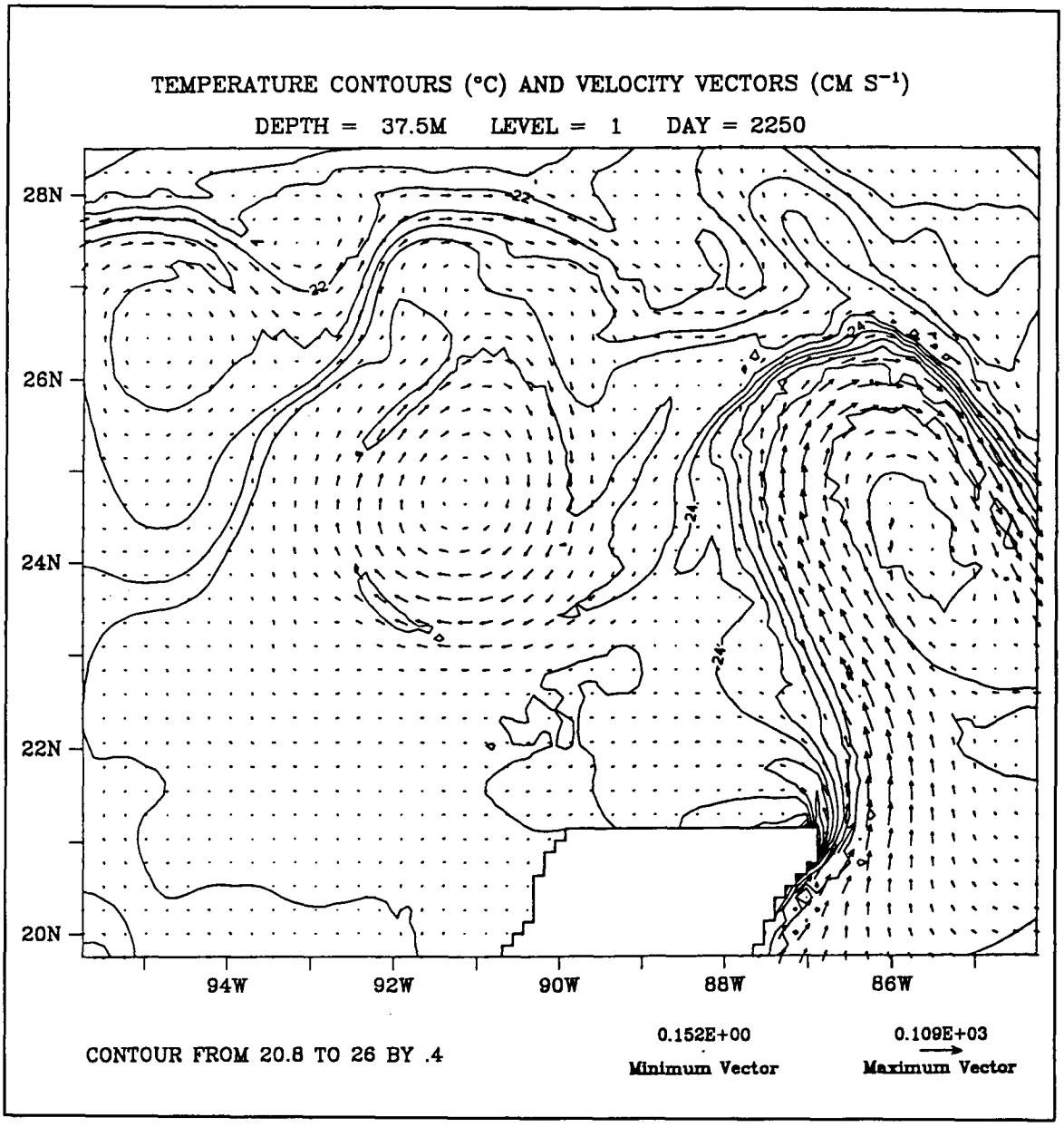

Figure 19a. Temperature contours (°C) and velocity vectors (cm s^{-1}) for the present-day seasonally forced model on day 2250 at 37.5 m.

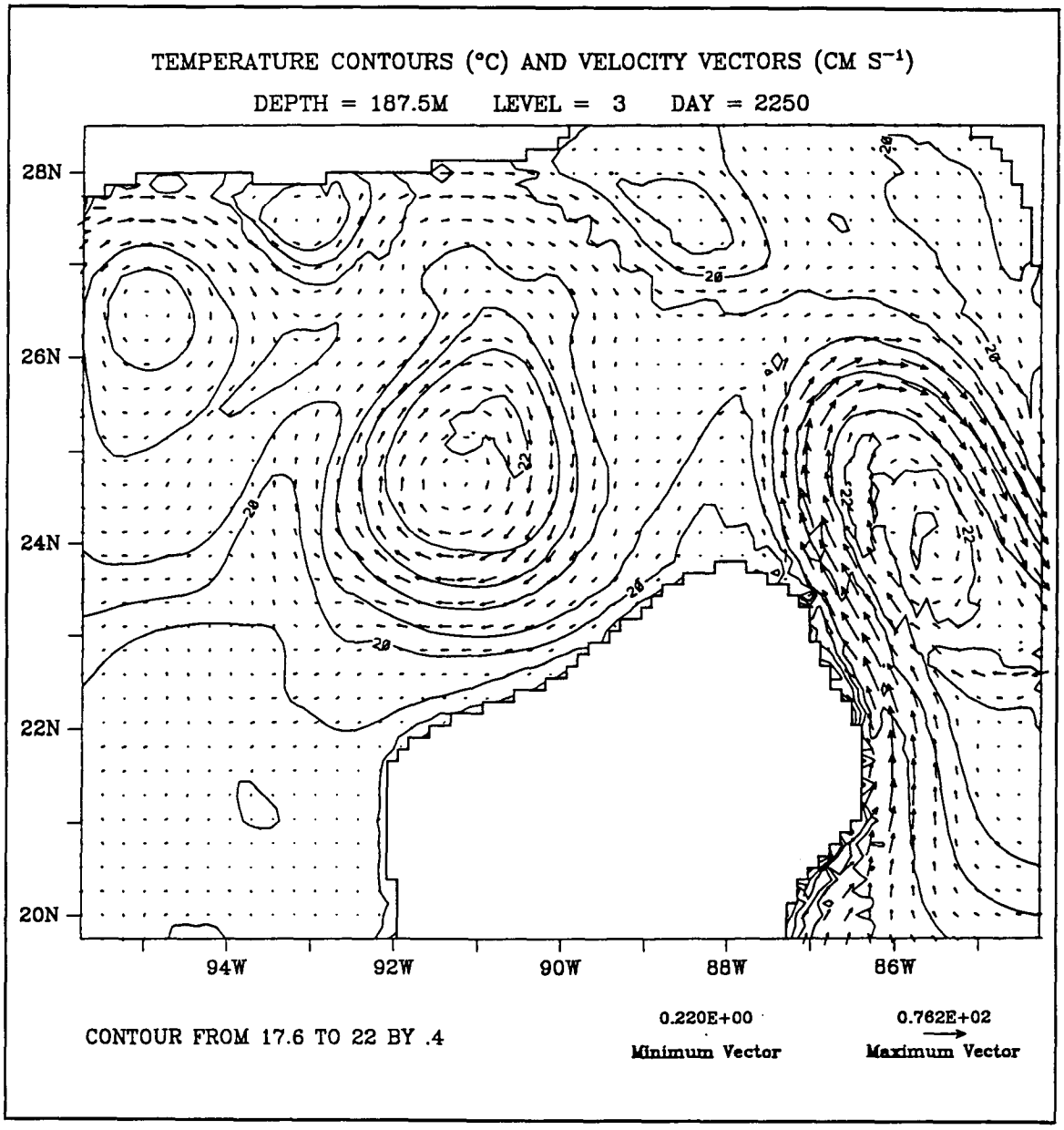

Figure 19b. Temperature contours (°C) and velocity vectors (cm s^{-1}) for the present-day seasonally forced model on day 2250 at 187.5 m.

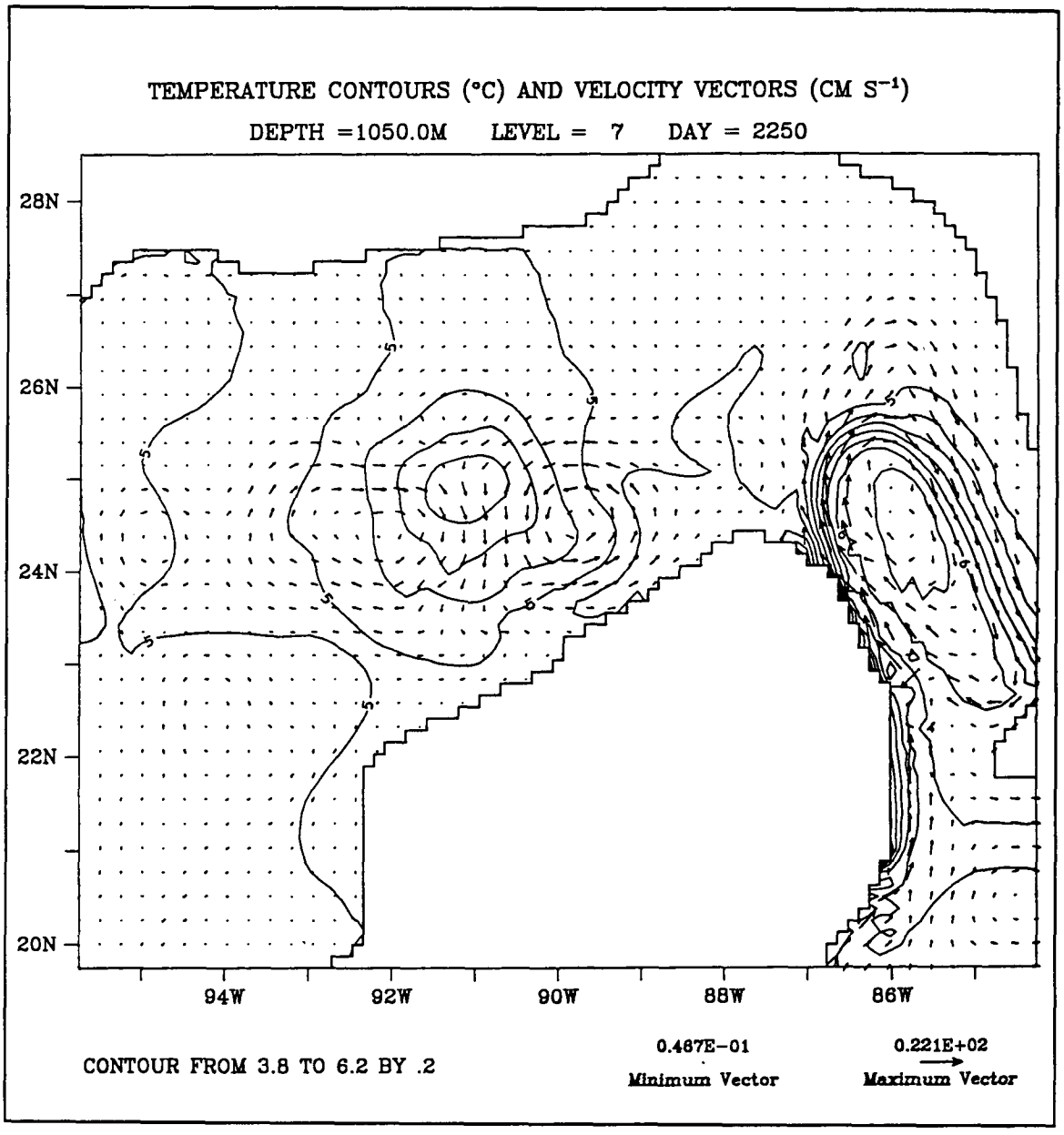

Figure 19c. Temperature contours (°C) and velocity vectors (cm s^{-1}) for the present-day seasonally forced model on day 2250 at 1050 m.

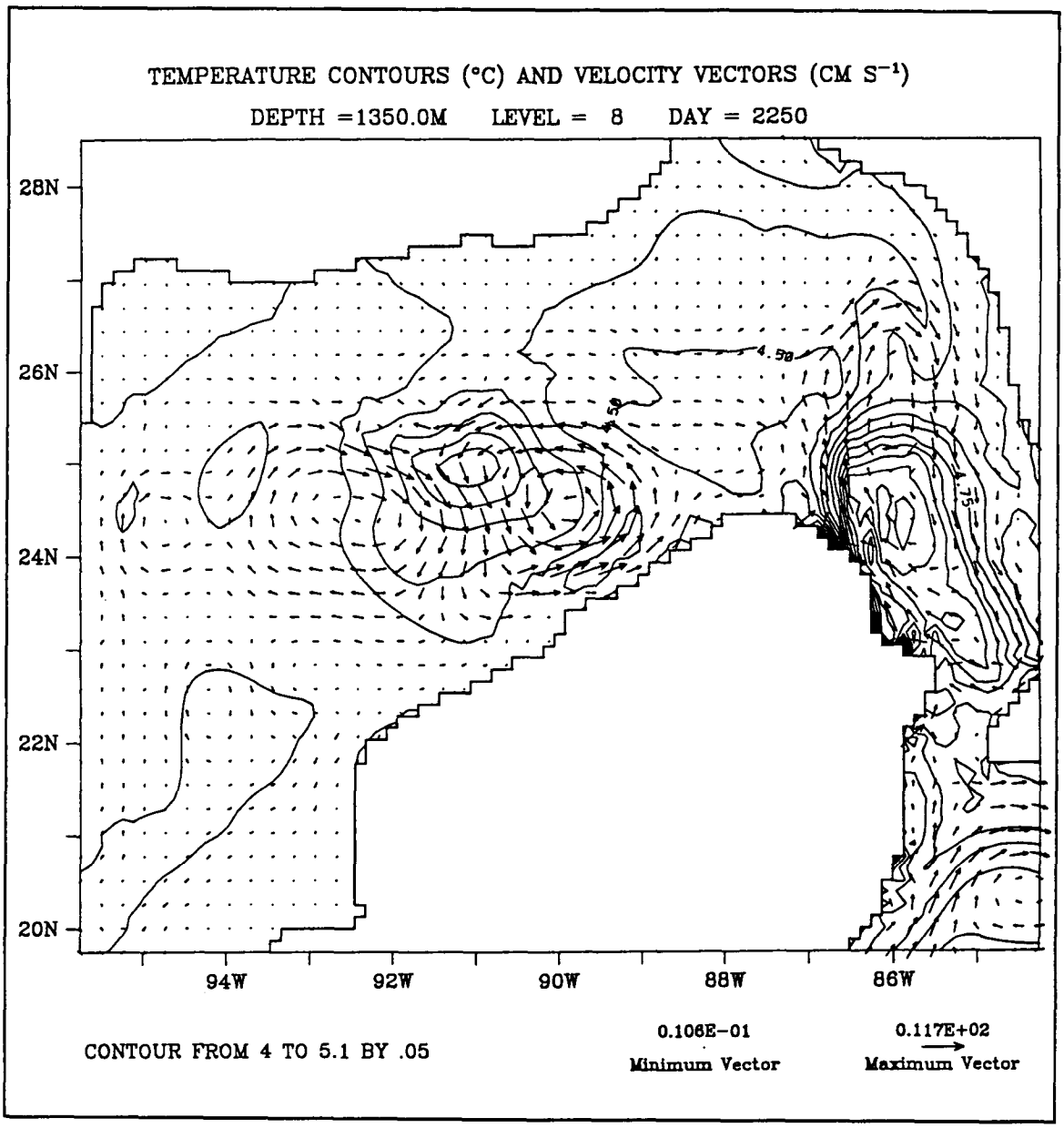

Figure 19d. Temperature contours (°C) and velocity vectors (cm s^{-1}) for the present-day seasonally forced model on day 2250 at 1350 m.

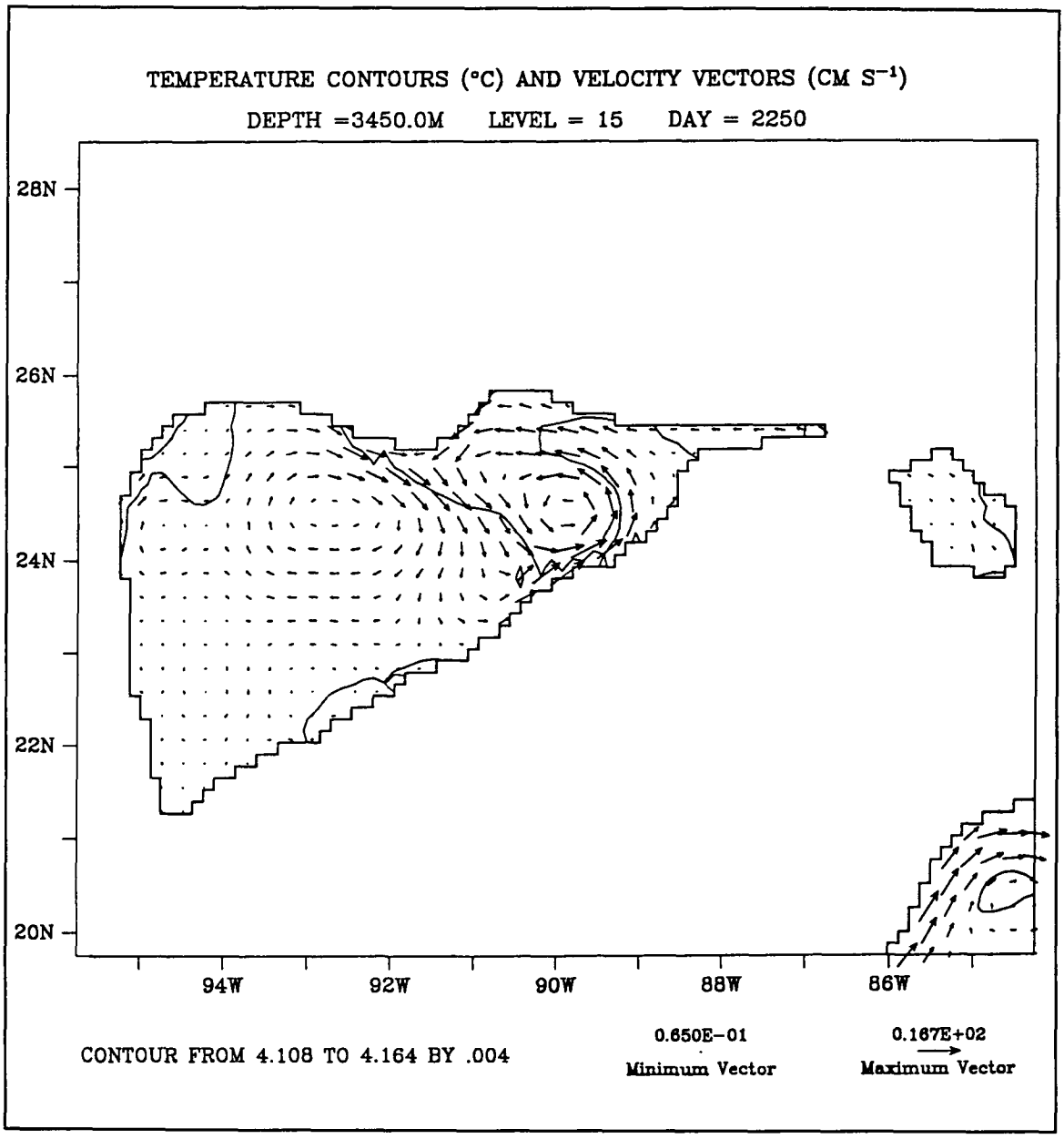

Figure 19e. Temperature contours (°C) and velocity vectors (cm s^{-1}) for the present-day seasonally forced model on day 2250 at 3450 m.

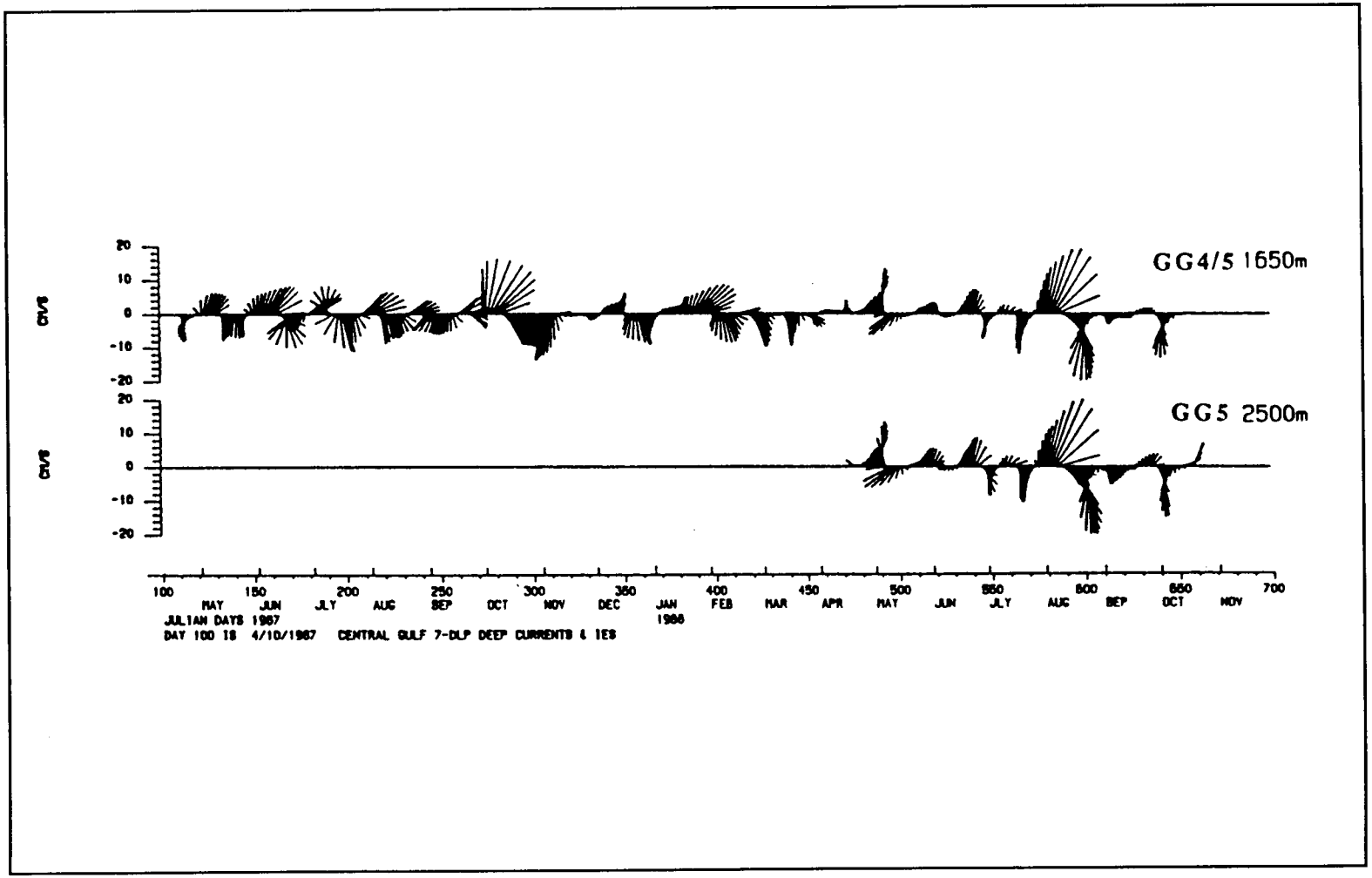

Figure 20. Seven-DLP stick vectors for the central Gulf of Mexico at 1650 m and 2500 m (from Hamilton 1990).

Detailed analysis of the model temperature and velocity fields has provided a complete picture of the formation and westward migration of the deep cyclones. Animations of the model velocity fields at 187.5m, 1650 m and 2550 m show that as the LC extends northward into the GOM during the ring-separation cycle, the deep circulation beneath the LC changes from anticyclonic to cyclonic (Figure 21). This change in circulation can also be observed in current meter records in the eastern GOM at depths of 1565 m, 2364 m, and 3174 m during the formation of two rings, labeled 'eddy B' and 'eddy C' (Figure 22 from Hamilton 1990).

The deep cyclone that forms beneath the ring in the model is highly coherent in the vertical and 'feels' the bottom bathymetry. The 3450-m isobath for the GOM is separated into two closed basins, a small basin to the east and a larger basin in the central and western region of the GOM. There is a narrow passage below 3000 meters that connects the deepest portions of the eastern and central basins (see Figure 2). As the ring migrates over this passage, the deep cyclone becomes constricted in the north-south direction, as if it were squeezing through the passage. The temperature signal of the ring is coupled to the velocity signal down to at least 2550 m (Figure 23). The influence of the bathymetry can also be seen on the temperature signal as it elongates east-west while passing over the narrow passage. Once inside the central basin, the deep cyclone reforms and strengthens.

All deep cyclones observed in this study followed nearly the same westward migration path. The position of the upper layer anticyclone changes relative to the position of the deep cyclone. Initially the upper layer anticyclone is northwest of the deep cyclone, but the cyclone moves counterclockwise relative to the anticyclone until the anticyclone moves over the Mexico slope. The deep cyclone does not move up over the slope, but is trapped by the bottom bathymetry below 3300 meters and decays rapidly (Figure 24). Although some of the upper layer anticyclones split in the model, the deep cyclones associated with them did not split. The deep cyclones remained coupled with the portion of the rings that moved toward the southwest.

This study suggests that the deep cyclone and surface anticyclone do not become decoupled as they migrate westward, but that they move relative to each other and that the deep cyclone appears to move faster than the surface anticyclone when measured at certain locations along the migration path. Because the deep cyclones all follow nearly the same path, it appears that they are guided by the bottom bathymetry, while factors controlling the migration paths of the surface anticyclone are more complex, and they do not appear to be dominated by the bottom bathymetry.

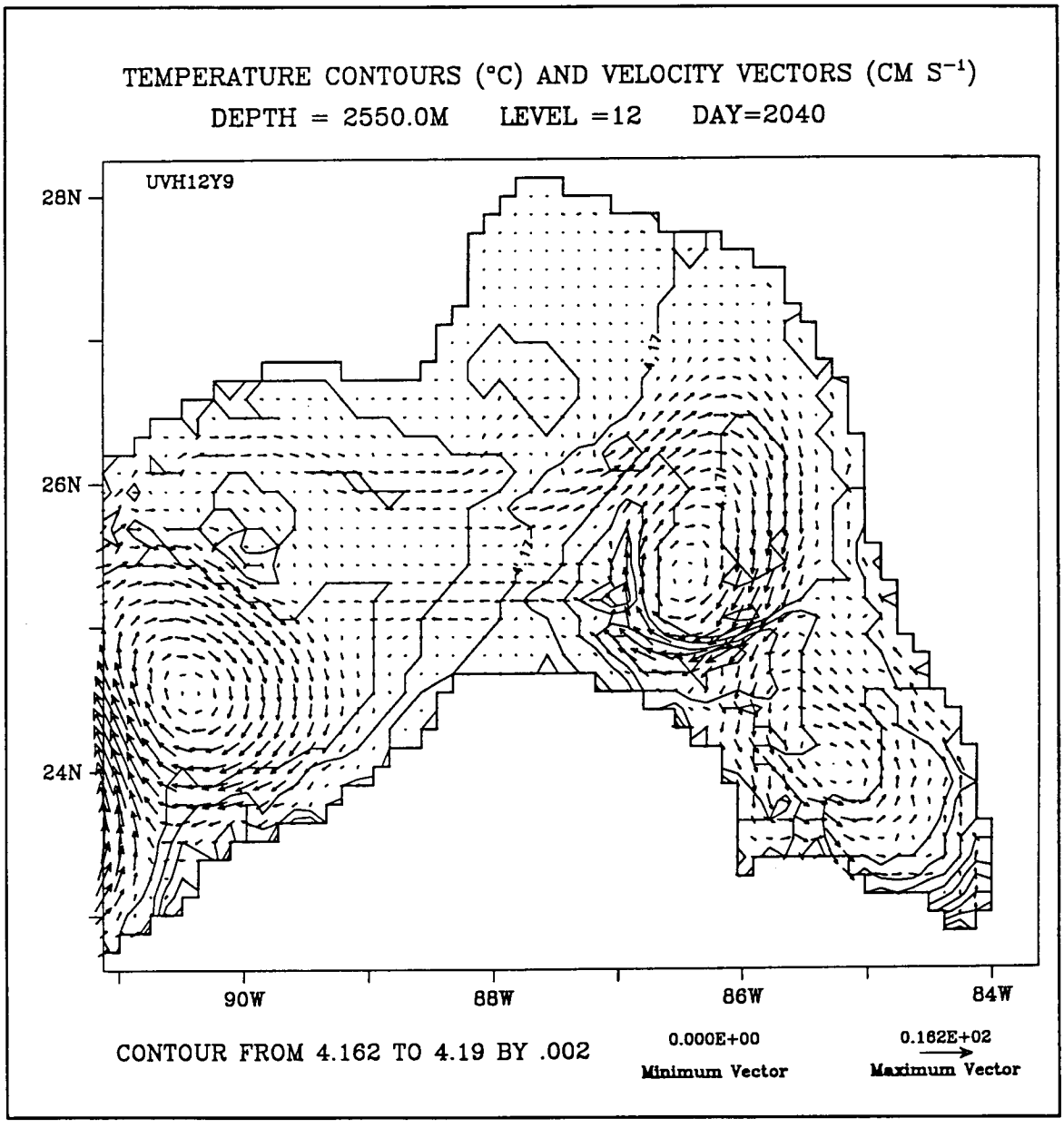

Figure 21a. Level 12 (2550 m) temperature and velocity fields for the eastern Gulf of Mexico for the present-day seasonally forced model on day 2040.

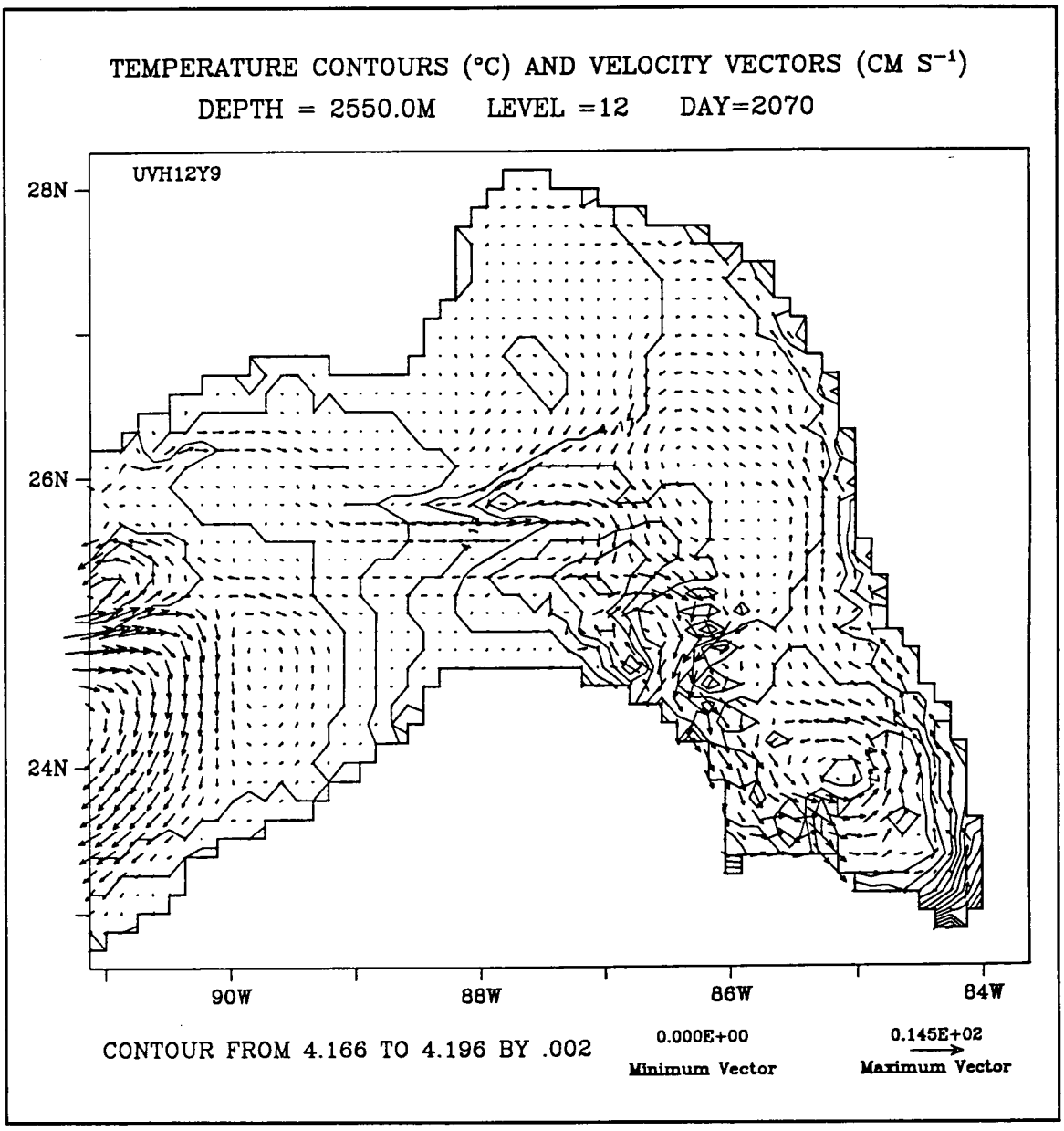

Figure 21b. Level 12 (2550 m) temperature and velocity fields for the eastern Gulf of Mexico for the present-day seasonally forced model on day 2070.

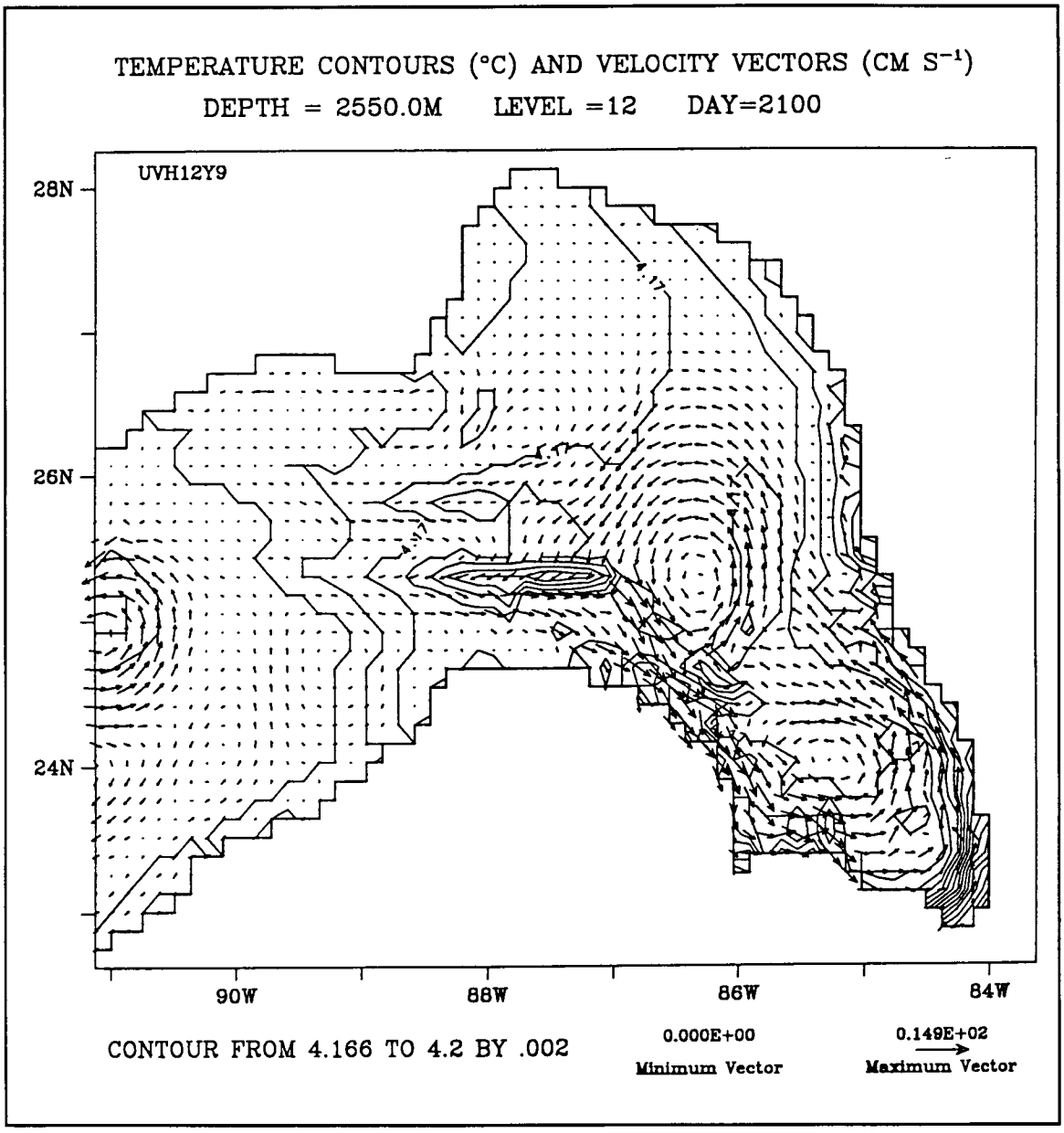

Figure 21c. Level 12 (2550 m) temperature and velocity fields for the eastern Gulf of Mexico for the present-day seasonally forced model on day 2100.

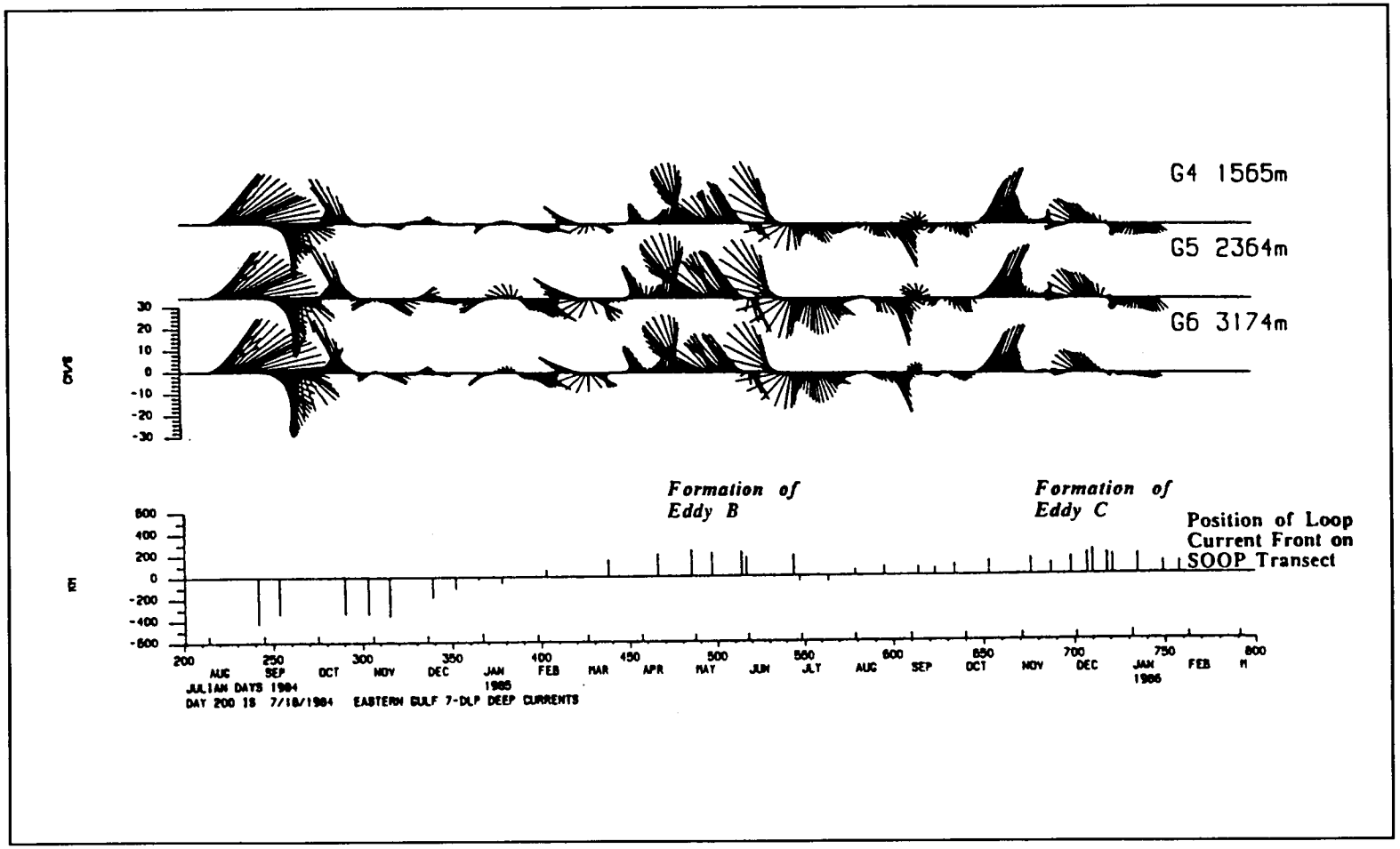

Figure 22. Seven-DLP stick vectors from Mooring G in the eastern Gulf of Mexico at 1565 m, 2364 m, and 3174 m. The periods of formation and shedding of rings Eddy B and Eddy C are indicated (from Hamilton 1990).

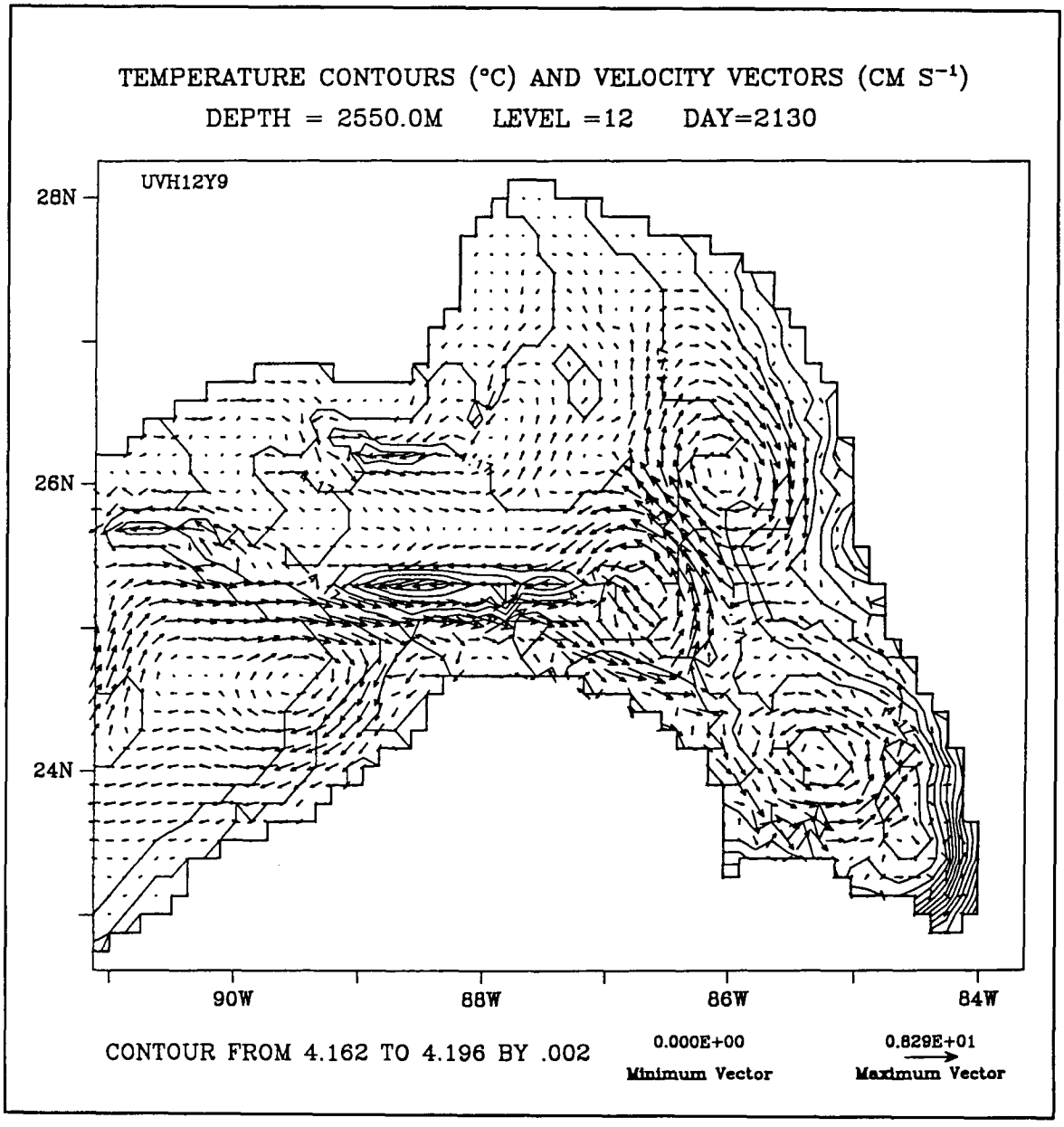

Figure 23a. Level 12 (2550 m) temperature and velocity fields for the central Gulf of Mexico for the present-day seasonally forced model on day 2130.

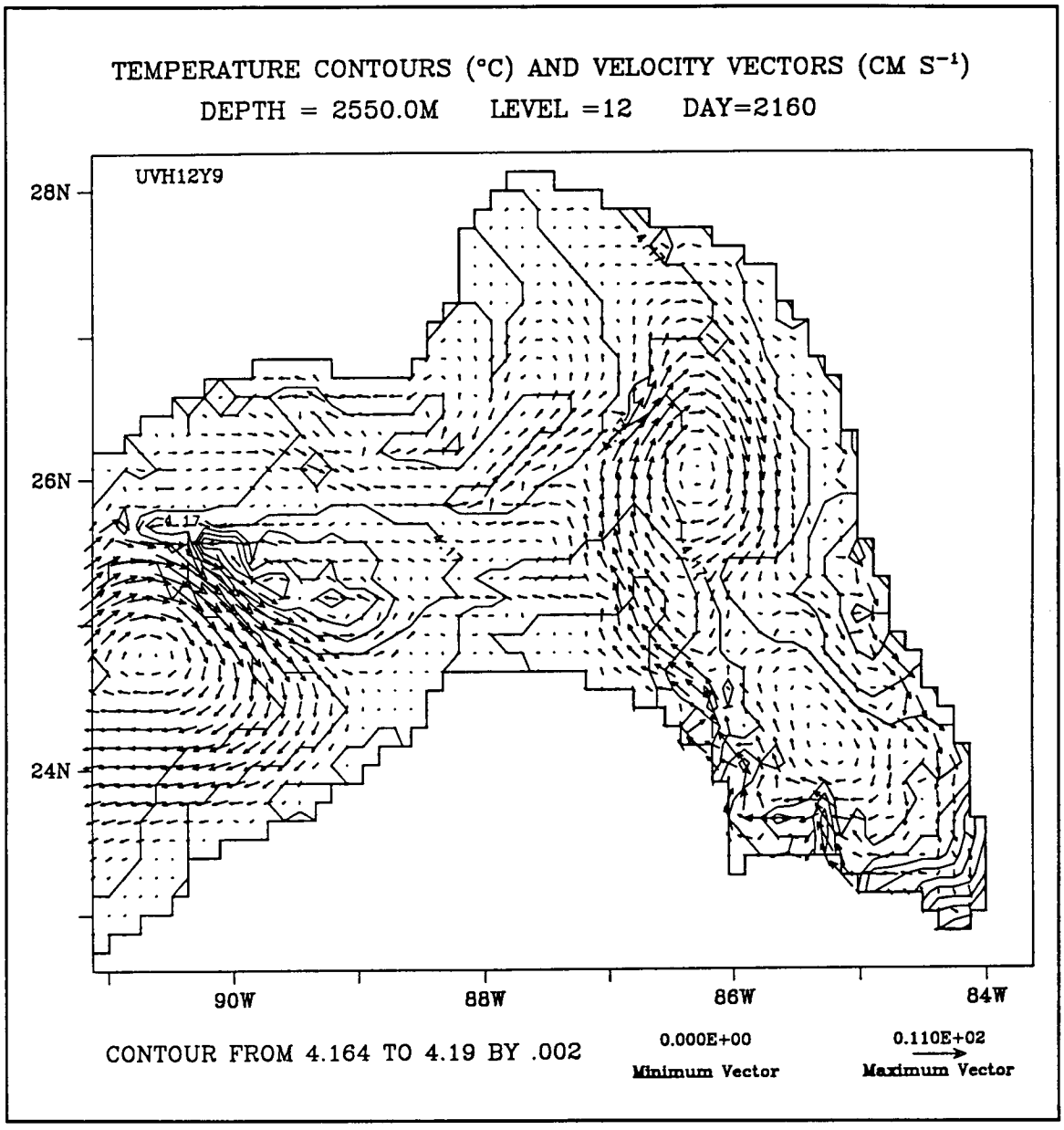

Figure 23b. Level 12 (2550 m) temperature and velocity fields for the central Gulf of Mexico for the present-day seasonally forced model on day 2160.

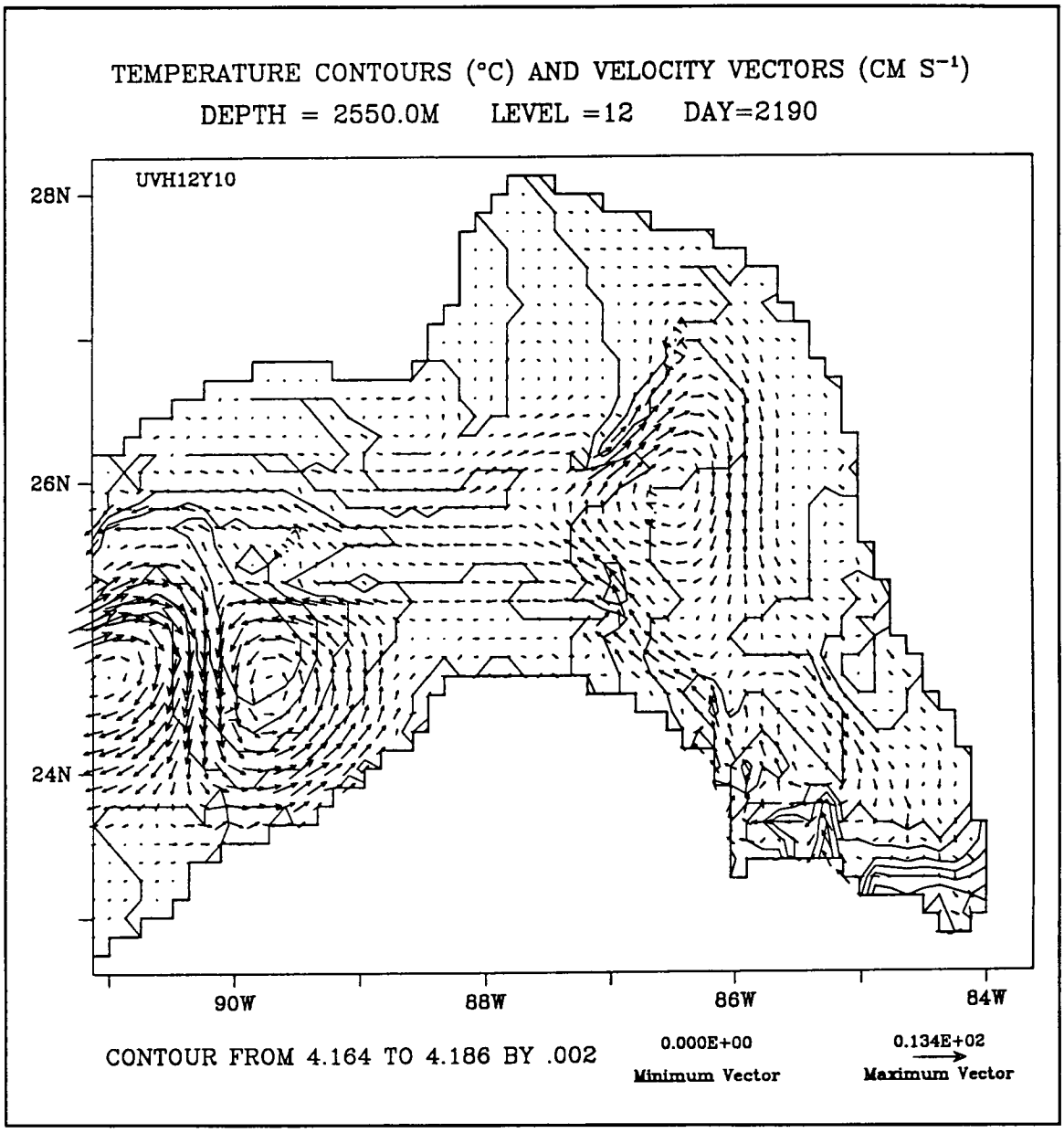

Figure 23c. Level 12 (2550 m) temperature and velocity fields for the central Gulf of Mexico for the present-day seasonally forced model on day 2190.

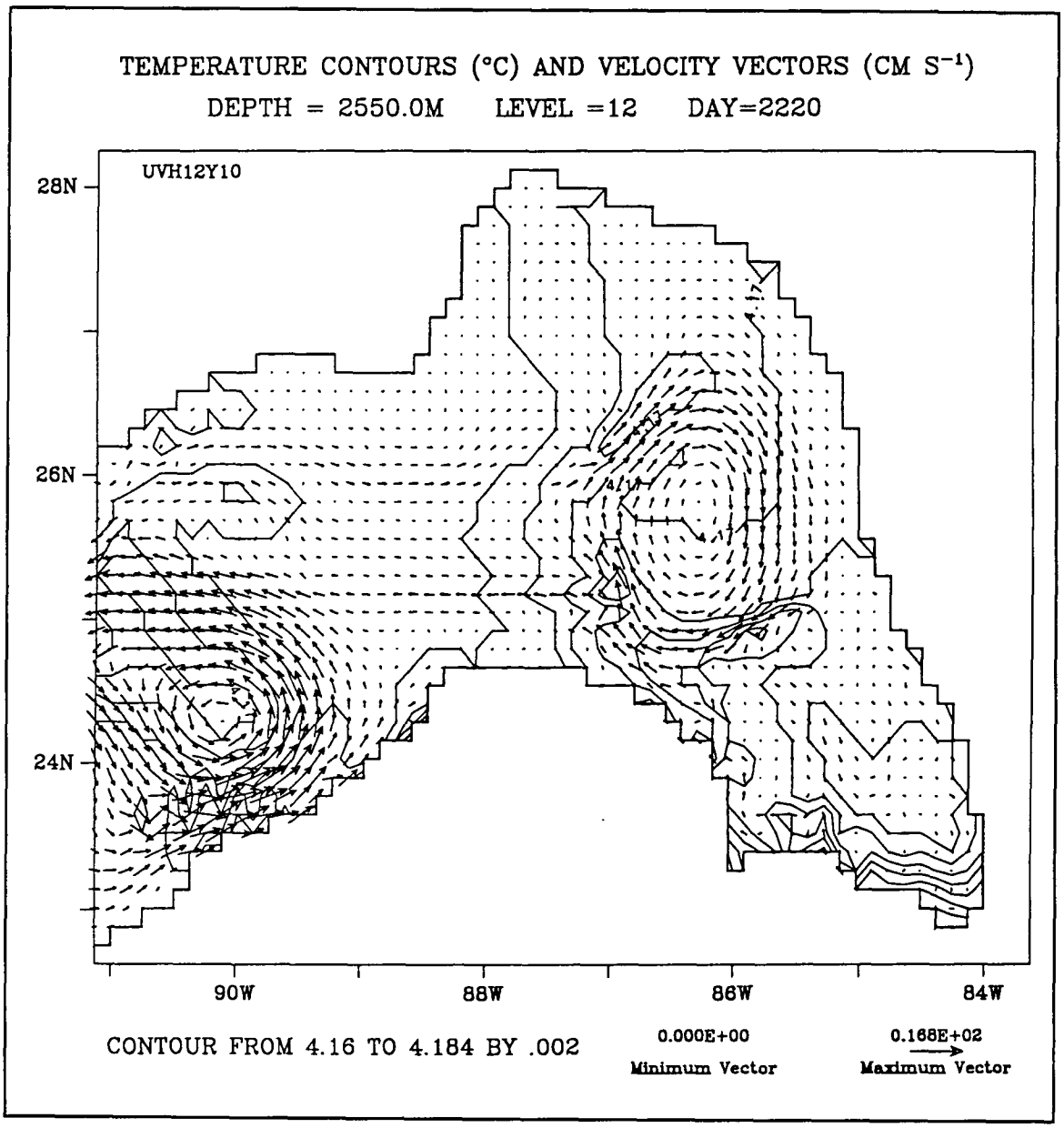

Figure 23d. Level 12 (2550 m) temperature and velocity fields for the central Gulf of Mexico for the present-day seasonally forced model on day 2200.

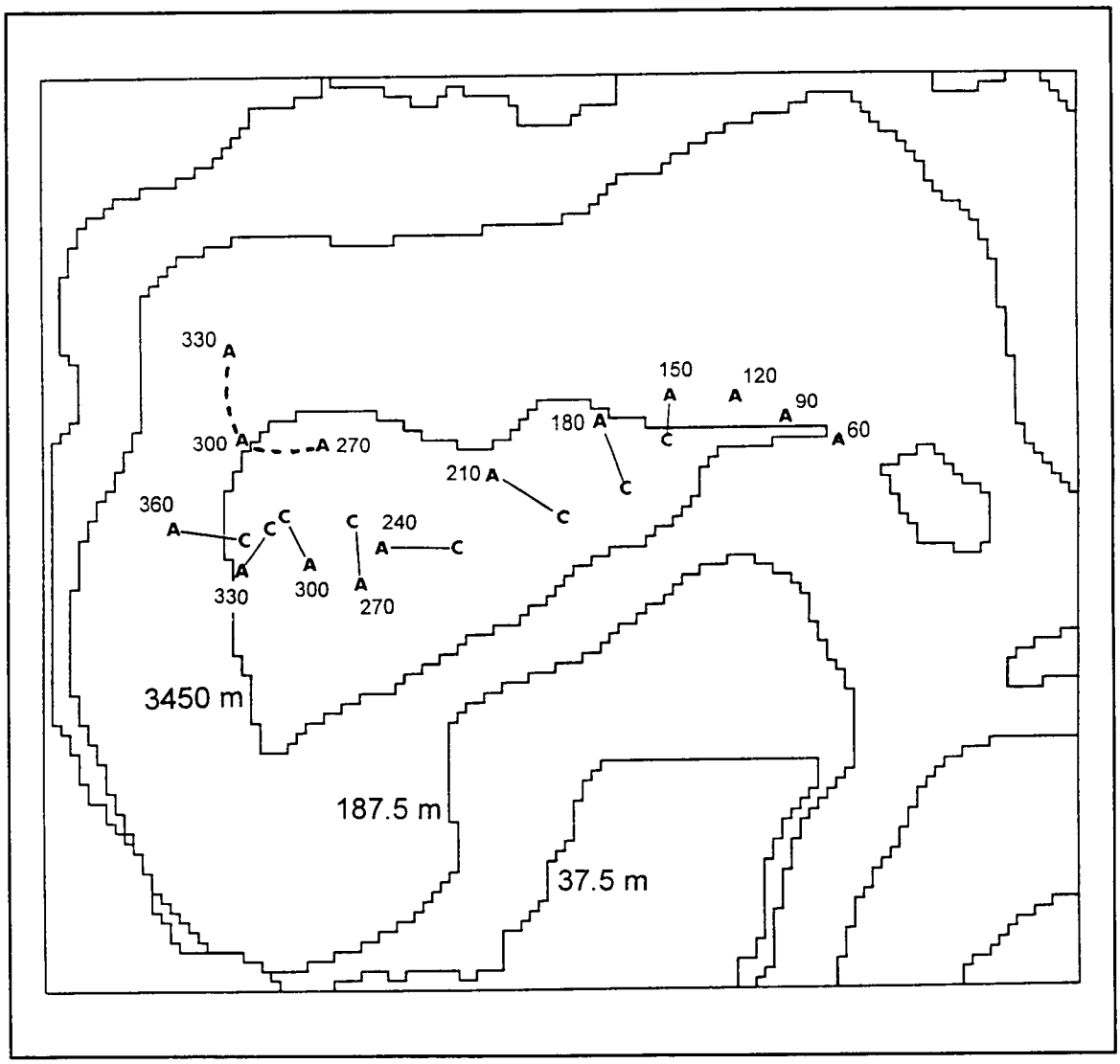

Figure 24a. Model migration paths and days of observations for surface anticyclones 'A' and deep cyclones 'C' for ring S10.

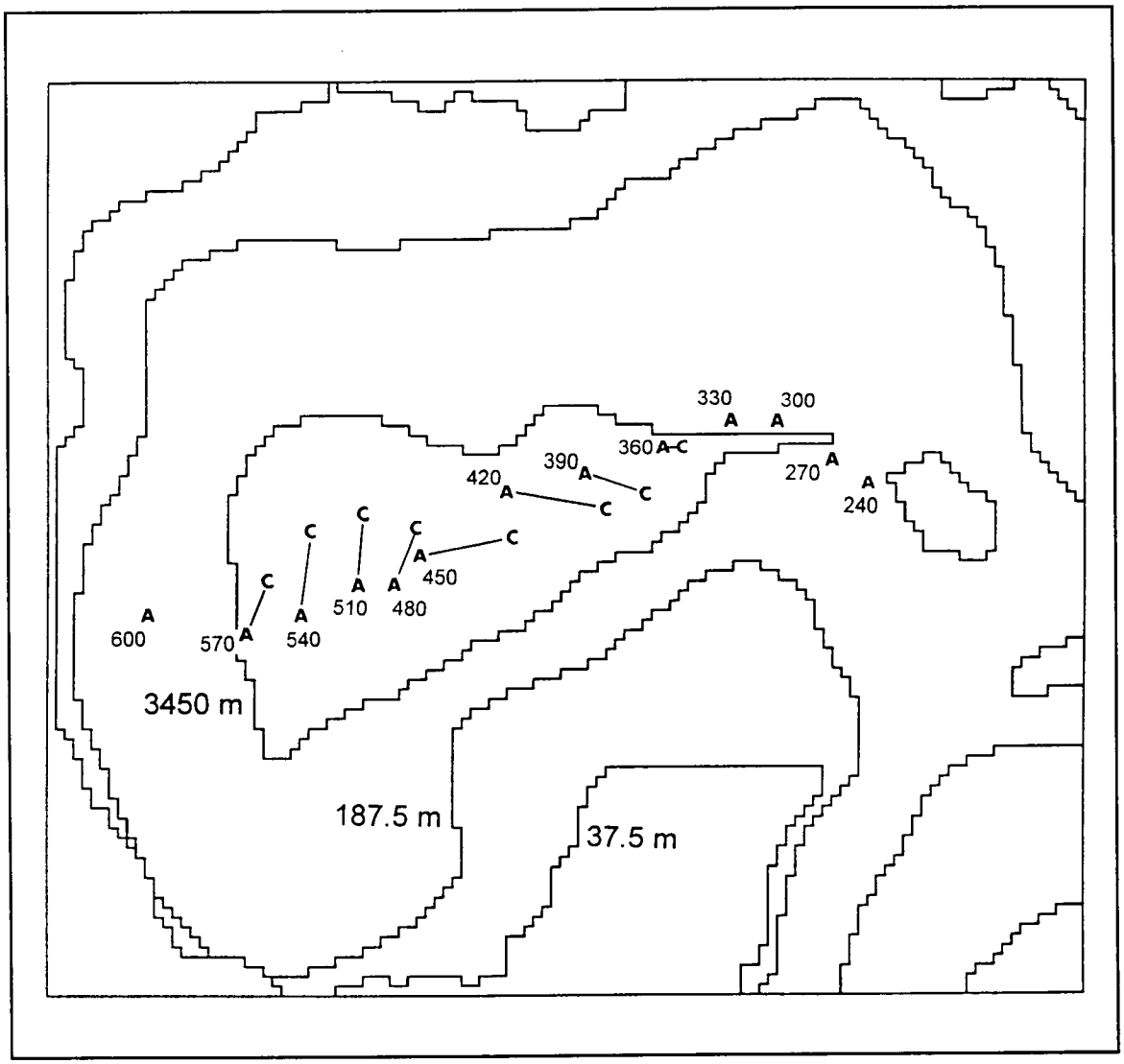

Figure 24b. Model migration paths and days of observations for surface anticyclones 'A' and deep cyclones 'C' for ring S11.

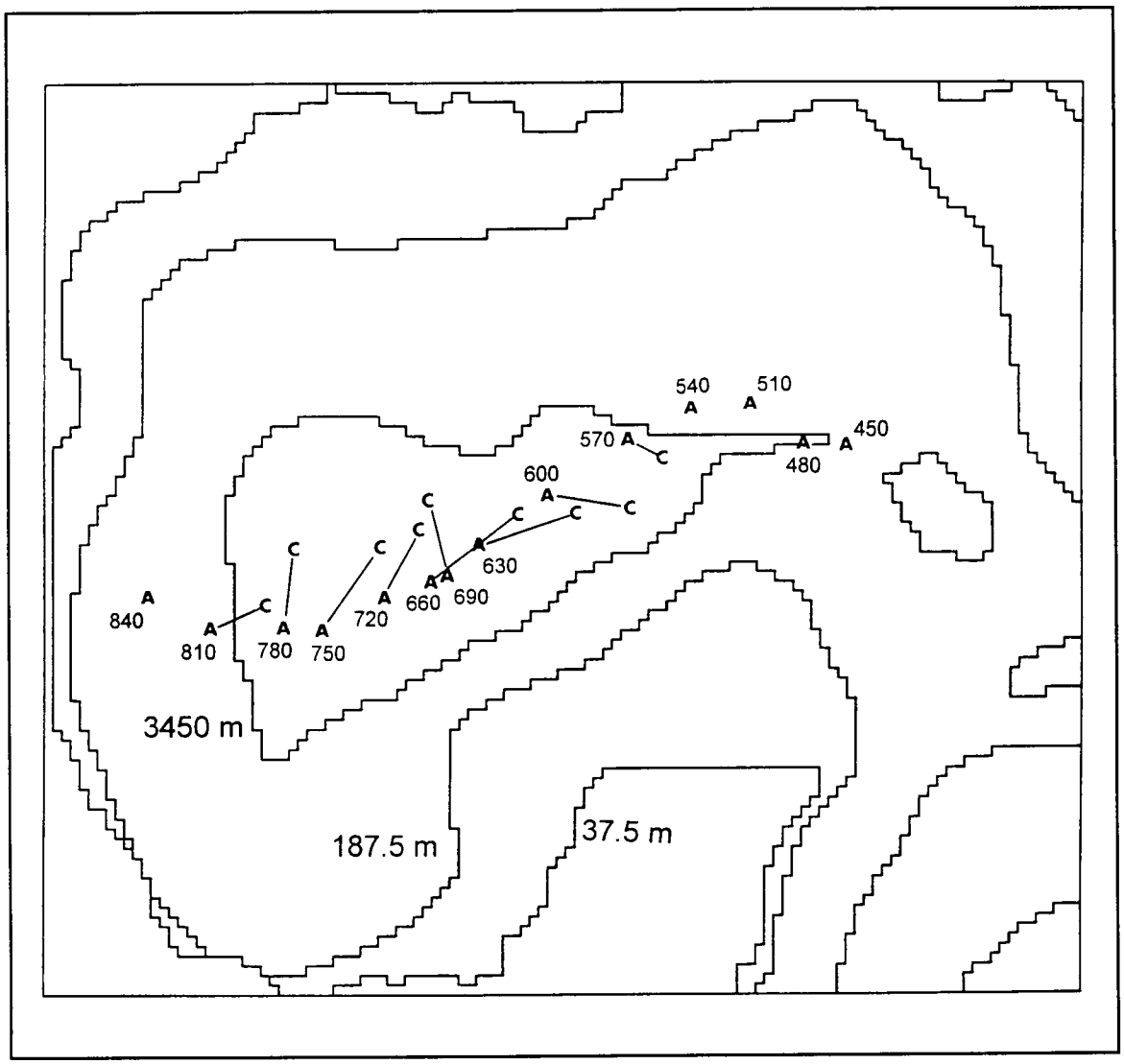

Figure 24c. Model migration paths and days of observations for surface anticyclones 'A' and deep cyclones 'C' for ring S12.

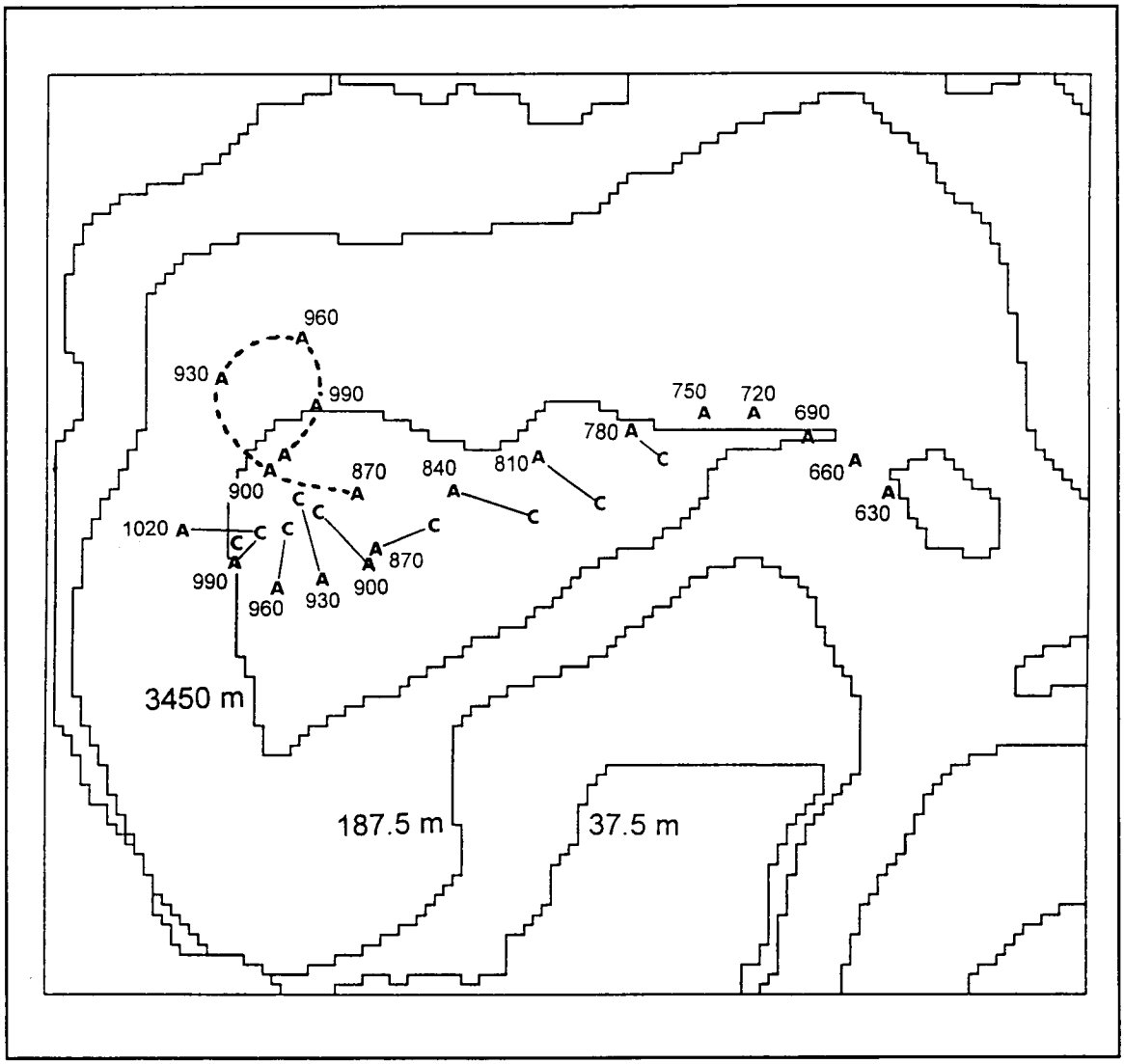

Figure 24d. Model migration paths and days of observations for surface anticyclones 'A' and deep cyclones 'C' for ring S13.

CHAPTER 4

LAST GLACIAL MAXIMUM SIMULATIONS

4.1 Introduction

There are many unknowns in modeling the circulation of past oceans. Therefore model verification needs to be done using the present-day circulation. To develop a model of a past system, we assume that the physical processes in the model remained the same, although the boundary conditions may be quite different. The past boundary conditions to be used in the paleo-circulation models should incorporate as much correct information as possible so they will best represent the past environment. Configuring the present-day model of the GOM for glacial environmental conditions required a new model grid representing the lowstand in eustatic sea level and changes in the surface temperature forcing, wind forcing, and volume flux through the Yucatan Channel. Details of all the forcing fields are described in greater detail in the following section.

4.2 Model Description

4.2.1 Model Grid

The GOM may have experienced as many as four eustatic sea-level oscillations during the last 100,000 years (Morton and Price 1987). The last sea-level cycle began with the Middle-Wisconsin high sea level estimated at 50,000-30,000 years B.P. (Morton and Price 1987). During the late Wisconsin glacial maximum, approximately 18,000 years B.P., sea level was at a lowstand and the Laurentide ice sheet over North America was at its greatest extent (Leventeer et al. 1982). Previous studies to determine relative sea-level change considered the biostratigraphy of planktonic foraminiferal assemblages from sediment cores, carbon and oxygen isotope analysis of sediment cores and seismic stratigraphy (Morton and Price 1987). The values of sea-level lowering for the GOM range from -140 m to -80 m (Bloom 1983). Suter et al. (1987) determined that sea level fell to the depth of the present shelf break (-120 to -130 m) by looking at buried fluvial systems and deltaic deposits at the shelf margin along the northern coast of the GOM.

Fairbanks (1989) reported that sea level was 121±5 m below present during the LGM based on the Barbados sea level curve, which was constructed by measuring the radiocarbon age and depth below present sea level of the Caribbean reef-crest coral *Acropora palmata*. Fairbanks (1989) had to take into account the apparent age of the sea water at Barbados and the late Quaternary mean uplift of Barbados. Another coral, *Porites asteroides*, sampled at 124 m below present sea level was determined to be 18,200 years old (Fairbanks 1989). The sea level lowering of -124 m was chosen for this study, which is the same value estimated by Curray (1965) for the GOM.

A new model grid was created to accommodate the drop in sea level. In order to continue using equally-spaced levels in the vertical, the number of levels had to be

increased from 15 to 16. The top 6 levels were changed from a thickness of 75 m to 80 m and the lower 10 levels remain 300-m thick. The total depth of the model grid is now 3480 m, which extends the deepest depth to four meters below the present-day grid. The new grid is illustrated in Figure 25 in which the present-day coastline is indicated for comparison. Since the GOM features broad, gently sloping shelves, the surface area of the GOM is dramatically reduced. This drop in sea level causes the shelves to nearly disappear, which is important in terms of air-sea exchanges of heat, momentum and moisture as well as biological productivity and sediment transport.

Although the numerical model code used in the present-day circulation study is used with few parameter changes, the viscosity and diffusivity had to be increased. Due to sea level lowering, the continental shelves essentially disappear in the LGM model grid and the upper six model levels, which are 80-m thick, impinge on the steep continental slope. The combination of high vertical resolution and steep topography causes topographically-induced numerical instabilities in the model. Although two additional passes of a double Hanning filter were used in particularly steep regions of the model grid in the upper 400 m, the viscosity and diffusivity had to be increased to 100 $m^2 \cdot s^{-1}$ each. The LGM model friction is 33% higher than the present-day seasonal simulation.

4.2.2 Wind Forcing

The wind stress estimates used to force the LGM simulations were derived from the atmospheric general circulation model of Kutzbach and Guetter (1986). In their study, the community climate model of the National Center for Atmospheric Research was configured to represent glacial maximum through interglacial environmental conditions. Changes in the following orbital parameters were incorporated in their model: date of perihelion, axial tilt and eccentricity. The effects of ice sheets, land albedo, sea ice and SST were included in the model's lower boundary conditions. The surface temperature field was derived from CLIMAP and perpetual January and perpetual July conditions were simulated. Although the model uses spectral representation of the horizontal atmospheric fields at nine levels in the vertical, the model fields are transformed into rectilinear coordinates and made available on a 4.4° by 7.5° grid in latitude and longitude, respectively. The glacial winds are interpolated to the model grid using an IMSL (1989) two-dimensional quadratic interpolation algorithm.

The LGM wind stress estimates are very different from the present-day wind fields over the GOM. A comparison of the Sverdrup volume transport in the GOM computed using present-day and LGM wind stress estimates was made to predict how the circulation in the GOM might have changed based solely on differences in the wind fields. The present-day wind-driven circulation is discussed first and then the predicted wind-driven circulation for the LGM is described.

The direction of the present-day winter wind stress is northeasterly over most of the GOM, except over the Campeche Basin where the winds are northerly (Figure 26). The magnitude of the winter wind stress is fairly uniform over most of the GOM with

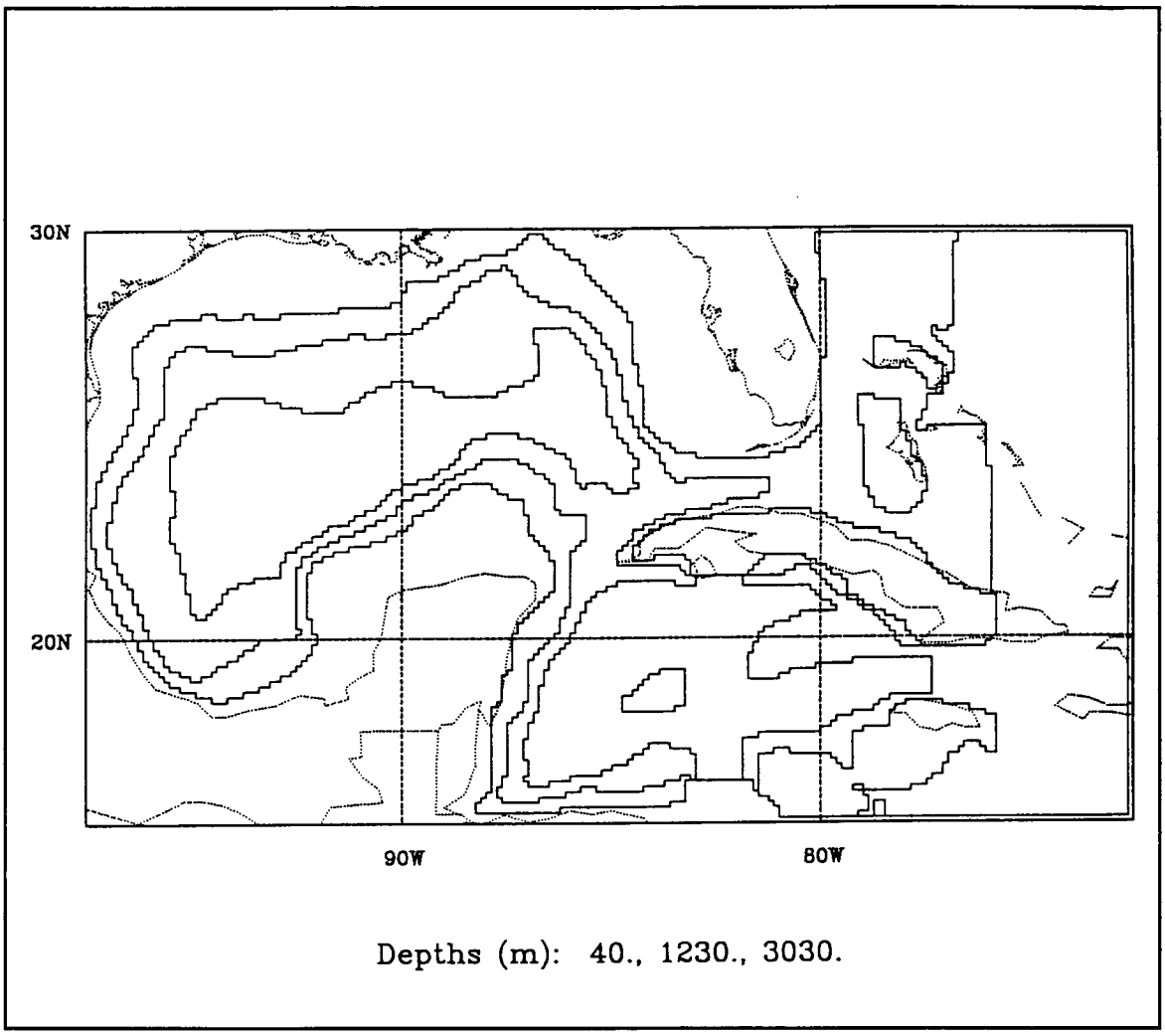

Figure 25. The last glacial maximum model grid. Solid lines represent model grid levels. Stippled line represents present-day observed coastline.

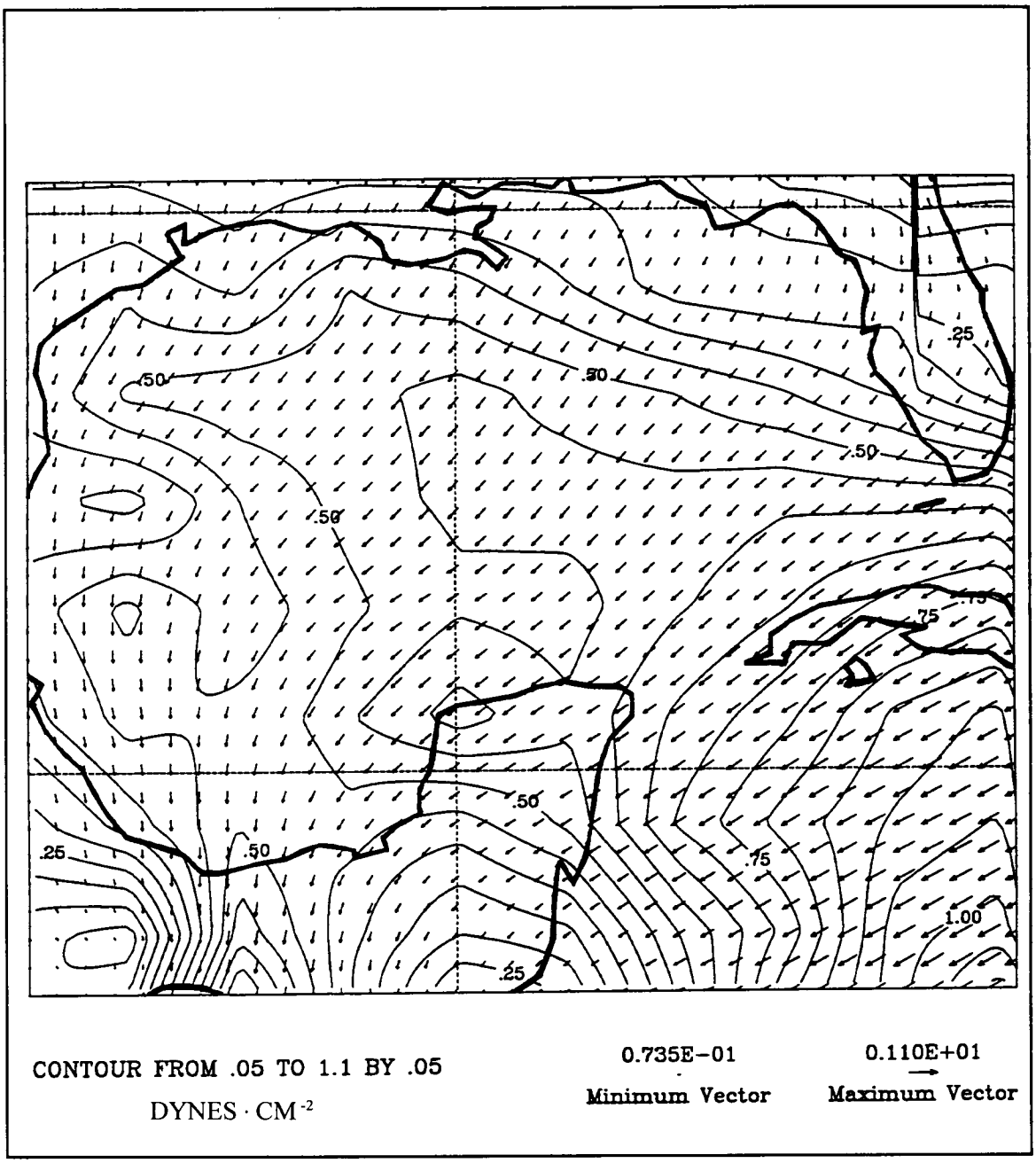

Figure 26. Hellerman and Rosenstein (1983) January wind stress field interpolated to 1/8° grid.

maximum values found over the southern Straits of Florida. The present-day Sverdrup volume transport for the GOM computed using the Hellerman and Rosenstein (1983) January wind stress indicates potential for a weak western boundary current along the Texas coast of 4.0 Sv and a broad return flow region over the entire northern GOM (Figure 27). There is also potential for a cyclonic gyre (1.25 Sv) in the Campeche Basin.

The present-day July wind field is characterized by mainly southeasterly winds in the northern GOM and easterly winds near the Yucatan peninsula and in the Campeche Bay (Figure 28). The strongest winds are in the northwestern GOM and very weak winds are observed over the northern part of the west Florida Shelf. The curl of the wind stress is greater in July and results in a stronger WBC from 21°N to the northern boundary with maximum transport of 5.75 Sv and a return flow region that reaches the west Florida shelf (Figure 29). There is potential for a very weak cyclonic gyre (.75 Sv) in the Campeche Basin. These Sverdrup volume transport calculations are in keeping with the findings of Sturges and Blaha (1976), Sturges (1994), and the present-day seasonal simulations discussed in the previous section.

The LGM wind field computed by Kutzbach and Guetter (1986) is much stronger than the present and shows greater seasonal variability. The LGM winter wind field was characterized by northeasterly winds over the Yucatan Peninsula with a maximum magnitude of 1.4 dynes·cm^{-2} along the western coast compared to .6 dynes·cm^{-2} for the present-day January wind field (Figure 30). The potential existed for upwelling along the northern and western Yucatan coast. The westerlies were displaced southward during the LGM winter and the northern half of the glacial GOM is also subject to upwelling favorable winds. The Sverdrup volume transport computed with the LGM winter winds indicates that a strong WBC (8 Sv) originated in the Campeche Basin (Figure 31). Weaker zonal bands of anticyclonic circulation are predicted for the northern GOM, but no organized WBC is predicted for the northern half of the basin.

The summer LGM wind field was similar in direction to the present-day wind stress field, but the magnitudes were much stronger (more than double in some areas) and the pattern of wind stress magnitude contrasts the present-day pattern (Figure 32). Easterly winds in the Campeche Bay during the present-day summer have a maximum magnitude of less than .7 dynes·cm^{-2}. During the LGM summer very strong northeasterly winds were present in the Campeche Bay with a maximum magnitude of nearly 1.8 dynes·cm^{-2}. The western Yucatan Coast was subject to more intense upwelling favorable winds in the LGM summer than during the LGM winter. There are very weak southeasterly winds over the present-day northeastern GOM for July, in contrast to very strong easterly winds during the LGM. During the LGM summer there was potential for a strong WBC to originate in the Campeche Basin, as in the LGM winter (Figure 33). The Sverdrup calculations predict a northern GOM characterized by alternating bands of cyclonic and anticyclonic circulation.

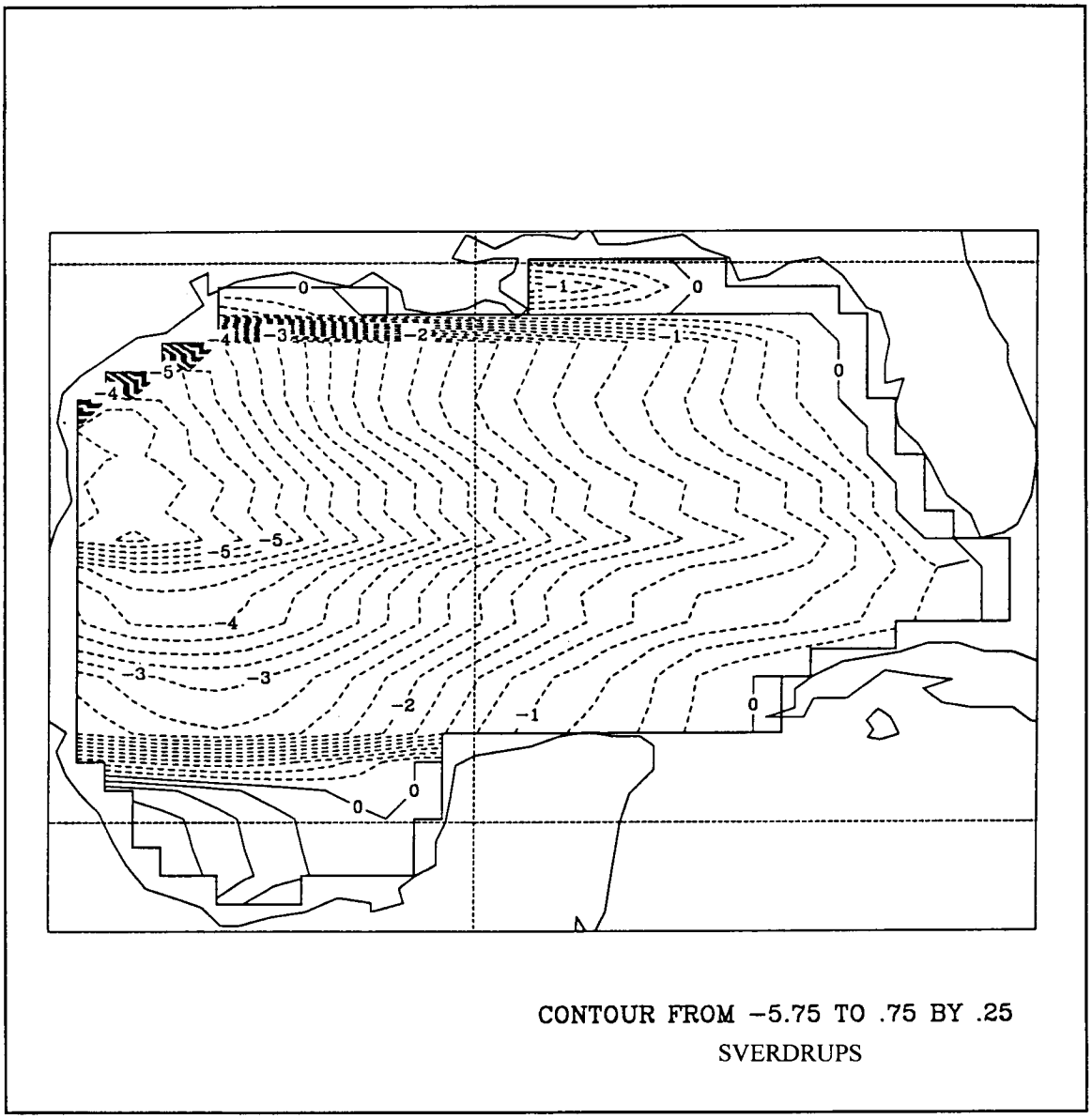

Figure 27. Sverdrup volume transport for the Gulf of Mexico computed using Hellerman and Rosenstein (1983) January wind stress field.

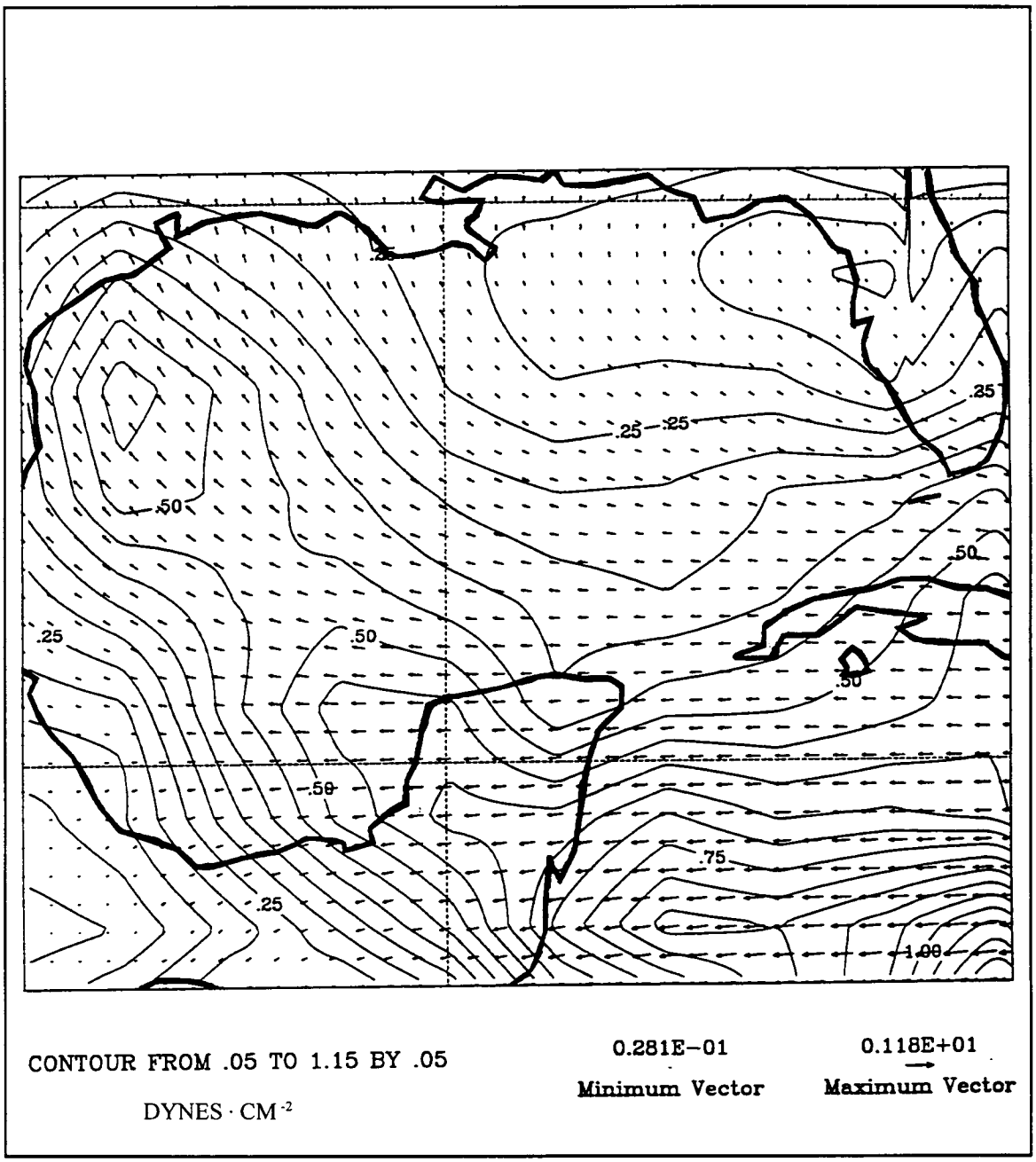

Figure 28. Hellerman and Rosenstein (1983) July wind stress field interpolated to 1/8° grid.

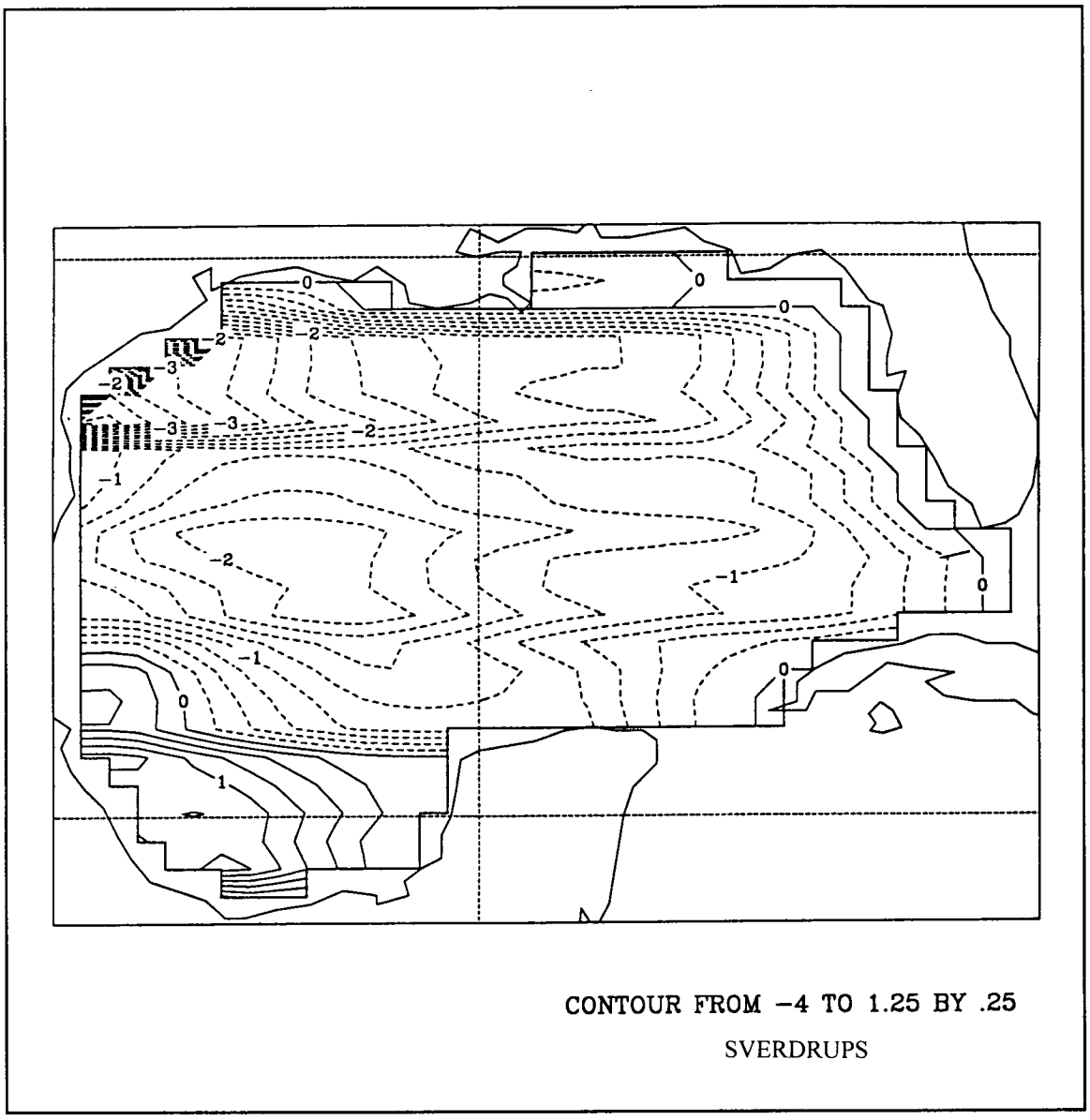

Figure 29. Sverdrup volume transport for the Gulf of Mexico computed using Hellerman and Rosenstein (1983) July wind stress field.

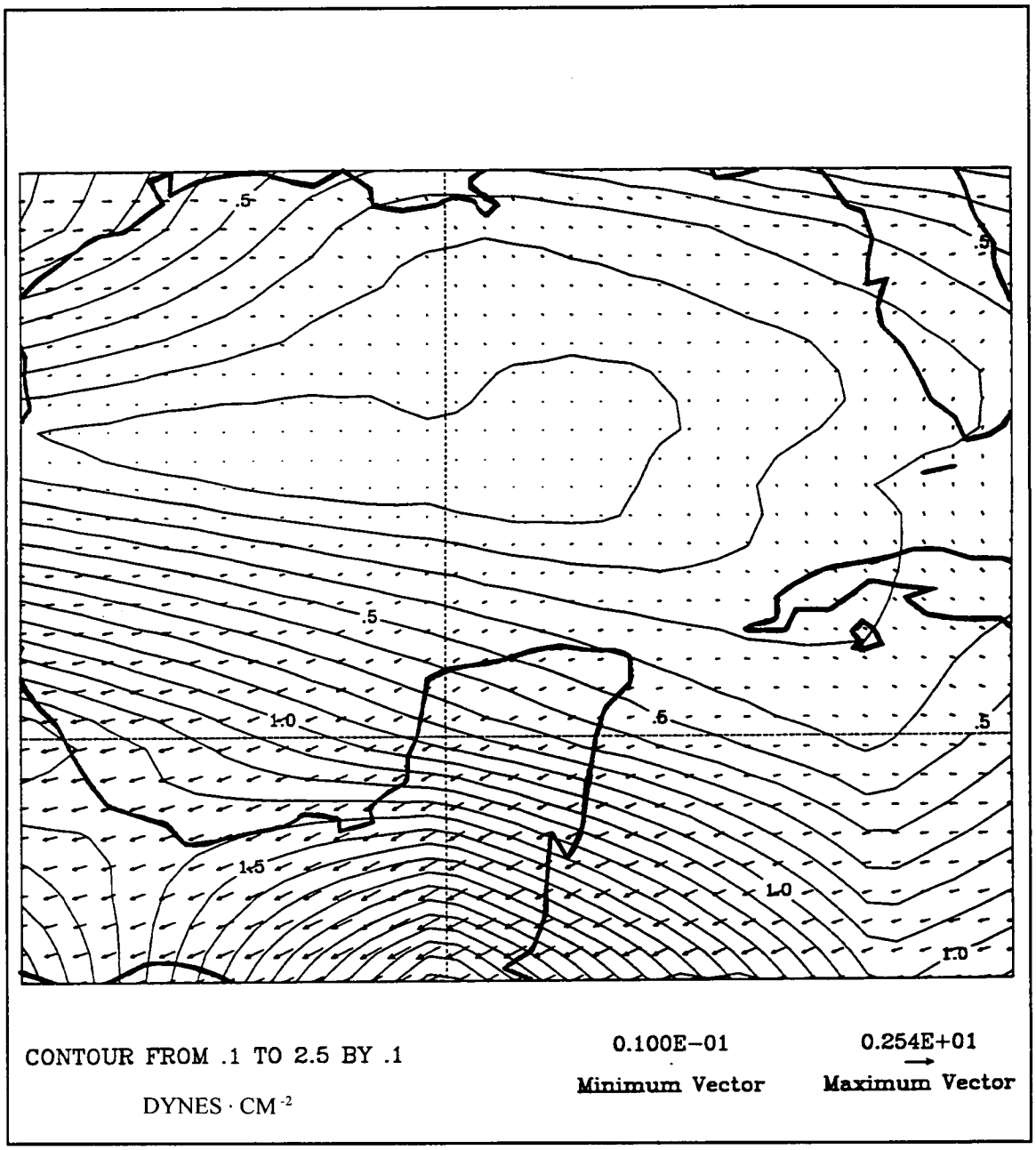

Figure 30. January wind stress field for 18 ka computed by Kutzbach and Guetter (1985) glacial atmospheric general circulation model.

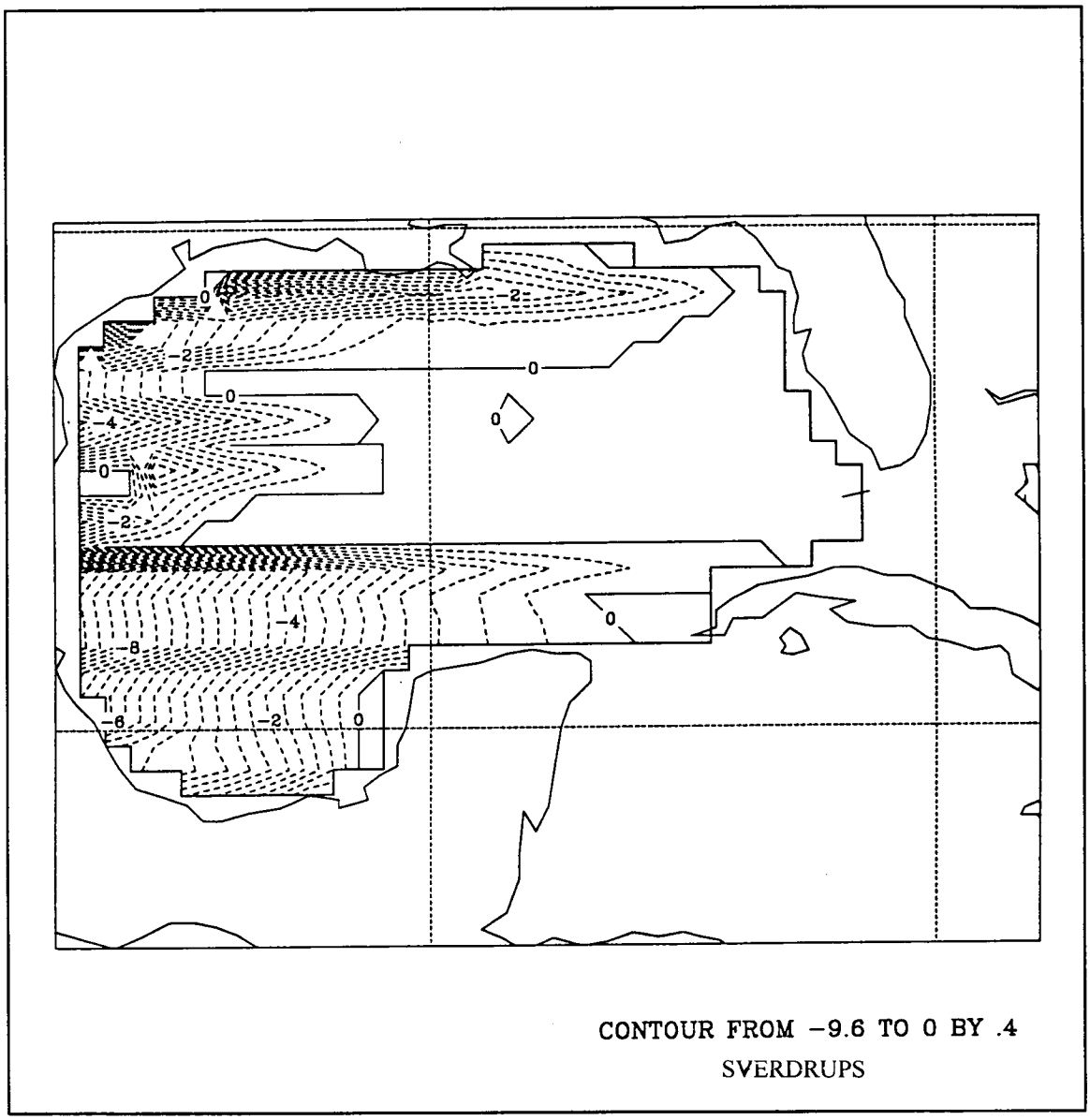

Figure 31. Sverdrup volume transport for the Gulf of Mexico computed using Kutzbach and Guetter (1985) January glacial wind stress estimates.

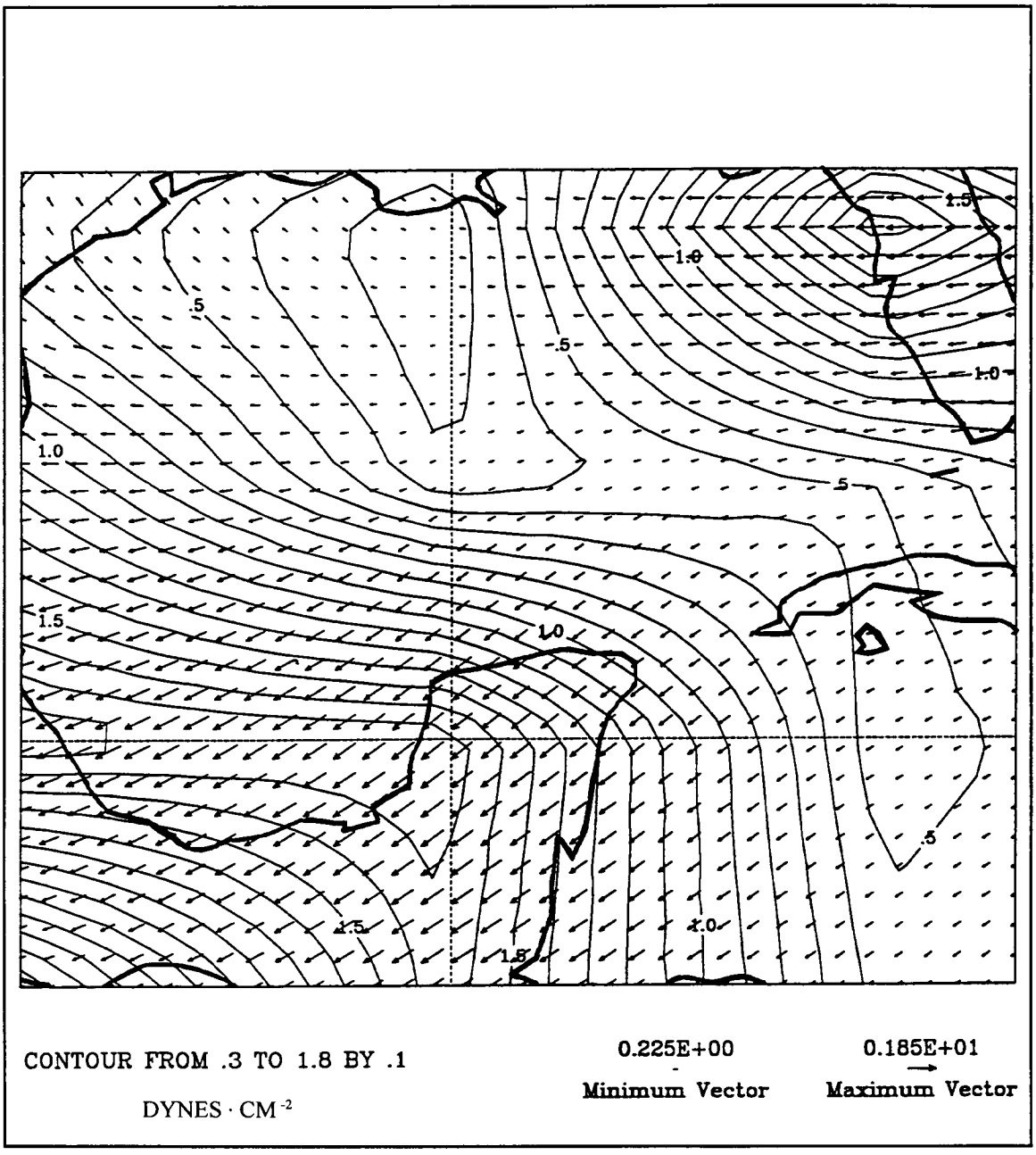

Figure 32. July wind stress field for 18 ka computed by Kutzbach and Guetter (1985) glacial atmospheric general circulation model.

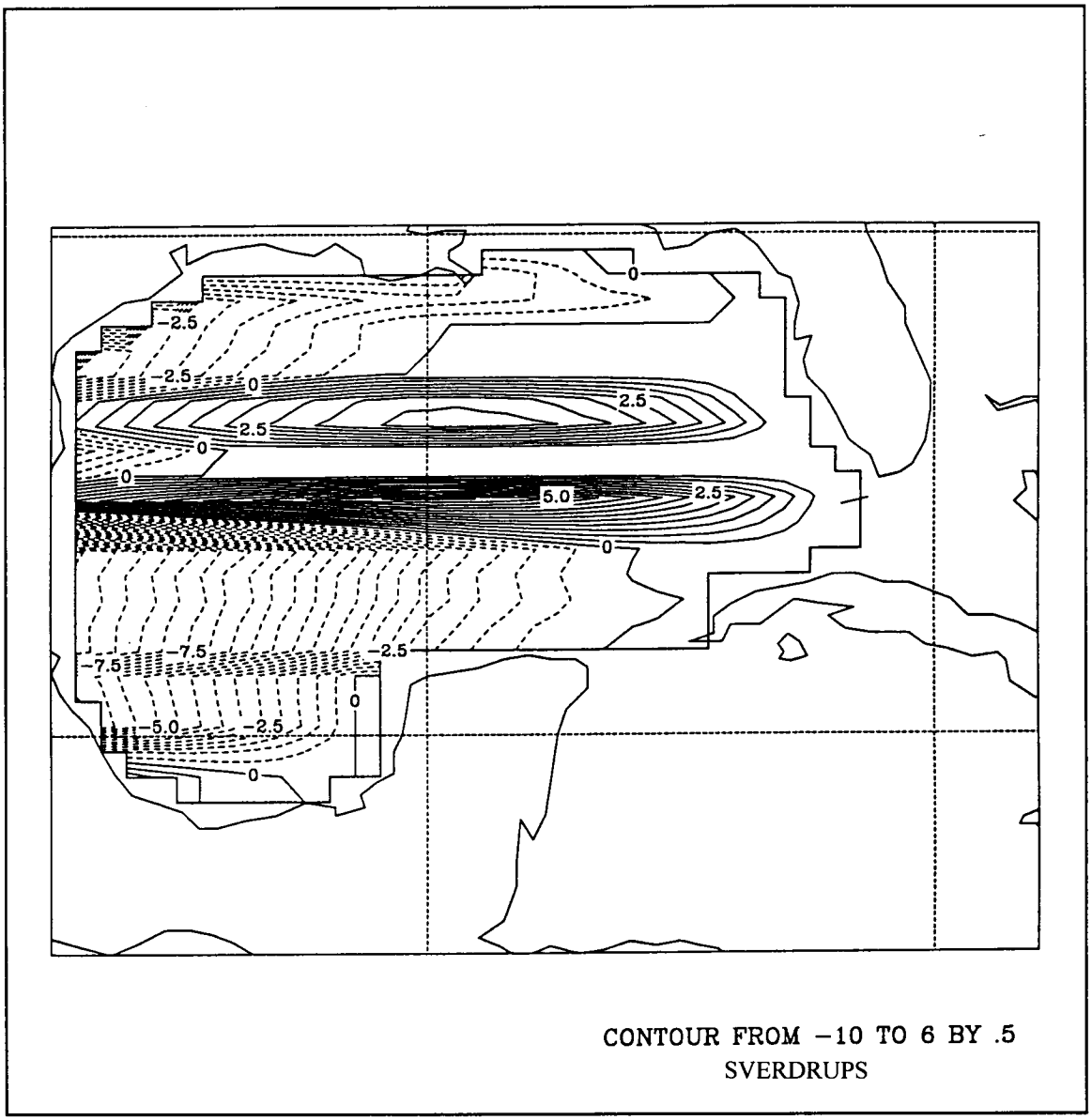

Figure 33. Sverdrup volume transport for the Gulf of Mexico computed using Kutzbach and Guetter (1985) July glacial wind stress estimates.

4.2.3 Sea-Surface Temperature

The CLIMAP SST for the LGM are used for the surface boundary condition on temperature. The CLIMAP data was created using sophisticated statistical techniques to infer glacial SST from abundance counts of fossil planktonic foraminifera found in the deep-sea sediments (CLIMAP 1981). These temperature estimates have been found by some authors to be too warm in the low latitudes (Rind and Peteet 1985), but the CLIMAP data is chosen for this study because it presently has the best spatial resolution and geographic coverage available for the GOM. The effect of using cooler SST values could also be analyzed using this numerical model, but the original CLIMAP values are used.

The CLIMAP data is available on a 2° grid and then extrapolated to the model coastline and interpolated to ⅛° using the IMSL (1989) two-dimensional quadratic interpolation algorithm and smoothed using a Hanning filter. Since the CLIMAP data represents true surface values, a constant was subtracted from each data point to compute the temperature field at the midpoint of the uppermost level (40 m) in the model. The constant was equal to the area-average decrease in temperature from the surface to 40 m for the Levitus data, which was 2.0°C for summer and .7°C for winter.

This next section compares the present-day and LGM estimates of SST in an effort to forecast differences in the surface circulation in the GOM that are related to lateral gradients in temperature. Both present and LGM winter temperature fields feature a north-south temperature gradient in the northern GOM that would result from wintertime atmospheric cooling (Figure 34). The maximum temperatures are nearly 5°C lower than present in the western Caribbean. Cooler temperatures along the eastern Yucatan Coast in both the present and LGM suggest upwelling along the western side of the Yucatan Current. The winter CLIMAP data has minimum temperatures less than 1°C lower than the present in the western GOM, and a large anticyclonic gyre is indicated in the western GOM that is not indicated by the present SST field.

The present-day and LGM summer SST fields are qualitatively similar (Figure 35). The temperature gradients are oriented more meridionally in the western and central Gulf in the summer than winter for both present and LGM. Although the present-day high temperatures are located on the extreme eastern and western boundaries of the GOM, the maximum temperatures in the LGM occur in the center of the large anticyclonic gyre in the western GOM. Both summer and winter CLIMAP SST fields indicate that there is a source of warm surface waters to the western GOM. It may be inferred from the gradient in temperature and salinity oriented toward the perimeter of the basin that a large anticyclonic circulation cell existed in the western basin. It is important to note that although the glacial temperature estimates represent a given season, the sampling interval within the sediment core can encompass a span of hundreds to thousands of years. The anticyclonic circulation inferred from the glacial estimates of temperature and salinity may not be due to a single persistent circulation feature, but could be due to a composite of smaller scale processes averaged over time. The seasonal averages presented in a later section are computed for only four years of model output.

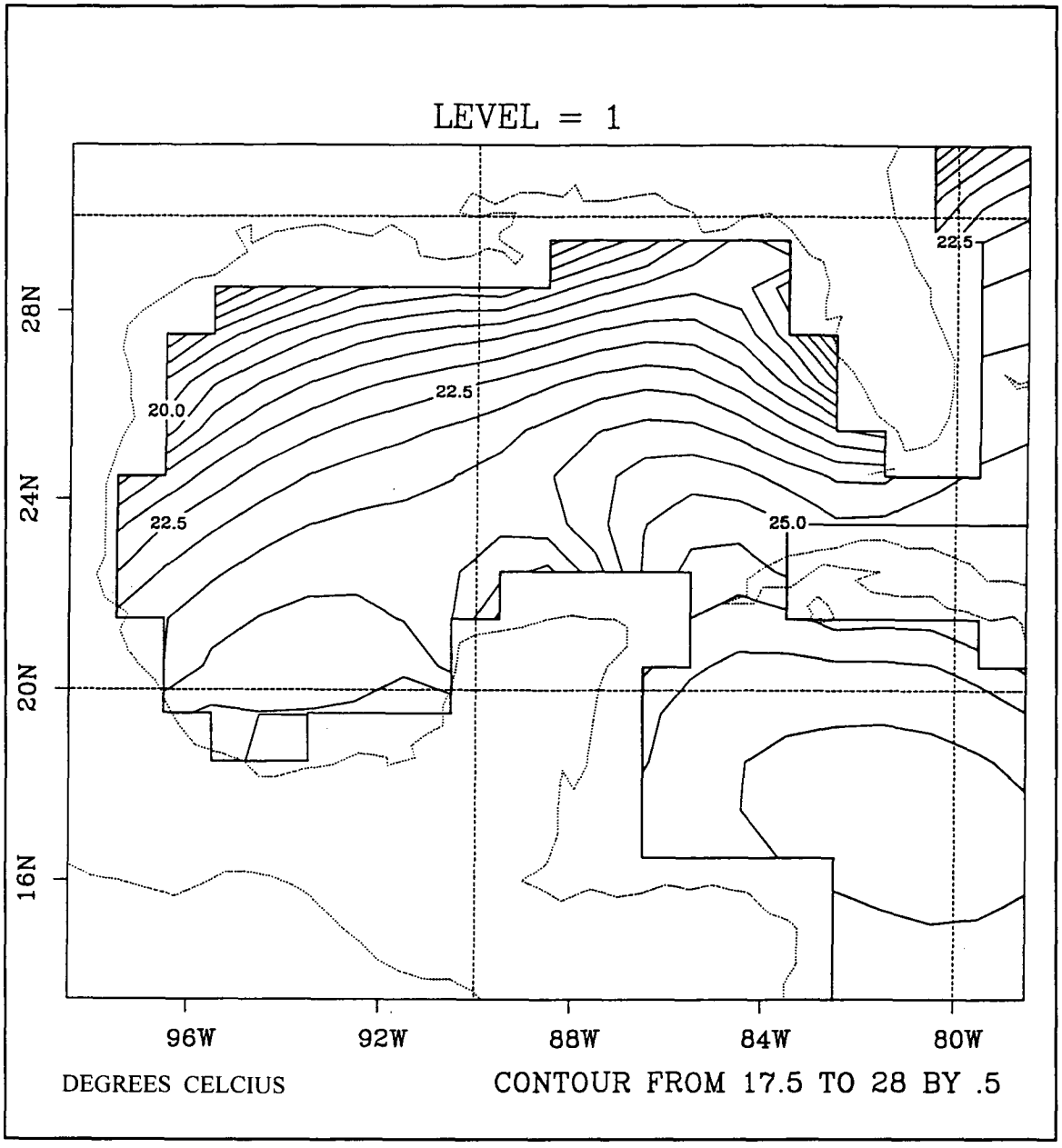

Figure 34a. Winter sea-surface temperature for the Gulf of Mexico from Levitus seasonal mean climatology (1982).

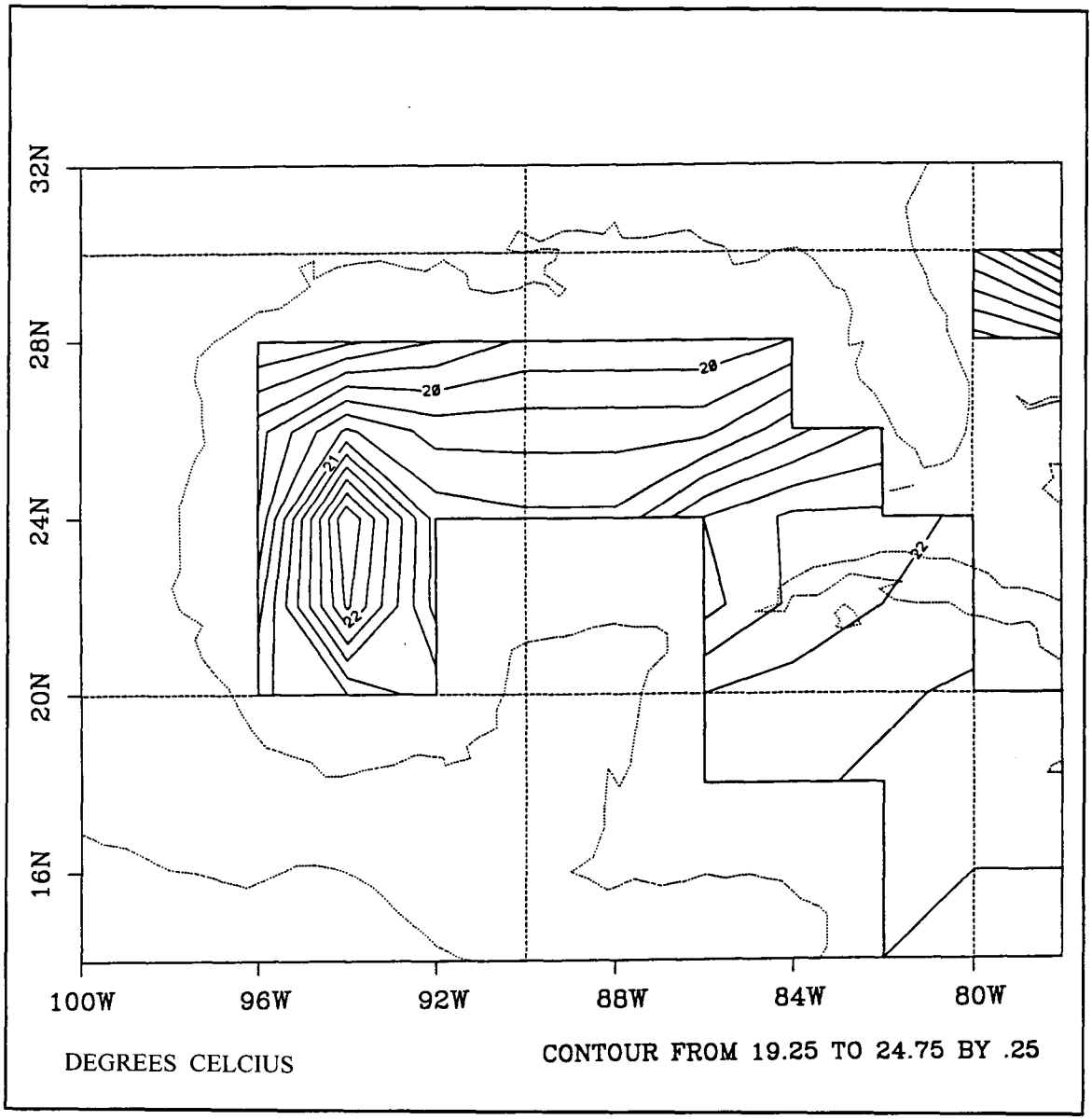

Figure 34b. Winter sea-surface temperature for the Gulf of Mexico from CLIMAP estimates (1976) for 18,000 years B.P.

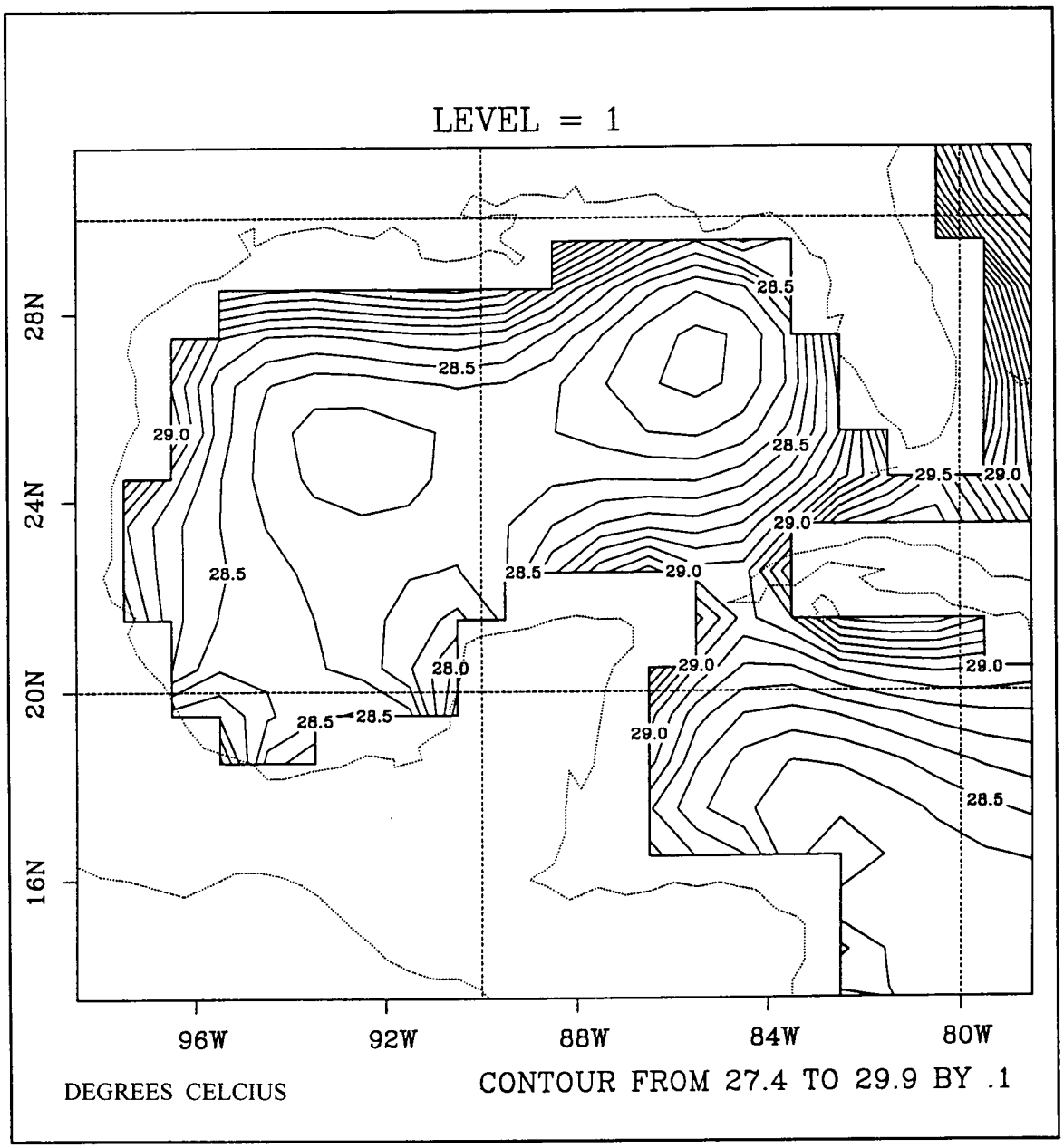

Figure 35a. Summer sea-surface temperature for the Gulf of Mexico from Levitus seasonal mean climatology (1982).

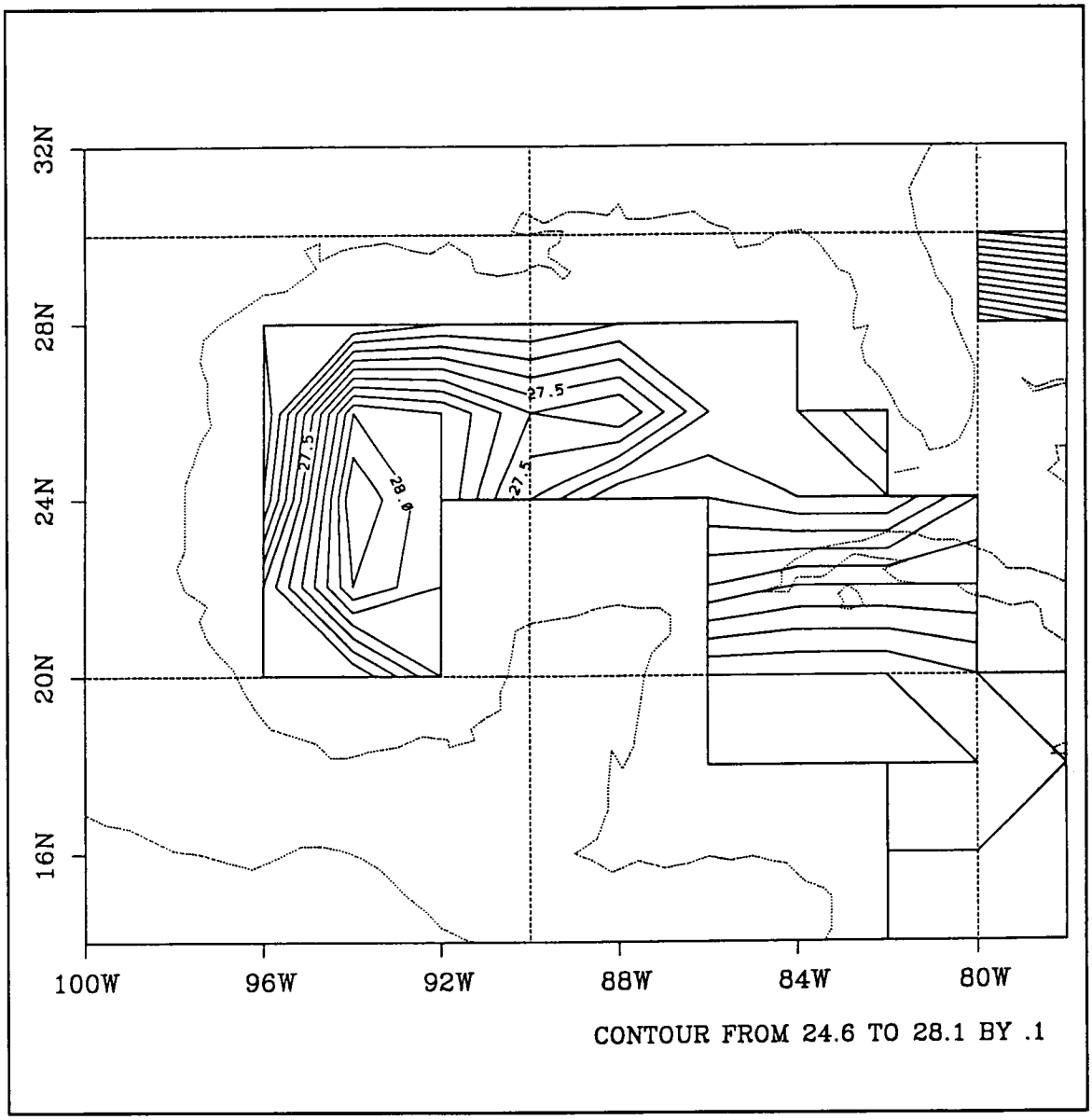

Figure 35b. Summer sea-surface temperature for the Gulf of Mexico from CLIMAP estimates (1976) for 18,000 years B.P.

4.2.4 Geostrophic Forcing

Forcing the inflow through the Yucatan Channel from the Caribbean is an integral part of this modeling study. The present-day inflow condition is based on measurements of the volume transport through the Florida Straits (SAIC 1992; Schott et al. 1988) and temperature-partitioning analysis of hydrographic data in the North Atlantic (Schmitz et al. 1992). The purpose for relaxing the temperature and salinities along a north-south vertical transect in the western Caribbean is to approximate the baroclinic shear corresponding to the observed geostrophic flow, and thus simulating the observed contributions of the individual water masses.

Without direct estimates of the LGM volume transport through the Florida Straits or a quantitative model of the global thermohaline circulation during the LGM, how can the correct inflow condition be specified? This modeling study does not attempt to define an optimum inflow condition for the LGM. Instead, two extreme inflow conditions are assumed that represent minimum and maximum estimated volume transports through the Florida Straits during the LGM. The two inflow conditions used to force the model are based on the present-day observed transport of the Florida Current, the sources of the Florida Current, the present-day and LGM wind field and the change in sill depths and widths of the passages into the Caribbean. Details of the method used to derive the minimum inflow condition are presented in Appendix B.

The LGM simulations are divided into two cases featuring the two extreme inflow conditions through the Yucatan Channel. The low transport case uses the minimum inflow condition based on the lower than present-day annual average wind-driven component of the Florida Current during the LGM (see Appendix B). The present-day annual average wind-driven component of the Florida Current is 17-18 Sv and annual average for the LGM is 12 Sv, which is a reduction of 33%. The minimum inflow condition is achieved by targeting the volume transport through the Yucatan Channel to attain an annual average equal to 67% of the annual mean volume transport of 28 Sv used in the present-day seasonal simulations. Therefore, the target annual mean volume transport through the Yucatan Channel in the LGM simulations for the low transport case is 19 Sv.

The maximum inflow condition is set equal to the present-day annual mean transport of the Florida Current. This condition can be justified, although some previous studies suggested stronger inflow into the Caribbean (e.g., Brunner and Cooley 1976; Brunner 1982; Brunner 1986). The intensity of the LGM trade winds over the Atlantic was stronger than present, which would likely have resulted in a stronger equatorial current system. However, there is no evidence that volume transport into the Caribbean increased (Lautenschlager et al. 1992). Due to the fall in sea level the sill depths of the passages were shallower and the passages were narrower, which would require much higher velocities through the passages to produce the same volume transport as present. The LGM high volume transport case uses the maximum inflow condition, which is achieved by setting the target annual mean volume transport through the Yucatan Channel to approximately 28 Sv.

4.3 High-Volume Transport Case

The amount of *u*-velocity added in the Caribbean was greatly increased in the high volume transport case because the cross-sectional area of forcing region and of the Yucatan Channel were smaller and larger velocities were required to produce a volume transport equal to the present-day model simulations. During the four years of model spin-up, an annual average volume transport of 28.4 Sv through the Straits of Florida was achieved. This is slightly higher than the annual average of 27.71 Sv from the present-day simulation.

4.3.1 Loop Current Rings

After 4 years of model spin-up, four years of model simulations were made with high transport and during this time there were eight rings shed by the LC, of which six entire life spans were observed (refer to Table 1). Although the LC appears to be more constrained by the coastline in the LGM simulations, the process of ring separation is not much different than the present. The geographic location of the ring separations is the same, as well as the 30-week ring-separation period. These results seem reasonable since the bottom bathymetry below 124 m for the present-day is unchanged from the LGM bathymetry and the volume transport for the LGM high transport case is unchanged from the present-day simulations.

Several characteristics of the six rings are summarized in Table 3. A comparison of Table 2 and Table 3 indicates that the LGM rings in the high-transport case are slightly smaller, slightly faster and have a slightly longer life span that the present-day rings. The migration paths of the LGM rings are somewhat different in the high-transport case, which may help explain the longer life spans. Of the six migration paths observed, there appeared to be only two main routes (Figure 36). The southerly route is very similar to the present-day migration path 1 and the northerly route is like the present-day migration path 3. Both of the rings that followed the northerly route partially merged with rings that were already present in the northwest GOM, as occurs in the present-day simulation. Unlike the present-day case where all rings following migration path 2 were likely to split, the only ring to split in the high-transport case was following the northerly route. The fact that only one ring splits and that the timing and location of the event were different from the present-day case, may be partly influenced by the higher eddy viscosity in the LGM simulations.

Once the rings reach the western wall in the LGM high transport simulations they all move along the Mexico slope into the northwest corner, but not as rapidly as in the present-day case. All rings decay in the northwest corner and none are advected eastward in the shelf break current as in the present-day case. Also no model rings decay over the Mexico slope as occurs in the present-day simulation. All these factors contribute to the longer life spans of the rings in the high-transport case of the LGM simulations. Since the rings have longer life spans and similar shedding frequency, there are more rings in

Table 3. Characteristics of model Loop Current rings for the LGM high transport case.

Ring	Size [1] (km)	Migration Speed (km d^{-1})	(cm s^{-1})	Time to W. Wall [2] (days)	Lifespan (days)	Ring Interaction
H1	360	4.22	4.88	210	385	none
H2	340	4.24	4.90	231	483	none
H3	340	3.90	4.52	252	294	none
H4	340	4.55	5.26	294	483	split
H5	340	4.18	4.84	294	315	none
H6	376	4.90	5.68	168	315	merge
H7	346					
Mean	349	4.33	5.01	242	380	
Std. dev.	14.0	0.35	0.40	49.2	86.1	

[1] Approximate diameter in the eastern GOM. Meaxured by taking an average of the north-south and east-west dimensions of each ring.

[2] Time to western wall is a visual estimate of the number of days that each ring took from just after separation to reach the outer shelf of the Mexico or Texas coast. The arrival of the ring at the western wall is characterized by some deformation of the ring, typically marked by a north-south elongation of the ring.

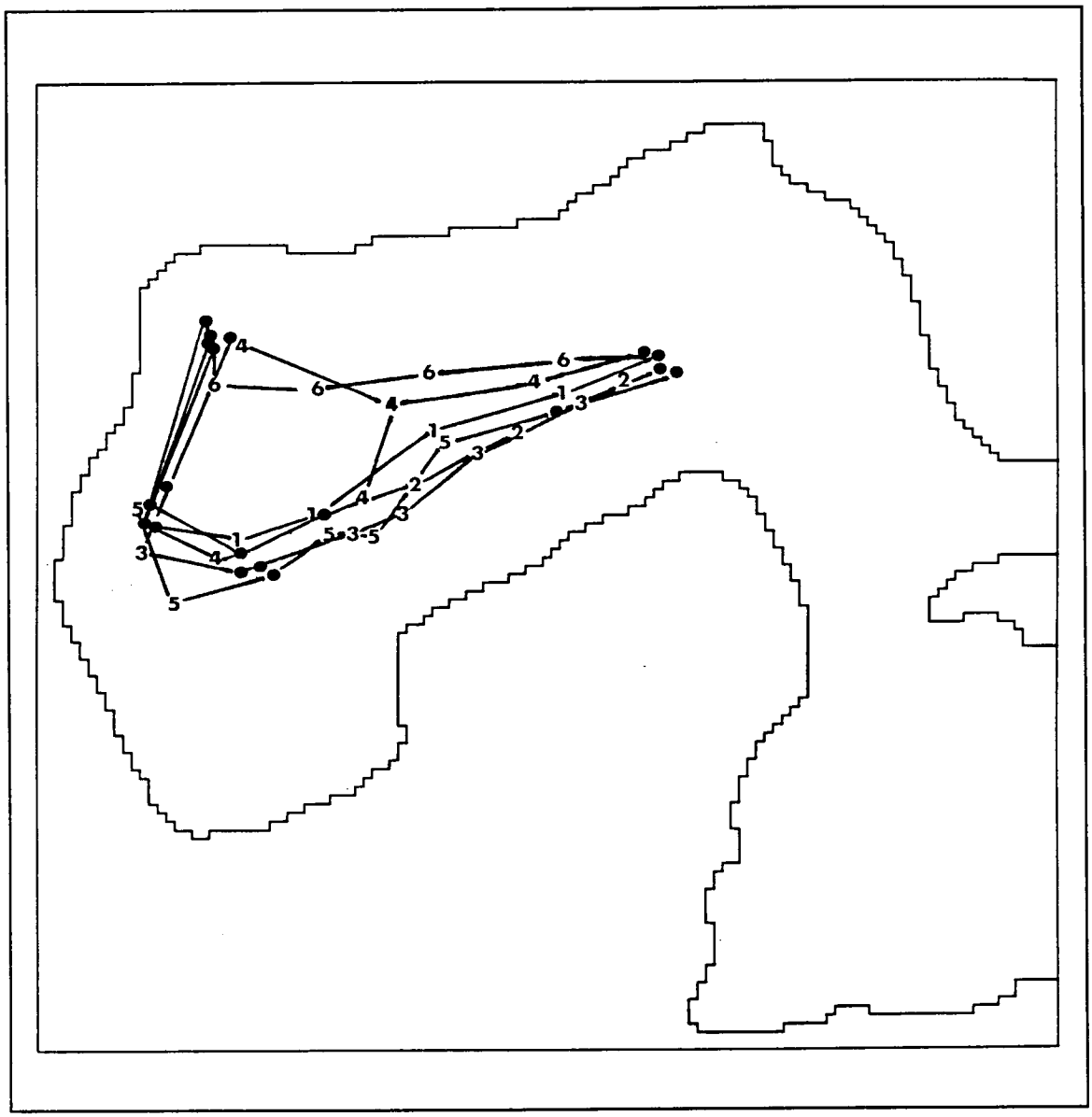

Figure 36. Model migration paths of Loop Current rings H1-H6 during the four-year simulation of the LGM high transport case.

the western GOM at one time than the present. The presence of the rings and the induced circulation associated with the rings, such as eddy-pairs, results in a western GOM characterized by more eddy activity than the present-day (Figure 37).

It should be noted that the density shear of the LC is derived from forcing with the present-day hydrographic data, we therefore do not attempt to verify vertical structure of the LGM rings, for which no observations are available. However, the temporal changes in the vertical structure of the rings may be worth noting, since the surface wind stress during the LGM was much greater and presumably resulted in a deeper mixed layer. Vertical cross-sections through the centers of rings H2 and H3 show that the high salinity core is present in the LC at approximately 200-m depth, although it is less saline than present (Figure 38). The high salinity core of ring H3 degrades rapidly, which is accompanied by a flattening of the isohalines, and is almost gone by the time the ring reaches the central GOM (Figure 38). Vertical cross-sections of temperature through the centers of H2 and H3 show similar structure to present-day rings, although the isotherms in the upper 200 m flatten-out to a greater degree than observed today (Figure 39).

4.3.2 General Circulation

The circulation in the eastern GOM during the LGM is dominated by the boundary fluctuations and ring separation process of the LC as occurs in the present-day GOM. As mentioned previously the LC behaved much like today and rings separate in approximately the same location with the same frequency. The more vigorous forcing for the high volume transport case resulted in higher velocities with depth in the Yucatan Current, LC and rings. Upwelling occurs along the eastern side of the Yucatan Peninsula as seen in the present-day simulations due to the strong velocities in the Yucatan Current impinging on the Yucatan Slope. The upwelling causes the western branch of the LC to be much cooler than the warmer surface waters of the central GOM during summer and can result in a ring that is cooler than the surrounding water at the surface (Figure 40).

The volume transport of the Florida Current ranges from 26.5 Sv to 30.5 Sv with a minimum in the summer and a maximum in the winter (Figure 41). This seasonal fluctuation in volume transport is out of phase with the present-day cycle which has its maximum in June.

The surface area of the eastern GOM was greatly diminished during the LGM because of the disappearance of the west Florida Shelf. The Dry Tortugas and Florida Keys become merged with the Florida Peninsula and the land boundary of Cuba is extended northward to create a relatively long and narrow southern Straits of Florida. The Tortugas gyre forms in the LGM simulation when the LC is fully extended as it does in the present-day simulation, but the narrowing of the southern Straits of Florida causes it to decay very rapidly after a ring has separated from the LC. The surface currents in the northeast GOM are weak and variable and appear to be strongly influenced by the boundary fluctuations in the LC.

The western GOM exhibits the greatest changes in circulation compared to the present. As already noted, there is a greater degree of eddy activity, but there are some

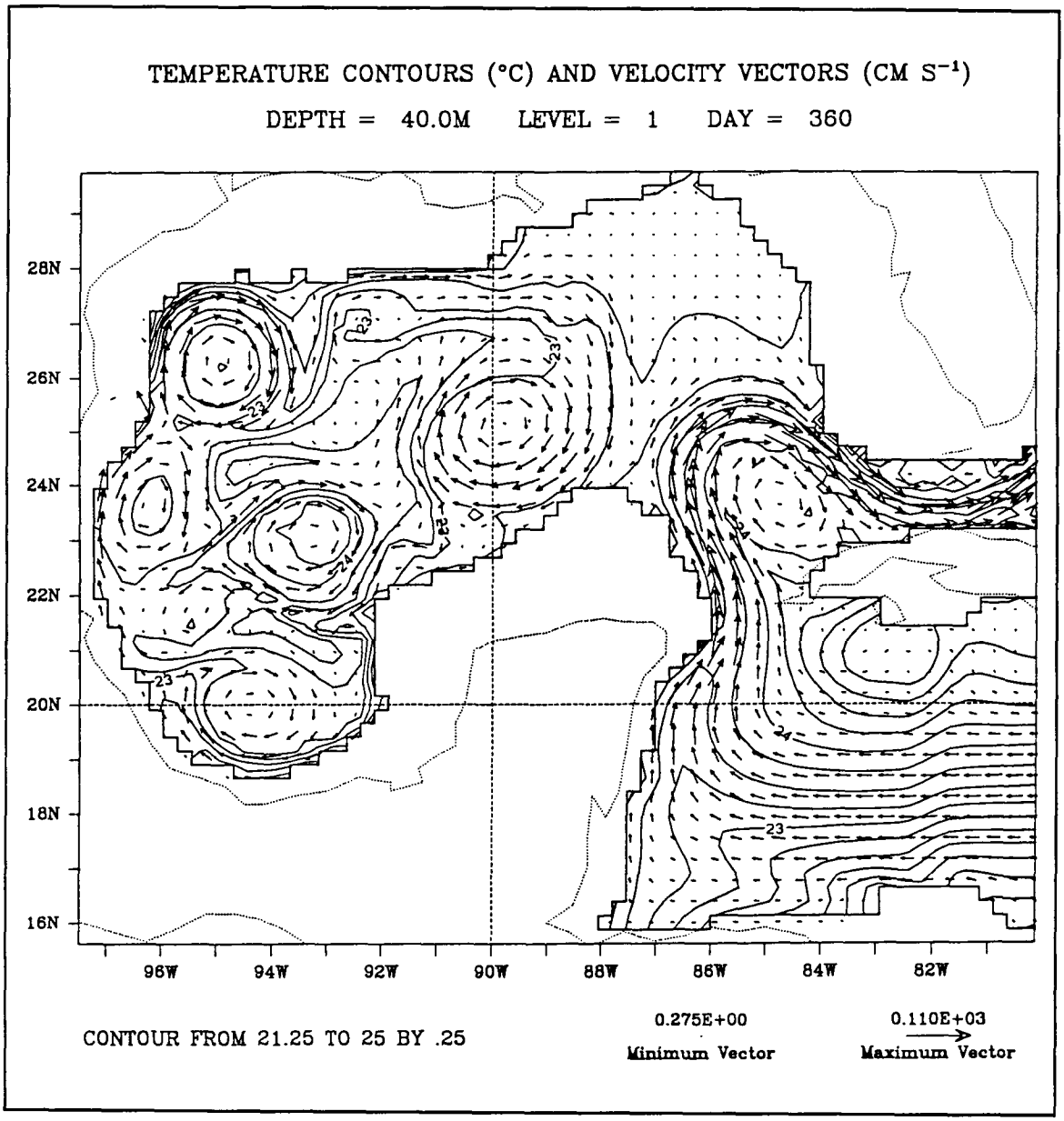

Figure 37. Level 1 (40 m) temperature and velocity fields for the LGM high transport case at model day 360 (November). Ring H2 has just separated from the Loop Current.

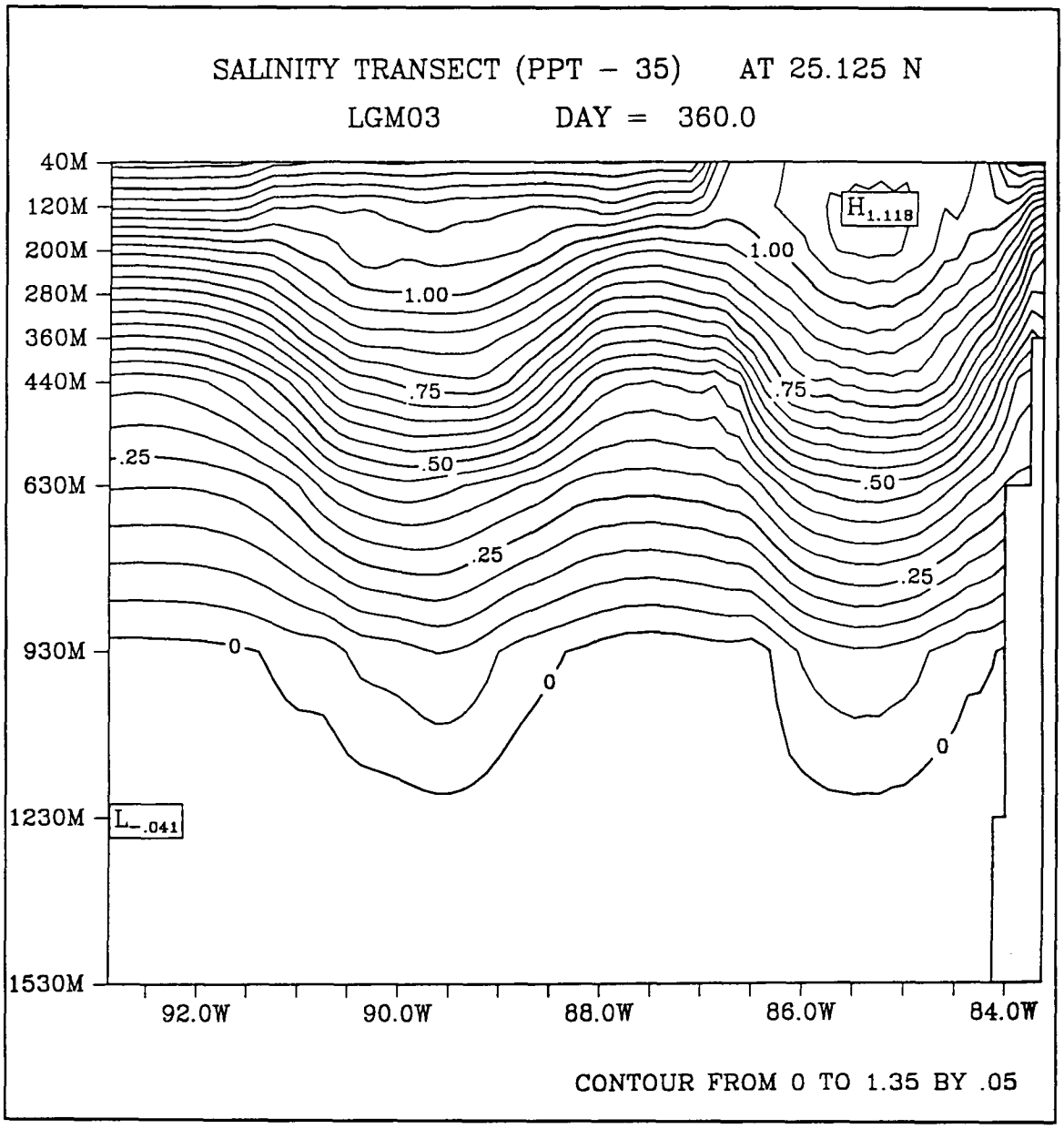

Figure 38a. Vertical cross-section of salinity (ppt-35) from the LGM high transport case through the Loop Current and ring H2 at model day 360 (November).

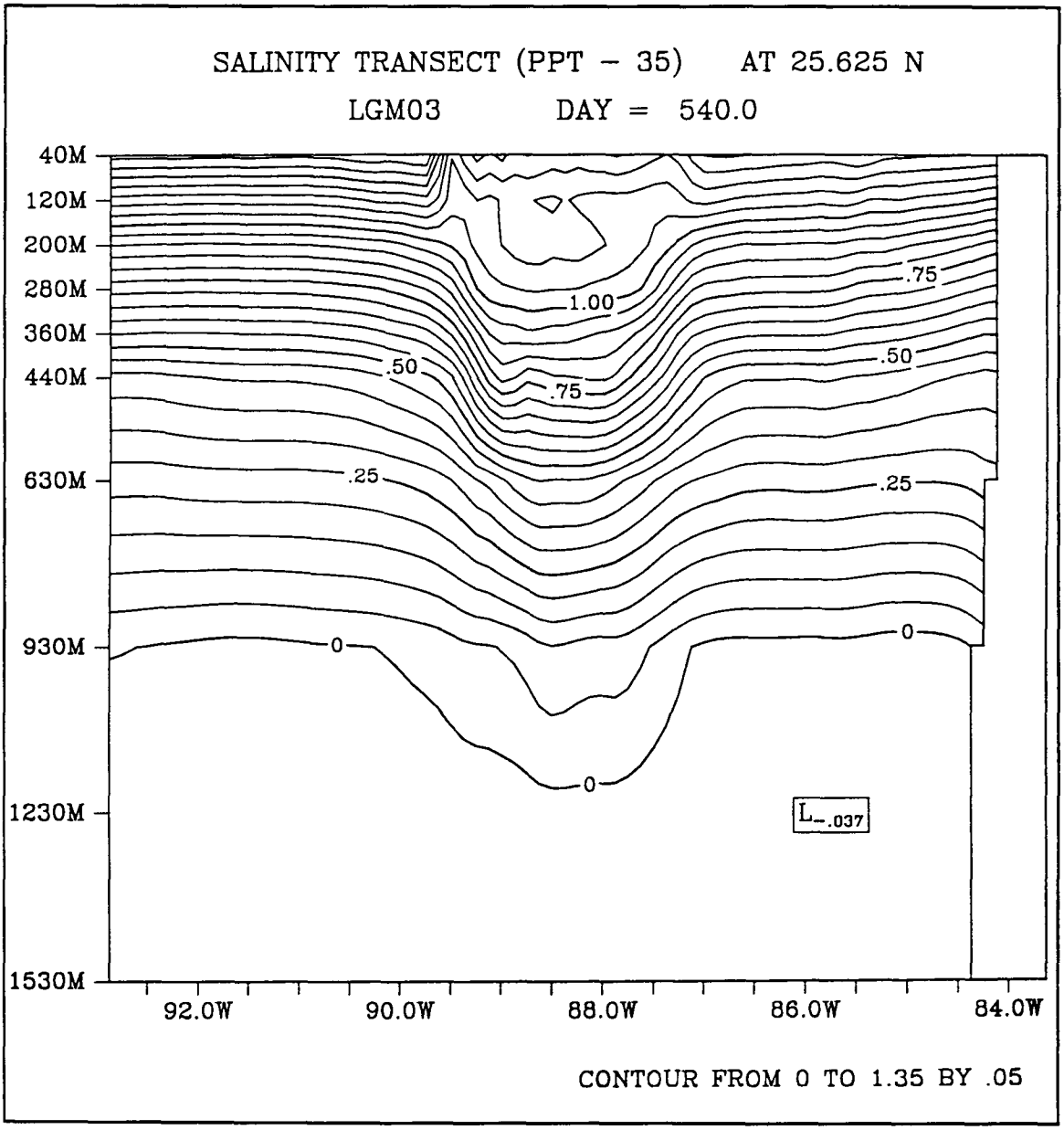

Figure 38b. Vertical cross-section of salinity (ppt-35) from the LGM high transport case through ring H3 on model day 540 (May).

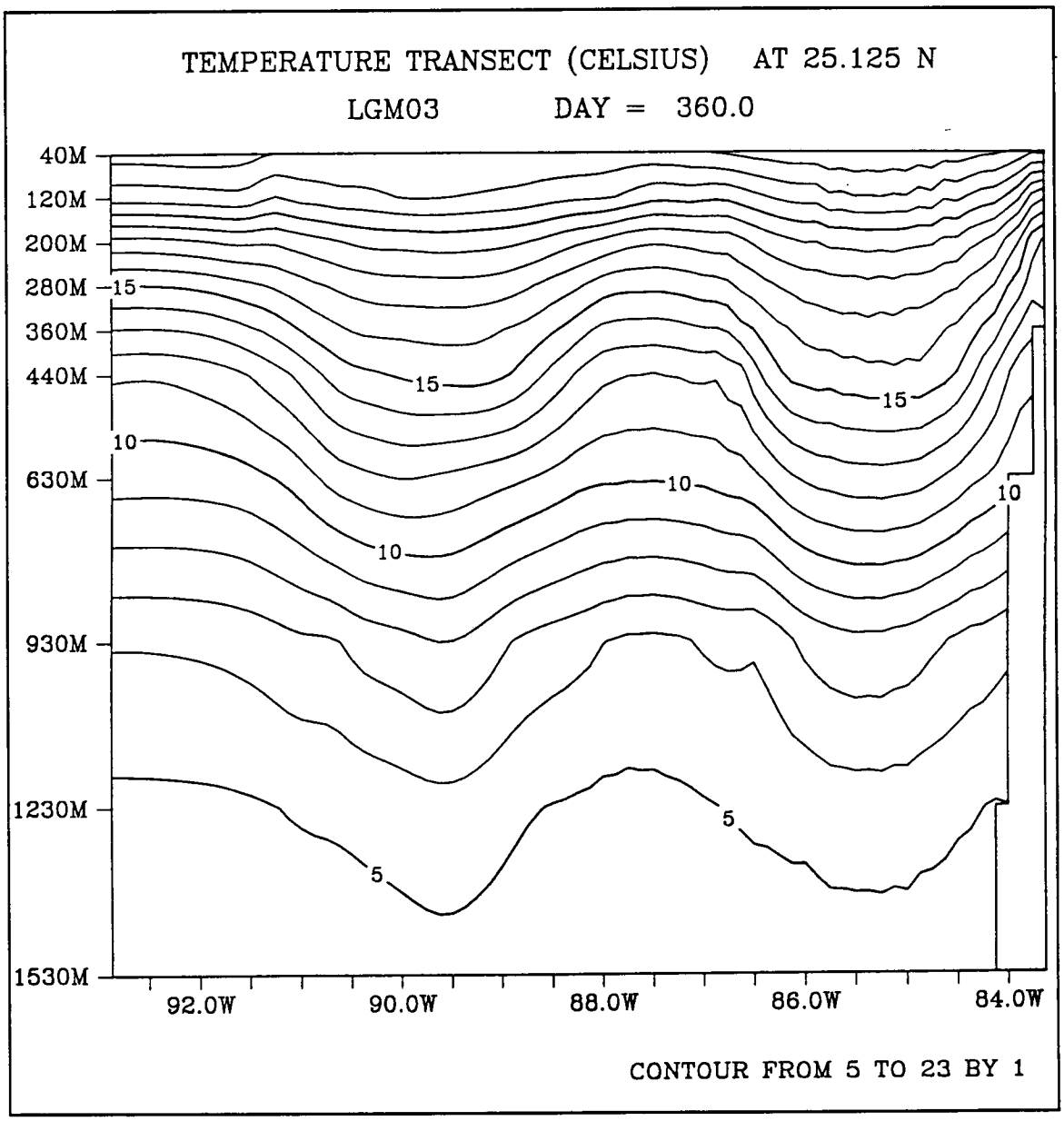

Figure 39. Vertical cross-section of temperature (°C) from the LGM high transport case through ring H2 at day 360 (November).

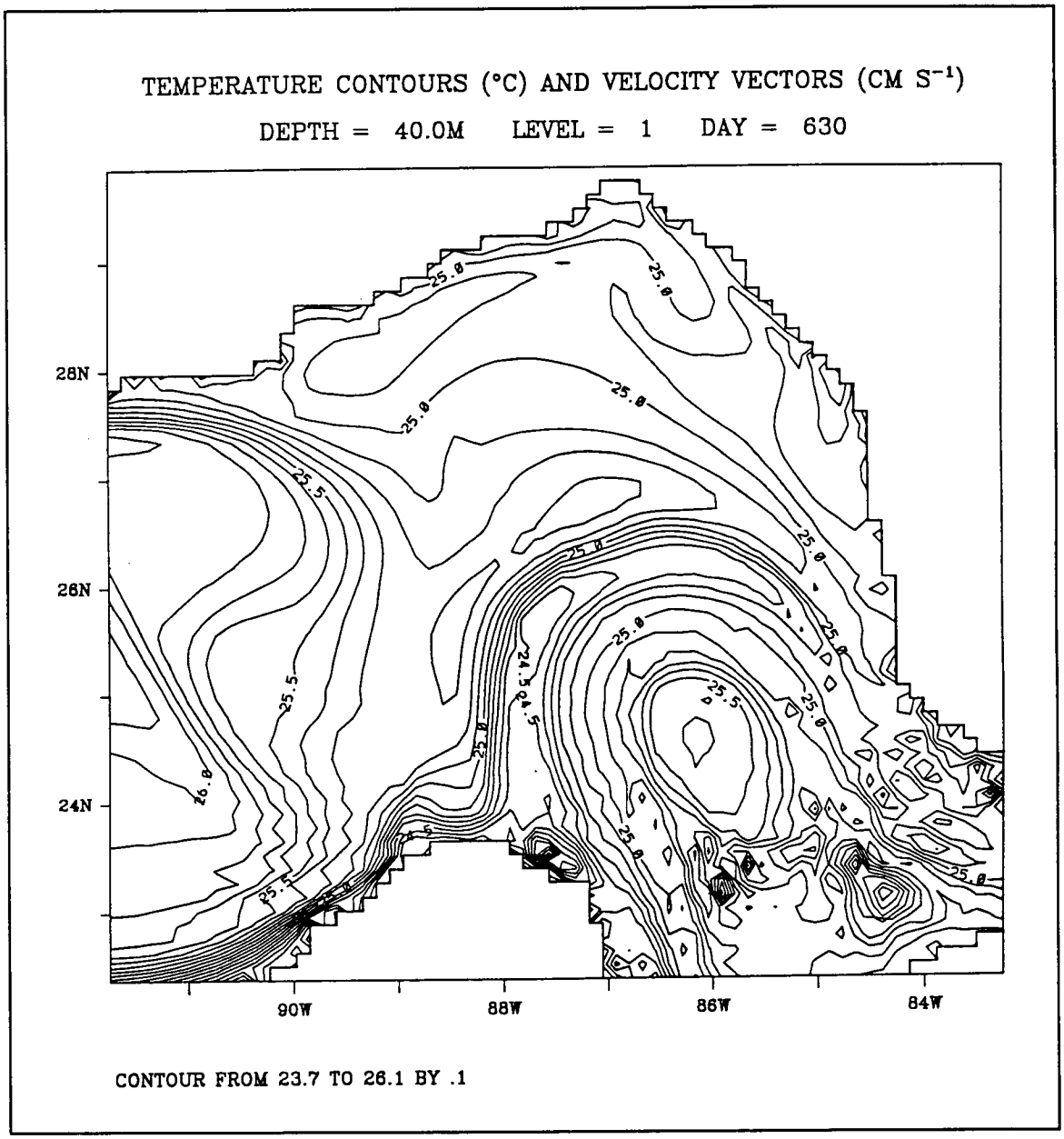

Figure 40. Level 1 (40 m) temperature field in the eastern Gulf of Mexico for the LGM high transport case at model day 630 (August).

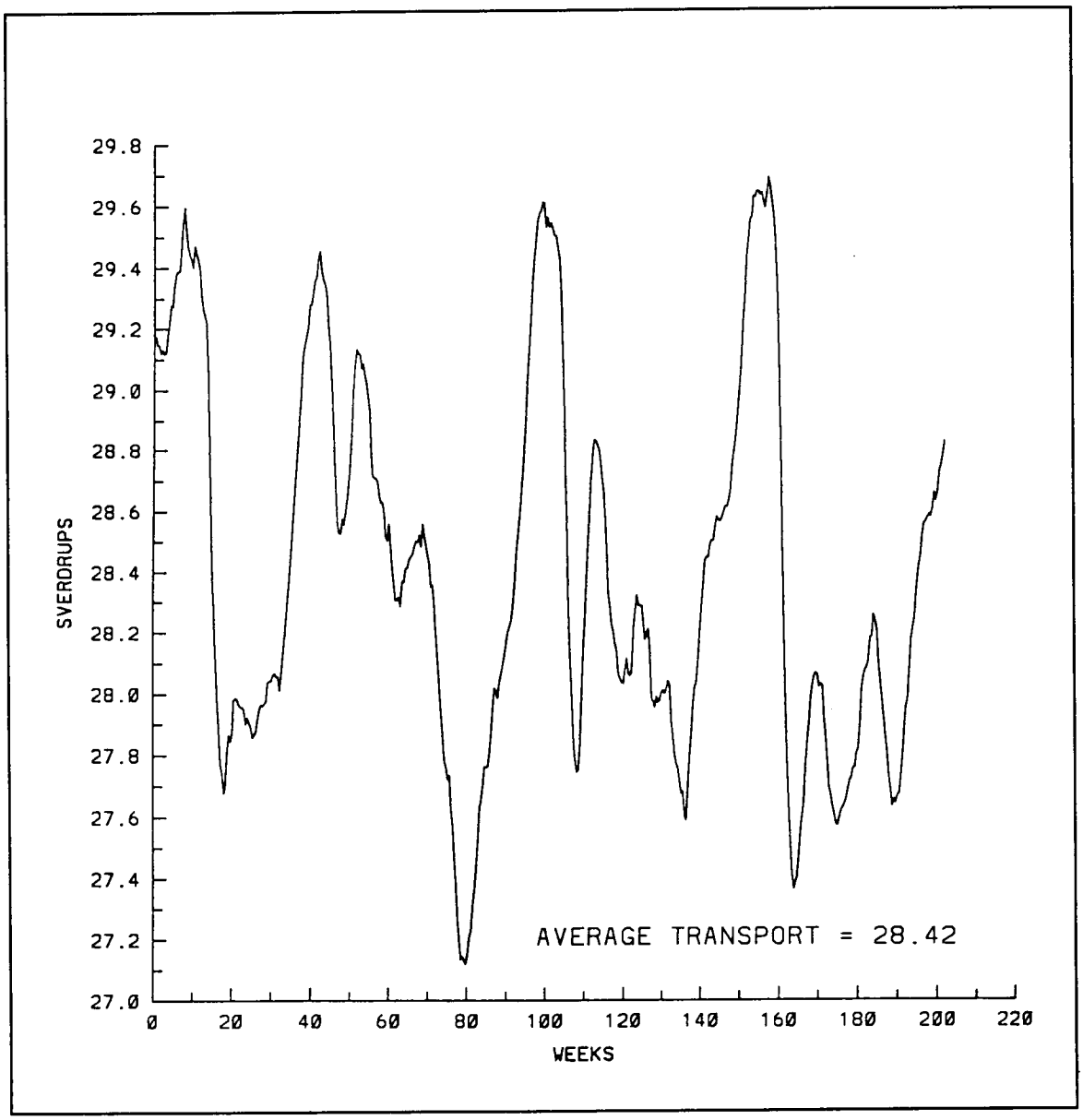

Figure 41. Time series of transport stream function (Sv) in the Florida Straits for the high transport case, model years 5-8. This data was processed with a 30-day running mean.

significant changes in the wind-forced circulation also. Upwelling occurs on the western side of the Yucatan Peninsula where the direction of the wind is favorable for upwelling throughout the year, but the magnitude of wind stress is nearly twice as large for summer as winter (Figures 30 and 32). Although the upwelling is present throughout the year, it is weakest in spring, strengthens in summer and is strongest in fall (Figure 42). The tongue of upwelled water generally extends westward from the coast at approximately 22°N where there is a change in the orientation of the coastline. The westward extent of the upwelled water is highly influenced by the eddy activity in the region. The upwelled waters can nearly reach the slope of Mexico if a ring is present in the western basin (Figure 43) or the tongue can be deflected southward into the Campeche Basin along the fronts of large anticyclonic eddies.

Upwelling is also observed in the northwest GOM in winter along the western and northern edges of the permanent anticyclone (Figure 42). Upwelling favorable winds are observed here in the winter only and the magnitude of the wind stress is only about one-third of that generated along the western Campeche Coast (Figure 30).

The circulation in the Campeche Basin is characterized by mesoscale eddies over the central and eastern portion. There may be only one large anticyclonic eddy or as many as two anticyclones and two cyclones at one time. Although eddy pairs commonly occur, a large cyclone by itself is not observed in the model output. Northward currents flow along the western boundary of the Campeche basin at all times in agreement with the Sverdrup volume transport calculation for the LGM.

A continuation of the northward current from the Campeche Basin into the northern GOM can occur in the LGM simulations, but does not exhibit a seasonal cycle. Both the timing and the location of the northern WBC with respect to the coast are variable and the northern WBC appears to be generated mainly by the addition of anticyclonic vorticity from the rings. A shelf break current occurs along the Texas-Louisiana coast and also appears to be dependent on the contribution of anticyclonic vorticity from rings.

The deep circulation in the high transport case is not significantly different than in the present-day simulations. The dominant feature of the deep circulation is the cyclonic gyre that forms beneath the LC as an eddy is being shed, which migrates westward along with the surface signature of the ring. The maximum velocities in the deeper layers are less than 20 $cm \cdot s^{-1}$ as observed today, but are generally greater than 14 $cm \cdot s^{-1}$. Several smaller cyclones and anticyclones can be observed as well as the large cyclone. The deep motions are vertically coherent, although the depth at which this occurs is slightly deeper.

4.4 Low-Volume Transport Case

Lowering the volume transport through the Yucatan Channel was accomplished by gradually reducing the amount of *u*-component of velocity added in the Caribbean. Due to the sensitivity of the model to small adjustments in this method of forcing, four years of model spin-up time were needed to reach the new target volume transport. The annual mean volume transport for the low transport case is 18.66 Sv through the southern

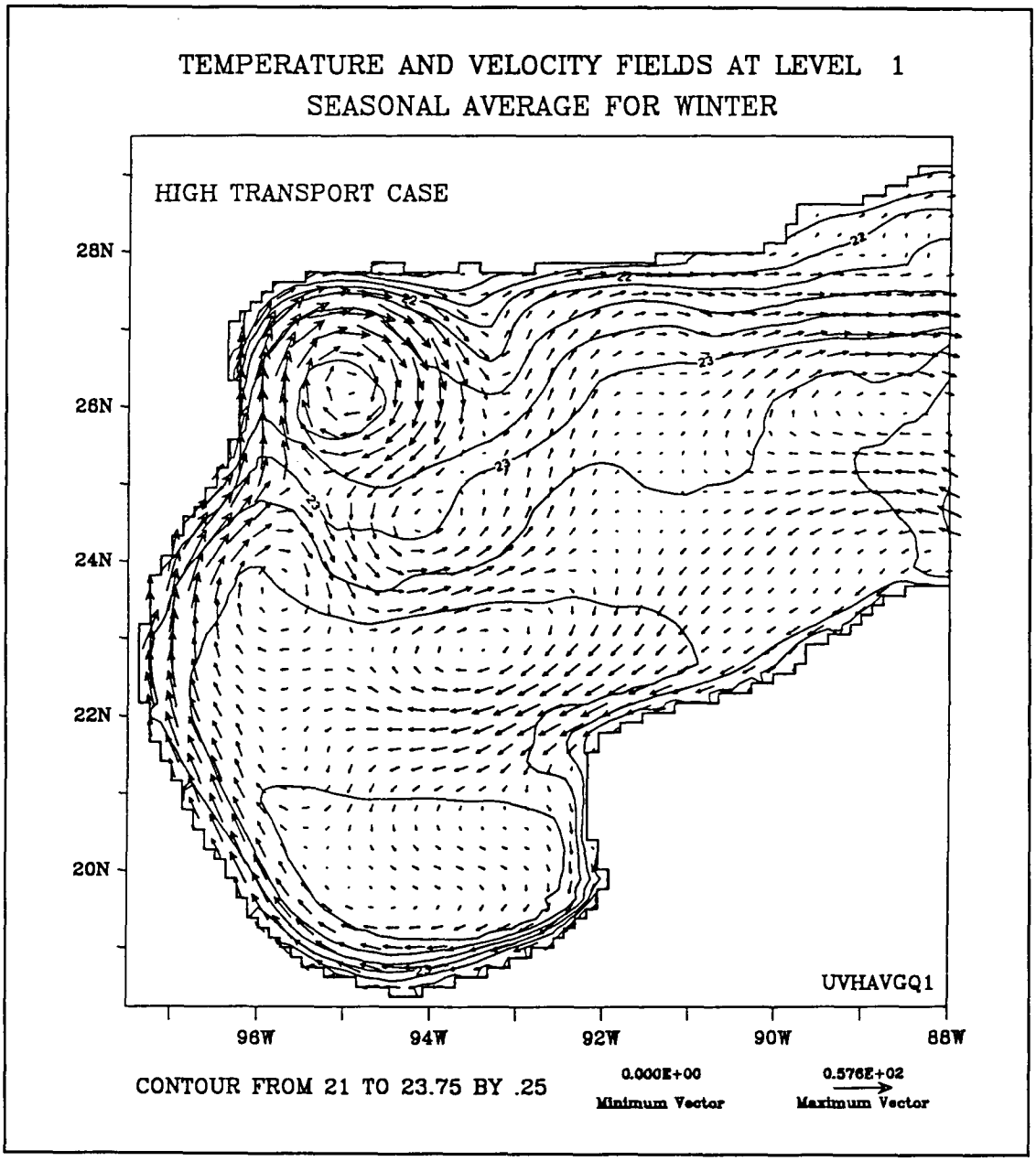

Figure 42a. Four-year average of level 1 (40 m) temperature (°C) and velocity (cm s^{-1}) fields for the LGM high transport case in the western Gulf of Mexico during Winter.

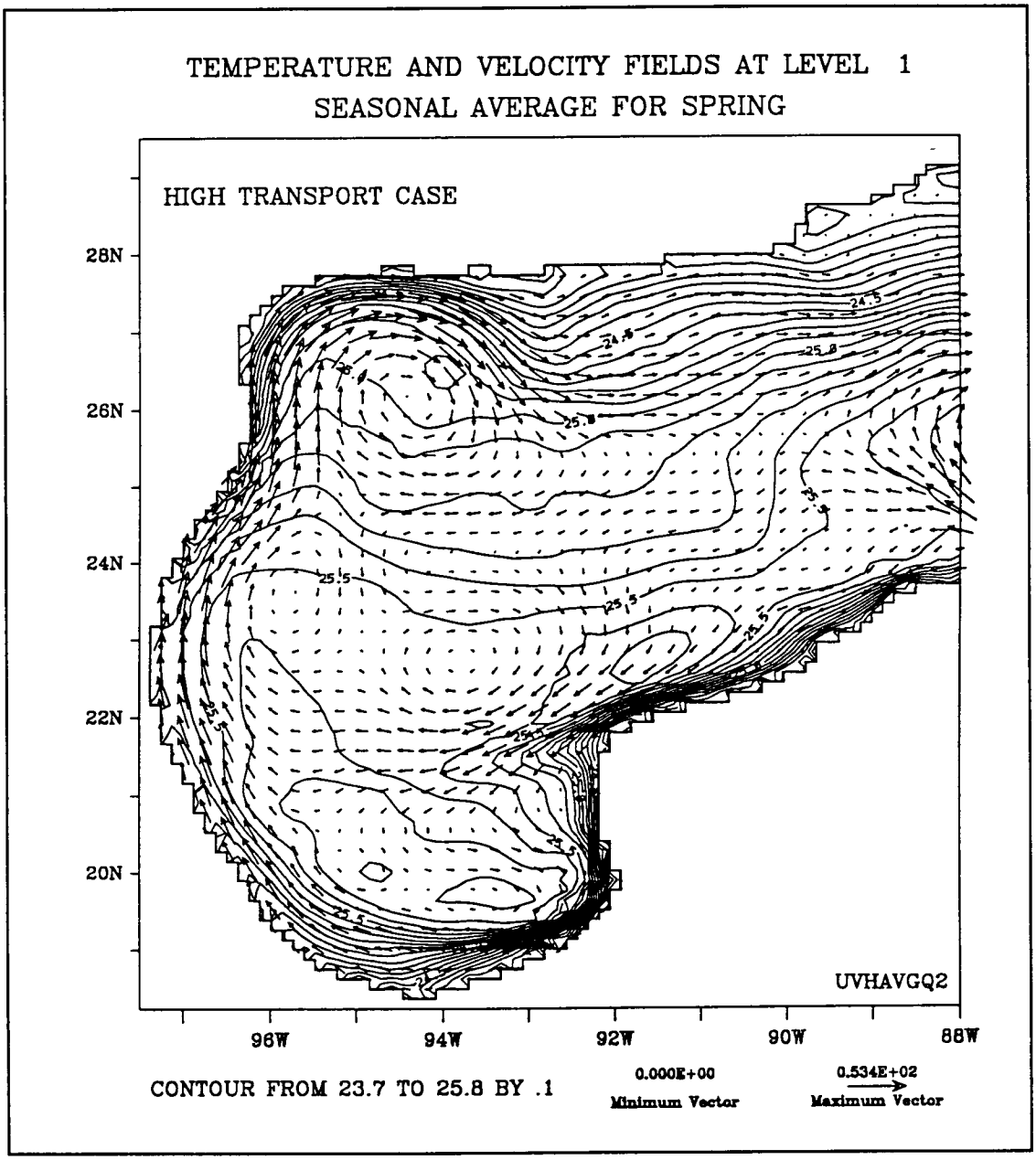

Figure 42b. Four-year average of level 1 (40 m) temperature (°C) and velocity (cm s^{-1}) fields for the LGM high transport case in the western Gulf of Mexico during Spring.

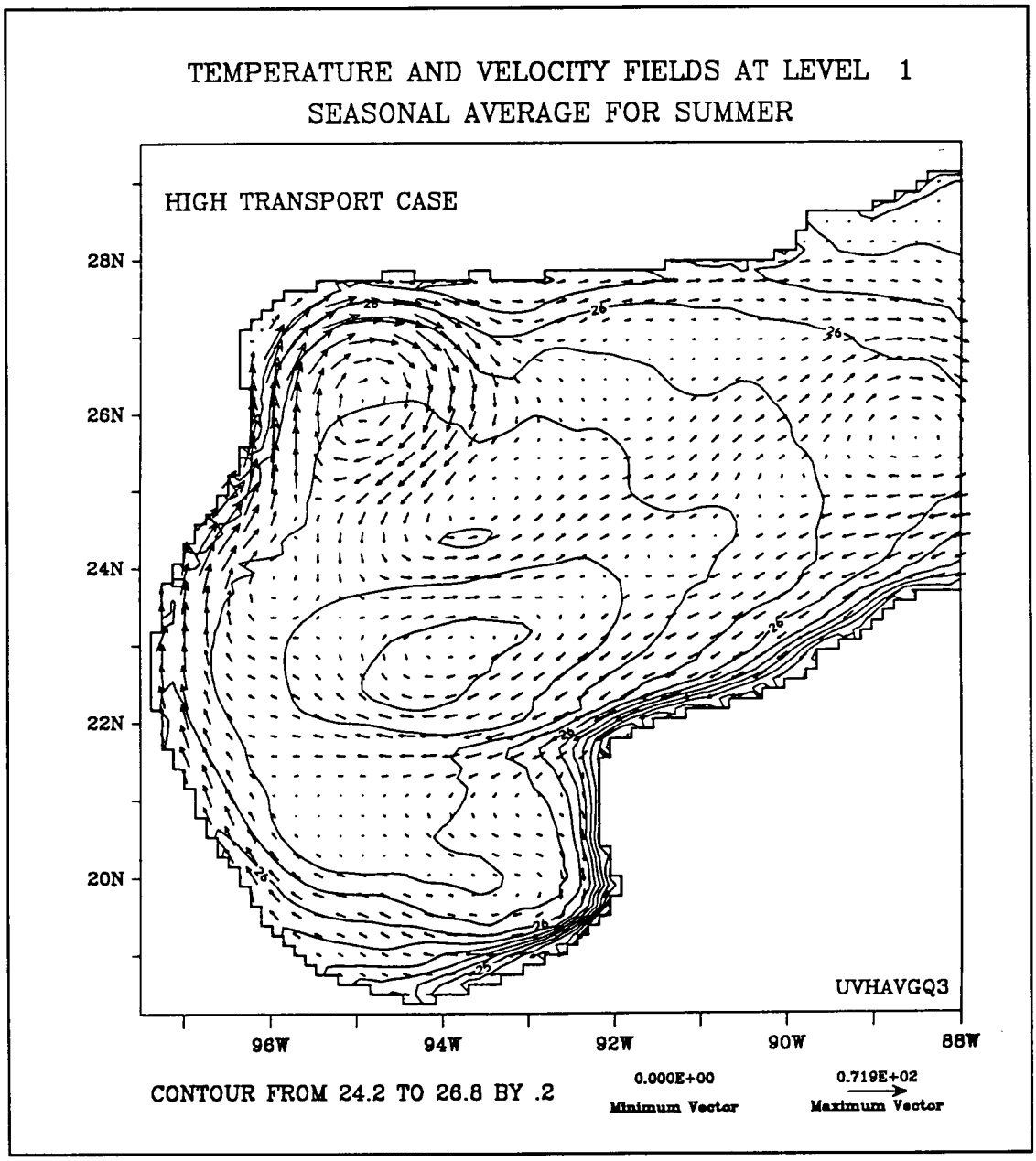

Figure 42c. Four-year average of level 1 (40 m) temperature (°C) and velocity (cm s^{-1}) fields for the LGM high transport case in the western Gulf of Mexico during Summer.

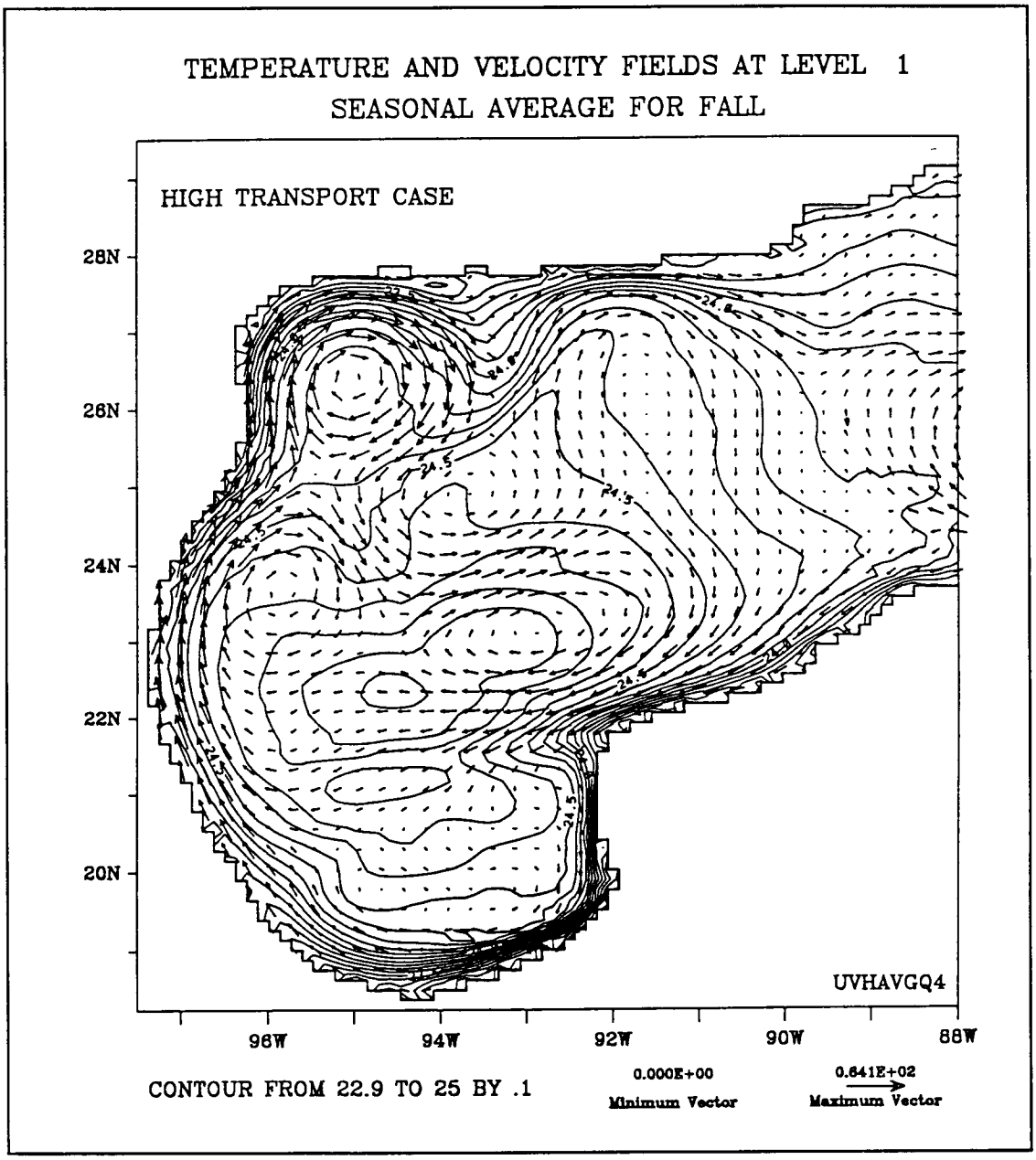

Figure 42d. Four-year average of level 1 (40 m) temperature (°C) and velocity (cm s^{-1}) fields for the LGM high transport case in the western Gulf of Mexico during Fall.

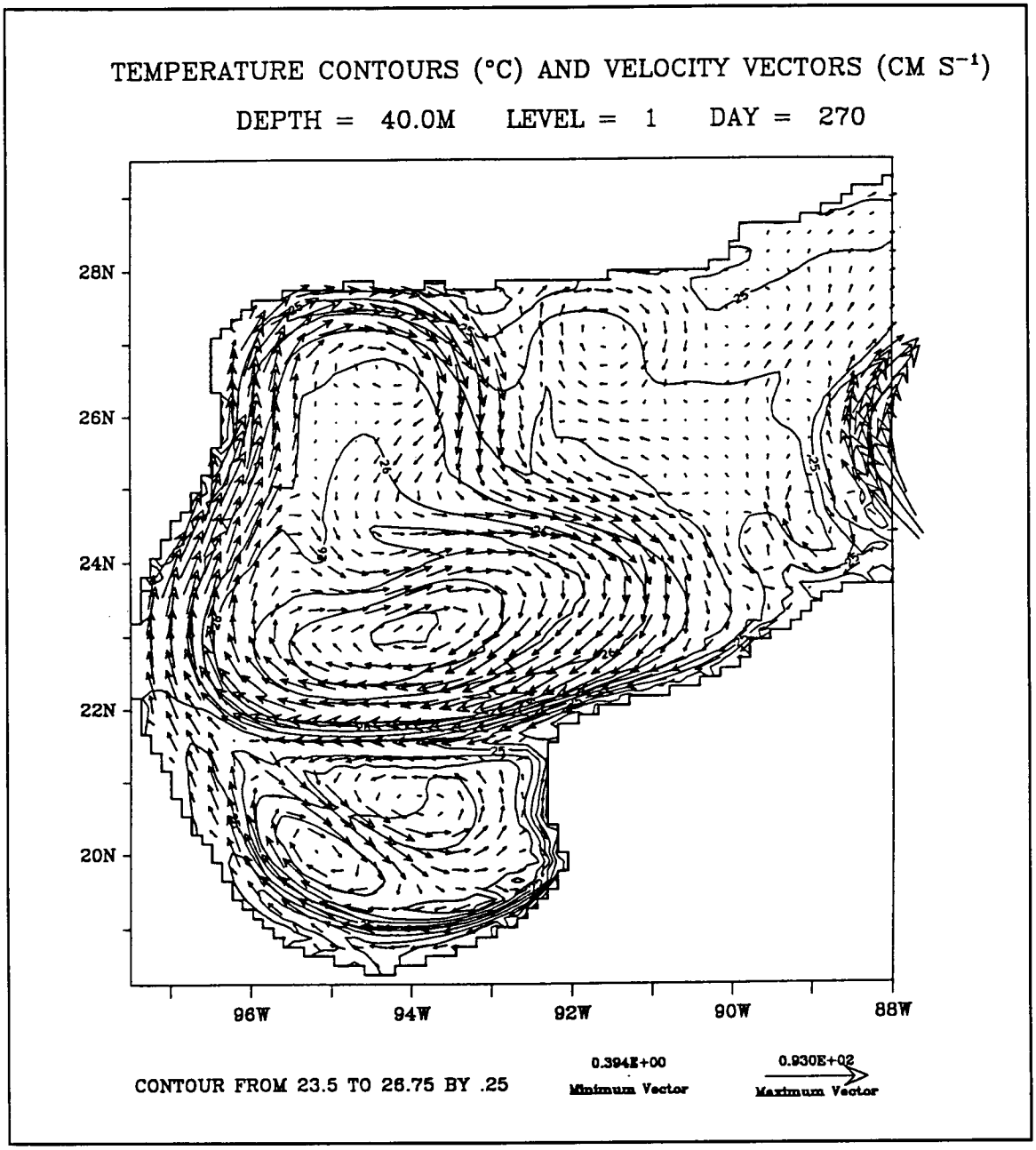

Figure 43. Level 1 (40 m) temperature and velocity fields for the LGM high transport case in the western Gulf of Mexico at model day 270 (August).

Straits of Florida (Figure 44). The flow through the Caribbean in the high transport case is characterized by a well-defined, vigorous current parallel to the South American coast which turns northward along the eastern Yucatan coast (Figure 37). In the low flow case the inflow forms a broad, relatively weak current (Figure 45), and results in a LC that has narrower annulus.

4.4.1 Loop Current Rings

The LC in the low transport case is weaker and narrower than in the high transport case. The rings separate in approximately the same location, but the LC reforms farther to the south after a ring has separated in the low transport case than in the high transport case or the present-day simulations. The characteristics of the low transport rings are summarized in Table 4. The low transport rings are only 4.3% smaller than the high transport case, while the change in volume transport was nearly one-third. Also the ring separation period was only reduced by nearly 7% from 30 weeks to 28 weeks. The westward translation speeds for the low transport and high transport cases are nearly identical.

A significant effect of lowering the inflow volume transport was to reduce the velocities of both the LC and the rings at all depths. The maximum velocities in the LC for the high transport case were 100-120 $cm \cdot s^{-1}$ compared with 80-100 $cm \cdot s^{-1}$ in the low transport case. The maximum swirl speeds of the rings at level 1 (40 m) were typically 70 $cm \cdot s^{-1}$ in the eastern GOM and 45-50 $cm \cdot s^{-1}$ in the central GOM for the high transport case. For the low transport case the maximum swirl speeds of the rings at level 1 were also 70 $cm \cdot s^{-1}$ in the eastern GOM, but they decreased quickly during westward migration and were typically 30-35 $cm \cdot s^{-1}$ in the central GOM. At 200 m the maximum velocities in the low transport case compared with the high transport case were nearly 20 $cm \cdot s^{-1}$ smaller, at 930 m they were reduced by nearly one-half and at 3330 m (the lowest level) they were reduced by more than one-third.

The effects of lowering the inflow can also be seen in the vertical structure of the rings. The vertical structure of the low transport rings is quite different from both the present-day observations and the high transport case. Both the isohalines and isotherms are much flatter with depth and the divergence of the isotherms with depth is not as great in the low transport case (Figure 46).

The average life span of the low-transport rings is longer than the high-transport rings, which can be explained by the difference in their migration paths. The rings in the high transport case followed either a northern migration path or a southern. Each ring that followed the northern migration path, which has a shorter distance, quickly merged with an older ring that was already in the northwest corner. All rings in the low transport case followed the southern migration path and were observed to slowly decay in the northwest corner until another ring arrived. The average life span of 451 days for the low transport case is three months longer than the average life span of one year observed today. This may result from the fact that none of the rings in the low transport case interacted with other rings and each ring followed the longest observed migration path.

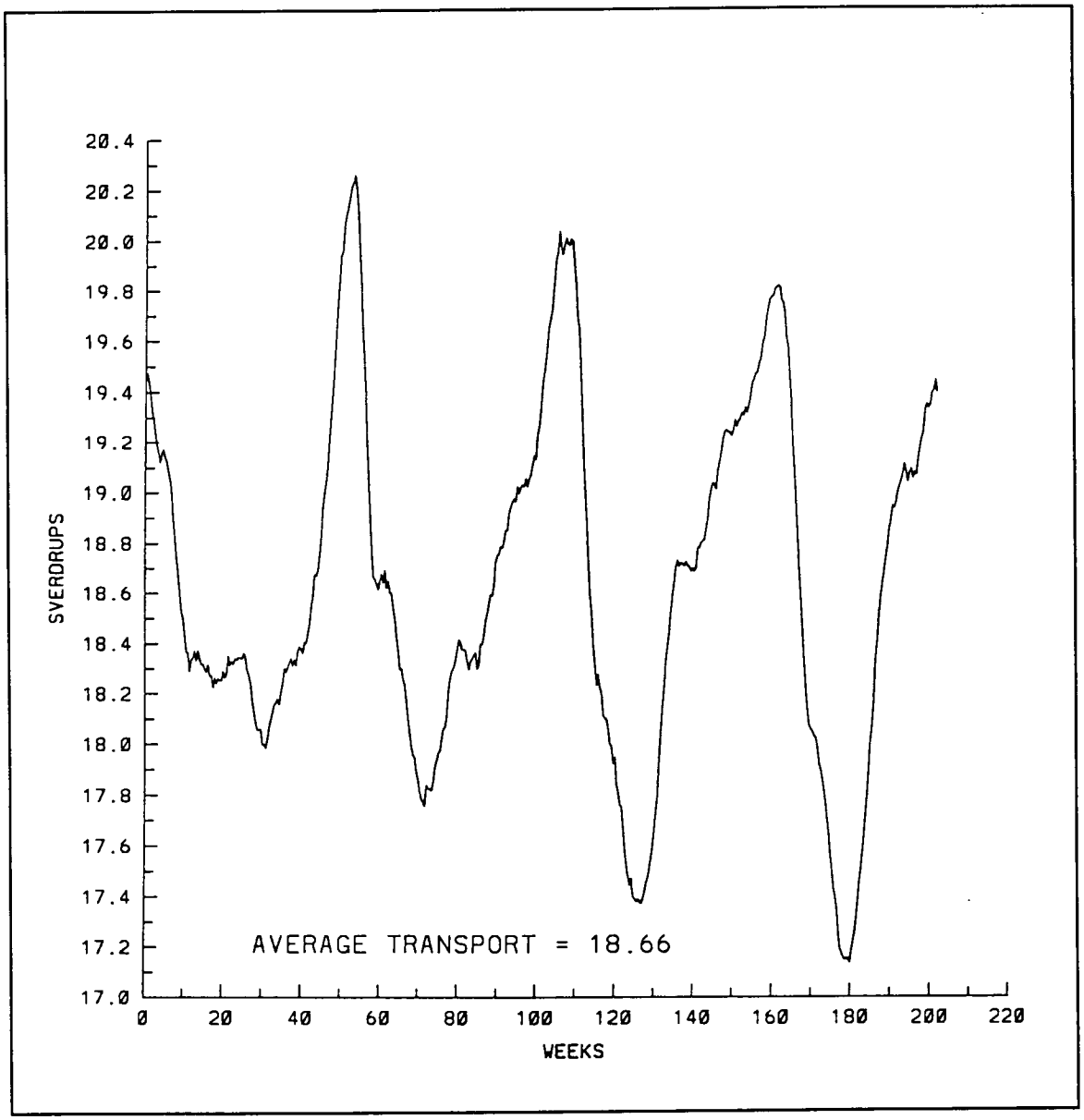

Figure 44. Time series of transport stream function (Sv) in the Florida Straits for the low transport case, model years 13-16. This data was processed with a 30-day running mean.

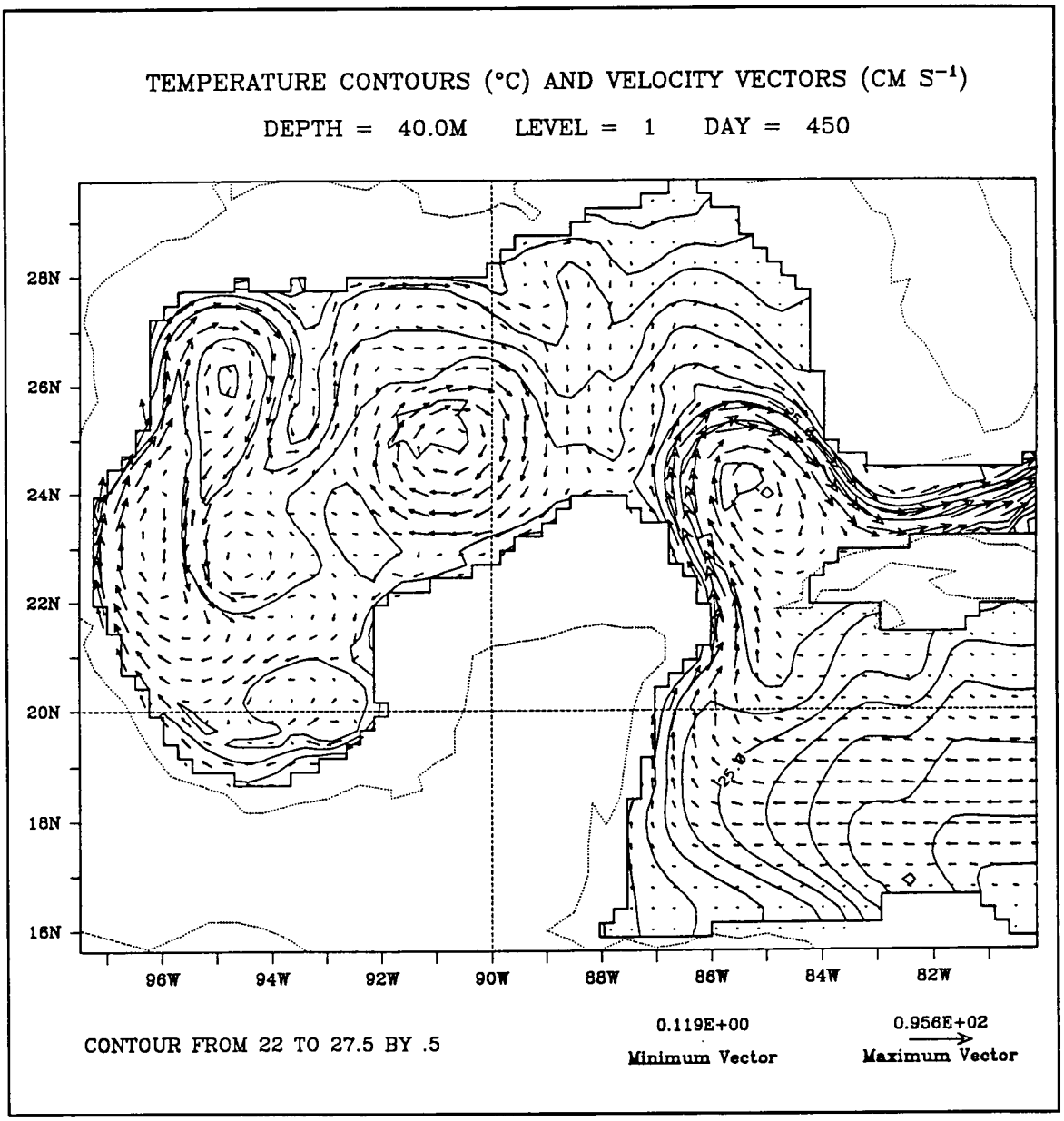

Figure 45. Level 1 (40 m) temperature and velocity fields for the LGM low transport case at model day 450 (February).

Table 4. Characteristics of model Loop Current rings for the LGM low transport case.

Ring	Size [1] (km)	Migration Speed (km d^{-1})	(cm s^{-1})	Time to W. Wall [2] (days)	Lifespan (days)	Ring Interaction
S1	320	4.71	5.45	180	483	none
S2	320	4.16	4.81	252	462	none
S3	340	4.43	5.12	180	441	none
S4	290	4.13	4.78	180	498	none
S5	360	4.60	5.32	180	482	none
S6	310	4.55	5.27	231	371	none
S7	393	3.96	4.58	180		
Mean	333	4.36	5.05	198	456	
Std. Dev.	34.4	0.28	0.33	30.6	46.2	

[1] Approximate diameter in the eastern GOM. Measured by taking an average of the north-south dimensions of each ring.

[2] Time to western wall is a visual estimate of the number of days that each ring took from just after separation to reach the outer shelf of the Mexico or Texas coast. The arrival of the ring at the western wall is characterized by some deformation of the ring, typically marked by a north-south elongation of the ring.

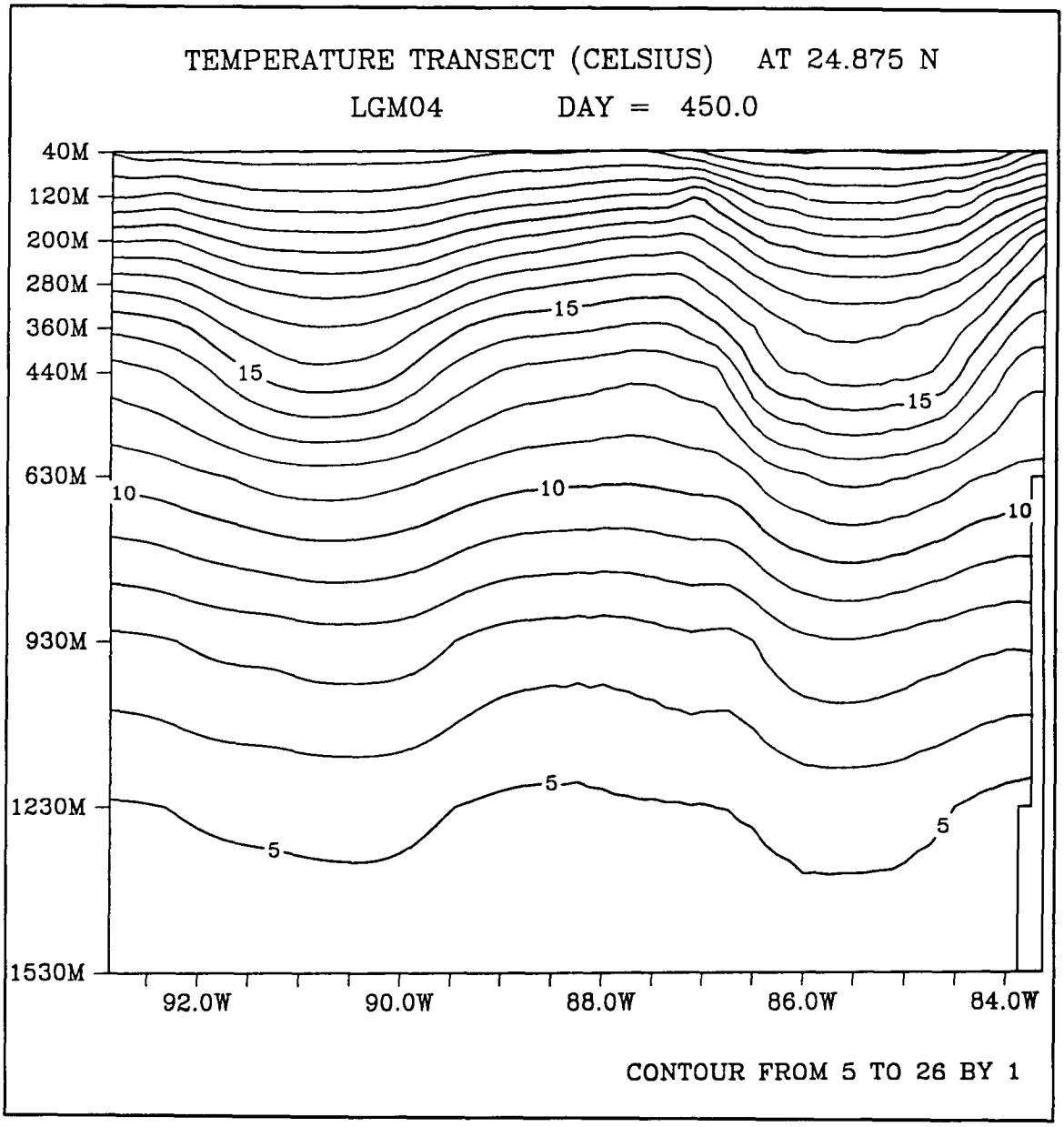

Figure 46a. Vertical cross-section of temperature through ring L2 in the LGM low transport case on model day 450 (February).

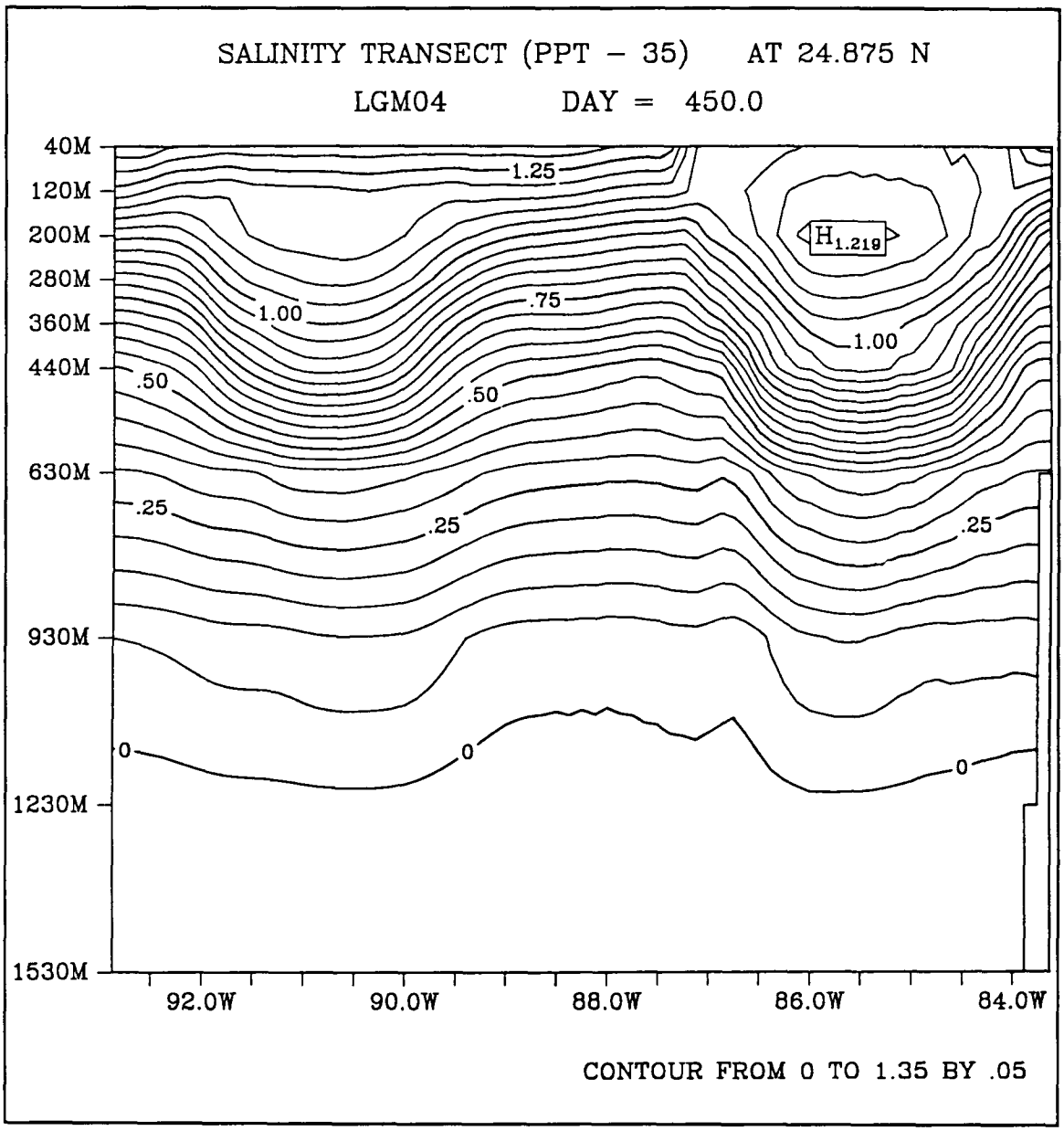

Figure 46b. Vertical cross-section of salinity through ring L2 in the LGM low transport case on model day 450 (February).

4.4.2 General Circulation

Most of the general circulation features discussed in the high transport results section are not significantly different in the low transport case. A circulation change is observed in the eastern GOM which is related to the intensity of the LC. In the low transport case the LC is narrower, which places the eastern branch farther offshore and creates a larger region between the eastern edge of the LC and the west coast of Florida. A larger Tortugas Gyre is generated when the LC overshoots the entrance to the southern Straits of Florida and a current extends northward from the eastern side of the gyre along the west coast of Florida into the northeast corner (Figure 47). The deep circulation in the low transport case is similar to the high transport case, except that the overall velocities are smaller.

4.5 Discussion

There are many similarities between the high transport and low transport cases in both the general circulation and the formation and structure of the rings. From the two simulations with different inflow conditions there is a common picture of a GOM during the LGM with a LC system and rings that behave nearly like those observed today, and circulation in the deep GOM that resembles the present-day simulations. The features that are present in the LGM simulation that are not observed today are a WBC originating in the Campeche Bay, upwelling off the western Yucatan Peninsula, upwelling in the northwestern GOM, increased eddy activity in the western GOM and variable or northward flow off the west coast of Florida.

Brunner and Cooley (1976) and Brunner (1982) inferred the physical oceanographic conditions in the GOM during the LGM from the distribution of glacial fauna in deep sea cores. Both Brunner and Cooley (1976) and Brunner (1982) estimated surface temperature and salinities for 18,000 years B.P. using multivariate statistical analysis on counts of planktonic foraminifera from trigger core tops in the GOM and Atlantic Ocean. The LGM temperature pattern in the western GOM is similar in Brunner and Cooley (1976) (Figure 48) to the CLIMAP data (Figures 34b and 35b) used to force the LGM simulations. The maximum summer CLIMAP temperatures are only .3°C warmer in the western GOM than Brunner and Cooley (1976), and the difference in maximum winter temperatures is less than .4°C. The eastern GOM is characterized by a greater northward intrusion of the LC in summer and winter in Brunner (1982) than the CLIMAP data. Also the Brunner (1982) temperature estimates indicate a warmer LC than the CLIMAP data.

All of these LGM temperature estimates suggest a single large gyre existed in the western GOM during both summer and winter, and the gyre is centered farther north and elongated more in the north-south direction in summer. Brunner and Cooley (1976) also present a gyre-like distribution of summer and winter salinities during the LGM, with the highest salinities near the margins and low values at the center of the gyre (Figure 49).

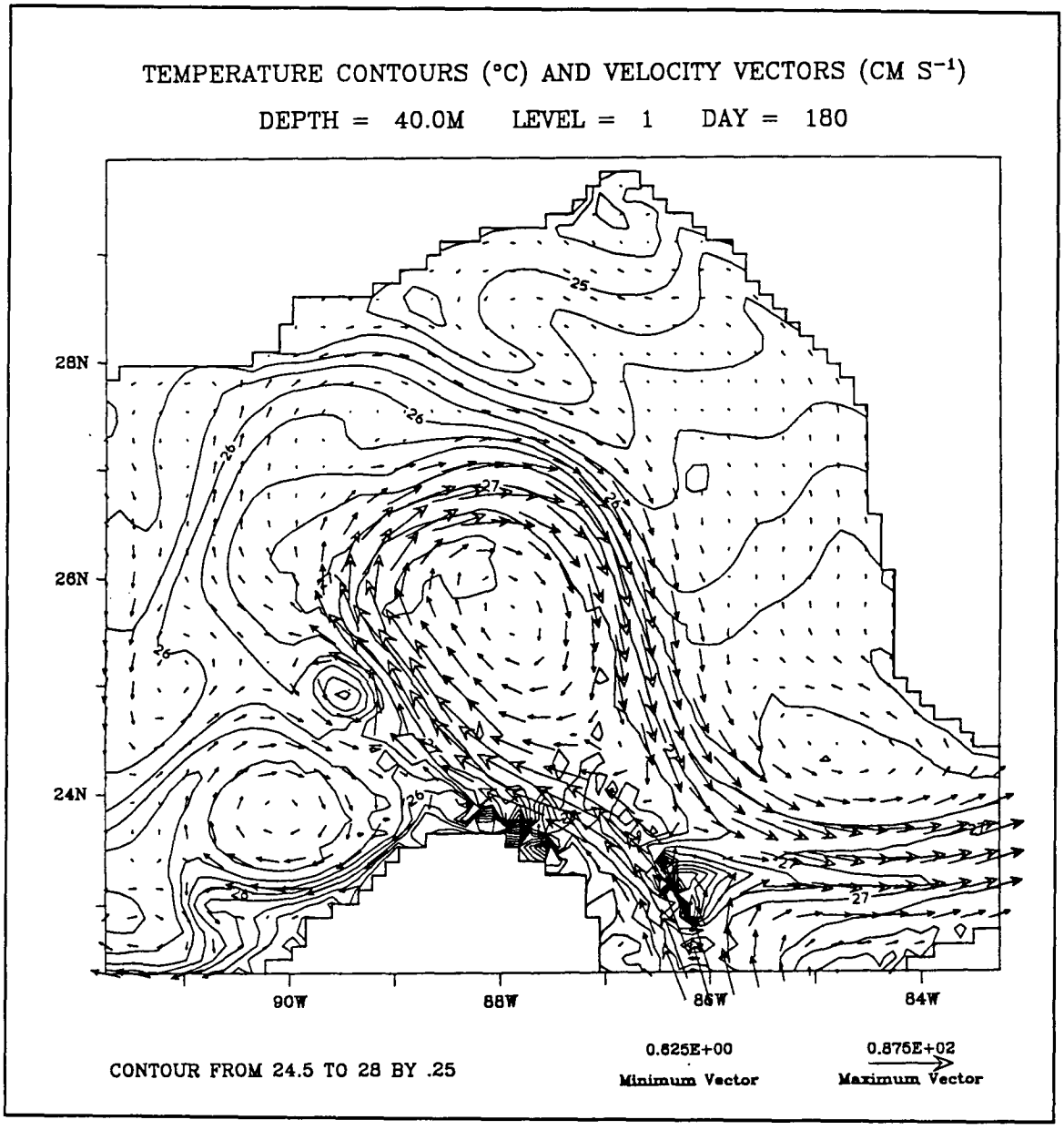

Figure 47a. Level 1 (40 m) temperature and velocity fields for the LGM low transport case in the eastern Gulf of Mexico on model day 180 (May).

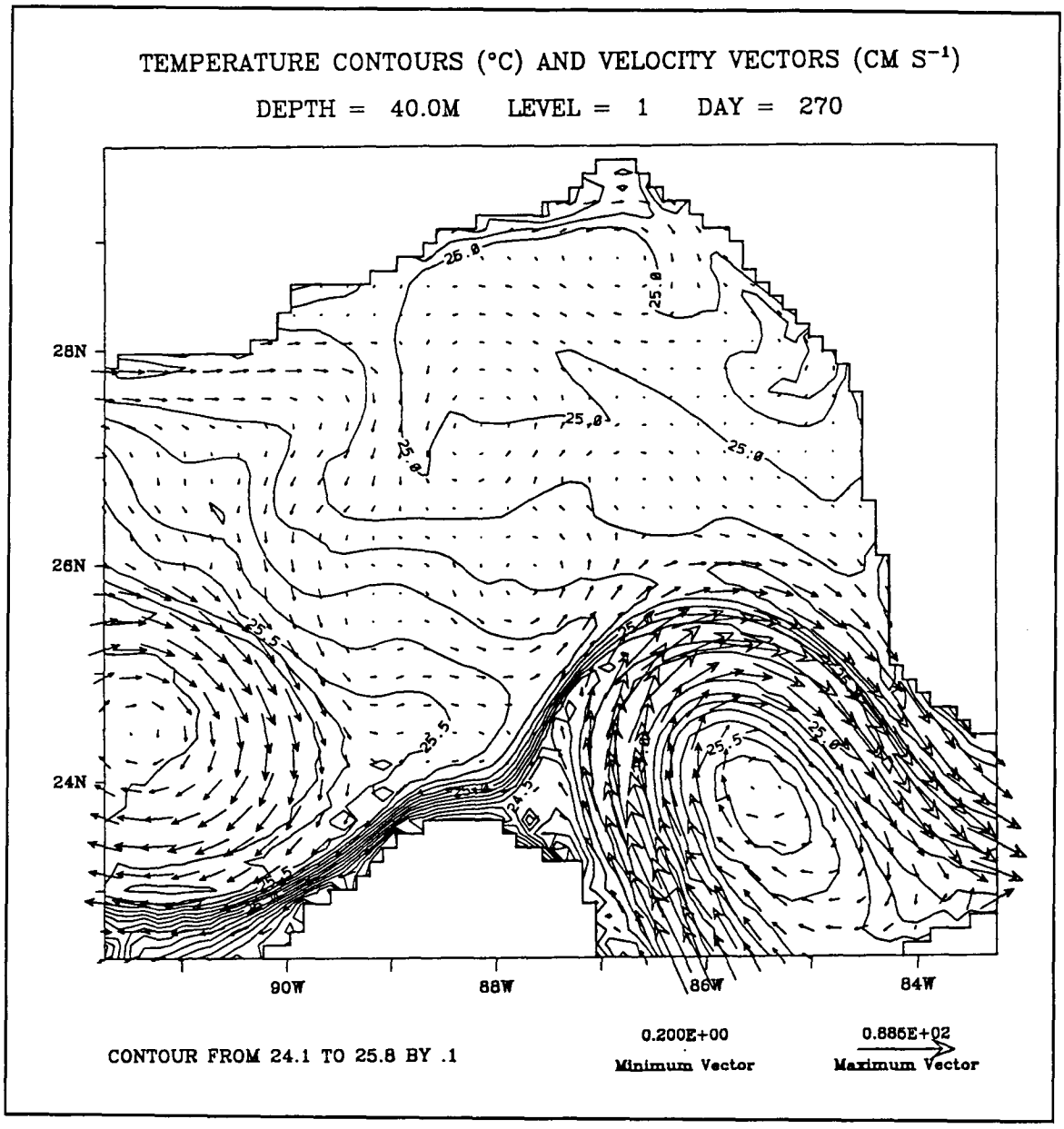

Figure 47b. Level 1 (40 m) temperature and velocity fields for the LGM low transport case in the eastern Gulf of Mexico on model day 270 (August).

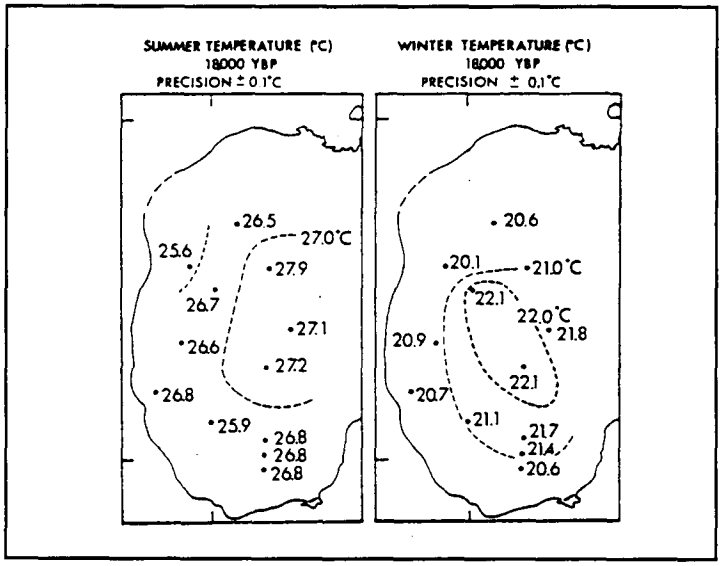

Figure 48. Sea-surface temperature (°C) for 18,000 years b.p. for (a) summer with an accuracy of ±1.1°C and (b) winter with an accuracy of ±1.3°C at an 80% confidence interval (from Brunner and Cooley 1976).

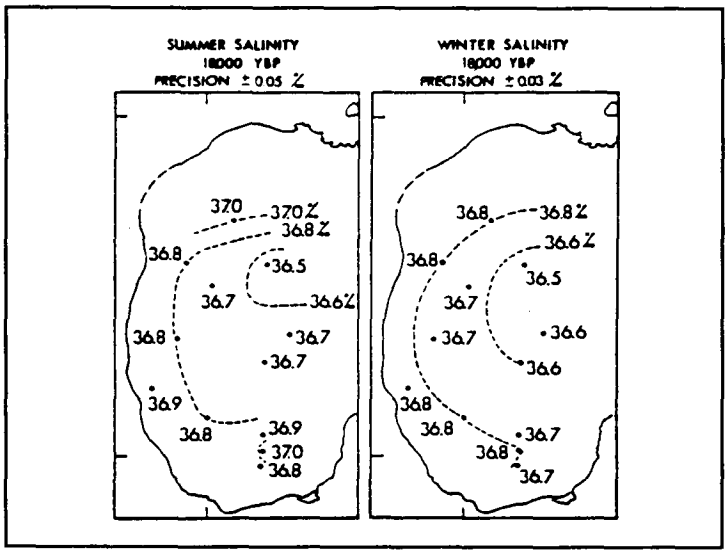

Figure 49. Sea-surface salinity (ppt) for 18,000 years b.p. for (a) summer with an accuracy of ±0.6‰ and (b) winter with an accuracy of ±0.5‰ at an 80% confidence interval (from Brunner and Cooley 1976).

Brunner and Cooley (1976) conclude that anticyclonic circulation must have existed in the western GOM during both summer and winter due to the density gradient indicated by the glacial temperature and salinity patterns.

Brunner and Cooley (1976) propose that a large anticyclone existed in the western GOM due to an intensified LC resulting from increased volume transport and vertical shear of the Yucatan Current. Increased flow through the Yucatan Channel would have resulted from increased intensity of the equatorial Atlantic currents due to increased trade wind activity (Brunner and Cooley 1976). Brunner and Cooley (1976) offer the following models to explain the anticyclonic circulation in the western GOM: (1) circulation in the GOM that is the same as the present, but with denser waters, (2) an increase in the volume transport and vertical shear of the LC so it could extend farther into the eastern GOM and shed rings large enough to nearly fill the western basin, and (3) increase the volume transport of the LC even more than the second model, in which case it would: "intrude into the western basin in an immense anticyclonic flow, sweeping the periphery of the Gulf basin into the narrow Florida Straits to become a major component of the Gulf Stream".

The hypothesis of greater volume transport entering the GOM during the LGM than present was not tested using the LGM model. The consequence of increased transport of the LC on the circulation in the GOM as described by Brunner and Cooley (1976) is not supported by the rotating tank experiments on the circulation of the GOM by Ichiye (1972). Ichiye (1972) performed a series of experiments whereby he increased the velocity and rotation speed of the inflow through the Yucatan Channel by varying the Rossby number and Reynolds number of the inflow. Results of only four of the experiments were discussed. Ichiye (1972) demonstrated that as the Rossby number and Reynolds number of the flow are increased, the region of influence of the LC and associated eddies will increase, but the direction of rotation may become cyclonic. The LC penetrated into the western GOM only for the case of relatively large values of Rossby number and Reynolds number, but the LC flowed counter-clockwise around the basin and the largest eddy that was generated north of the Yucatan Channel was cyclonic (Ichiye 1972).

The estimated temperature and salinity patterns for the LGM can be explained by a combination of physical oceanographic process generated by the LGM simulations. The temperature gradient extending southward from the center of the western gyre into the southern Campeche Basin can be produced by the upwelling off the western Yucatan Peninsula, which is strongest in winter and weak in summer. The WBC in the Campeche Bay is produced year round in the model as predicted by the Sverdrup volume transport calculations. The WBC has an east-west temperature gradient perpendicular to the direction of flow that frequently extends northward into the northwest GOM. The north-south temperature gradient off the slope of northern Texas and Louisiana also is observed year-round. This is due to both the decay of rings and the coastal upwelling along the Texas-Louisiana coast that is a maximum in LGM winter. The temperature maximums near the center of the western basin may be explained by the warm-core rings which have longer residence times in the western GOM in the LGM simulations. There

is a large amount of eddy activity in the western GOM in the LGM simulations and closed contours of the western gyre are not a persistent feature.

The intensity of the Florida Current during the late Quaternary is inferred from sedimentary analysis of piston cores made in the Yucatan Channel and the Straits of Florida by Brunner (1986). The cores were divided into Ericson zones based on the presence or absence of *Globorotalia menardii* and *Globoratalia inflata* (Brunner 1986). The X and Z zones approximate the last interglacial and present interglacial respectively and the Y zone approximates the last glacial.

In the central portion of the southern Straits of Florida at approximately 82°W, the channel is narrower than the eastern and western portions. Therefore, the axis of the current would be most confined by the channel in the central portion. The thickness of the biostratigraphic zone Y is much thicker than the biostratigraphic zone Z in the central portion of the Straits compared to the eastern and western portions (Figure 50a). In this same section of the channel, the overall proportion of sand-size material is less in the Y zone than in the Z zone (Figure 50b) and the overall accumulation rates of silt and clay-size material in the Y zone are more than in the Z zone (Figure 50c). According to Brunner (1986), all of these factors may indicate a reduction in flow rates in the southern Straits because: "sand and silt-rich facies occur in contourite drifts where bottom currents are most rapid or close to the sea floor".

Brunner (1986) offers an interpretation of the data that attempts to support the hypothesis of greater volume transport of LC system resulting from intensification of LGM global ocean circulation. Another interpretation of the sediment data in Figure 50 could signify lower bottom current velocities in the central southern Straits during the LGM, which would be the result of lower volume transport of the LC. A comparison is made of the current speeds through a north-south vertical cross-section at 82°W in the southern Straits of Florida for the present-day seasonal simulation and the LGM low transport case (Figure 51). This comparison indicates that although the maximum velocities through the section are the same for the present-day simulation and the LGM low transport simulation, lower current speeds occur along the channel walls for the case with lower total transport.

There is also some sedimentological evidence in support of lower volume transport of the flow entering the Yucatan Channel from the Caribbean during the LGM. Brunner (1984) looked at the biostratigraphy and sedimentology of 5 piston cores in the Yucatan Channel. Brunner (1984) found that the high sand content of the foraminiferal ooze found in the Yucatan Channel indicated current winnowing. Brunner (1984) reported that although foraminiferal sands can accumulate if the productivity of the surface waters is high, the net sedimentation rates decrease with increasing sand content in the Yucatan Channel. Brunner (1984) concluded that percent sand-size material is proportional to bottom current velocity in winnowed sediments and that cycles of current winnowing may be caused by changes in current transport in response to glacial cycles. Out of the 5 piston cores, the net sedimentation rate and percent of sand-size material for all of the Ericson zones of the Quaternary were only reported for core number 19 located at 23°46.4'N and 86°21.5'W (Brunner 1984). The average sand content in core 19 (in

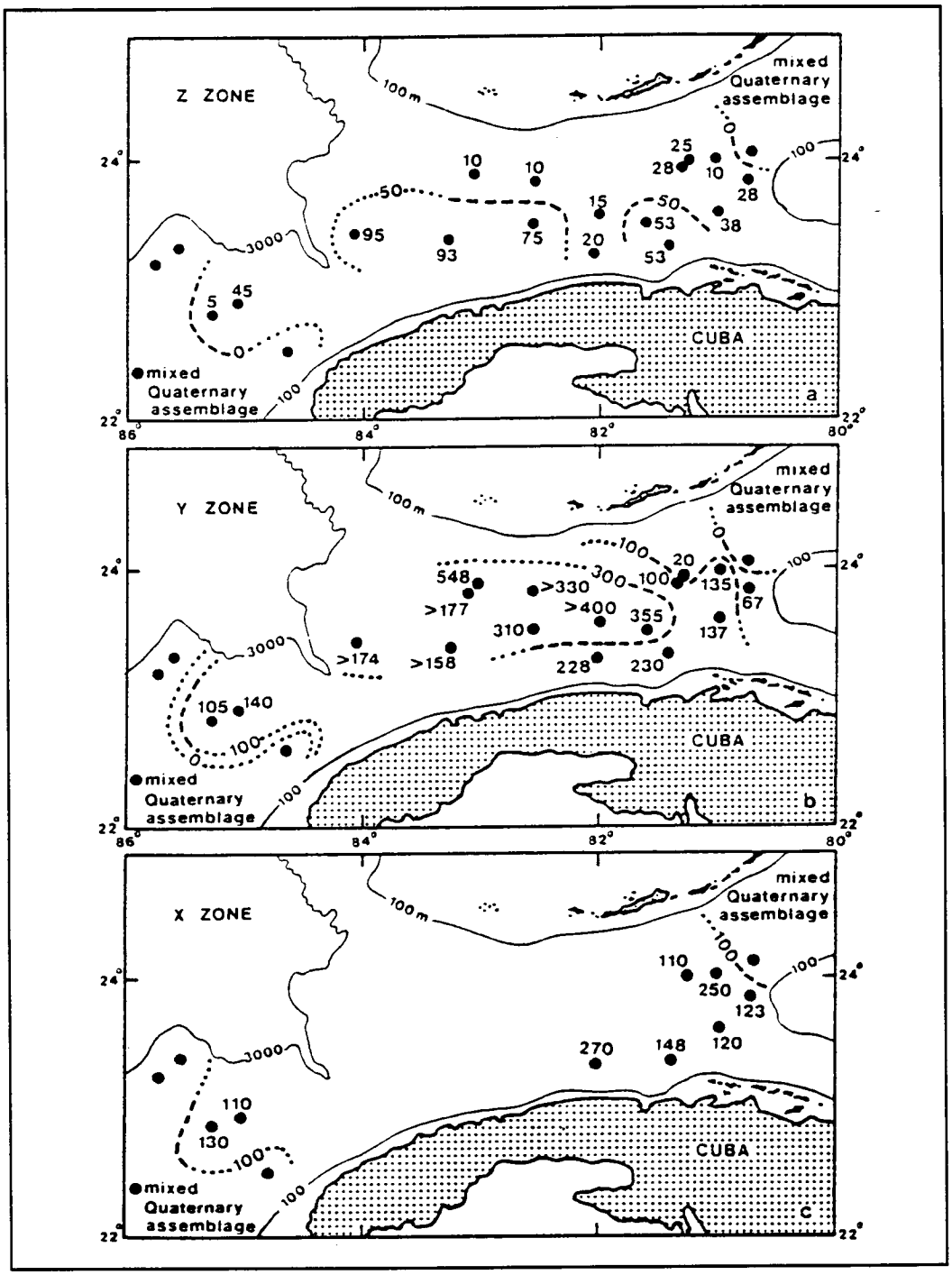

Figure 50a. Thickness (cm) of late Quaternary biostratigraphic zones Z, Y, and X (from Brunner and Cooley 1976).

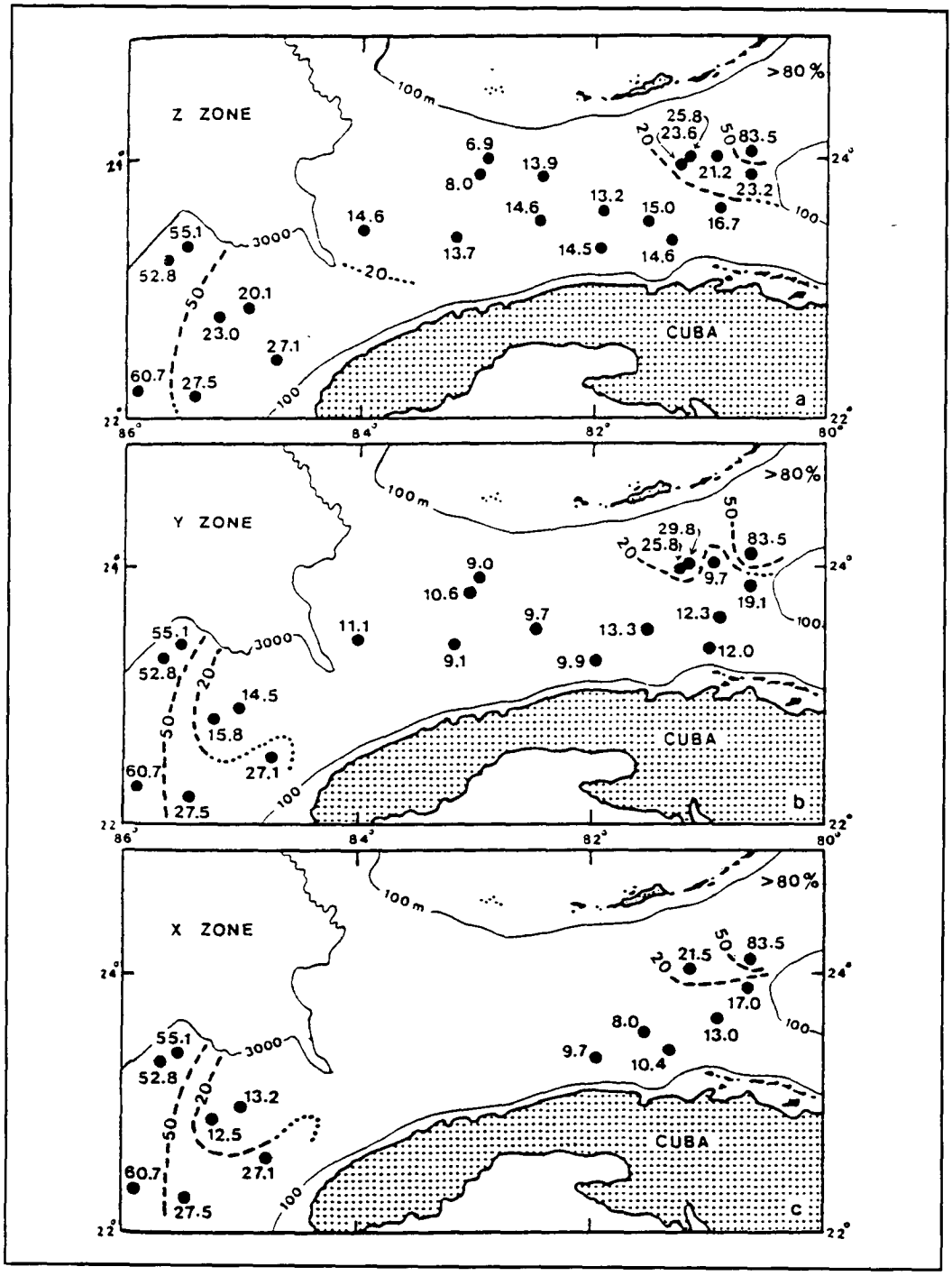

Figure 50b. Areal distribution of the proportion of sand-size material in the Z, X and Y zones (from Brunner and Cooley 1976).

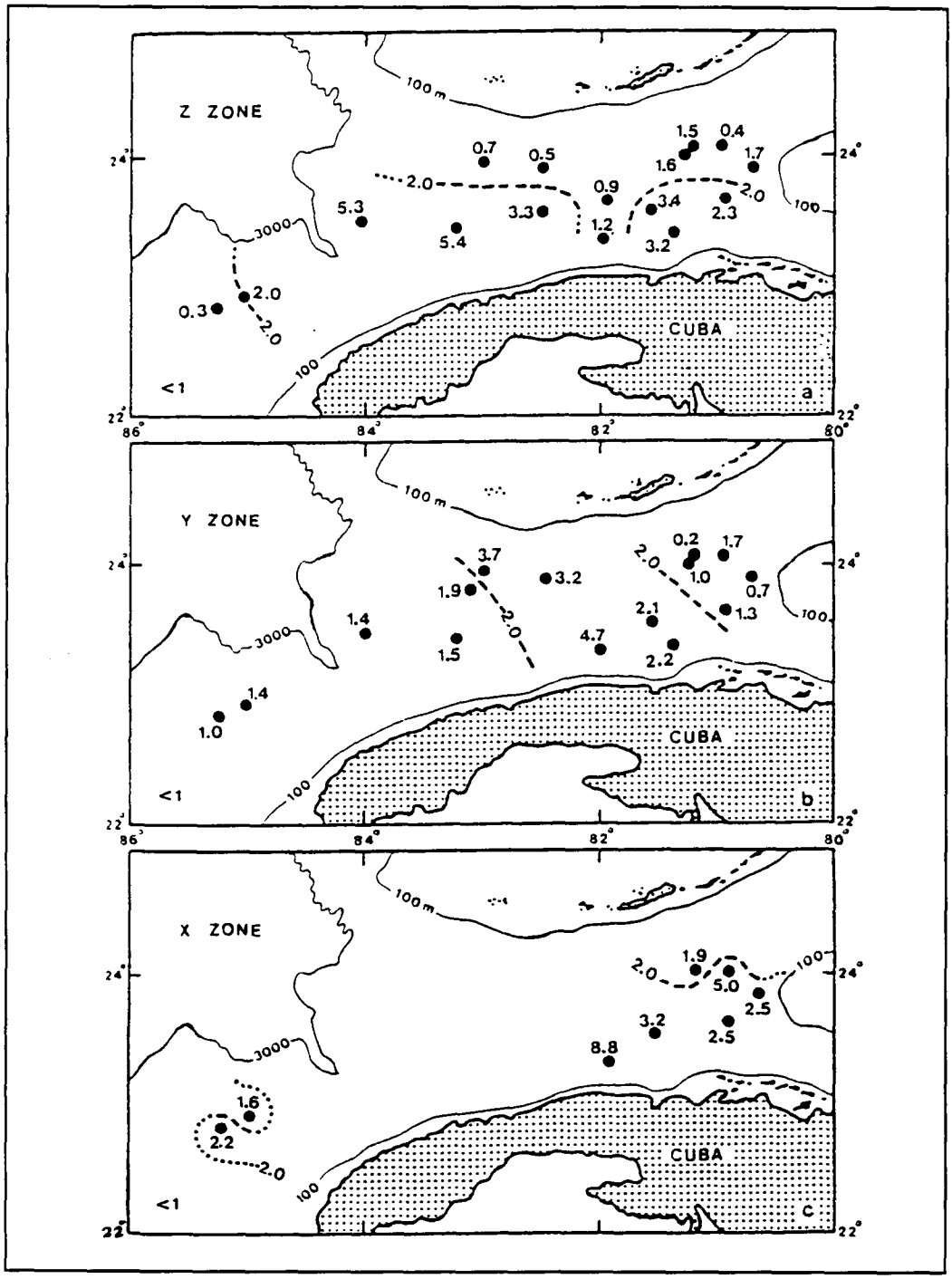

Figure 50c. Accumulation rates (g/cm^2/1000 yr) of silt and clay-size material in the Z, Y and X zones (from Brunner and Cooley 1976).

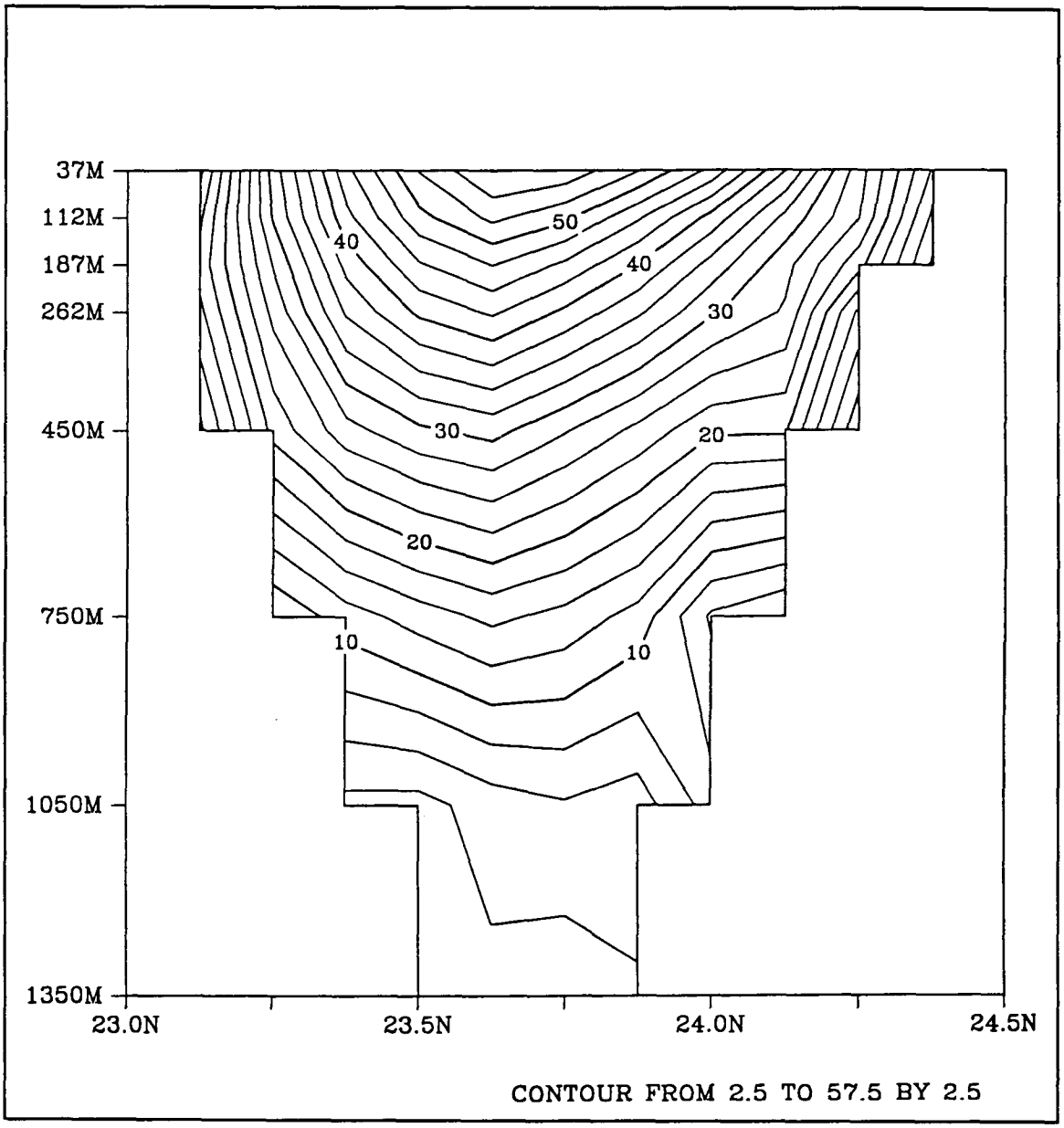

Figure 51a. Vertical profile of the annual average current speed ($cm \cdot s^{-1}$) in the Florida Current at 82°W looking upstream for year 10 of the present-day seasonally-forced simulation.

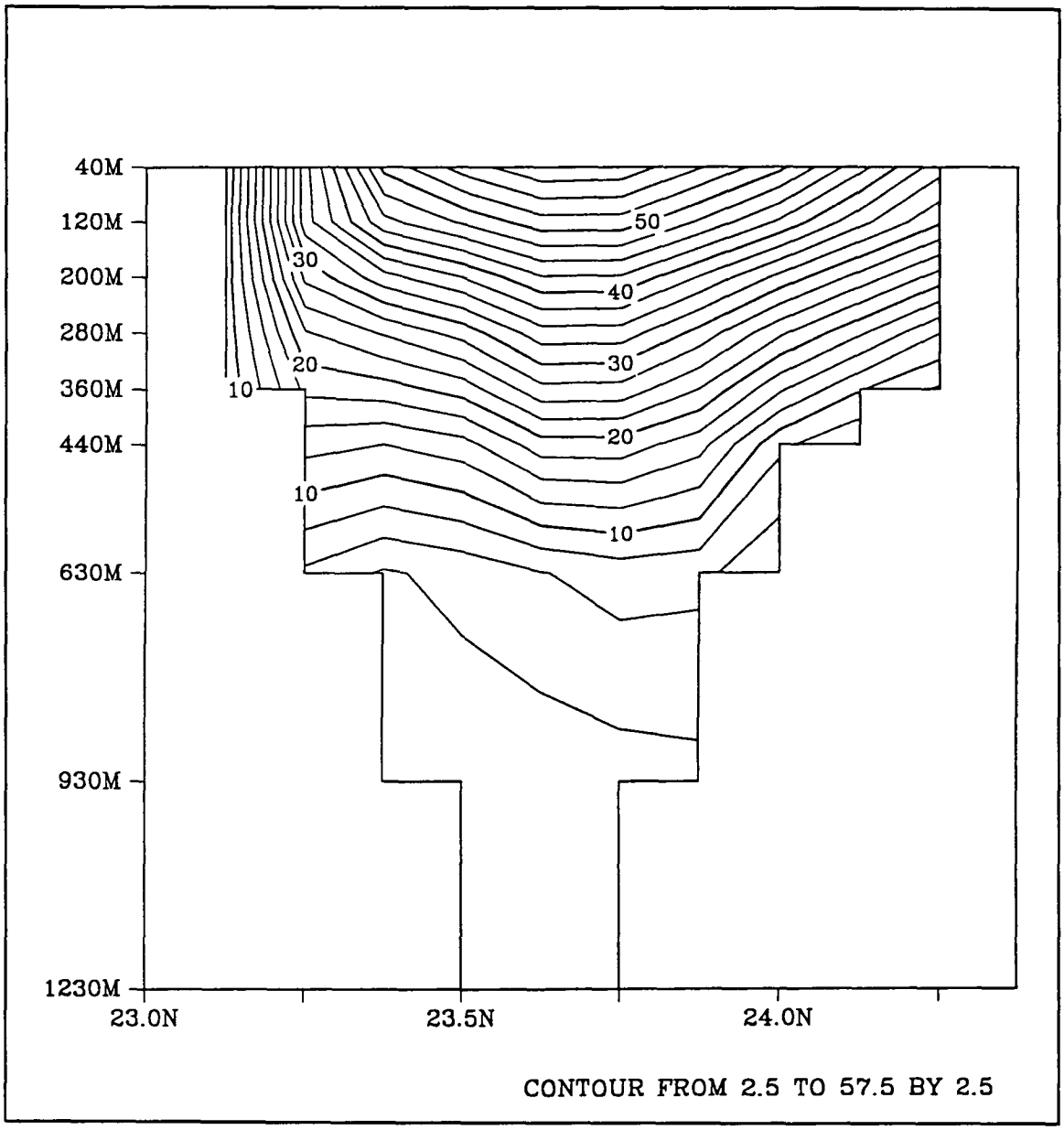

Figure 51b. Vertical profile of the annual average current speed ($cm \cdot s^{-1}$) in the Florida Current at 82°W looking upstream for year 2 of the LGM low transport case.

percent) of each of the interglacial zones Z, X and V were 31.8, 42.6 and 37.5, respectively. The glacial zones Y and W had average sand contents (in percent) of 25.4 and 23.9, respectively. These data clearly indicate higher sand content and presumably greater bottom current velocities during interglacial periods than during glacial periods in the Yucatan Channel, although Brunner's (1984) conclusion (not based on core 19 data) was the the opposite.

The hypothesis of lower than present volume transport of the Florida Current is also in agreement with the paleoceanographic modeling study by Lautenschlager et al. (1992) as mentioned in Chapter 1. A comparison of the global annual average of surface horizontal velocity using present-day boundary conditions (control run) and ice age boundary conditions is presented in Lautenschlager et al. (1992). The intensity of the surface equatorial currents in the Atlantic are shown to increase, but a larger percentage of the flow is directed southward along the east coast of South America in the Brazil Current in the LGM simulation than control. The velocity vectors in the Caribbean and the eastern Gulf of Mexico are smaller in the LGM model results than in the control run, indicating weaker surface currents.

CHAPTER 5

SUMMARY AND CONCLUSIONS

5.1 Present-Day Model Simulation

A numerical ocean model is developed for the study of the circulation in the GOM under present and past environmental conditions. The model is first initialized with present-day annual mean temperature and salinity fields and forced with annual mean wind stress in order to calibrate model parameters and test the method of forcing the model with geostrophic currents in the Caribbean. The annual cycle is then implemented through seasonally-varying surface boundary conditions and seasonal adjustment of the geostrophic forcing in the Caribbean. The seasonal variation of the volume transport of the LC is achieved through forcing the seasonal variation in the vertical shear of the Caribbean Current with observed climatological hydrographic data. Detailed analysis of the present-day seasonal simulations was made to satisfy the following objectives: (1) verify the ability of the model to produce realistic results, (2) learn more about the deep circulation in the GOM, which is not well understood, and (3) provide a basis for using the model to study circulation in the GOM during the LGM.

The model is useful for simulating seasonal changes in certain circulation patterns in the GOM as well as the impact of rings on other features of the general circulation. Some of the observed physical oceanographic processes reproduced in the model output are the Catoche Tongue upwelling, Campeche Bay cyclone, seasonal cycle in the WBC, the shelf break current off Louisiana and Texas, southward flow on the west Florida Shelf and the Tortugas Gyre. The model results show very realistic simulation of ring formation, migration and decay. The model does not accurately reproduce the observed circulation on the Texas-Louisiana shelf. This is in part due to the rather coarse resolution of the wind data set used and also due to the lack of bouyancy forcing which is provided by the fresh water flux of the Mississippi River, which are significant factors in forcing the westward near shore currents along the Louisiana-Texas coast (Oey 1995). The model also exhibits a fixed ring-separation period of 30 weeks, which is slightly less than the primary mode of between eight and nine months (Sturges 1994 and Vukovich 1995).

To study the deep circulation the model temperature and velocity fields were saved every three days for three years of model time at four levels in the vertical. Computer animations were made at each level to provide a continuous description of the entire water column covering six complete ring life spans. Snapshots of the model temperature, salinity, velocity and transport stream function at every grid point were saved every three months for more detailed analysis of the vertical structure. The ability to look at the temperature and velocity of the entire water column with very fine temporal and spatial resolution has led to some new conclusions about the forcing mechanisms of the large cyclonic gyres that dominate the deep circulation. They have been described as expressions of topographic Rossby waves that may be excited during ring separation, but

are thought to become decoupled from the LC rings because they migrate westward at a greater speed than the surface rings (Hamilton 1990). One can observe a connection between the deep cyclones and the surface temperature signal of the rings in the model output and conclude that they migrate westward as a pair. Analysis of the deep circulation in the eastern GOM indicates that the deep cyclones are formed beneath the LC during the final stages of ring separation. The deep cyclones in the model appear restricted by the bathymetric contours to a narrow migration path, but the surface anticyclones follow three main paths similar to those observed by Vukovich and Crissman (1986).

5.2 Last Glacial Maximum Model Simulation

This paleoceanographic study is significant because it uses a small grid size in the horizontal and vertical within a limited model domain to be truly eddy-resolving. The LGM simulations for both the high and low transport cases produce a LC and ring separation process much like we observe today. Varying the volume transport of the LC during the LGM simulations resulted in variations in the size, migration paths and life spans of the rings. A change in the general circulation between the high and low transport cases is the development of a northward current in the low transport case off the west coast of Florida associated with the cyclonic circulation of the Tortugas Gyre.

There are several significant differences between the present-day simulations and the LGM simulations in the western GOM that may explain the distribution of glacial fauna. A gyre-like pattern of temperature and salinity is estimated for both winter and summer during the LGM from statistical analysis on counts of glacial planktonic foraminifera in trigger-core tops in the western GOM (CLIMAP 1976 and Brunner and Cooley 1976). Temperatures and salinities were high in the center of the gyres and decreased toward the boundaries of the western basin.

In the present-day western GOM a seasonal WBC, forced by the seasonal cycle in wind stress curl (Sturges 1993), is positioned along the northern half of the western boundary. A WBC is also generated in the LGM simulations, but it originates in the southern Campeche Basin, flows northward to at least 24°N, but frequently extends into the northwestern GOM. An east-west temperature gradient is associated with the WBC along most of its path. South of the Texas coast a persistent north-south temperature and salinity gradient is caused by the presence of rings that enter the northwest corner and eventually decay. Southward displacement of the westerlies during winter produces upwelling off south Texas and Louisiana and generates even cooler temperatures along the coast.

The gradients in glacial temperature and salinity fields in the southern portion of the western gyre may also be explained by upwelling. Although wind direction over the western Yucatan Peninsula is favorable for upwelling year-round, the maximum in wind stress occurs in summer. A tongue of upwelled water extends westward from the western Yucatan Peninsula in late summer and can extend all the way across the western basin depending on the location of rings and other mesoscale eddies. The combination of

upwelling regimes, the WBC, and the longer residence times of the rings in the western GOM (especially in the low transport case) is consistent with the gyre distribution of glacial temperature and salinity in the western GOM.

There is sedimentation data for both the Yucatan Channel and the southern Straits of Florida that appears to support the hypothesis of lower transport of the LC system during the LGM than the present. Overall accumulation of silt and clay-size sediment in the central portion of the southern Straits of Florida is greater for the LGM than for the present (Brunner 1986), which may indicate weaker bottom velocities in the Florida Current during the LGM than the present. Also a greater percent of sand-size material was observed in each of the interglacial zones, Z, X, and V than in the glacial zones Y and W in a piston core in the Yucatan Channel (Brunner 1984). Brunner (1984) assumed that the percent of sand-size material is proportional to bottom flow velocities, which may indicate weaker bottom current velocities through the Yucatan Channel during the LGM than the present.

The model results for the LGM suggest that both the distribution of glacial fauna in the western GOM and sedimentation patterns in the southern Straits of Florida and the Yucatan Channel are consistent with lower than present volume transport of the LC system. These findings are in agreement with the LGM global ocean model results of Lautenschlager et al. (1992).

5.3 Future Work

An updated version of the Modular Ocean Model was released in the summer of 1995 that includes a free-surface boundary condition. The implementation of the free-surface may improve simulating ring dynamics and near-shore processes. Better vertical grid resolution on the Texas-Louisiana shelf and incorporation of fresh-water flux of the Mississippi River would improve the present-day simulation in that region. The LGM simulations would be improved by quantitative estimates of the inflow into the Caribbean during the LGM from both the North Atlantic and South Atlantic and subsequently an estimate of the glacial volume transport of the Florida Current.

REFERENCES

Barron, E.J. 1989. Model simulation of the Cretaceous ocean circulation. Science 244: 684-688.

Barron, E.J. and W.H. Peterson. 1990. Mid-Cretaceous ocean circulation: results from model sensitivity studies. Paleoceanography 5:319-337.

Bloom, A.L. 1983. Sea level and coastal changes, pp. 723-735. In H.E. Wright and D.G. Frey, eds. Late Quaternary Environments of the United States, Vol. 2, The Holocene. Princeton Univ. Press, Princeton, NJ.

Blumberg, A.F. and G.L. Mellor. 1987. A Description of a three-dimensional coastal ocean circulation model, pp. 1-16. In N.S. Heaps, ed. Three-dimensional Coastal Ocean Models. Coastal and Estuarine Sciences, Vol. 4.

Böning, C.W., R. Döscher and H.-J. Isemer. 1991. Monthly mean wind stress and Sverdrup Transports in the North Atlantic. J. Phys. Oceanogr. 21:221-235.

Brooks, D.A. 1984. Current and hydrographic variability in the northwestern Gulf of Mexico. J. Geophys. Res. 89:8022-8032.

Brunner, C.A. 1986. Deposition of a muddy sediment drift in the southern Straits of Florida during the Late Quaternary. Mar. Geol. 69:235-249.

Brunner, C.A. 1984. Evidence for increased volume transport of the Florida Current in the Pliocene and Pleistocene. Mar. Geol.. 54:223-235.

Brunner, C.A., 1982. Paleoceanography of surface waters in the Gulf of Mexico during the Late Quaternary. Quat. Res. 17:105-119.

Brunner, C.A. and J.A. Cooley. 1976. Circulation in the Gulf of Mexico during the last glacial maximum 18,000 yr ago. Geol. Soc. Am. Bull. 87:681-686.

Bryan, K. 1969. A numerical model for the study of the world ocean. J. Comput. Phys. 4:347-376.

Climate: Long-Range Investigation, Mapping and Prediction (CLIMAP). 1976. The surface of ice-age earth. Science. 191:1131-1137.

CLIMAP Project Members. 1981. Seasonal reconstruction of the Earth's surface at the last glacial maximum. Geol. Soc. of Am. Map and Chart Ser., MC-36.

Cochrane, J.D. and F.J. Kelly. 1986. Low-frequency circulation on the Texas-Louisiana continental shelf. J. Geophys. Res. 91:10645-10659.

Cox, M.D. 1984. A primitive equation three-dimensional model of the ocean. Tech. Rep. 1. Geophys. Fluid Dyn. Lab, NOAA. Princeton, NJ. 250 pp.

Curray, J.R. 1965. Late Quaternary history, continental shelves of the United States, pp. 723-735. In H.E. Wright and D.G. Frey, eds. The Quaternary of the United States. Princeton University Press, Princeton, NJ.

Dietrich, D.E. and C.A. Lin. 1995. Numerical Studies of eddy shedding in the Gulf of Mexico. J. Geophys. Res. 99:7599-7615.

Elliot, B.A. 1982. Anticyclonic rings in the Gulf of Mexico. J. Phys. Oceanogr. 12:1292-1309.

Emery, W.J., W.G. Lee, and L. Magaard. 1984. Geographic and seasonal distributions of Brunt-Väisälä frequency and Rossby radii in the North Pacific and North Atlantic. J. Phys. Oceanogr. 14:294-317.

Fairbanks, R.G. 1989. A 17,000-year glacio-eustatic sea level record: influence of glacial melting rates on the Younger Dryas event and deep-ocean circulation. Nature. 342:637-642.

Haidvogel, D.B., J.L. Wilkin, and R.Young. 1991. A semi-spectral primitive equation ocean circulation model using vertical sigma and orthogonal curvilinear horizontal coordinates. J. Comput. Phys. 94:151-185.

Hamilton, P. 1990. Deep currents in the Gulf of Mexico. J. Phys. Oceanogr. 20:1087-1104.

Han, Y. 1984. A numerical world ocean general circulation model. Part II. Baroclinic experiment. Dyn. Atmos. Ocean. 8:141-172.

Hellerman, S. and M. Rosenstein. 1983. Normal monthly wind stress over the world ocean with error estimates. J. Phys. Oceanogr. 13:1093-1104.

Hirst, A.C. and J.S. Godfrey. 1993. The role of Indonesian throughflow in a global ocean GCM. J. Phys. Oceanogr. 23:1057-1086.

Hoffman, E.E. and S.J. Worley. 1991. Circulation of the Gulf of Mexico. J. Geophys. Res. 91:14221-14236.

Hsu, S.A. 1988. Coastal Meteorology. Academic Press Inc., San Deigo, CA. 260 pp.

Hurlburt, H.E. and J.D. Thompson. 1980. A numerical study of Loop Current intrusions and eddy shedding. J. Phys. Oceanogr. 10:1611-1651.

Ichiye, T. 1972. Experiments on circulation of the Gulf of Mexico and the Caribbean Sea with a rotating tank, pp. 37-57. In Mem. IV Congr. Nac. Ocean. Mexico.

IMSL Fortran Subroutines for Mathematical Applications. 1989. Math/Library version 1.1. Houston, Texas. 1152 pp.

Indest, A.W. 1992. Ring dynamics in the western Gulf of Mexico. Ph.D. Thesis. Old Dominion University. Norfolk, VA. 127 pp.

Kutzbach, J.E. and P.J. Guetter. 1986. The influence of changing orbital parameters and surface boundary conditions on climate simulations for the past 18,000 years. J. Atmos. Sci. 43:1726-1758.

Kutzbach, J.E., P.J. Guetter, and W.M. Washington. 1990. Simulated circulation of an idealized ocean for Pangaean time. Paleoceanography. 5:299-317.

Lautenschlager, M., U. Mikolajewicz, E. Maier-Reimer, and C. Heinze. 1992. Application of ocean models for the interpretation of atmospheric general circulation model experiments on the climate of the last glacial maximum. Paleoceanography. 7:769-767.

LeGrand, P. and C. Wunsch. 1995. Constraints from paleotracer data on the North Atlantic circulation during the last glacial maximum. Paleoceanography. 10:1011-1045.

Lee, T.N., K. Leaman, E. Williams, T. Berger, and L. Atkinson. 1995. Florida Current meanders and gyre formation in the southern Straits of Florida. J. Geophys. Res. 100:8607-8620.

Leventeer, A., D.F. Williams, and J.P. Kennett. 1982. Dynamics of the Laurentide ice sheet during the last deglaciation: evidence from the Gulf of Mexico. Earth and Planetary Science Letters. 59:11-17.

Levitus, S. 1982. Climatological Atlas of the World Ocean. NOAA Prof. Paper 3. 173 pp.

Lewis, J.K., and A.D. Kirwan. 1987. Genesis of a Gulf of Mexico Ring as determined from kinematic analyses. J. Geophys. Res. 92:11727-11740.

Luther, M.E. and J.J. O'Brien. 1985. A model for the seasonal circulation in the Arabian Sea forced by observed winds. Prog. Oceanogr. 14:353-385.

Luther, M.E., J.J. O'Brien and W.J. Prell. 1990. Variability in upwelling fields in the northwestern Indian Ocean, 1, Model experiments for the past 18,000 years. Paleoceanography. 5(3):433-445.

Maier-Reimer, E., U. Mikolajewicz, and K. Hasselmann. 1991. On the sensitivity of the global ocean circulation to changes in surface heat fluxes. Report #68, Max-Planck-Institut für Meteorol., Hamburg.

Molinari, R.L., J.F. Festa, and D.W. Behringer. 1978. The circulation in the Gulf of Mexico derived from estimated dynamic height fields. J. Phys. Oceanogr. 8:987-996.

Morton, R.A. and W.A. Price. 1987. Late Quaternary sea-level fluctuations and sedimentary phases of the Texas coastal plain and shelf, pp. 181-198. In D. Nummedal, O.H. Pilkey and J.D. Howard, eds., Sea-Level Fluctuation and Coastal Evolution. The Society of Economic Paleontologists and Mineralogists.

Oey, L.-Y. 1995. Eddy- and wind-forced shelf circulation. J. Geophys. Res. 100:8621-8637.

Pacanowski, R., K. Dixon, and A. Rosati. 1991. "The GFDL Modular Ocean Model Users Guide version 1.0", GFDL Ocean Group Technical Report #2. Princeton, N.J.

Prell, W.L., R.E. Marvil, and M.E. Luther. 1990. Variability in upwelling fields in the northwestern Indian Ocean, 2, Data-model comparison at 9000 years b.p. Paleoceanography. 5:447-457.

Prell, W.L., J.V. Gardner, A.W.H. Be and J.D. Hays. 1976. Equatorial Atlantic and Caribbean foraminiferal assemblages, temperatures and circulation: interglacial and glacial comparison. Geol. Soc. Am. Mem. 145:247-266.

Rind, D. and D.M. Peteet. 1985. Terrestrial conditions at the last glacialmaximum and CLIMAP sea-surface temperature estimates: Are they consistent? Quat. Res. 24: 1-22.

Ruiz Rentería, F.G. 1979. Upwelling north of the Yucatan Peninsula. M.S. Thesis. Texas A&M University. College Station, Tx. 82 pp.

Schmitz, W.J. and P.L. Richardson. 1991. On the sources of the Florida Current. Deep-Sea Res. 38(Suppl.):S379-S409.

Schmitz, W.J., J.D. Thompson, and J.R. Luyten. 1992. The Sverdrup circulation for the Atlantic along 24°N. J. Geophys. Res. 97:7251-7256.

Schott, F.A., T.N. Lee, and R. Zantopp. 1988. Variability of structure and transport of the Florida Current in the period range of days to seasonal. J. Phys. Oceanogr. 18:1209-1230.

Science Applications International Corporation. 1986. Gulf of Mexico Ship-of-Opportunity Data Report. OCS Report/MMS 86-0028. U.S. Dept. of the Interior, Minerals Mgmt Service, Gulf of Mexico OCS Regional Office, New Orleans, La. 632 pp.

Science Applications International Corporation. 1992. Straits of Florida Physical Oceanographic Field Study, Final Interpretative Report. Volume I: Executive Summary. OCS Report/MMS 92-0024. U.S. Dept. of the Interior, Minerals Management Service, Gulf of Mexico OCS Regional Office, New Orleans, La. 19 pp.

Semtner, A.J. 1974. An oceanic general circulation model with bottom topography. Tech. Report #9. Dept. of Meteorology, Univ. of Calif. Los Angeles, Ca. 99 pp.

Semtner, A.J. 1986a. History and methodology of modeling the circulation of the world ocean, pp. 23-32. In J.J. O'Brien, ed. Advanced Physical Oceanographic Numerical Modeling. D. Reidel. Norwell, Ma.

Semtner, A.J. 1986b. Finite-difference formulation of a world ocean model, pp. 187-202. In J.J. O'Brien, ed., Advanced Physical Oceanographic Numerical Modeling. D. Reidel. Norwell, Ma.

Suter, J.R., H.L. Berryhill, and S. Penland. 1987. Late Quaternary sea-level fluctuations and depositional sequences, Southwest Louisiana continental shelf, pp. 199-219. In D. Nummedal, O.H. Pilkey and J.D. Howard, eds. Sea-Level Fluctuation andCoastal Evolution. Soc. Econom. Paleont. Mineral.

Sturges, W. 1994. The frequency of ring separations from the Loop Current. J. Phys. Oceanogr. 24:1647-1651.

Sturges, W., and J.P. Blaha. 1976: A western boundary current in the Gulf of Mexico. Science. 192:367-369.

Sturges, W., J.C. Evans, S. Welsh and W. Holland. 1993. Separation of warm-core rings in the Gulf of Mexico. J. Phys. Oceanogr. 23:250-268.

Sturges, W. 1993. The annual cycle of the western boundary current in the Gulf of Mexico. J. Geophys. Res. 98:18053-18068.

Vazquez de la Cerda, A.M. 1993. Bay of Campeche cyclone. Ph.D. Thesis. Texas A & M University. College Station, Tx. 91 pp.

Vidal, V.M.V., F.V. Vidal, and J.M. Perez-Molero. 1992. Collision of a Loop Current anticyclonic ring against the continental shelf slope of the western gulf of Mexico. J. Geophys. Res. 97:2155-2172.

Vukovich, F.M. and B.W. Crissman. 1986. Aspects of warm rings in the Gulf of Mexico. J. Geophys. Res. 91:2645-2660.

Vukovich, F.M. 1995. An Evaluation of the Loop Current's eddy-shedding frequency. J. Geophys. Res. 100:8655-8659.

Yasuda, I. 1995. Geostrophic vortex merger and streamer development in the ocean with special reference to the merger of Kuroshio warm core rings. J. Phys. Oceanogr. 25:979-996.

APPENDIX A

NUMERICAL MODEL FORMULATION

The Modular Ocean Model is a three-dimensional primitive-equation ocean model. The ocean is assumed to be incompressible. In order to simplify the equations, the following approximations are made: thin shell approximation, hydrostatic assumption and the Boussinesq approximation. There are constant eddy viscosity coefficients, κ and A_H, and constant eddy diffusivity coefficients, μ and A_M. The variables are projected onto a spherical coordinate system with a, Ω, λ, ϕ, and z, used to represent the earth's radius, angular speed, latitude, longitude and height, respectively. The following seven equations are solved for u-, v-, and w-components of velocity, pressure p, density ρ, potential temperature T and salinity S:

$$\frac{\partial u}{\partial t} + Lu - \frac{uv\tan\phi}{a} - fv = -\frac{1}{\rho_o a\cos\phi}\frac{\partial p}{\partial \lambda} + \mu\frac{\partial^2 u}{\partial z^2} + A_M\left[\nabla^2 u + \frac{(1-\tan^2\phi)u}{a^2} - \frac{2\sin\phi}{a^2\cos^2\phi}\frac{\partial v}{\partial \lambda}\right], \tag{1}$$

$$\frac{\partial v}{\partial t} + Lv - \frac{u^2\tan\phi}{a} + fu = -\frac{1}{\rho_o a}\frac{\partial p}{\partial \lambda} + \mu\frac{\partial^2 v}{\partial z^2} + A_M\left[\nabla^2 v + \frac{(1-\tan^2\phi)v}{a^2} + \frac{2\sin\phi}{a^2\cos^2\phi}\frac{\partial u}{\partial \lambda}\right], \tag{2}$$

$$\frac{\partial p}{\partial z} = -\rho g, \tag{3}$$

$$\frac{1}{a\cos\phi}\frac{\partial u}{\partial z} + \frac{1}{a\cos\phi}\frac{\partial(v\cos\phi)}{\partial\phi} + \frac{\partial w}{\partial z} = 0, \tag{4}$$

$$\frac{\partial T}{\partial t} + LT = \kappa\frac{\partial^2 T}{\partial z^2} + A_H\nabla^2 T, \tag{5}$$

$$\frac{\partial S}{\partial t} + LS = \kappa\frac{\partial^2 S}{\partial z^2} + A_H\nabla^2 S, \tag{6}$$

$$\rho = \rho(T, S, p). \tag{7}$$

The additional forcing terms in the above equations are the advection operator,

$$L(\alpha) = \frac{1}{a\cos\phi}\frac{\partial(u\alpha)}{\partial\lambda} + \frac{1}{a\cos\phi}\frac{\partial(v\alpha\cos\phi)}{\partial\phi} + \frac{\partial(w\alpha)}{\partial z},$$

the horizontal Laplacian operator,

$$\nabla^2\alpha = \frac{1}{a^2\cos^2\phi}\frac{\partial^2\alpha}{\partial\lambda^2} + \frac{1}{a^2\cos\phi}\frac{\partial(\frac{\partial\alpha}{\partial\phi}\cos\phi)}{\partial\phi},$$

and the Coriolis parameter,

$$f = 2\Omega\sin\phi .$$

The boundary conditions applied to the governing equations are: zero flux of momentum, heat and salt at the ocean bottom; wind stress and fluxes of heat and salt are prescribed at the surface; no slip at the vertical walls; no flux of heat or salt at the vertical walls; a rigid-lid at the surface (w=0 at z=0); and flow parallel to the slope at the ocean bottom. Due to the rigid-lid approximation, this version of the model can not be used to solve for sea-surface elevation and therefore does not contain tides.

The finite-difference method was used to construct the model on a staggered grid referred to as the Arakawa B-grid or B scheme. This scheme was chosen over other arrangements of grid points because it works better with a high number of vertical levels and is better for the resolution of eddy dynamics (Semtner 1986a). The arrangement of grid points is such that the temperature, salinity, actual depth and transport stream function lie at the center of the grid box and velocity lies at the centers of the vertical edges. The vertical component of velocity is computed at the vertical interface between two grid boxes.

The type of numerical solver implemented is the five-point conjugate gradient method, which is faster and more accurate than the successive over-relaxation method of the Bryan-Cox model (Pacanowski et al. 1991), while retaining its ability to work with steep gradients in bathymetry.

APPENDIX B

MINIMUM INFLOW CONDITION FOR THE LGM SIMULATIONS

The last glacial maximum simulations were designed to test the model's response to varying the inflow into the GOM. We first assume that the annual average volume transport into the GOM through the Yucatan Channel is equal to the outflow through the Florida Straits. We then tried to determine how much the inflow during the LGM may have differed from the present. Therefore it was necessary to evaluate the sources of the present-day Florida Current and the percent contributions of each of the sources, before we could predict how much the total flow may have changed.

The widely accepted value for the total flow of the Florida Current at 24°N is 30 Sv (Schmitz et al. 1992). The wind-driven component of the Florida Current can be estimated by computing the annual mean Sverdrup volume transport for the North Atlantic from present-day wind stress climatology. The annual mean Sverdrup volume transport at 24°N is 18 Sv computed using the Hellerman and Rosenstein (1983) wind stress climatology (Böning et al. 1991). This value compares well with the estimate of 17 Sv of wind-driven transport entering the Caribbean reported by Schmitz et al. (1992). Schmitz and Richardson (1991) estimate that the remaining 13 Sv or 45% of the total flow in the Florida Current is of South Atlantic origin to compensate for the cross-equatorial transport of NADW.

The Sverdrup volume transport calculation is repeated using the Kutzbach and Guetter (1986) LGM wind stress field for January and July (Figure 52). The maximum volume transport in the North Atlantic gyre in January is 23.73 Sv at 24.4°N, but less than 22 Sv could flow into the Caribbean east of Cuba (Figure 52a) at this latitude. The north Atlantic Gyre is shifted north in the summer (Figure 52b) and has a maximum Sverdrup volume transport of only 5.5 Sv, but less than 2 Sv could enter the Caribbean east of Cuba. There is a very large seasonal difference in the volume transport of the North Atlantic gyre computed using the Kutzbach and Guetter (1986) wind stress estimates. As discussed in Chapter 3, it is not practical to directly force changes in the total transport produced by the inflow condition. Therefore the wind-driven component of the Florida Current for the LGM low transport simulations was set equal to the average of the maximum possible transports entering the Caribbean east of Cuba during January and July. This calculation produces an annual average wind-driven component of the Florida Current of 12 Sv, which is ⅓ of the present-day value of 17-18 Sv.

How much of the total transport of the Florida Current is represented by the wind-driven flow during the LGM? Reliable quantitative estimates of the thermohaline circulation for the LGM are not yet available and it is not possible to determine how much South Atlantic water entered the Caribbean as cross-equatorial compensation flow of glacial NADW. This study assumes that the ratio of wind-driven transport to total transport of the Florida Current was the same during the LGM as today. Therefore the target volume transport of the low inflow condition is achieved by reducing the target volume transport of the present-day seasonal forcing case by ⅓.

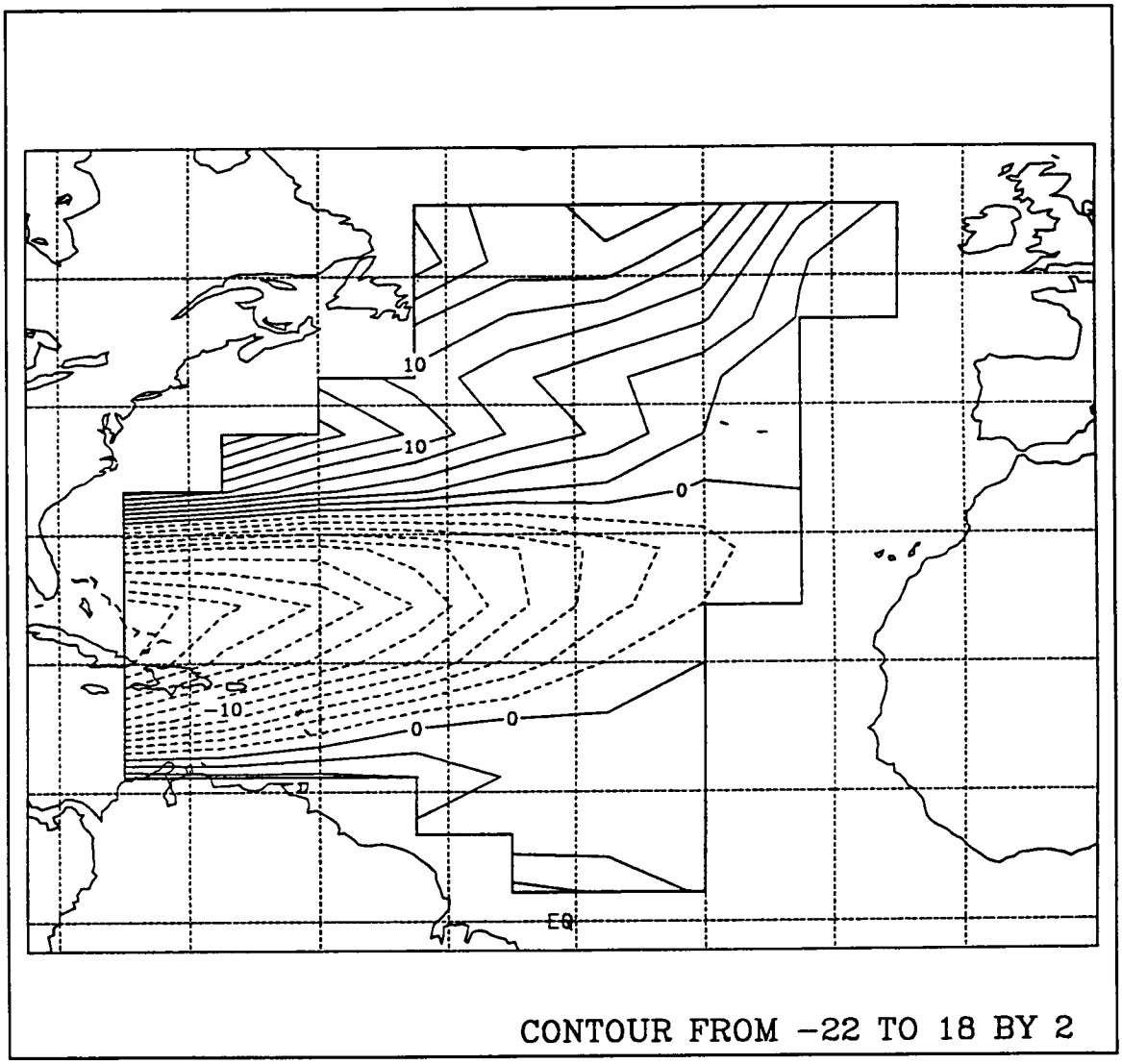

Figure 52a. Sverdrup volume transport (Sv) for the North Atlantic computed using Kutzbach and Guetter (1986) wind stress field for 18,000 years B.P. on a 7.5° longitude by 4.4° latitude grid for January.

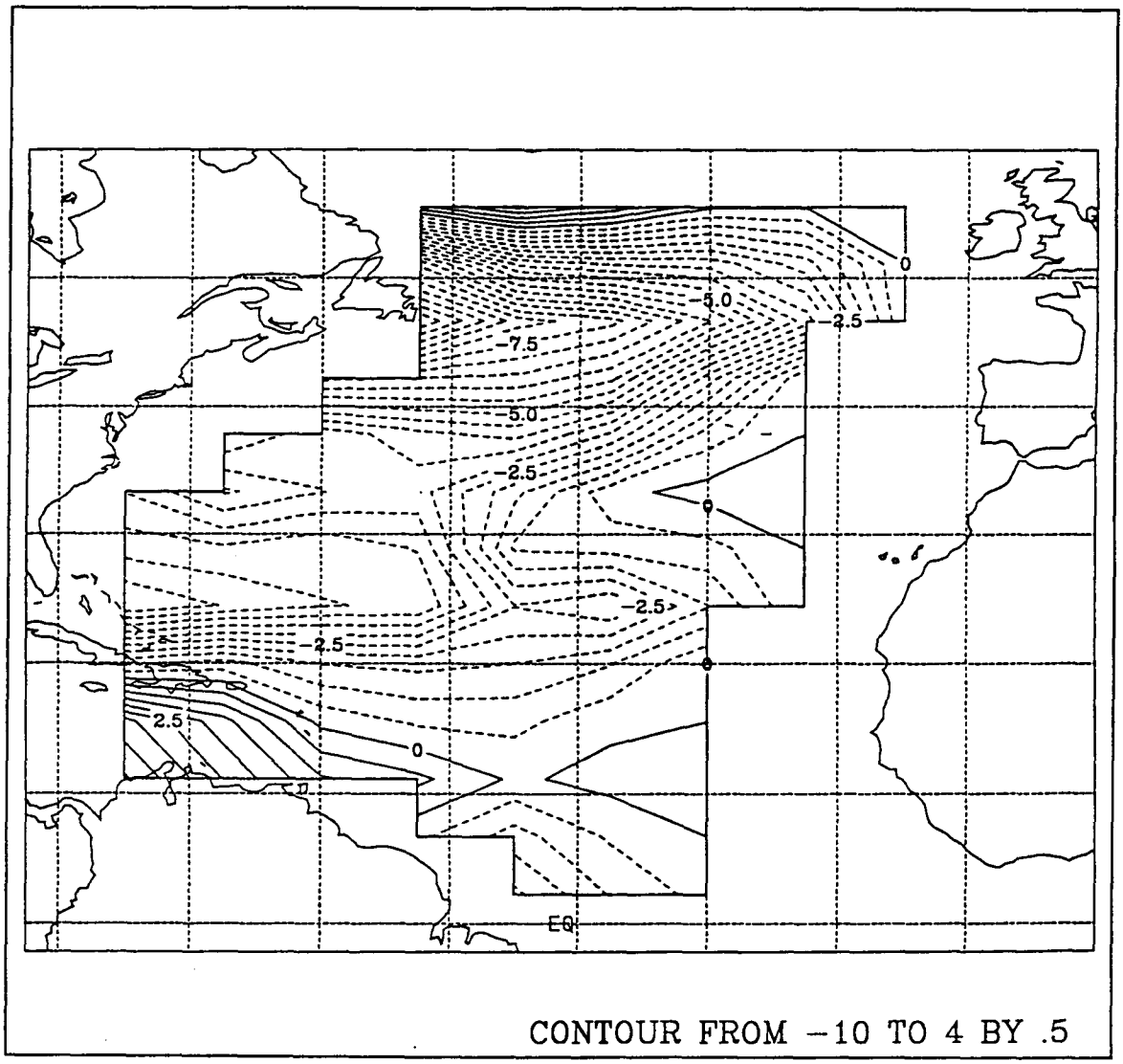

Figure 52b. Sverdrup volume transport (Sv) for the North Atlantic computed using Kutzbach and Guetter (1986) wind stress field for 18,000 years B.P. on a 7.5° longitude by 4.4° latitude grid for July.

The Department of the Interior Mission

As the Nation's principal conservation agency, the Department of the Interior has responsibility for most of our nationally owned public lands and natural resources. This includes fostering sound use of our land and water resources; protecting our fish, wildlife, and biological diversity; preserving the environmental and cultural values of our national parks and historical places; and providing for the enjoyment of life through outdoor recreation. The Department assesses our energy and mineral resources and works to ensure that their development is in the best interests of all our people by encouraging stewardship and citizen participation in their care. The Department also has a major responsibility for American Indian reservation communities and for people who live in island territories under U.S. administration.

The Minerals Management Service Mission

As a bureau of the Department of the Interior, the Minerals Management Service's (MMS) primary responsibilities are to manage the mineral resources located on the Nation's Outer Continental Shelf (OCS), collect revenue from the Federal OCS and onshore Federal and Indian lands, and distribute those revenues.

Moreover, in working to meet its responsibilities, the **Offshore Minerals Management Program** administers the OCS competitive leasing program and oversees the safe and environmentally sound exploration and production of our Nation's offshore natural gas, oil and other mineral resources. The MMS **Royalty Management Program** meets its responsibilities by ensuring the efficient, timely and accurate collection and disbursement of revenue from mineral leasing and production due to Indian tribes and allottees, States and the U.S. Treasury.

The MMS strives to fulfill its responsibilities through the general guiding principles of: (1) being responsive to the public's concerns and interests by maintaining a dialogue with all potentially affected parties and (2) carrying out its programs with an emphasis on working to enhance the quality of life for all Americans by lending MMS assistance and expertise to economic development and environmental protection.